THE UNIVERSITY
of EDINBURGH

DEVELOPMENT OF A SOLAR POWERED REFRIGERATION SYSTEM

STIRLING-CYCLE BASED

By

Jafar Mohammad Salim Daoud

Doctor of Philosophy

The University of Edinburgh

2019

Lay Summary

Solar energy has potential for cooling due to the coincidence with cooling demand and the adequate solar power per square meter. It has been successfully applied in cooling through photovoltaic (PV) powered vapour compression cycles (VCC) and heat powered sorption technologies but in remote areas and where electricity grids are not reliable. Although, efficient working Stirling-cycle coolers were successfully built, the solar powered Stirling-cycle has not been commercially successful due to the high initial cost of the Stirling machines and solar tracking system. The Stirling-cycle machine is particularly complex and hence expensive at high power generation due to the heat exchangers and engine high-temperature material. On the other hand, the Stirling cycle enjoys the potential for high efficiency, quietness, and use of environmental friendly gases. In this study, the performance of bare Stirling-cycle machines with long stroke to bore ratio is studied to replace complex heat exchangers with large cylinder walls. A new type of isothermaliser, which is a large surface device almost filling working spaces is used to increase the heat transfer, has cylindrical surface deployed to enhance heat transfer and hence power density. The effect of different engine arrangements on vibration, start-up capability and flywheel elimination are investigated. Implementation of the balanced compounding technology, which eliminates the need for kinematic drive and rotational parts, is studied. A novel thermal coupling method integrated within solar thermal collectors is suggested and the whole solar cooler is analysed. Based on a theoretical model, the new isothermaliser improves the power density by 275% and 250% compared to the existing conventional Stirling engine and refrigerator, respectively. Also, an extended mathematical model showed that the multi-cylinder configuration of at least 3 hot and 3 cold cylinders removes vibrations caused by non-uniform force distribution, brings the system to self-start, eliminates the need for a flywheel and works as free piston machine with the balanced compounding technology. A theoretical model reveals that if the developed machine is directly deployed inside the cylinders of line focused solar collectors it might give a solar coefficient of performance of 0.367 for near ambient cooling. This figure is close to the efficiency of commercial solar-powered vapour compression coolers if the efficiency of the PV and VCC is 10% and 3.5, respectively.

Abstract

Solar refrigeration has been tirelessly studied since the 1970s. Yet, no renewable technology has been superior to the conventional grid powered technology for household applications. However, Photovoltaic (PV) powered vapour compression coolers and thermal collector powered sorption technologies are affordable in the market for off-grid cooling. The Stirling cycle is more than 200 years old technology but had limited success. For solar powered applications, it is complex, expensive and only commercially feasible at high-temperature differences in both motoring and refrigeration modes. That's because high power machines need efficient, compact and hence complex heat exchangers, high temperature materials, pressurised light gases, complex driving mechanism, expensive solar tracking and solar thermal coupling mechanism. In this study, the Stirling-cycle machine is thermodynamically and technologically studied and designed to work with input temperatures between 450 K and 600 K that can be achieved by line-focus solar collectors. The Franchot-type machine, which is a double acting Stirling machine that uses one hot and one cold cylinder to form 2 alpha-type Stirling machines, has been redesigned to use long and direct-heated and cooled cylinders at low temperature differences. In addition to the polytropic processes, a novel simple isothermaliser was presented to improve the power density of the Franchot machine. The isothermaliser is either passive or active if it is thermally insulated or connected to external heat source, respectively. A simple balanced compounding mechanism, where compression pistons are mechanically coupled to expansion ones, is suggested and studied theoretically. A novel thermal coupling mechanism with evacuated tube collectors is suggested for the solar-powered engine. To minimise material use, unpressurised ambient air and short regenerator connections are only considered with the suggested Stirling-cycle machine.

In this study, the Franchot machine is mathematically studied in the Matlab/Simulink environment using the second order model for the three-control volume machine, assuming the expansion and compression are polytropic processes. In the initial study, the model is built on ideal processes in order to understand the response of the machine for changes in the speed, gas pressure, phase angle, dead volume and geometry. In

successive chapters, introduction of different non-ideal processes and effects is considered and coupled to the ideal model.

It is found that the Stirling cycle performance can be improved by the optimisation of load, losses, gas pressure, engine speed, phase angle and geometrical parameters (e.g. cylinder diameter, length and dead volume). Increasing the gas pressure and engine speed enhances the power as they increase Reynolds' number which in turn improves the in-cylinder heat transfer. Varying the phase angle and dead volume at a given speed can maximise the power approaching the Curzon and Ahlborn efficiency, which is the efficiency of any heat engine at maximum power. On the other hand, the Stirling-cycle refrigerator has a monotonic response approaching Carnot efficiency at very low cooling power and maximum cooling density at very low efficiency. Therefore, the optimised engine parameters at maximum power generation is used for the refrigerator. In comparison to the Stirling engine with adiabatic cycle, the polytropic model of the isothermalised engine predicts about 275% and 211% power density improvements at the maximum power point for the active and passive isothermalisers, respectively. Similarly, in comparison to the adiabatic cycle refrigerator, the isothermalised refrigerator could have about 250% and 190% cooling power improvements at a COP of 3.25 for the active and passive isothermalisers, respectively. Conceptually, the suggested balanced compounding mechanism generates low side forces, reduces the machine length and complexity and adds self-starting capability. Simplicity and compactness are also enhanced by the removal of complex heat exchangers and using of a novel thermal coupling mechanism with the line solar collector. The solar refrigerator could deliver a specific cooling power peak of 367.5 W/m^2 for air conditioning relative to a peak solar irradiance of 1 kW/m^2. This number can be approximately computed by multiplying solar irradiance by Curzon efficiency, COP of 4 and solar collector efficiency of 50%. Therefore, the solar Stirling refrigerator might have the potential to compete with the vapour compression cycle for domestic applications.

Acknowledgement

First and foremost, praises and thanks to Allah, the Almighty, for His showers of blessings throughout my research work to complete the research successfully.

I am extremely grateful to my parents for their love, prayers, caring and sacrifices for educating and preparing me for my future understanding, their patience and continuing support to complete this research work.

I would like to express my deep gratitude to my supervisor, Dr. Daniel Friedrich, for giving me the opportunity to work with him and providing invaluable guidance throughout this research. He has taught me the methodology to carry out the research and to present the research works as clearly as possible.

Finally, my thanks go to all people who have supported me to complete the research work directly or indirectly. I am especially grateful to the British council for granting me the PhD scholarship.

Jafar Mohammad Salim Daoud

2019, Edinburgh, UK

Declaration

I declare that this thesis was composed by myself, that the work contained herein is my own except where explicitly stated otherwise in the text, and that this work has not been submitted for any other degree or professional qualification except as specified. I carried out all aspects of data collection, data analysis, writing of the manuscript and generating figures. The co-author was responsible for providing feedback on study, design and corrections to the manuscript. Daoud JM is the student and author of the declaration and listed publications. Friedrich D is the supervisor.

The main work presented in Chapter 3 was published in *International Journal of Energy Research (IJER)* [1] as *Performance investigation of a novel Franchot engine design* by [*Daoud JM, Friedrich D]*.

The engine relevant work presented in Chapter 4 was published in the *Journal Inventions* [2] as Parametric study of an air charged Franchot engine with novel hot and cold isothermalisers by [*Daoud JM, Friedrich D*].

The work presented in Chapter 5 was published in the *Journal Applied Thermal Engineering* [3]as *Design of the multi-cylinder Stirling engine arrangement with self-start capability and reduced vibrations* by [*Daoud JM, Friedrich D*].

The thermodynamic cycle interpretation presented in Chapter 3 and the balanced compounding work presented in Chapter 6 were published in the *Journal Energy Conversion and Management (ECM)* [4] as *A novel Franchot engine design based on the balanced compounding method* by [*Daoud JM, Friedrich D*].

Parts of the work of Chapter 5 and the main work presented in Chapter 7 were submitted to *18th Stirling Engine Conference (ISEC)* as *A new duplex Stirling engine concept for solar-powered cooling* by [*Daoud JM, Friedrich D*].

Jafar Mohammad Salim Daoud

Table of Contents

List of figures

List of tables

Nomenclature

A_x	*Total cylinder wall area*	*m^2*
c_v	*Gas specific heat capacity at constant volume*	*J/kg.K*
c_p	*Gas heat specific capacity at constant pressure*	*J/kg.K*
d	*Piston rod diameter*	*m*
d_h	*Hydraulic diameter*	*m*
D_x	*Cylinder bore in each compartment*	*m*
F	*Force*	*N*
f	*Engine frequency*	*Hz*
H	*Enthalpy*	*J*
h_x	*In-cylinder heat transfer coefficient*	*$W/m^2.K$*
k	*Working gas stiffness*	N/m
L	*Total cylinder length*	*m*
M	*Total working gas mass*	*kg*
$\dot{m}_l$	*Gas leakage*	*Kg/m^3*
m_x	*Gas mass in compartment x*	*kg*
m	*Reciprocator mass*	*kg*
n	*Engine speed, Number of phases*	*RPM*
N	*Number of engine cylinders*	
Nu	*Nusselt number*	
p	*Instantaneous gas pressure*	*N/m^2*
P	*Average mechanical power*	*W*
P_{ins}	*Instantaneous mechanical power*	*W*
Q_x	*Heat exchanger thermal energy*	*J*
rc	*Compression space clearance*	*m*
re	*Expansion space clearance*	*m*
R	*Ideal gas constant*	*J/kg.K*
Re	*Reynolds number*	
T_x	*Instantaneous temperature of compartment x*	*K*
v_x	*Volume of compartment x*	*m^3*
W	*Cycle work*	*J*

Greek letters

ε	*Regenerator effectiveness*	
γ	*Heat capacity ratio*	
ρ	*Charge gas density*	*kg/m^3*
θ	*Thermodynamic phase angle*	*deg*
θ_s	*Phase shift*	*deg*
ω_o	*Resonant frequency*	*Rad/s*
ζ	*Efficiency*	

Subscripts

c	*Compression space*
e	*Expansion space*
h	*Hot cylinder*
k	*Cold cylinder*
l	*Chilling cylinder/ load*
r	*Regenerator*
rh	*Regenerator hot side*
rk	*Regenerator cold side*
x	*Specific compartment*

CHAPTER

1 Introduction

During the last two centuries, humankind has consumed a large amount of fossil fuel, which has taken millions of years to be generated. It is expected that we will continue consuming energy at high rates and, as a consequence, increase the instability of fuel prices and release a large amount of CO_2 [5][6]. Thus, finding alternative resources especially for high-energy consumption applications will reduce the fossil fuel depletion and enhance energy and economy security.

Refrigeration, which is the process of bringing a space temperature below the ambient, is one of the applications that consumes large quantities of energy and accounts for more than 33% of the global electricity consumption [7]. In a cold country like Germany, refrigeration counts for 14% of its total electricity consumption [8]. In hot countries, electricity consumption for refrigeration is more significant. For example, the summer electricity consumption for refrigeration approaches 40% in China [9] and 40% of commercial power consumption in the USA [10]. In developing countries like Egypt and Saudi Arabia, household air conditioning alone is responsible for 32% and 72% of the electricity consumption, respectively [11][12]. Refrigeration is not only important for human comfort but also for vaccine storage and food preservation. More than 33% of the world's food production is wasted due to technological and financial limitations in poor countries [13]. The demand for refrigeration is expected to increase due to the global warming, population growth and improving lifestyle. In addition to that, energy crises, fuel prices, environmental issues and electricity grid reliability, especially in rural and remote areas, require the reliance on electricity independent resources. Refrigeration is considered a main source of unevenly distributed electric loads [14].

Solar powered refrigeration can reduce electricity requirements for refrigeration by 21-70% based on the location, building standard and internal load situation of the

building [15]. Moreover, solar energy is renewable, safe, freely available, coincides with cooling demand and can be used to generate heat, cold and power which improves grid security and reduce the reliance on electricity grids.

1.1 Solar energy

The Sun is a giant nuclear reactor distant from the Earth by about 150 million km, so that the light requires 8.3 min to reach us [16]. The Sun is in its midlife and it has been shining for about 4.6 billion years. Due to hydrogen fusion at the Sun's core, it radiates a huge amount of energy spread out to the universe. However, the Earth intercepts a small fraction of this irradiance but only 0.035% of the irradiance reaches the earth is enough to supply the whole world's energy needs [17]. The earth receives an average solar irradiance of 1367 W/m^2 [18] from which about 13% is absorbed by the atmosphere and 13% reflected back to space. Thus, the solar irradiance has a peak of around 1 kW/m^2 on the surface of the earth.

The absorbed solar irradiance by both the air and the earth surface causes the earth to heat up. Thus, the needs for ambient refrigeration increase with solar irradiance [19]. However, solar irradiance is not the same for all locations on Earth. Countries located in the equatorial Sun Belt receive abundant energy and have a higher average temperature in comparison to countries closer to Earth's poles making them generally hotter than other countries. Hence, the need for air refrigeration for the equatorial belt countries is larger than that for near pole countries. Because of the seasonal earth tilt of -23.45° to 23.45° from the poles [20], the maximum direct solar irradiance travels to the north in northern summer and to the south in northern winter which causes temperature variations on the surface of the earth, accordingly. In addition to that, daylight hours increase in summer and decrease in winter. However, the Earth cools down by emitting some of its energy to the outer space. This reduces the refrigeration needs at night to about one third of the day load [21]. Thus, the peak of solar irradiance coincides with the peak of ambient temperature not only monthly [22][23][24][25] but also on daily [26][27] and hourly bases [28]. Besides this, the power density of the solar energy makes the Sun a perfect renewable energy source for air conditioning. For

example, a typical house with a plan area of 100 m^2 intercepts a peak of 100 kW of solar irradiance while an economical 1-Ton (3.5 kW) air conditioner draws around 1 kW of electrical power. Nevertheless, solar cooling suffers from the intermittent nature of solar irradiance for which refrigeration is still needed, e.g. at night or at cloudy days when there is temporary absence of solar irradiance.

1.2 Solar Thermal collectors

Solar energy can be harnessed by converting the solar irradiance into electricity via photovoltaic (PV) panels and into heat by thermal collectors, both of which are commercially available for households and the commercial sector. For simplicity, reliability and cost, the domestic solar collectors are statically mounted to avoid tracking power and control requirements and running maintenance. They are able to absorb the direct and diffused irradiance caused by the particles in the atmosphere [5].

Solar thermal collectors can benefit from the whole solar spectrum having an average solar to thermal efficiency of 50% and wide range of temperatures depending on the collector type [32]. They are also able to generate heat during cloudy periods due to the potential to capture diffused irradiance. However, additional components are required to convey the heat to a remote location such as a heat transfer fluid (HTF), fluid pump, piping and heat exchangers [33]. Selection of an HTF depends on different criteria such as the heat capacity, availability, boiling and freezing temperatures and safety. Different fluids can be used such as thermal oils, molten salt, air, water or water-glycol mixture. HTF leaking must be minimised or prevented to reduce maintenance cost and increase safety [34]. The pump requires operational maintenance, an external power source and heat exchangers. All of which increases the complexity and cost of the system. Hence, a machine that is closely attached to the solar thermal collector which can eliminate some or all of the heat conveying components would reduces the complexity created by the pump and plumbing work. The complexity of the thermal collectors increases with the generated temperature (e.g. high temperature collectors > 500° C require a two axis solar tracking system and expensive materials). Thus, most of them are used for domestic water heating where

only low temperature (<80° C) is needed and can be obtained by stationary flat plate collectors.

1.3 Solar Stirling-cycle refrigeration

Solar refrigeration can be classified based on the type of solar collector into PV powered and thermally powered refrigeration. The PV collector generates electricity which is then conveyed to a remote refrigerator to ease transferring the cold to the load and can provide electricity for other applications when cooling is not needed. However, this technology is less attractive than grid-connected VCC due to the high levelised cost of energy (LCOE) corresponding to installation cost, PV cost and PV efficiency in comparison to the grid powered refrigeration [6][37]. Moreover, it requires the conversion of electricity into mechanical energy by an electric motor. AC motors require electronic inverters or power trackers which increase the drive losses, maintenance requirement and cost [38]. Using a DC motor is a simple and highly recommended option. It can be coupled to the PV directly eliminating the need for power tracker or inverter but is still expensive [29]. In a recent study based on the total solar system cost per kW of cold production, Ferreira and Kim [39] showed that the PV driven VCC is the cheapest available solar cooling technology. Many units are commercially available for off-grid cold generation such as Solarchill, Dulas VC65-2 and SunDanzer [13][40]. These are powered by an electric DC motor and use ice storage banks instead of batteries to overcome the intermittent nature of solar energy.

The Stirling-cycle refrigerator is a cooling technology that is simple, has safe and quiet operation, low maintenance requirement, high theoretical efficiency and uses environmentally friendly gases [41][42]. The Stirling refrigerator is already competitive in high-lift refrigeration where it achieves better performance and is cheaper than some cryocooling technologies [41]. The one stage Stirling refrigerator reaches its performance peak for an absolute temperature ratio of around two [43] for which the performance of the VCC deteriorates [44]. Although, the ideal Stirling cycle can achieve Carnot COP the Stirling-cycle refrigerator has not been commercially successful at low lift refrigeration due to the lower cooling capacity [45], complexity

of heat exchangers and working gas pressure. In contrast to VCC refrigerators, only few solar Stirling refrigerators are available for limited applications due to their initial costs [46]. Berchowitz et al. have developed a free piston refrigerator for domestic refrigeration [47] and portable coolers [48][49]. The refrigerator showed a total of 35% of Carnot efficiency. The portable coolers are powered by a PV collector and have a COP of three which is 33% of Carnot COP. Oguz and Ozkadi [50] tested the free piston Stirling refrigerator for domestic refrigeration and showed that the main challenge is due to the complicated heat exchangers. Thus, the Stirling cycle can be an alternative to the VCC if the cost and complexity of the heat exchangers are reduced while maintaining the performance.

Thermal driven refrigeration benefits from the high efficiency of thermal collectors which balance the low efficiency of heat engines. The efficiency of the heat engines is dependent on the solar collector temperature. As the heat engine efficiency is much lower than an electric motor efficiency, it requires the use of high-temperature and efficient solar collectors not only to enhance the solar to mechanical efficiency but also to increase the power density of the heat engine. Kim and Ferreira [32] showed that the thermomechanical driven VCC is more expensive than PV driven VCC using an electric motor due to the cost of solar collectors. Klein and Reindl [29] calculated the maximum solar to mechanical efficiency of a Rankine cycle powered by stationary collectors to about 4.5%. They suggested a high-temperature collector with Rankine-cycle to power the VCC for only large refrigeration systems (e.g. 3.5 MW of cold production) because of the economy of scale of tracking systems. However, cheap energy storage can be included in the hot and cold side of the machine [15]. Thermally driven refrigeration raises the issues of hermetic sealing, mechanical coupling and commercialising the prime mover and solar collector for low power applications [51].

The Stirling engine is particularly interesting due to the simplicity of operation that does not require valves, high theoretical efficiency even at low pressure, use of benign gases and ability to be directly coupled to solar collectors. Hence, requiring no auxiliary components such as heat transfer fluid, controller, fluid pump and auxiliary power supply [52][53]. Heat exchangers, high pressures, high temperatures and solar

collector tracking are responsible for the high cost of dish Stirling machines although they are necessary to improve the power density of Stirling machines [54]. Moreover, coupling and hermetic sealing of both the engine and the compressor is another obstacle. Ferreira and Kim [39] suggested using dish Stirling powered VCC refrigerator with electric coupling for which the power is transferred electrically from the dish focal point to a remotely located machine. They showed it can be cheaper than the absorption refrigerator powered by parabolic trough but not competitive to the PV powered VCC. In this scenario, the engine and refrigerator work on high efficiency and are hermetically sealed. This scenario suggests using a commercial electric generator and motor that each have 90% efficiency which reduces the total efficiency to 81% [51] and increases the cost compared to a system with direct mechanical coupling.

However, different coupling mechanisms between the heat engine and heat pump like direct [55], pneumatic [56][57], hydraulic [58][59][60][61][62] and magnetic [63][64][65][66][67] coupling have been reported with the Stirling engine. All of these coupling mechanisms allow the engine to drive a linear compressor with hermetic sealing but need both machines to be closely coupled. This leads to efficiency improvement (due to the elimination of additional electrical components), hermetic sealing and compact machine design. However, positionally attaching the machine to the dish focal point is technically challenging. The combined machine is heavy and bulky and has high heat rejection due to the refrigerator. The cold transfer from the focal point to the load requires a special engineering solution. However, ThermoLift presented a novel idea to overcome this challenge by installing the machine in the dish base [68]. In their design shown in Figure 1-1, two small mirrors are added in the focal point to reflect the solar irradiance to the dish base where the stationary machine is located. The new design is based on their 3.5-ton gas-fired model that has a calculated COP of 0.8-1.2 for air conditioning and a maximum experimental heating COP of 1.65 at 8^{o}C [69].

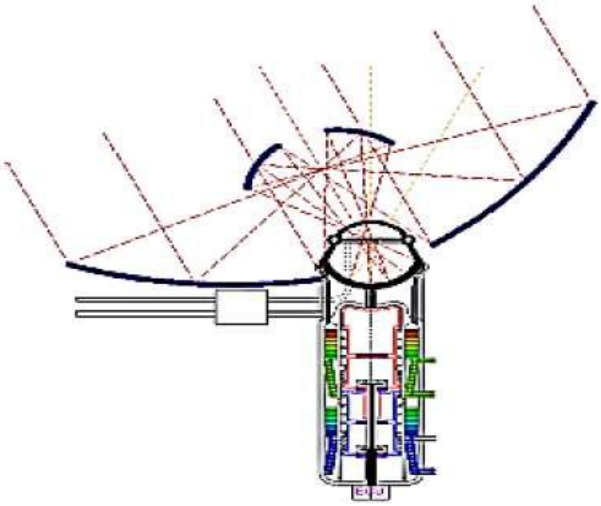

Figure 1-1: Proposed dish power Stirling heat activated heat pump [68].

In this study, line focus collector is adopted as it has the advantage of using a simpler solar tracking system and also permits a Stirling-cycle refrigerator to be directly coupled to the engine. Assuming that the Stirling engine has a practical efficiency of 55% of Carnot efficiency and solar collector efficiency of 50%, the solar to mechanical efficiency of 13% at 300^{o} C and direct coupling is comparable to the dish Stirling engine of 17% at 550^{o} C and having electrical coupling of 80% efficiency. A temperature of 180^{o} is particularly interesting, as it can be achieved using stationary collectors. Thus, cost and simplicity reduction are anticipated but auxiliary parts are needed to transfer the solar heat to the engine.

1.4 Summary

Solar energy coincides with cooling needs and has adequate density to power solar refrigeration. Simple and cheap solar thermal collectors are available with an average efficiency of 50%, but thermal refrigeration requires expensive collectors due to the need for high-temperature that requires a complex solar tracking system.

The PV powered VCC is currently the cheapest technology for near ambient solar refrigeration, especially for domestic applications. Currently, the Stirling cycle cannot compete with the VCC at near ambient refrigeration in terms of cost. However, Stirling-cycle heat activated heat pump has potential for solar near ambient

refrigeration as it is quiet, has the highest theoretical performance which allows for further development, uses natural working fluids such as air and can be hermetically sealed.

The low temperature thermal collector is not suitable for refrigeration due to the low efficiency and large size of the machine used. The dish Stirling engine is expensive and requires complex sun tracking in addition to coupling problems. So far, no Stirling engine has been designed to work directly inside evacuated tube collectors. If such a machine is built the Stirling engine will benefit from a temperature reaching 300^{o} C and deal directly with the absorbed solar irradiance, the number of auxiliary devices will be minimised and coupling the engine to a refrigerator will avoid the size and weight issues of the Stirling-cycle machines.

1.5 Aim of this work

This thesis aims to develop a low-lift solar powered cooling system for household applications. It strives to improve the Stirling-cycle machine thermodynamically and mechanically. Initially, air as working fluid seems to be interesting for its availability and safety. The Stirling-cycle machine will be studied in order to improve its efficiency, power density, simplicity and coupling capability to solar collectors.

The following points are sought in this study

- To mathematically investigate the method of direct cylinder wall heating and cooling without the use of complex heat exchangers or materials of the Stirling-cycle engine and refrigerator.
- To enhance the power density of the directly heated and cooled Stirling-cycle machine by using cylindrical isothermalisers.
- To improve the kinematic drive mechanism. This goal is achieved by applying the free piston technology on the directly heated and cooled Stirling-cycle machine. The capability of the Stirling engine to be self-starting will be investigated. Also, the Stirling cycle machine will be studied to reduce

potential vibrations and to find the optimal phase angle at different operating points.

- To investigate the performance of the solar refrigeration system, with directly heated and cooled Stirling engine working cylinders inside the evacuated tube collectors, for different load temperatures, solar irradiances and engine parameters.

1.6 Contribution to knowledge

This work focuses in the design of the Stirling-cycle machine based on novel ideas. The Stirling-cycle machine is studied and designed based on improved thermodynamic and mechanical characteristics. Thus, the following contribution to knowledge can be found in the thesis:

- **Use of direct cylinder-wall heating and cooling method combined with increased stroke to bore ratio and eliminated axial heat flow of double acting Stirling-cycle machine**. The new Stirling-cycle machine uses piston cylinder heating and cooling and does not require additional heat exchangers. The engine has long stroke to bore ratio and hence, the cylinders are longer than the cylinders of conventional machines. Also, all the cylinder area participates in heat exchanging whereas in conventional machines, displacers and pistons shade some of the heat exchanging area.
- **Simplified model with a definition of the regenerator end temperatures**. The mathematical model that describes the polytropic Stirling engine cycle was derived using energy and mass balance equations and the three-control volume approach. The regenerator end temperatures are redefined based on the polytropic cycle taking into consideration the working gas temperatures instead of the fixed heat source temperatures.
- **Performance of the cylinder wall heated and cooled machine.** The novel engine design is investigated mathematically for different machine variables such as the piston diameter, phase angle, engine speed, charge gas pressure and dead volume. The machine is studied without considering the mechanical and

gas friction losses in order to understand the response and investigate the capabilities of the ideal machine.

- **Improvement of the machine power capability and reduction of the gas flow rate.** The effect of a novel isothermaliser on the performance of the cylinder wall heated and cooled machine is investigated for power density improvement and gas flow reduction. The isothermaliser is an extended cylindrical surface attached to the machine piston cylinder for which the heat transfer path is annular and has constant hydraulic diameter along the cylinders.
- **Selection of the best mechanical arrangement of the novel engine cylinders.** Based on regenerator connection, mechanical vibration, power pulses and start-up capability, the novel multi-cylinder engine is optimised for the best phase angles and mechanical arrangements. For which, the engine has reduced linear vibration as well as reduced power pulses without using a flywheel.
- **Balanced compounding of the novel engine.** The balanced compounding mechanism is investigated for the novel machine so that it provides short regenerator connections. A more confined range of phase angles was found for this driving mechanism. The machine with this driving mechanism is investigated for the start-up capability. Switching the position of cold cylinders with hot cylinders in the heat activated heat pump is studied for its effect on force balancing and piston side forces hence the accompanied mechanical friction. The effect of changing different engine parameters such as the moving mass, piston diameter cylinder length, source temperature, dead volume and engine loading condition is investigated.
- **Solar coupling and total solar system performance.** Assessment of the direct thermal coupling of the machine to solar collectors is provided with a novel coupling mechanism.

It is expected that this machine design will be of interest to engineers and scientists working in the fields of thermodynamics, external combustion machines and refrigeration.

1.7 Thesis structure

This chapter introduces the importance of solar cooling, the relation between cooling demand and sun availability, a review of solar Stirling-cycle refrigeration and summarises the aims of this research.

Chapter 2 provides a literature review on the Stirling cycle and focusses on the Franchot machine, heat exchanger problem, phase angle effect, multi-cylinder configuration and free piston driving mechanism.

Chapter 3 presents a novel and simple cylinder wall heated and cooled Stirling machine and comprehensive performance evaluation of this machine with respect to the phase angle, engine speed, charge density, piston diameter and dead volume. The performance evaluation is performed with a specially developed polytropic, second-order mathematical model for both the engine and refrigerator.

Chapter 4 strives to improve the power density of the Stirling cycle by developing special isothermalisers for this purpose. In addition, a comparison of the potential improvements with the conventional Stirling cycle is given.

Chapter 5 investigates the effect of cylinder arrangement and increasing the number of cylinders on the engine vibrations and start-up capability.

Chapter 6 investigates the characteristics of a new driving mechanism based on the balanced compounding mechanism, for which neither rotational parts, start-up mechanisms nor complex engine to heat pump couplings are needed.

Chapter 7 provides a comprehensive evaluation of the solar-powered cooler including some of the potential losses of the Stirling-cycle machine. The performance of an optimised solar system and a sensitivity study are provided and discussed.

Chapter 8 gives a general summary of the thesis, highlights the main findings and gives potential improvements and future recommendations.

CHAPTER

2 Literature review

In this chapter, a more in detail look into the Stirling-cycle machines is provided. The literature review of the Stirling machine defines the problem areas concentrating on the Franchot Stirling machine. The heat transfer problem and cranking mechanisms are reviewed for the Franchot machines.

2.1 Introduction

The Stirling engine shown in Figure 2-1 is an external combustion engine that was patented by Robert Stirling in 1816 [70]. Robert Stirling wanted to find a safer alternative to dangerous steam engines by inventing an air engine. The steam engines existing at that time were causing severe casualties to the workers when the steam boilers exploded. The Stirling engine era was ended due to advances in the steam, internal combustion and electric motors. The Stirling engines of the 19^{th} century were characterised by having low power density, non-advanced materials and air as working fluid. In the 1930s the Stirling engine started to gain more interest. Different working gases and new materials (i.e. stainless steel) and cranking mechanism (i.e. rhombic drive) were used. The peak development was achieved by Philips when they made portable electricity generators in the late 1940s for small radios. Unfortunately, the product has never been commercialised and only several hundred were distributed to universities all over the world [71]. The engines at this phase of development had higher power density, efficiency, pressure and temperature compared to the early engines. Currently, the most advanced Stirling engine is power dense and efficient, uses advanced materials and uses advanced cranking mechanisms like the free piston and swash plate for multi-cylinder configurations [52].

Figure 2-1: Stirling engine at the National Museum of Scotland [72].

2.2 Stirling engine

Heating and cooling the gas inside a closed compartment generates pressure variations. However, no mechanical energy will be generated, as the volume is constant. Adding a piston to such a system enables variations in the volume hence converts the pressure variations into mechanical energy and thus a heat engine is created. Due to the heat capacity of the piston housing material and working gas, the continuous heating and cooling of these elements will cause energy loss. The ingenious Robert Stirling patented the Stirling engine with distinct heat accepting and rejecting spaces. Thus, the engine has fixed material temperature and the heat loss due to heating and cooling the same material is avoided.

Due to the reciprocating nature of the pistons, the working gas shuttles back and forth between the hot and cold spaces. This, in turn, creates thermal loss in the gas stream. Robert Stirling realised this problem and patented a temporary heat storage element called economiser, which is now known as the regenerator. The regenerator works as thermal sponge, which absorbs the heat from the hot gas stream and reemits it back at gas counterflow. One might wonder about the importance of putting such an obstacle into the working gas passage given that the Stirling engine is capable to work without a regenerator [73]. With the absence of the regenerator, five times more heat is needed [74]. Thus, besides its role as a temporary thermal storage element to increase the efficiency, the regenerator reduces the thermal loads on the heat exchangers and separates the hot and cold sides of the engine.

Figure 2-2 shows the thermodynamic cycle of a Stirling engine having two opposite pistons. The expansion piston always leads the compression piston by an arbitrary phase angle. The ideal Stirling cycle comprises two isothermal and two isochoric processes as follows:

- 1-2 Isothermal compression: the engine requires some work in order to compress the working fluid. The expansion piston remains stationary close to the regenerator and the compression piston moves to the left. The isothermal compression keeps the working gas temperature constant and the heat is rejected at the cold side of the engine.
- 2-3 Isochoric heating: the gas flows from the compression to the expansion space. It passes through the regenerator absorbing heat from it. The expansion and compression pistons move in the same direction keeping the total volume of the engine constant. In this process, no work is required or generated since there is no change in the total engine volume.
- 3-4 Isothermal expansion: the engine generates positive work and absorbs energy from the hot reservoir. The isothermal expansion implies that the hot side gas temperature remains constant.
- 4-1 Isochoric cooling: the gas flows from the expansion to the compression space through the regenerator. It stores the heat in the regenerator that is

equivalent to the energy absorbed in process 2-3. In this process, no mechanical work is required or generated since there is no change in the total engine volume.

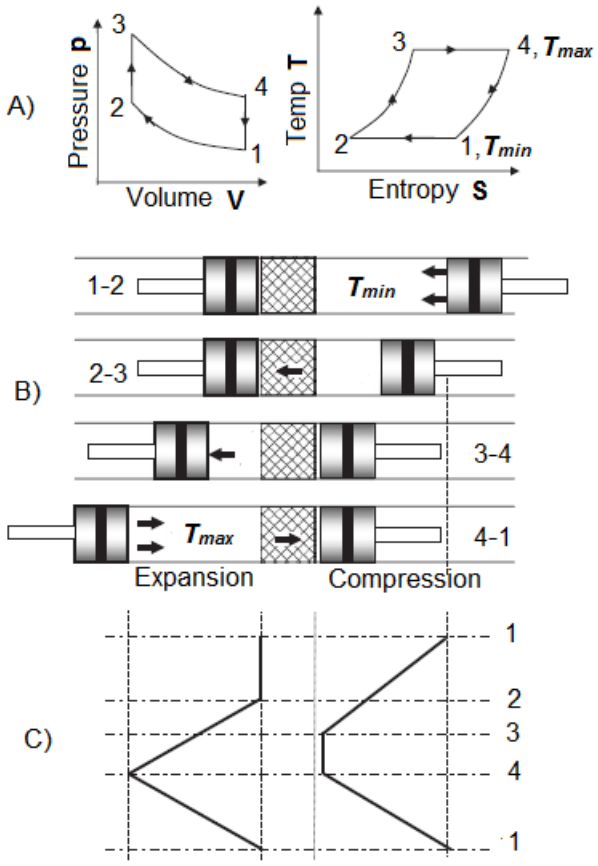

Figure 2-2: Thermodynamic processes in the ideal Stirling-cycle engine A) PV and TS diagram B) piston arrangement and C) time displacement diagram [70].

Amazingly, the Stirling engine was patented 40 years before the birth of modern thermodynamics. It was believed that the Stirling engine can work on efficiencies of more than 100% and that a perpetual motion machine is possible [75]. At that time, it was thought that an undestroyed magic fluid called "Calorie" shuttles between the hot and cold chambers. In 1855, John Ericsson, one of the famous inventors of heat engines attempted to violate the first law of thermodynamics [75]. He said 'we will show practically that bundles of wire are capable of exerting more force than shiploads of coal' [76]. A claim that he was never able to prove. Before that, in 1843, Joule proved that mechanical energy could be transformed into heat. This experiment was the foundation for the first law of thermodynamics in which the generated work cannot

exceed 100% of the input energy. This implies that perpetual machines can never be built. In 1824 and before formulating the second law of thermodynamics and even before Joules' experiment, Sadi Carnot defined the maximum efficiency of any reversible heat engine. The Carnot efficiency set another limit below the 100% depending on the working temperatures. The Schmidt analysis of the Stirling engines that assumes isothermal processes and sinusoidal variation of swept volumes shows that Stirling engines are theoretically capable of achieving the Carnot efficiency which is given in Equation 2.1 [77]

$$\zeta_c = 1 - \frac{T_k}{T_h} \qquad 2.1$$

where T_k and T_h are the cold and hot engine compartment temperatures, respectively.

However, in order for an ideal machine to achieve the Carnot limit, the gas in both the expansion and compression spaces must be kept at the source temperatures. Hence, the heat transfer rate must be infinite to support this claim. In reality, neither the cylinder walls nor the heat exchangers have unlimited heat transfer [70]. There must be a temperature difference between the heat exchanger walls and working gas for the heat transfer to take place [78]. This difference in temperature makes the Carnot efficiency unachievable, as the hot gas temperature is lower than the hot heat exchanger temperature and the cold gas temperature is higher than the corresponding heat exchanger temperature. At the heat transfer, the temperature difference between the walls and working gas is maximum and the gas temperature in the hot space is equal to that in the cold space. On the contrary, the Carnot efficiency based on the working gas temperatures will be zero and no work will be generated. If the bulk gas temperatures are equal to the corresponding cylinder temperatures then no heat will be exchanged. Hence, no power will be generated although the efficiency is maximised. Therefore, there exists a temperature difference for maximizing the power but at an efficiency smaller than the Carnot efficiency. This is called the maximum power point.

In 1975 Curzon and Ahlborn [79] obtained the efficiency limit for any heat engine operating at the maximum power point given by Equation 2.2. They assumed isothermal expansion and compression using the finite time thermodynamics in which the heat transfer is finite. Although, the efficiency is known by "Curzon and Ahlborn efficiency" it was obtained by many researchers and it can be traced back to 1929 [80].

$$\zeta_{CA} = 1 - \frac{\sqrt{T_k}}{\sqrt{T_h}} \qquad 2.2$$

Wu [81] applied the finite time thermodynamics to Carnot engines with finite heat capacity of external reservoirs. He obtained exactly the same maximum power point equation. Kaushik and Kumar [82] and Blank et al. [83] showed numerically that the Stirling engines have an efficiency at the maximum power point equal to the efficiency obtained by Curzon and Ahlborn with ideal regeneration. Others [84][85][86][87][88][89][78][90] optimised the response of the heat engine considering heat leakage, internal irreversibility and external irreversibility on Carnot heat engines. They found that the maximum power efficiency is smaller than the Curzon and Ahlborn efficiency if more irreversibilities are considered. The Curzon and Ahlborn efficiency provides a practical limit of the Stirling engine efficiency. This efficiency relative to Carnot efficiency is larger than 50% for $T_k < T_h$. It approaches 100% as the temperature ratio $\frac{T_k}{T_h}$ approaches zero. By dividing the Curzon and Ahlborn efficiency by the Carnot efficiency, the relative efficiency can be written as

$$\zeta_{relative} = \frac{1}{1 + \sqrt{\frac{T_k}{T_h}}} \qquad 2.3$$

2.3 Reversed Stirling cycle

Thermodynamically, the heat flows naturally from hot to cold bodies. Thus, heating can be naturally obtained by only using heat exchangers connected between higher and lower temperature reservoirs. Heating can be easily provided by a solar thermal collector, burning wood or an electric heater. On the other hand, refrigeration which is the process of bringing a space temperature below ambient is harder. It requires pumping the heat from a low temperature reservoir to a higher temperature one which does not happen naturally. The second law of thermodynamics implies that external work should be added to the system in ordered for refrigeration to take place. Thus, generating cold needs heat pumping technologies. The Stirling cycle is reversible and thus can generate a temperature difference by applying mechanical work. If the hot side is cooled to the ambient temperature, then the cold side will be below the ambient and hence a Stirling-cycle refrigerator is created. The Stirling-cycle refrigeration concept was first imagined in 1834 by John Herschel and the first machine was built by Alexander Kirk in 1860 [44][91]. The ideal reversed Stirling cycle has four thermodynamic processes. Two isothermal and two isochoric processes explained by the opposite piston configuration (shown in Figure 2-2) as follows:

- 1-2 Isothermal compression: the compression piston retracts, keeping the expansion piston near the regenerator. Work is being added to the system and energy is removed at higher temperature side.
- 2-3 Isochoric cooling: the compression and expansion pistons move together making a constant volume. The gas moves from the compression side to the expansion side through the regenerator. The gas delivers energy to the regenerator and cools down. In this process, no work is required or generated since there is no change in the total engine volume.
- 3-4 Isothermal expansion: the expansion piston moves causing the gas to expand and decrease its pressure. The compression piston stays still and external heat is absorbed by the low-temperature side causing the refrigeration to take place.

- 4-1 Isochoric heating: the compression and expansion pistons move together. The gas flows from the expansion to the compression space through the regenerator absorbing the same energy, which was stored previously in process 2-3. In this process, no work is required or generated since there is no change in the total engine volume.

These processes are represented in the P-V diagram as shown in Figure 2-3.

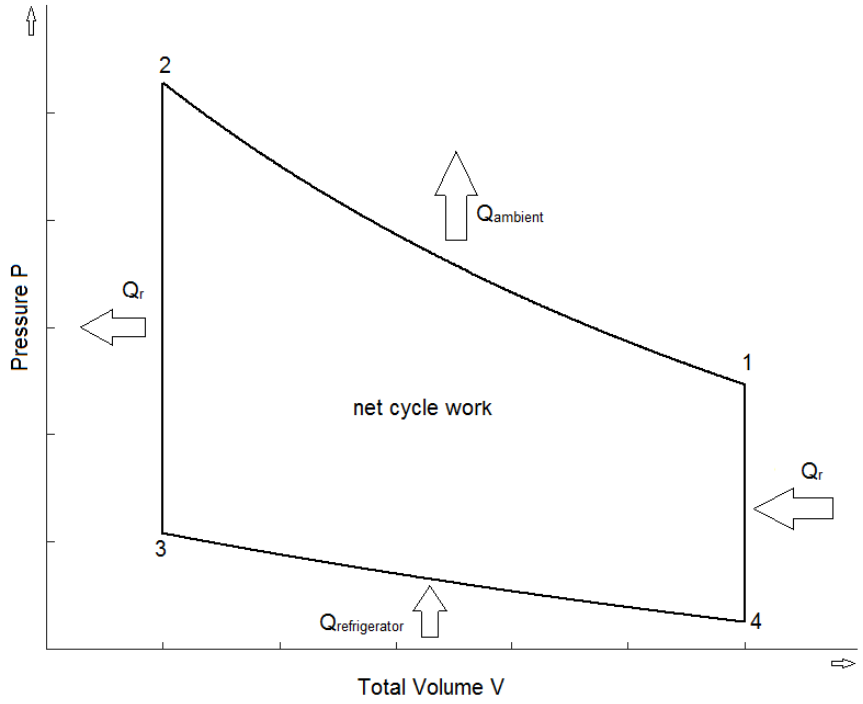

Figure 2-3: PV diagram of the ideal reversed Stirling cycle.

The efficiency of the refrigeration cycle is measured by the coefficient of performance (COP). The COP is analogous to the efficiency of a heat engine with the difference that the COP can be larger than one. The cooling COP is calculated by dividing the cold energy produced by the supplied mechanical energy. The ideal COP of a Stirling-cycle refrigerator, that works between low temperature T_l and warm temperature T_k, is given from the reversed Carnot cycle by Equation 2.4

$$COP = \frac{T_l}{T_k - T_l} \qquad 2.4$$

Leff and Teeters [92] reported that the assumptions made by Curzon and Ahlborn cannot be applied to heat pumps. They showed that there is no maximum due to the monotonic response of the cooling power to the COP. Thus, they concluded that Carnot efficiency could be ideally approached when the cooling power is zero and the COP approaches zero for the highest cooling rate. They attributed the monotonic response of the heat pumps to possible unbounded working gas temperatures. In contrast, the heat engine works between two temperature limits (heater and cooler temperatures). Continued heat rejection and absorption are attained as the gas temperature keeps increasing in the warm reservoir and decreasing in the cold reservoir, respectively. The maximum cooling power occurs when the gas temperature in the expansion cylinder approaches absolute zero or the compression temperature is extremely high hence, the COP is zero. The maximum COP occurs when both temperatures are equal to each other for which the cooling power is zero.

Blanchard [93] reported that there is no natural maximum COP for heat pumps. Instead, he searched for the minimum input power for a given heating power. He obtained an equation based on the finite time thermodynamics for the optimal COP, which depends on the temperature of the reservoirs, cold and hot heat transfer ratios and the temperature difference between the working gas and hot reservoir. Wu [94] studied the endo-reversible Stirling refrigerator numerically for the maximum specific cooling load. He found that the specific cooling load could be maximised but it drops to zero when the COP equals Carnot COP, where the total conducting area is finite. Chen [95] numerically studied the Stirling refrigerator with irreversibilities by the finite time thermodynamics. He found that the cooling power increases monotonically with input power and the COP decreases with increasing cooling power if the regenerator is ideal. Hence, due to the limited heat transfer, there is no maximum input power or cooling power and the maximum COP approaches Carnot COP. In practice, losses act against cooling power. For example, Chen [95] derived an equation for the

maximum cooling power and its corresponding efficiency considering the regenerator losses and assuming two isothermal and two isochoric processes. He also obtained the maximum heating rate and its corresponding efficiency of the endo-reversible heat pumps. Others [88][96][97][98][99][100][101] studied the effect of the finite thermal conductance, internal irreversibility and heat leakage between the reservoirs on the cooling power and COP and concluded that a cooling power maximum can be found.

2.4 Heat activated heat pump

The heat-activated heat pump resembles a heat engine driving a refrigerator, which has thermal efficiency as a combination of the engine and refrigerator efficiencies as given by Equation 2.5.

$$COP_{total} = \frac{T_l(T_h - T_k)}{T_h(T_k - T_l)} \qquad 2.5$$

This machine is implemented as one Stirling machine in a back-to-back arrangement and called duplex machine as shown in Figure 2-4. This configuration is characterised by two distinct cold spaces. Usually, a double acting power piston is used to couple both of the machines mechanically. The PV diagram of this machine can be separately obtained for the prime mover and refrigerator [102]. Duplex Stirling-machine uses the free piston drive where no kinematic drive is required. The duplex machine is efficient, reliable and compact, can generate power in addition to cold and has low operating cost and long life [103][104].

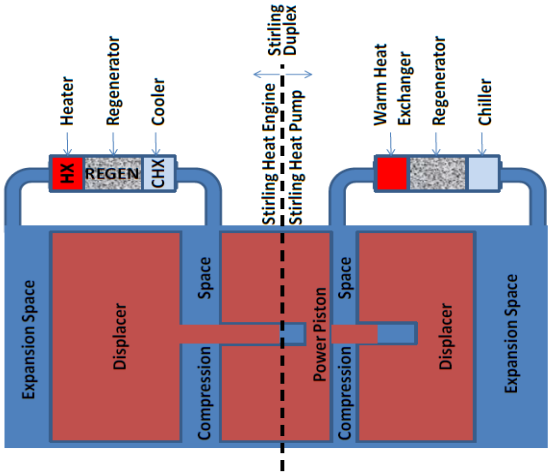

Figure 2-4: Duplex Stirling machine with a common power piston [105].

In the Vuilleumier cycle which was patented in 1918 [106], only two reciprocating displacers are needed which form three working spaces. In contrast to the duplex machine, which has two cold spaces and two gas circuits, the Vuilleumier cycle has only one cold space and has all compartments connected pneumatically. The pressure wave generated by the hot displacer motion is transferred directly into the cold space by shuttling the other displacer between the cold space and chilled reservoir with a phase shift between the displacers. Hence, instead of transferring the energy mechanically, it is transferred pneumatically. Synchronising the displacers' motion can be obtained by either mechanical or magnetic cranking mechanisms. No work is generated or required because the total volume is constant. In reality, the machine requires some work to run due to the friction. Otherwise, it will fail to start-up [103]. Moreover, Vuilleumier machine is larger, heavier and less efficient than the duplex Stirling machine [107][108]. That's due to the small pressure variation which is caused by the small volumetric compression [109].

2.5 Single acting Stirling engine

In the single acting Stirling machines, the working gas is in contact with only one face of the power piston. Three classical single acting Stirling machines have been found in the literature: alpha, beta and gamma. These machines are classified based on cylinder coupling as shown in Figure 2-5 [53][70][110].

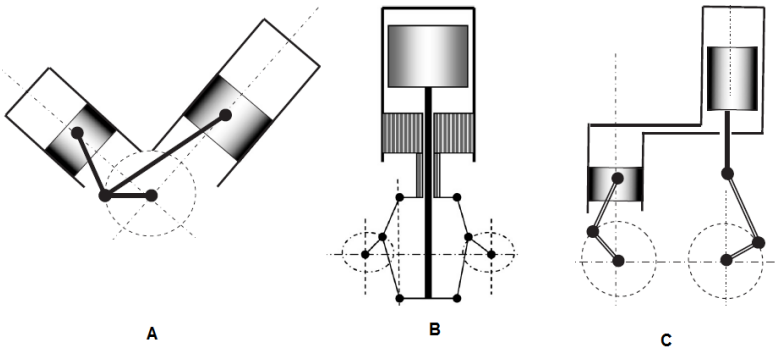

Figure 2-5: Classical Stirling machine arrangements: A) alpha type B) beta type and C) gamma type [111].

The alpha type is the simplest and easiest Stirling machine to construct. In the alpha type machine, the expansion and compression piston are in separate cylinders. Each piston is sealed to keep the working fluid inside the engine [53]. The phase angle between the hot and cold space in the alpha type engine is fixed by the mechanical drive. Alpha type coupling uses simple cranking mechanisms like the slider-crank, Ross-Yoke and Rocker-V. In addition, these mechanisms can convert the linear reciprocating motion into a rotary motion. A disadvantage of this arrangement is the need for temperature resistant seals in the hot cylinder, whilst the compression cylinder seal is continuously cooled as it is in touch with the cold cylinder [112].

In the beta type machine, a displacer and power piston are compactly deployed in one cylinder [112]. To reduce sealing problems, the power piston in this configuration is located in the cold space of the engine and the displacer seal is located on the side closest to the cold space. the displacer role is to shuttle the working gas between the hot and cold chamber and does not participate in power generation or consumption [112]. This requires only the power piston to be completely sealed in order to contain the working gas and to transform the pneumatic power into mechanical power. A displacer needs to be a good thermal insulator. Piston coupling is complicated due to the tandem motion of pistons which requires complex kinematics like the rhombic drive mechanism [53]. The rhombic drive is dynamically balanced and it generates low side loads. On the other hand, it is complex, requires two gears, has large bearing surfaces and many moving parts [52].

In the gamma type machines, the displacer still exists and the power piston is moved to a distinct cylinder via a connecting tube. However, it has smaller power density in contrast to the beta type due to the dead space on the cold side. The two-cylinder configuration makes it possible to use simpler cranking mechanisms similar to the alpha type. The gamma type with the slider-crank mechanism is the most commonly used type [53].

The Stirling engine is a heat engine that has its efficiency and power density increase with increasing driving temperatures. Thus, the Stirling engine can be subcategorised based on the driving temperatures into low-temperature difference (LTD), moderate temperature difference (MTD) and high-temperature difference (HTD) Stirling engines. The LTD engines are those capable to work at temperature levels obtained by flat plate solar collectors (up to 120^{o} C). MTDs work on temperatures generated by line solar concentrators (up to 300^{o} C) and HTDs have their temperature level achievable by point solar concentrators.

LTDs usually work on air, use simple materials and driving mechanism and have low efficiency and power density [113][114]. They are used for low power applications such as in toys, water pumping, fanning, microchip cooling, and demonstration. The HTDs are characterised by using light gases like helium and hydrogen, high pressures and temperatures, high power density and high efficiency [37]. They are suitable for solar electricity generation using parabolic dish concentrator where high temperature is generated. The engine can be added to the focal point due to its small weight and size. The dish Stirling engine broke the records by achieving a solar to electricity efficiency of three times the efficiency of PV panels [115][116]. So far the HTD Stirling engine has not been commercialised for household applications due to a number of remaining challenges such as, working gas leakage, use of sophisticated materials and technologies, solar thermal collectors and total system cost in particular due to the heat exchangers and cranking mechanism [33][117][118][119]. The MTD Stirling engine has a performance between the LTD and HTD and uses less sophisticated materials than the HTD. However, it is not simple to manufacture, uses light gas for improved performance and suffers from gas leakage and complicated heat

exchangers. Auxiliary devices might be needed to transfer the heat from the solar collector to the solar powered MHD engine which adds to the problems and cost. The Stirling engine that can be powered by a line concentrator has not been commercialised for household applications. Trolove and Raine [120][121] performed an experimental work on a novel design in which a Stirling engine is thermally coupled to a parabolic trough by horizontal heat pipes. While direct coupling is the only advantage, heat pipes which are auxiliary devises are still needed, have limited working temperatures and heat transfer rates. In addition, the engine is still having the heat exchanger problems and only two heat pipes are used per engine because the engine is positioned between two collectors.

2.6 Double acting Stirling engine

Double acting engines in which the working gas is in contact with both sides of the pistons were developed by Babcock in 1885 [70]. Figure 2-6 shows the Siemens and Franchot engines in which each expansion compartment is connected to a compression compartment through heat exchangers, namely: heater, regenerator and cooler. These engines have many features which make them preferable over single acting engines [122]: half the number of reciprocating parts, which results in simpler kinematics [123], absence of the displacer, elimination of the pressurised crankcase due to the smaller gas leakage on the piston rods, compactness and higher power density.

The Siemens (also known as Rinia) engine which is shown in Figure 2-6A is ascribed to Sir William Siemens in 1863 [124]. Each cylinder has an expansion (hot) and compression (cold) space separated by the power piston. Similar to the alpha engine each hot space is connected to a cold one in another cylinder via a regenerator. Hence, the Siemens arrangement is still prone to shuttle and heat conduction losses and is difficult to build due to the regenerator connections [52]. The Siemens engine was brought to practice when the swash plate and wobble yoke were commercialised [124][76][125]. The wobble yoke has been commercialised for four cylinders [126].

The Franchot engine which is shown in Figure 2-6B was invented in the 19th century by Charles Louis Franchot [127]. In the Franchot engine, only two pistons are required, the phase angle can be freely controlled and each cylinder is either hot or cold which eliminates the shuttle and axial conduction losses within each cylinder [128]. A different type of this engine is reported by Raballand [129] where flapping plates replace the linear reciprocating pistons.

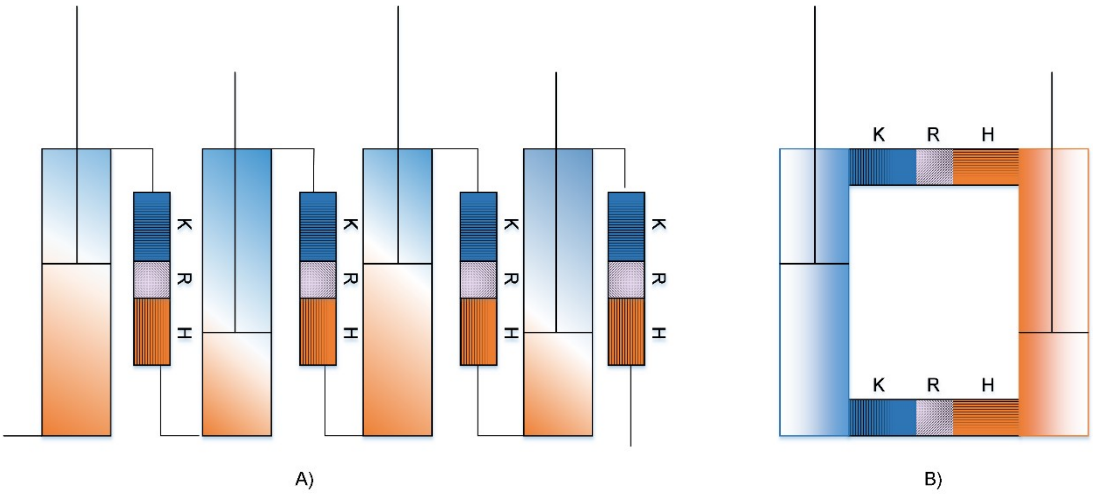

Figure 2-6: Double acting Stirling engines. A) Siemens engine and B) Franchot engine. The work volumes are connected to each other through the cooler (K), regenerator (R) and heater (H).

The Franchot engine has received only limited attention due to sealing problems as the expansion piston and piston rod are in the hot cylinder. Some studies [8][12] reported that keeping the seal at an acceptable temperature level in the hot cylinder is less severe for low temperature engines and can be overcome by using a clearance seal. Bartolini et al. [131][132][133][134] reported using a clearance seal to eliminate the wear and lubrication problem hence reduces the piston friction losses and increases the reliability of the engine. They suggested a dynamic labyrinth seal, which has a tortuous clearance to only allow low gas leakage. In their engine known as Franchot-Bartolini configuration, there are upper and lower Stirling engines in a Franchot configuration while heat exchangers are only added to the upper Stirling engine. The gas leakage and heat conduction from the upper to lower engine give the power to the lower engine. The labyrinth seal is installed to the lower side of the Franchot-Bartolini engine which has lower temperatures. Hirata [135] recommended using a sliding ceramic type piston in the hot chamber of 327° C. Furthermore, low friction PTFE seals can be used at

temperatures up to 300° C [118]. Graphite seals can be used at even higher temperatures but are limited to about 400° C with air to prevent oxidation [136][137]. Thus, the Franchot engine can be a good alternative at low temperatures where the sealing problem is less severe.

The first application of the Franchot machine was in domestic refrigeration in 1957 built by Finkelstein [76]. The vapour compression refrigerator was superior to the Franchot type refrigerator for normal domestic refrigeration temperatures although the COP was in favour of the Franchot machine at -20° C. The research on the domestic Franchot refrigerator was discontinued due to limited financial support and machine optimising efforts. In cryogenic refrigeration, the double-acting Stirling cycle refrigerator is not used due to the need for only low cooling capacities and hence a single acting refrigerator is sufficient [124]. Recently, Single-Phase Power manufactured a helium-charged Franchot-cycle heat pump, SPP 4-106, to produce high-lift temperature up to 200° C for industry (see Figure 2-7). The SPP 4-106 can also accept waste heat temperatures up to 250° C to work as a prime mover [130][138].

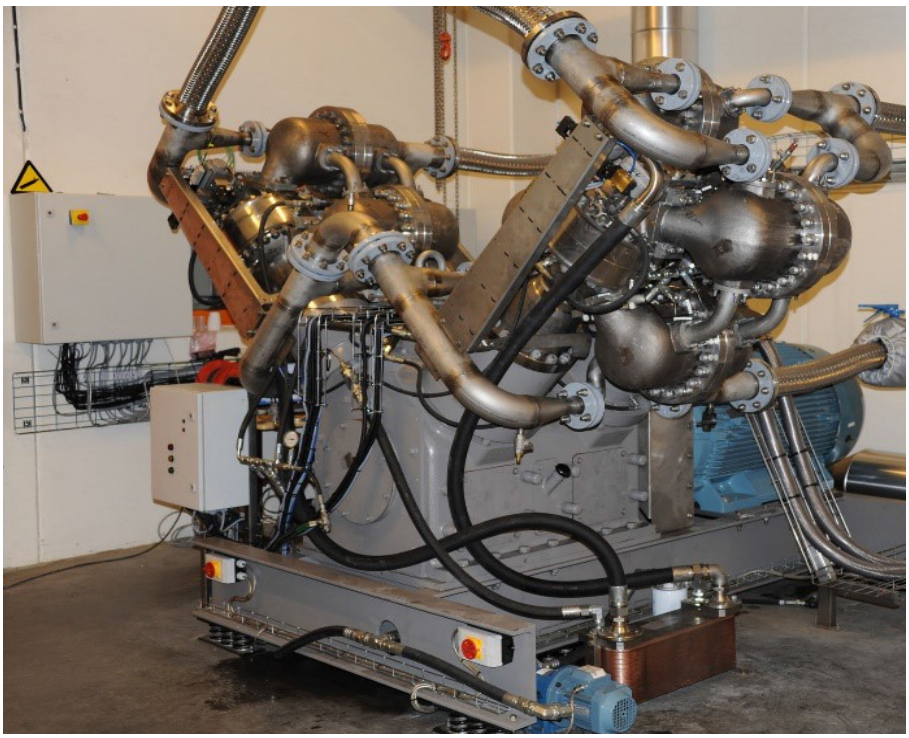

Figure 2-7: Installation of the SPP 4-106 at the dairy plant Tine Frya [138].

2.7 Phase angle

The phase angle is the thermodynamic shift between the leading expansion and lagging compression processes in the Stirling cycle machines. In alpha type engines, the phase angle of 90° can achieve the maximum power but requires efficient heat exchangers to support the power generated [43][139][140][141]. However, many researchers [142][143][144] showed that it is important to use larger than 90° phase angles to achieve the optimal performance of the Stirling engine. Hoegel [122] showed that the Siemens engine is superior to the Franchot engine at the same operational conditions, i.e. temperatures, charge density and phase angle. This is mainly due to the gas leakage through the power pistons, which is caused by a higher-pressure difference in the Franchot engine at a 90° phase angle. He showed that the 30% difference in the pressure amplitude at 90° phase angle was responsible for increasing the losses from 0.1% (in the Siemens engine) to 3.9% (in the Franchot engine). However, the pressure difference can be reduced by increasing the phase angle in the Franchot engine. Høeg et al. [130] showed that the Franchot engine in the SPP 4-106 heat pump is chosen for the ability to use phase angles other than 90°, especially with low-temperature sources. Martaj and Rochelle [145] studied the Franchot engine with a common recuperator-regenerator, which has limited heat transfer, and showed that an increase in efficiency of 18% was obtained for a phase angle of 120° in comparison to 110°. Hoegel [122] showed that the maximum power occurs around 150° and 160° for hydrogen and helium charged engines, respectively. For nitrogen, the engine gave negative power at 150° thus, increasing the heat transfer rate in the heat exchangers was essential to achieve positive power. This shows that the optimal performance critically depends on the heat transfer rate which is directly related to the thermal conductivity of the working gas. Minasian's [146] studied the 3-cylinder Siemens engine mathematically and showed that increasing the phase angle from 60° to 120° will reduce the hysteresis and viscous losses from 19.5W to 1.1W for an indicated power of 38.1W. Moreover, it leads to a reduction in the natural frequency of the free piston engine from 30 Hz to 19.4 Hz, which further reduces the losses to 0.9W. Carlsen et al. [147][148] reported that 120° is a common phase angle for Stirling engines and that 145° is proposed to compromise between the cooling power and efficiency of heat pumps. Li and Grosu

[149] theoretically studied a Stirling refrigerator and found that maximum cooling power and COP occur at 90°, however, they assumed isothermal expansion and compression processes of the Stirling refrigerator. Bauwens [43] and Tekin and Ataer [150] found that the maximum specific refrigeration occurs near 90° and the COP increases with increasing phase angle for both ideal and non-ideal heat exchangers. Thus, it can be concluded that increasing the phase angle from 90° to 180° will result in an efficiency increase and power density decrease for both the heat engine and heat pump and that there is no optimal working phase angle. However, the Stirling machines are commonly designed close to 90° phase angle to increase the power density and reduce the cost of these machines if good heat exchangers are used.

2.8 Cylinder configuration

It has been reported that at least three cylinders are needed to build a working model of the double acting engine [52][70][151][152]. However, this is only true for the Siemens configuration whilst the Franchot engine runs with only two cylinders. The number of cylinders affects the phase angle and phase shift of the Siemens engine. For each cylinder thermodynamically connected to an adjacent cylinder, the phase angle can be written as a function of the number of cylinders N as $\theta = 180 - \frac{360}{N}$ for $N > 2$ [122]. The phase shift which determines the sequence of the reciprocating pistons is given by $\theta_s = \frac{360}{N}$ [153]. This phase shift gives a full cycle, which leads to a consistent phase angle between all hot and cold volumes, hence the force and power of the engine will be uniformly distributed and all engines will be symmetric. The Siemens configuration produces consistent power through a cycle and can self-start. For any Stirling machine, the preferred phase angle is within the range 90°-140° [154]. For this range to be achieved, the four-cylinder Siemens configuration which has 90° phase angle is needed. For the three-cylinder engine, a phase angle of 60° is obtained although it has a phase shift of 120°. The small phase angle engine has high fractional volumetric variation hence contributes in increasing the hysteresis losses [146]. On the other hand, the Franchot engine, which has only one hot and one cold cylinder, has an arbitrary phase angle undefined by the number of cylinders.

It has not been reported that the Franchot engine can self-start. The self-starting capability weighs heavily in favour of the Siemens configuration over the Franchot engine [124]. However, several researchers reported that a dual Franchot engine could self-start if they are phase shifted by 90°, which is equivalent to the four-cylinder Siemens configuration in terms of number of cylinders, phase shift and phase angles. Arthur and Varela [155] patented a dual Franchot engine for a hybrid automotive. They suggested using a dual Franchot engine working in its highest efficiency to drive a linear alternator to generate electricity. They suggested a synchronising crank to keep the phase shift and phase angle at a predefined value of 90° and to keep the stroke for the dual Franchot engine unchanged. The SPP 4-106 [130] uses the dual Franchot engine concept with the slider-crank drive to fix the phase shift at 90° but works on larger than 90° phase angles. The 90° phase shift gives the smoothest torque curve and causes the engine to self-start. Fette [156] manufactured a self-starting dual Franchot engine that uses liquid pistons. All liquid pistons were phase shifted by 90° and the phase angle was kept at 90° using additional solid pistons. The dual Franchot engine is still having the phase angle independent from the phase shift as a compression and expansion volume never share the same piston or cylinder. Thus, it has the advantage to work on any phase angle to achieve the best thermodynamic performance while working at fixed phase shift of 90° to achieve the best mechanical performance.

Kinematic Stirling engines use kinematic drives such as the slider crank mechanism to convert the reciprocating into rotational motion and fix the relation between different engine parameters, such as the phase angle, phase shift and stroke length. However, kinematic Stirling engines are not cost effective in comparison to Stirling engines with free piston technology [157][151]. Double acting and single acting Stirling engines can use the simple slider-crank drive [158][52] but at the cost of vibration. The Franchot and dual Franchot engines have an uneven distribution of masses and cranks, which creates dynamic imbalances. These imbalances cause first order vibrations. For example, reciprocal vibrations and rocking couples are found in single acting Stirling engines due to the phase angle while rocking couples are found in the Siemens configuration because of the absence of piston pairs. Walker [127] suggested using the wobble drive with the Franchot engine for railway applications. The Stiller-Smith

mechanism is also reported to be used with the dual Franchot engine with a phase shift of 90° due to the uneven distribution of pistons [122]. The Stiller-Smith mechanism has a cross slider link for which its centre travels in a circular path and hence piston motions are perfectly sinusoidal [159]. Furthermore, Stirling engine vibrations can be reduced by dynamic balancing which adds counterbalancing weights [160]. Vibrations can also be reduced by inherent balancing, in which many cylinders participate in generating opposite vibrations that cancel each other out [161]. Inherent balance is applied successfully to internal combustion engines for which rocking couples, reciprocal vibrations and torque pulsations are reduced. A rotating shaft is dynamically balanced if it is statically balanced and the resulting turning moment about the axis of rotation is zero. This can be obtained if there is a uniform distribution of moving masses on the crankshaft. To remove the rocking couples in the inline topology, the summation of the primary forces and the algebraic sum of the couples at any point in the plane of cylinders should be zero. The rocking couples can be removed if there are piston pairs moving together. However, this is not possible in the Siemens engine.

The free piston Stirling engine (FPSE) was introduced by Beale in 1969 and patented in 1972 for single acting engines. It has the crankshaft replaced by gas or mechanical springs [162][163]. The force that is needed to complete the compression stroke is stored in the spring instead of being transferred through the crankshaft. In other words, some of the expansion energy is stored as potential energy in the spring for the compression to take place. The absence of the crankshaft results in the removal of the rotating parts, lubrication system, support structure and piston rods. This implies that the FPSE has small side thrust forces, reduced mechanical wear and good hermetic sealing which makes it compact, more reliable, cheaper and more efficient than conventional engines [162]. The FPSE is preferred for dish solar systems and for applications where rotation is not needed, like heat pumping, water pumping, and electricity generation [164]. However, the FPSE experiences variations of the stroke length and phase angle as a response to the load and has hysteresis losses due to the internal friction of the springs which is dissipated as heat [152][157][165][107][164][166][167]. To obtain the maximum power of the FPSEs, the maximum power speed must match the resonant frequency. Hence, they are

suitable for constant speed applications, given that controlling the FPSE is harder than the kinematic engine. The FPSE might experience overstrokes at which, the power piston strikes the cylinder heads [125][168]. Hence, auxiliary devices might be needed to limit the stroke.

The free piston concept can be extended to the multi-cylinder configuration where higher power density and an economic number of moving parts and springs are obtained. The reliability of the multi-cylinder FPSE can be increased if the pistons are replaced by membranes to avoid mechanical frictions and to ease sealing [151]. Unlike the single acting engine where the phase angle is a function of spring stiffness, the multi-cylinder engine (Figure 2-8A) has its phase angle governed by the number of cylinders. Experimental working models of the three-cylinder engines have been shown by Formosa et al.[169], Fenies et al.[151] and Minassians [146][152][170].

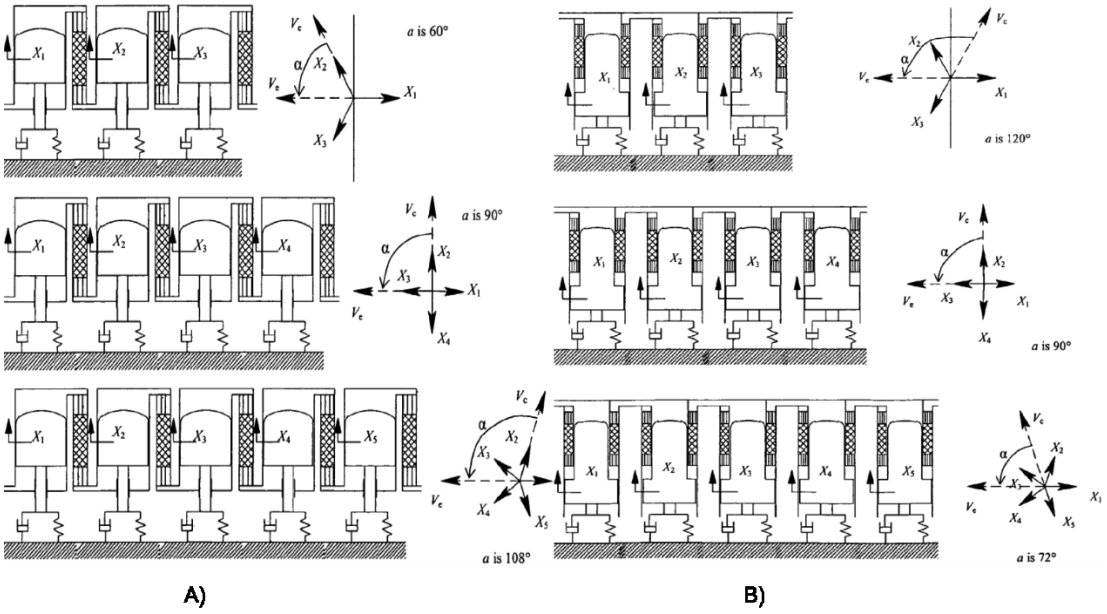

Figure 2-8: Multi-cylinder FPSE: A) conventional type and B) stepped piston type [154].

In their patent in 2007, Berchowitz and Kwon [154] proposed a new design for the multi-cylinder FPSE with stepped pistons where the phase angle matches the phase shift. So that the highly favourable phase shift of 120° is equal to the phase angle in a three-cylinder engine. In their design, both the cold space and hot space move in phase and have the same displacement but the cylinders are not double acting as shown in Figure 2-8B. Minassians et al. [146][152][170] proposed and experimentally studied a

reversing mechanism within only one piston in the three-cylinder engine so that the phase angle is forced to 120°. Their proposed mechanism requires two of the engine pistons to be mechanically linked so that they move parallel to each other. Also, the engine must work under ambient pressure which works against the working gas pressure and forces the two parallel pistons to retract.

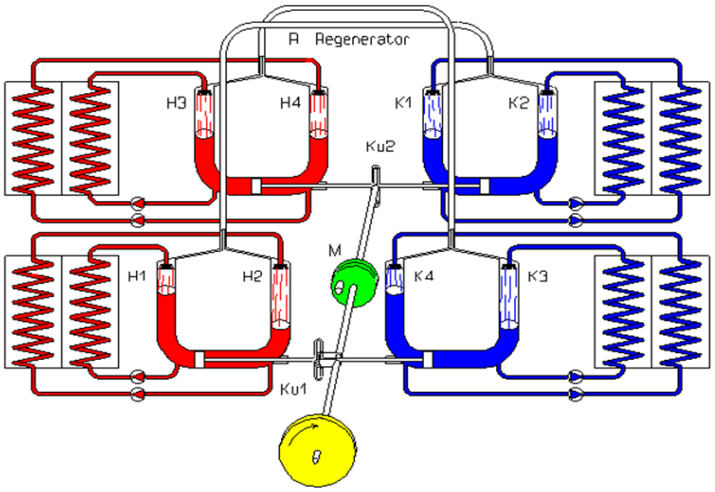

Figure 2-9: Water-type dual Franchot engine with solid pistons and mechanical drive [171].

A liquid piston engine (also known as Fluidyne) was invented by Colin D. West in 1969 [172]. In liquid piston engines, the mechanical pistons and piston rods are replaced by liquid columns and the coupling forces in the FPSE are replaced by the hydrodynamic and hydrostatic forces [173]. Due to the oscillatory nature of the liquid piston, it was successfully applied to water pumping application as the reciprocating water piston can work as a pump with a help of check valves [174]. Hence, no external pump is needed and the pumped water can be used to cool the compression space. Some others [175][176] suggested using the Fluidyne for heat pumping for which a rotational motion is not needed. In multi-cylinder liquid piston engines such as the Siemens configuration, each hot to cold space shares the same liquid column so that they are coupled pneumatically and hydraulically which defines the phase angle. This cannot be applied to the Franchot engine since the cold spaces are only coupled to the hot volumes by the working gas, which leaves the phase angle undefined. For the dual Franchot engine, each hydraulic column is either hot or cold. This makes both of the Franchot engines independent from each other both pneumatically and hydraulically.

Thus, the compression work is uncompensated by the expansion work and the liquid piston Franchot engine cannot work as a FPSE. The liquid-piston dual Franchot engine manufactured by Fette [156] is shown in Figure 2-9. It uses an external kinematic drive and solid pistons to fix the strokes, phase shift and phase angles.

In 1978, Finkelstein [165] presented a novel coupling mechanism called the balanced compounding of Stirling machines for which he was granted a patent in 1980 [177]. Instead of storing some of the expansion energy in a rotating crankshaft, mechanical springs or hydrostatic columns, an opposite engine group is added where the energy is stored in the working gas spring and each expansion piston is rigidly coupled to a compression piston. Both engine groups are coupled mechanically through straight piston rods. Thus, in this arrangement, each piston rod connects two cylinders. Hence, an even number of double acting Stirling machines is required. This coupling has an advantage over other free piston and multi-cylinder coupling techniques by requiring no additional springs or crankshafts. Figure 2-10 A shows the balanced compounding of the 4-cylinder engine where each cylinder has a hot and a cold space. The piston rods are located on the cold cylinder side. Hence, piston rods can be as short as possible due to the absence of a temperature gradient between the facing parts.

By rearranging the engine compartments, a balanced compound 4-cylinder engine where each cylinder is either hot or cold can be obtained as seen in Figure 2-10 B. This is similar to the dual Franchot engine, which eliminates heat conduction and shuttle losses in each cylinder but has heat losses due to the piston rods. Hot spaces are both gas and mechanically coupled to the cold spaces by the regenerators and piston rods, respectively. As each Franchot engine comprises two opposite alpha type Stirling engines, the four Stirling engines produce forces evenly distributed in a cycle shifted by 90^{o}. This makes a dual Franchot engine in which compression work is directly drawn from expansion work. The cross and long regenerator connections that appear in the figures are needed to keep the phase angle advanced by 90^{o} for all of the four hot spaces. Rearranging the cylinders to group similar temperature cylinders will result in long and unequal regenerator connections. Hence, in the current configuration, two heat combustors are needed. Finkelstein showed in his patent many variations of the

FPSE based on the balanced compounding technique. For example, a one-cylinder engine in which different work volumes are coupled mechanically using two concentric shafts can be equivalent to the 4-cylinder engine.

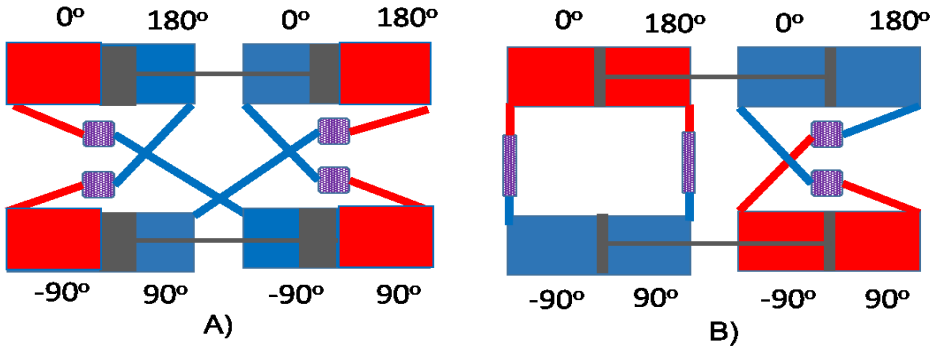

Figure 2-10: Balanced compounding of the 4-cylinder engine: A) mixed temperature cylinders and B) similar temperature cylinders.

Similar to the FPSE, the balanced compounding mechanism has virtually no side forces, absence of rotating parts, hence, increased seal life, improved engine performance, ability to hermetically seal engine compartments and most importantly the absence of mechanical drive and mechanical springs. The balanced compound engine was investigated based on the phasor diagram and ideal Schmidt analysis of the isothermal Stirling engine [165]. The analysis shows that the proposed engine can generate net positive power. In 1980, Finkelstein [178] obtained an analytical solution for the balanced compounding Vuilleumier cycle with two hot, two warm and two cold cylinders which required 8 regenerators with long connections, six hot heat exchangers and two piston rods. His model was based on ideal assumptions, isothermal expansion and compression processes and works only with FPSE. The analytical solution showed that the piston oscillation is sinusoidal and the phase shift is 90°. In 1992, Finkelstein [179] analysed the balanced compound Vuilleumier heat pump using a simpler model based on the sinusoidal variations of the swept volumes. The new model showed negligible differences with his previous model. The new model can be used for both the kinematic and free piston machines. Balanced compounding has been successfully and commercially implemented in duplex machines [102].

In 2007, McConaghy [180] patented a new arrangement for $3-ph$ AC power generation which is composed of two engines working opposite to each other and

coupled electrically. Each engine is a three-cylinder gamma type engine for which, each cylinder has a piston and a displacer rigidly coupled by a piston rod. This design makes it possible to get rid of the piston rods between different cylinders and to hermetically seal all engine compartments but it still has a bounce volume, displacers and double the number of sliding objects. In addition to that, the operation is dependent on the load. In 2014, Dadd [181] patented a linear multi-cylinder Stirling machine that has the same number of piston rods and cylinders. In this machine, the hot and cold volumes are coupled by gas, common piston rods and linear power transmitters such as linear motors and generators (see Figure 2-11).

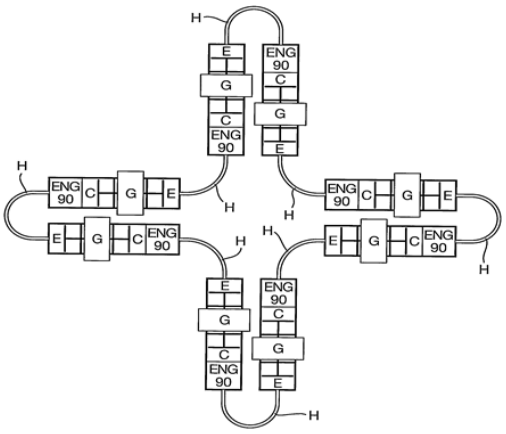

Figure 2-11: Linear multi cylinder Stirling cycle machine with load coupling [181].

2.9 Heat addition and rejection mechanism

In internal combustion engines, the air and fuel are mixed and explosively burned inside the working cylinders and thus, the temperature of the mixture rises very fast. The exhausted gas is discharged to the atmosphere requiring no heat exchanger. In contrast, Stirling engines exchange the heat with the working gas through finite surfaces, which limit the heat transfer. However, heat is transferred to the working gas by forced convection due to the oscillatory nature of the piston. Hence, the heat transfer can be enhanced by enhancing the working gas dynamics. West [182] argued that it is very hard to increase the heat transfer in a conventional Stirling engine by increasing the working gas density because of the reduced thermal diffusivity. This will increase the difference between the cylinder and working gas temperature. It is also reported that the mismatch increases by increasing the specific heat ratio γ [43]. Light gases

like hydrogen and helium have higher heat transfer per unit pressure drop than air [41][122]. Hence, using light gases allows the Stirling machine to work at larger power densities (see, Figure 2-12) [183]. Hydrogen is found to have the best power density among other gases including helium [71][115]. However, hydrogen causes corrosion, is explosive and hard to trap. In contrast, air is easier to seal, harder to penetrate through the material, cheap, readily available and requires no space for storage [41][117]. In addition, sealing the engine is less important if air is chosen as the working fluid. This reduces the complexity since an air pump can replenish the gas loss instead of using a spare gas bottle beside the engine. Tekin and Ataer [150] showed numerically that air can achieve better COP than helium for near ambient refrigeration and at pressures less than 2.5 bar. Walker et al. [41] suggested air as a refrigerant at speeds of 15-25 Hz where the losses due to air are acceptable. Moreover, he advised the open cycle for ambient refrigeration in which, the air can be discharged from the expansion chamber. Thus, no heat exchanger is required and water vapour when condensed acts as a coolant and lubricant, especially for dry seals. Haywood [45] simulated the open air cycle using the commercial software 'SAGE' where a boundary valve replaces the expansion heat exchanger. The space cooling and heating COPs were two and three, respectively.

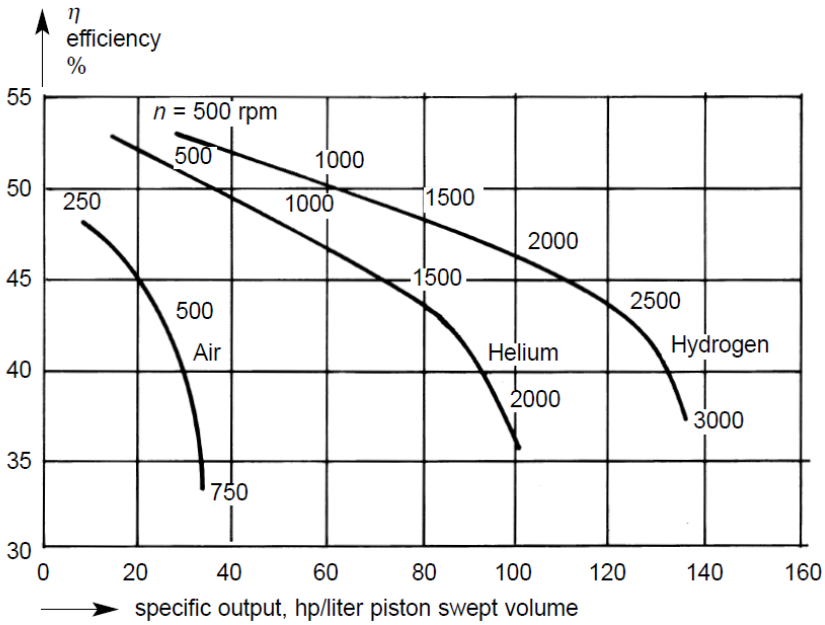

Figure 2-12: Effect of light gases on the power density of Stirling engines [76].

2.9.1 Plain cylinder

In plain cylinder Stirling engines, heat is exchanged through the cylinder end plates and wall surface nearby [184][185][186]. For example, in beta and gamma engines, a light displacer that has low thermal conductivity shuttles the working gas between the hot and cold end plates of the same cylinders. However, the cold heat exchanging area is larger than the hot one because the power piston is located on a cold cylinder which adds to the total cold area. The length of the displacer needs to be long enough to reduce shuttle, enthalpy and conduction losses due to the temperature gradient along the cylinder. The heat transfer can be enhanced by increasing the end plate areas of the displacer containing cylinder [78]. This will increase the size of the engine, limiting its applications to low power applications. LTDs reported by Kongtragool et al. [187] effectively reduce the wall area by using a short displacer with relatively large diameter [53]. They can be directly deployed to low-cost low-temperature flat plate collectors [188][189][190][73][191]. However, the advantages of LTD Stirling engines are balanced by lower efficiencies and power densities. Enhancing the power by increasing the temperature difference is possible but requires an increase of the displacer length, which will decrease the shuttle and heat conduction losses. Accordingly, high-temperature high-power engines have a large wall area of the displacer-containing cylinder, which is not participating in heat addition or rejection. Moreover, a long displacer increases the volume and weight of the Stirling engine. The MTD engine has low heat transfer area and a long displacer. It needs the heating and cooling to be concentrated in small areas, which reduce the in-cylinder heat transfer. Figure 2-13 shows the geometry differences between a gamma type LTD and MTD with plain cylinders.

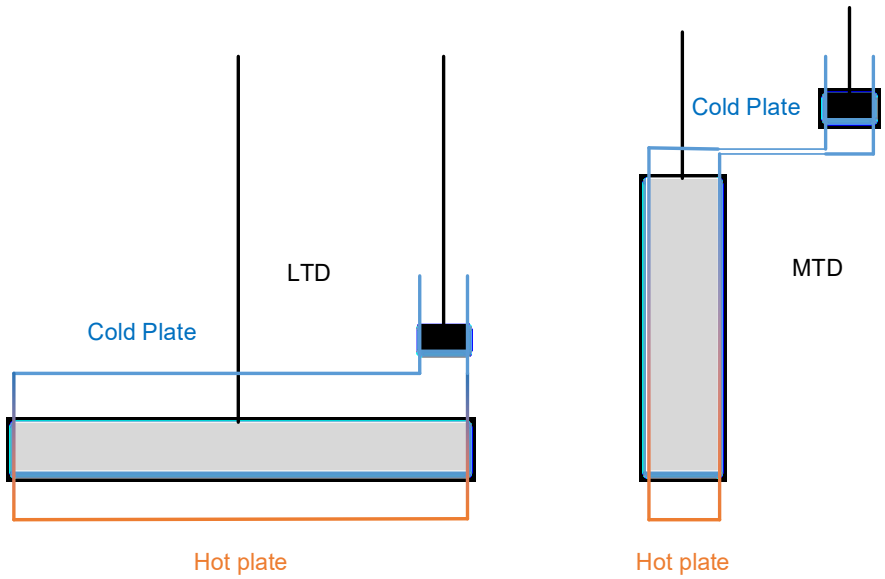

Figure 2-13: Heat transfer area in the LTD and MTD gamma type Stirling engine.

2.9.2 Heat exchangers

In general, the Stirling machine with bare cylinders has inadequate area for heat transfer [43][117][147]. To increase the heat transfer, additional heat exchangers which are connected in series to the gas circuit are needed [139]. The heat exchangers increase the heat transfer area and make it possible to operate at high power densities. In reality, they are responsible for increasing gas friction losses and dead volume (also called un-swept volume) of the system [110][139]; in addition to the dead volume in the regenerator, the cylinder clearance, and the connecting lines. While the dead volume should ideally be zero [70], in practice dead volumes make up over 50% of the total engine volume with a direct influence on the engine power [113][110]. The heat exchangers are particularly responsible for increasing the Stirling engine complexity and cost [117][151]. However, additional heat exchangers do not lead to an increase in the efficiency at maximum power [192]. The most commonly used heat exchangers with Stirling engines are reported in [123][122][193]. Due to heat exchanger cost and complexity, it is not worth to use them with the LTDs. For HTDs, the heat exchangers need to be small and efficient to decrease the dead volume and hence, increase the indicated power.

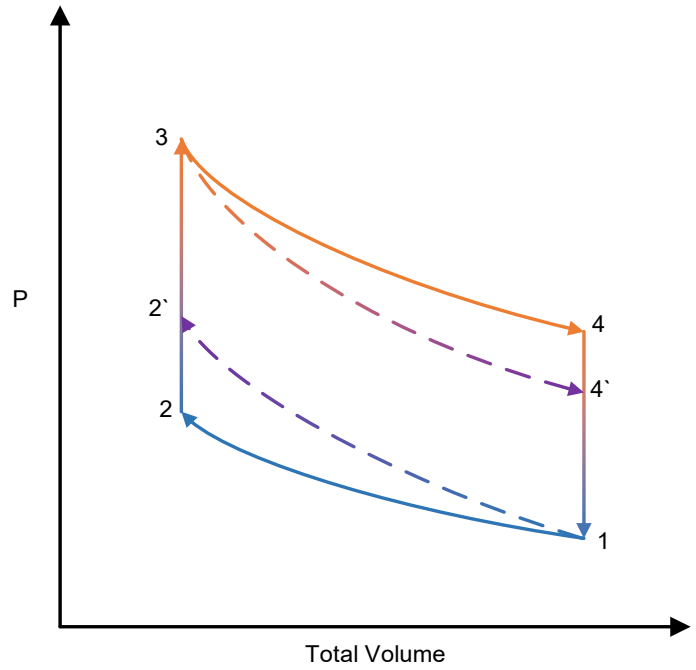

Figure 2-14: PV diagram of the Stirling engine ideal adiabatic cycle 1-2`-3-4` and the ideal isothermal cycle 1-2-3-4.

A Stirling engine with heat exchangers has a thermodynamic cycle different from the ideal one. As the speed increases, the isothermal expansion and compression processes become more adiabatic [117][123][107] which produces lower cycle work and efficiency than the isothermal processes [43][194][195][147]. Figure 2-14 clearly shows the differences between the ideal isothermal and adiabatic processes on the cycle work. The real efficiency is even worse than the ideal adiabatic efficiency due to the non-adiabatic cylinders and non-isothermal heat exchangers which increase the irreversibilities [182][196]. Carlsen et al. [147] numerically analysed the Stirling engine taking the heat transfer in the adiabatic chamber into account. They showed the adiabatic cycle efficiency tends to less than 50% of the isothermal efficiency. Haywood [45] showed that the actual processes for the Stirling engine are always polytropic which is the greatest contributor to the discrepancy between the ideal adiabatic and practical cycle of Stirling machines.

The COP of the adiabatic cycle increases with decreasing temperature difference such as for near ambient refrigeration but the COP relative to Carnot (COP_r) decreases. The COP has a limited value due to the mismatch between the working gas and the heat exchanger temperature while the Carnot COP approaches infinity. Walker [124]

reported that the COP_r of the Stirling cycle refrigerator with adiabatic cycle has a maximum for temperatures between 100-150 K and approaches zero for zero temperature difference refrigeration. Bauwens [43] showed numerically that the adiabatic process plays the major role in decreasing the COP_r at low-lift refrigeration which is hard to improve without decreasing the refrigeration load. As result of the adiabatic losses, the COP_r at low-lift temperatures approaches zero when the hot side is getting close to the cold side temperature [124]. In contrast, the isothermal cycle has always a COP ratio of 100% for all temperature ranges. Thus, the polytropic cycle would have a COP_r between the isothermal and adiabatic cycles at near ambient refrigeration.

2.9.3 Isothermaliser

Enhancing the in-cylinder heat transfer will increase the power and efficiency by modifying the machine internal heat transfer area [117][197]. The improvement in heat delivery without increasing the dead volume is called isothermalisation [139]. Carlsen et al. [147] numerically showed that increasing the in-cylinder heat transfer towards isothermal in the Stirling cycle machines with heat exchangers will increase their efficiency to 100% of Carnot efficiency. Bauwens [43] claimed that increasing the heat transfer in the compression space is more important than the expansion space. Walker [124] suggested isothermalising the Stirling-cycle heat pumps as they are designed to maximise the heat transfer. Orlowska [198] suggested adding the isothermaliser in particular to the compression space to improve the COP of a refrigerator. The isothermalisers differ from the heat exchangers in that they are within the expansion and compression spaces and not in series with them. At the maximum power point, the engine efficiency cannot exceed the Curzon and Ahlborn limit [79]. That is because the increased heat transfer is still finite and does not bring the working gas to the cylinder wall temperature. Accordingly, the expansion and compression processes are neither isothermal nor adiabatic, but polytropic. The temperature difference causes irreversibility but helps to increase the heat transfer without increasing the gas flow rate or heat exchanging area. Hence the gas friction losses at the same heat transfer rate are decreased in comparison to the use of external heat exchangers.

One of the known methods to isothermalise the working space is using interleaving fins. The fins increase the heat transfer area by creating augmentations in the cylinder end plates. However, the heat transfer changes with piston position [110]. When a finned displacer or piston compresses, the conjugate fins get closer to each other allowing the heat transfer to be largest. On the other hand, when a finned piston or displacer expands the distance between the fins gets larger, decreasing the heat transfer. Hauser et al. [199] designed an apparatus to calculate the heat transfer in an engine with layer-type interleaving fins. They found an improvement in the heat transfer in comparison to the bare cylinder. W. Martini [110] argued the best interleaving fins are the nesting cones although they increase gas friction. Benson [200] patented multiple concentric interleaving fins for isothermalising the working spaces in external combustion heat engines including the Stirling engine. Alexandravichus [201] experimentally tested tubular isothermalisers, he found the working gas temperature is not constant and a maximum power point exists. Many further researchers [115][185][202][184] showed that the multi-piston Stirling engine has enhanced heat transfer due to the total surface area of piston containing cylinders and the dead volume does not increase. Kongtragool and Wongwises [114] concluded that better performance can be achieved as the number of cylinders increases which increases the total heat exchanging area. Cinar and Karabulut [115] argued that the increase in augmentation is proportional to the power produced. Bergman et al. [139] claimed there will be a geometrical limitation for increasing the heat transfer by an isothermaliser. Carlsen et al. [147] claimed that it is harder to isothermalise a cylinder than insulating it and using heat exchangers.

Others suggested heat injection in both the cold and hot chambers. Siegel et al. [203] patented injectors for the Stirling engine which requires external heat exchangers, thermal fluid, injectors and liquid pumps. This complicates the Stirling machines and increases the number of moving parts. Smith et al. [204] suggested a mechanism to separate the thermal fluid from the working gas in the double-acting Franchot-Stirling machines. Their design required the use of four pumps and four external heat exchangers. In the liquid piston Franchot engine designed by Fette [156], the hot and cold liquid pistons are reheated and recooled and then injected into the hot and cold

spaces respectively (see Figure 2-9). Jang et al. [205][206] tested an LTD gamma type Stirling engine with water spraying inside the working chambers. Surprisingly, the power consumption of water pump was much larger than the power generated.

Since liquids take the shape of their container, the Fluidyne Stirling engine seems interesting for isothermalising the workspace. Fluidyne can easily increase the number of pistons and change the pistons geometry which increases the heat transfer to achieve near-isothermal operation [207][208]. The liquid can pass through small channels like tubes, honeycomb, fins and wire mesh. The internal fins or tubes can be added to the cold and hot spaces where the liquid itself is generally used to transport the heat [117][197][172]. However, Fluidyne has high fluid friction especially with isothermaliser, suffers from low power density, is liable to evaporation, might create gas bubbles in the liquid, causes the regenerator to clog if the liquid splashes and has high piston mass [197][209][210][211].

So far, the Stirling engine isothermalisers have not been deployed with solid pistons because of the geometry limitation and complex fin design.

2.10 Stirling cycle modelling

Although the Stirling machine appears to be simple, even its idealised mathematical models do not reflect this simplicity. Furthermore, there are different mathematical models and thermodynamic analyses. The power and efficiency can be obtained using mathematical models classified into zero, first, second and third order models [110][148][212]. Thermodynamic analysis can be subcategorised into isothermal, adiabatic and polytropic based on the thermodynamic process assumption in the swept volumes.

Zero-order models are based on empirically derived numbers, such as the Beale and West numbers, these empirical models correlate the power output to easily measured quantities such as the engine speed, temperature, swept volume and average pressure [187][213][70]. However, these models cannot be used to predict the performance

change due to changes in the configuration such as different strokes, bores, driving mechanism, phase angles, losses and heat transfer rates.

The first order model, which is also called the analytical model, uses algebraic equations to describe the engine performance. In 1871 Schmidt was able to describe analytically the isothermal expansion and compression of a closed cycle [117]. Schmidt showed that a solution is possible for a closed loop isothermal model and gave an explicit form of the solution for a sinusoidal piston movement. This model became the basis of mathematically derived models. However, the first order models can be applied to non-isothermal processes but obtaining an analytical solution will be difficult especially when the losses are considered.

The second order models have been studied extensively since Finkelstein's first second order model in 1960 and are still being used to accurately model the Stirling engines [214][77]. These models use time differential equations of a set of mass and energy conservation equations for each control volume. They are widely used with decoupled analysis, where the solution starts from the ideal model, then variant losses are subtracted from it as they are independent of each other [110][77]. This makes the second order model more accurate than the first order model and gives it more flexibility in finding a solution for each loss separately.

The third order models use differential equations in time and space (1D, 2D and 3D). These models use conservation of mass, energy and momentum equations. A workspace can be subdivided into multiple control volumes taking into account the major engine losses [52]. This increases the number of equations and needs fast computers to aid in obtaining solutions.

Among the mathematical models, the second order and third order models are the most accurate [215]. The second order models offer a good compromise between accuracy, ease of implementation and computational cost.

More important than the mathematical model is the thermodynamic analysis as it describes the working gas temperature inside the working volumes. The isothermal

analysis assumes the gas temperature is constant, adiabatic assumes the temperature of heat exchangers is only constant and no heat transfer occurs in the swept volumes and polytropic analysis assumes limited heat transfer in the working spaces. The isothermal model overestimates the power of real engines by more than 200% and always gives the Carnot efficiency due to the infinite heat transfer in the working spaces [117]. It is good for fast calculation of the performance of low speed Stirling machines for its simplicity. In Stirling engines running at 15 Hz or more, the processes are more nearly adiabatic in both the expansion and compression cylinders [123][107]. Thus, the adiabatic analysis is more realistic than the isothermal analysis but it is more complicated. The most realistic approach is the polytropic analysis as the thermodynamic processes are neither isothermal nor adiabatic hence the heat transfer rate must be considered [45][104]. A new model called polytropic analysis of Stirling engines with various losses (PSVL) was developed by Babaelahi and Sayyaadi [216]. It assumes that the expansion and compression process are neither isothermal nor adiabatic; instead, they are polytropic processes, at which heat conduction through the cylinder walls takes place. In this model, the energy is only added and removed from the engine through tubular heat exchangers while the polytropic expansion and compression is used to include expansion and compression losses. Later the PSVL model was modified by the same authors. They coupled the convective heat transfer to the expansion and compression processes which lead to more accurate predictions of the GPU-3 engine [195]. Hosseinzade et al. [196] developed a new polytropic-finite speed thermodynamic (PFST) model which considers the processes in the heat exchangers as polytropic and uses finite speed thermodynamics in working volumes. Their model shows high accuracy in predicting the thermal efficiency of the GPU-3 engine of +2% difference but the brake power was overestimated by +36.2%. Li et al. [217] proposed a new polytropic Stirling model with losses (PSML). They coupled various types of losses to the engine model including the imperfection of the regenerator. Their model shows higher accuracy of calculating the power than the PFST model over a range of speeds and high accuracy in calculating the thermal efficiency. Recently, a new model called comprehensive polytropic Model of Stirling engine (CPMS) predicted the GPU-3 Stirling engine power and efficiency with error

percentages +1.13% and 0.45% respectively [218]. This accurate result is obtained by extending the polytropic assumption in the PSVL to include the heat exchangers.

The accuracy of the polytropic models depends on the accuracy of the heat transfer models, which depends on the flow characteristics of the working gas and the heat exchangers. Some researchers used constant heat transfer rates. For example, Martaj et al. [219] assumed average gas temperature to study a low temperature differential Stirling engine with constant heat transfer. The heat is added to the gas by a flat plate and not by cylinder wall. Neither the convective heat transfer coefficient, gas temperature nor the conducting area was variable. In other publications, the instantaneous convective heat transfer is considered. Shazly et al. [186] used equations based on Nusselt, Grasshof and Prandtl numbers to calculate the natural heat convection for a direct solar-powered Stirling engine. Others [220][214] used non-dimensional correlations to describe the instantaneous convective heat transfer in Stirling engines such as Woschni correlation. A number of other contributions used correlations based on forced convective heat transfer and Nusselt numbers [139][221][215]. Most of these correlations were originally developed for internal combustion engines or compressors [222][223][224]. Stirling engines differ from these due to the absence of valves and thus the swirl gas velocity inside Stirling engines is higher [139][225]. The calculation of the heat transfer for the under-squared engine, which has a large stroke to bore ratio and high Reynolds number, is different from internal combustion engines as it requires a tailored heat transfer correlation. Toda et al. [225] showed experimentally that the in-cylinder heat transfer for Stirling engines is not accurately described by the widely used Dittus-Boelter model for turbulent flow namely $Nu = 0.023Re^{0.8}$. Xiao et al. [226] showed that the classical heat transfer correlations poorly describe the heat transfer in the Stirling engine heat exchangers especially the unidirectional correlations at high Reynold's number. In particular, the in-cylinder heat transfer is turbulent while heat transfer in the heat exchangers is laminar. Organ [141] attributed this discrepancy of the heat transfer to the flow nature in the Stirling engine: the flow is unsteady, oscillatory, compressible, not isothermal, with laminar acceleration, turbulent deceleration and flow that is not fully established at entry.

As the heat transfer rate by convection can be modelled using the Nusselt number of the pipe model aRe^b for Stirling engines [222], Toda et al. [227] quantified the in-cylinder heat transfer which is tailored to Stirling engines. In their model, the time-variant heat-transfer coefficient is different during expansion stroke and compression stroke at the same cylinder. Therefore, they obtained two correlations for the heat transfer valid for a considerable range of Reynold's numbers, which are adopted in this study as it can be said to match Organ's explanations.

2.11 Main points in this chapter

For solar powered refrigeration, a duplex system based on the Franchot engine is particularly interesting. It presents a solution for increasing the power density, reducing heat losses and allowing high-temperature differences. The sealing problem of the hot piston Franchot engine for moderate temperature range can be overcome by using clearance, PTFE or graphite seals.

Cylinder configuration is important to the Stirling engine performance. It can lead to engine capabilities such as self-starting, enhanced power generation, changed phase angle and improved kinematics through balanced compounding mechanisms.

High temperature and gas pressure are responsible for increasing the material cost, complexity and insulation requirements. Light gases are hard to maintain and must be regularly replenished. Air has potential for low power applications and cooling, especially for near ambient cooling. This study uses unpressurised air as a working fluid so that, replenishing the working gas loss is easy without the need for hermetic designs that usually increase weight.

Stirling engine heat exchangers are responsible for increasing its dead volume, complexity, cost and losses but increase the power density. In addition to that, they are indirectly responsible for decreasing the COP_r for low-lift refrigeration as they are used with adiabatic processes. Isothermalisers have not been effectively deployed to Stirling engines especially to the solid piston engines. Using the cylinder end plate as

heat exchangers is very simple but has low power density. However, no design has been found that benefits from the cylinder wall area so that the heat addition and removal are only considered through the cylinder wall.

The second order model combined with the polytropic analysis is accurate enough to predict the performance of a Stirling engine. It does not require huge computer power and the fast calculations enable optimisation and parametric studies.

2.12 Knowledge gaps

Given that the Stirling engine can theoretically achieve Carnot efficiency, no Stirling machine was successful for near ambient cooling due the low power density and complexity of the heat exchangers. This study will theoretically investigate if the Stirling cycle is suitable for near ambient solar cooling. From the literature review of the Stirling-cycle machines presented in this chapter, the following knowledge gaps have been found and will be addressed in this thesis.

- **Benefitting from the whole area of the Stirling machine cylinders for heat exchanging and study the resulting polytropic cycle.** To reduce the complexity and accompanied losses of the adiabatic Stirling machines, an enhanced heat exchanging mechanism is needed which benefits from most of the machine material to improve heat transfer. Heating and cooling the complete cylinders is novel and will be emphasised by the large stroke to bore ratio. It effectively benefits from the wall area which is preserved for thermal separation between hot and cold sides in traditional Stirling engines. This has not been studied before in terms of power capabilities and effect of different machine variables. Studies were done on cylinder end plate and near head cylinder heating and cooling but not on total cylinder wall. The published studies of Stirling machines with direct heating and cooling are either studied with adiabatic or isothermal expansion and compression but not polytropic.
- **Power enhancement using simple isothermalisers with fixed hydraulic diameter.** It is not expected for the heat transfer in bare cylinders to be

adequate for high power applications. Also, isothermalisers are not used with solid piston machines due to geometry limitation. In this study, cylindrical isothermalisers will be theoretically studied for the first time and the effect on the heat transfer and gas friction will be addressed using appropriate mathematical analysis.

- **Mechanical assessment and self-starting capability of the kinematic Franchot engine.** There is a lack of studies about the Franchot engine and the vibrational and start-up assessment of the Stirling engines with the simple slider-crank mechanism. Reducing the power pulses, which is related to reducing the angular vibrations, through changing the arrangement and number of engine cylinders will be studied. Also, the effect of changing the cylinder arrangement on the phase angle, reciprocating vibration and couple forces will be provided. The importance of adding a flywheel and start-up mechanism will be discussed based on the theoretical performance of the kinematic Franchot engine. This study is important to inspire the design of a free piston Franchot engine to enhance its mechanical characteristics.
- **Balanced compounding of the multi-cylinder Franchot engine**. The free piston technology and especially the balanced compounding methods were not studied with the Franchot engine especially with long strokes. Different engine variables need to be studied for their effect on engine response. For example, the number and the arrangement of the engine cylinders needs to be studied for its effect on phase angle. The effect of reciprocator mass, dead volume and source temperatures on engine frequency will be investigated and the engine dimensions will be optimised for the best performance.
- **Direct coupling of the Stirling machine to solar line collectors.** No Stirling engine design was found in the literature for direct thermal coupling with line collectors. The cold power production of the developed Stirling machine per square meter of solar collectors needs to be addressed as a comparative index to other cooling technologies.

CHAPTER

3 Cylinder wall heated/cooled air filled Franchot machine

In the previous chapter, different heat exchanging methods for the Stirling machines and in particular the Franchot ones have been reviewed. The easiest method for delivering the energy is by directly heating and cooling the cylinder end plates. In this chapter, a novel Franchot machine which has two cylinders, each with a distinct temperature, is designed to be completely heated and cooled by the cylinder wall instead of the cylinder end plates. The novel machine has large stroke to bore ratio to increase the wall area. An ideal mathematical model is derived for this machine with a derived mathematical definition of the regenerator end temperatures. The performance of the heat engine and refrigerator is theoretically investigated for different parameters.

3.1 Introduction

Adding heat exchangers to the Stirling cycle machine leads to an improvement of the power density by increasing the heat transfer rate. The Franchot machine has the potential to improve the power density and efficiency without adding heat exchangers due to many features discussed in section 2.6. In particular, the thermal separation between the cylinders reduces the shuttle losses, axial heat transfer and the enthalpy loss due to the gas leakage across the piston. Also, the thermal separation between cylinders makes it possible to completely heat or cool the cylinders. It allows more area to participate in heat conduction in each cylinder with relatively short pistons and large stroke to bore ratio. The heat delivery can benefit from the cylinder wall area along the piston motion and the small hydraulic diameter of the cylinders. The wall area of a constant volume cylinder is always larger than the end plate area if the cylinder length is larger than 50% of the diameter. The absence of shuttle losses allows

using large stroke to bore ratios that have a small hydraulic diameter and larger cylinder area, which enhance heat transfer. The use of cylinders instead of the auxiliary complicated heat exchangers is expected to simplify the machine manufacturing and hence decrease the price.

3.2 Novel engine design

Figure 3-1 is a schematic diagram of the proposed cylinder wall heated/cooled Franchot engine with large stroke to bore ratio. The whole expansion and compression cylinders work as heat exchangers and power cylinders at the same time. Thermal energy is added through the hot (expansion) cylinder and removed from the cold (compression) cylinder. Two regenerators connect the cold spaces to the hot spaces. The Franchot engine consists of two opposite alpha engines with two separate gas circuits, which each have three working volumes. The dead volume in this design is attributed to the regenerator and the cylinder clearances. However, small diameters make small clearance volumes, which might be ignored if the stroke matches the cylinder length.

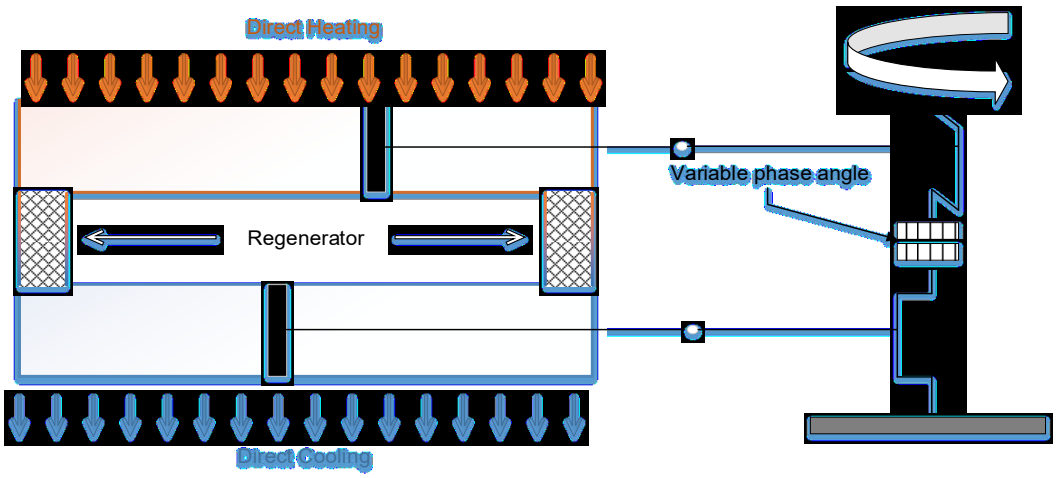

Figure 3-1: The proposed plain cylinder Franchot engine.

The engine is designed based on a pure thermodynamics approach. The thermodynamic goal is to obtain the maximum power point, which has a lower efficiency than the Carnot efficiency. The maximum power efficiency, known as the Curzon and Ahlborn efficiency, is due to the gas to wall temperature difference that in

turn improves the heat transfer (see section 2.2). So, the expansion and compression processes are neither isothermal nor adiabatic, they are polytropic. Hence, the temperatures are not constant during the expansion and compression strokes.

The isothermal and polytropic thermodynamic cycle and piston displacements of a Stirling engine having two opposite pistons are shown in Figure 3-2. The ideal isothermal engine given by cycle 1-2-3-4 has two isothermal and two isochoric processes. In contrast, the cylinder wall heated and cooled Stirling engine has a reduced polytropic cycle (1`-2`-3`-4`) due to the difference between the gas and cylinder wall temperatures. The polytropic cycle can be explained based on the displacements of the opposite engine pistons as follows:

- 1`-2` Polytropic compression: In this process, the expansion piston stands still close to the regenerator and the compression piston moves inward. The engine requires some work in order to compress the working fluid and the pressure increases. Heat is rejected at the walls of the cold cylinder due to the gas temperature difference with the cold cylinder walls.
- 2`-3` Isochoric heating: In this process, the expansion and compression pistons move outward and inward, respectively. They move with each other and keep the total engine volume constant. The gas flows from the compression to the expansion space and passes through the regenerator, which absorbs heat from it. In this process, the pressure increases and no work is required or generated since there is no change in the total engine volume.
- 3`-4` Polytropic expansion: In this process, the compression piston stands still and the expansion piston moves outward. Energy is absorbed in the working gas of the hot cylinder due to the temperature difference between the hot cylinder walls and working gas. The cycle generates positive work and the gas pressure decreases.
- 4`-1` Isochoric cooling: In this process, the expansion piston moves inward and the compression piston moves outward. Both move with each other keeping the total volume of the engine constant. The gas flows from the expansion to the compression space through the regenerator and the working gas pressure

decreases. The gas re-absorbs the heat which was absorbed in step 2`-3` into the regenerator. In this process, no mechanical work is required or generated since there is no change in the total engine volume.

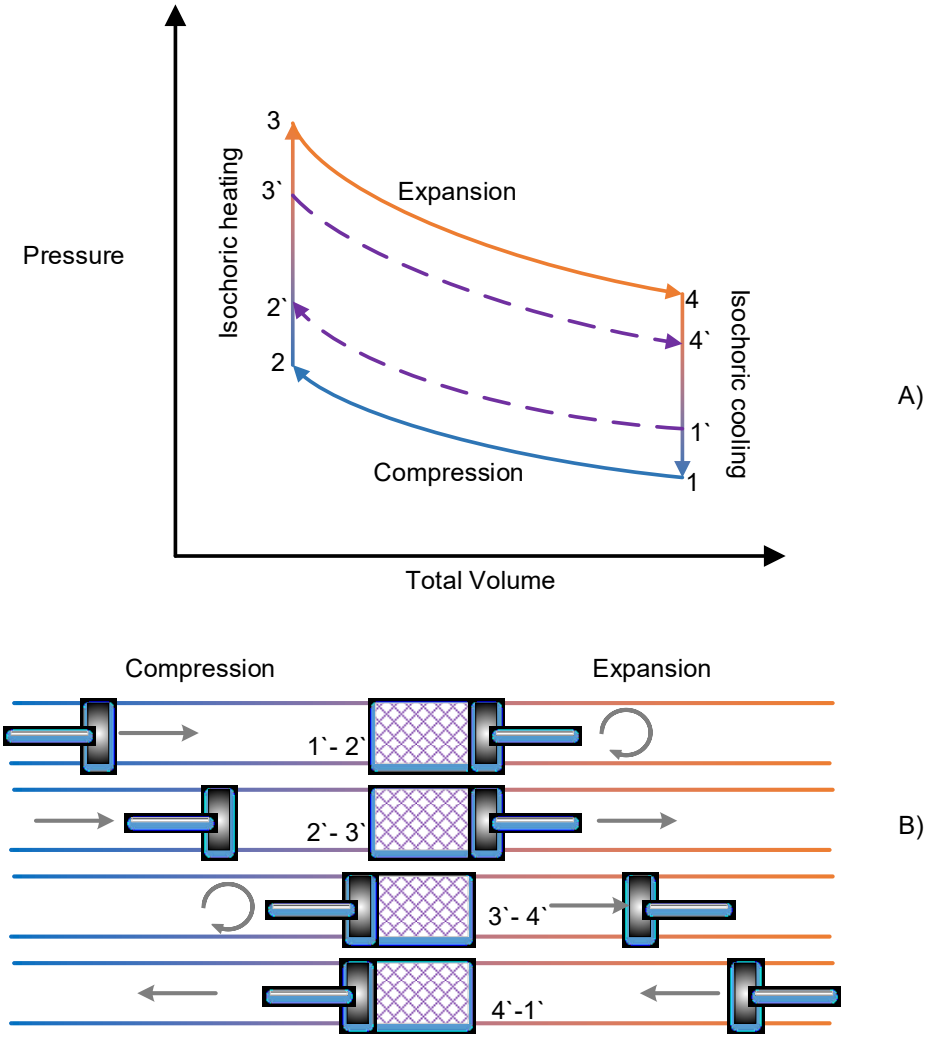

Figure 3-2: Thermodynamic cycle of the Stirling engine: A) PV diagram of the ideal (1-2-3-4) and polytropic (1'-2'-3'-4') cycle and B) piston displacements.

3.3 Modelling of the novel engine

The Franchot engine, which is heated and cooled by cylinder walls, is modelled using a second-order model. Each half of the Franchot engine has an independent gas circuit as shown in Figure 3-3. The three control volumes approach was chosen since each half consists of three consistent working spaces: the regenerator, expansion and compression space.

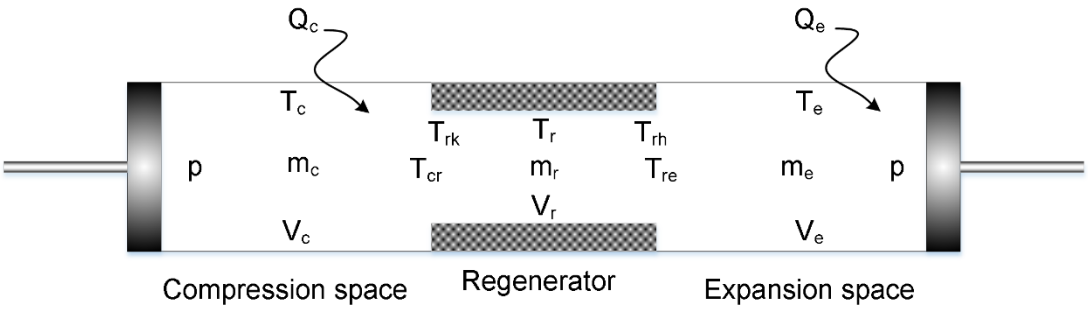

Figure 3-3: Schematic model of three-control volume Stirling engine showing the expansion, regenerator and compression spaces.

The heat transfer during a cycle of this engine is not constant and cannot be accurately described by an adiabatic or isothermal model. This is due to the variations in working gas temperature, wall area and convective heat transfer coefficient in the heated/cooled cylinders. This can be better described by the polytropic model taking into account the heat transfer between the cylinder wall and working gas. This model is limited to the ideal Stirling engine with polytropic expansion and compression and does not include the mechanical connection or hydraulic losses. Later, the mechanical connection will be considered in chapters 5, 6 and 7 and hydraulic losses will be considered in chapter 4. On the other hand, shuttle, axial heat conduction and enthalpy loss due to gas leakage across the pistons do not exist in the Franchot engine. The aim of this model is to investigate the upper limit performance of the polytropic cycle engine given that other losses can be separately minimised.

3.3.1 Ideal model assumptions

The mathematical model describes the ideal system through the following assumptions:

- The engine is modelled as three compartments: compression, expansion and regenerator.
- Each compartment has uniform instantaneous temperature, pressure and mass.
- Mass is preserved and the total amount is constant.
- No pressure drop occurs.

- No fluid leakage occurs across the power pistons.
- The ideal gas law applies.
- The engine speed is constant and the variation of swept volumes is described by sinusoidal waves.
- The steady state of the cycle occurs.
- The kinetic energy of the working fluid is neglected.
- The regenerator is ideal.
- The cylinder wall temperatures are constant and uniform.
- No mechanical losses occur.

These assumptions lead to a model, which describes the ideal polytropic cycle of the Franchot engine but with limited heat transfer. This model can be used to analyse the upper-performance limits. In subsequent chapters, a number of these assumptions will be assumed and quantified.

3.3.2 Thermodynamic modelling

The Stirling engine is modelled through mass and energy balances in the three control volumes that are connected through mass and energy flow across the volume boundaries. The three control volumes resemble the actual compartments of the cylinder wall heated and cooled Franchot engine.

The mass balance of the three control volumes is given by

$$M = m_e + m_c + m_r \qquad 3.1$$

where $M, m_e, m_c \; and \; m_r$ are the total constant gas mass inside the engine, the expansion volume gas mass, the compression volume gas mass and the trapped regenerator gas mass. Due to the constant total gas mass, the derivative of Equation 3.1 is given by

$$0 = \dot{m}_e + \dot{m}_c + \dot{m}_r \qquad 3.2$$

By assuming that the working gas is an ideal gas, the equation of state for the three control volumes can be written as

$$pv_x = m_x R\, T_x \qquad 3.3$$

where p is the instantaneous pressure, v_x is the control volume, m_x is the control volume gas mass, R is the ideal gas constant and T_x is the control volume gas temperature.

The energy balance equation for the expansion space is given by

$$\dot{Q_e} + c_p \dot{m}_e T_{re} = p\dot{v}_e + c_v(\dot{m_e} T_e) \qquad 3.4$$

where $Q_e, c_p, c_v \; and \; T_{re}$ are the energy absorbed by the expansion cylinder, gas specific heat capacity at constant pressure, gas specific heat capacity at constant volume and the temperatures of the gas entering and leaving the hot regenerator end, respectively.

Using the ideal gas law, Equation 3.4 becomes

$$\dot{Q_e} + c_p \dot{m}_e T_{re} = p\dot{v}_e + \frac{c_v}{R}(p\dot{v}_e) \qquad 3.5$$

Rearranging Equation 3.5 results in

$$\dot{m}_e = \frac{\frac{p\dot{v}_e}{R} + \frac{v_e\dot{p}}{\gamma R} - \frac{\dot{Q}_e}{c_p}}{T_{re}} \tag{3.6}$$

Similarly, the compression cylinder mass flow rate is given by

$$\dot{m}_c = \frac{\frac{p\dot{v}_c}{R} + \frac{v_c\dot{p}}{\gamma R} - \frac{\dot{Q}_c}{c_p}}{T_{cr}} \tag{3.7}$$

Using the ideal gas law and assuming that the regenerator average temperature is constant, the regenerator mass flow rate is calculated as

$$\dot{m}_r = \frac{V_r}{RT_r}\dot{p} \tag{3.8}$$

The differential form of the pressure is obtained from combining Equations 3.2, 3.6, 3.7 and 3.8 to obtain

$$\dot{p} = \frac{-p\left(\frac{\dot{v}_e}{T_{re}} + \frac{\dot{v}_c}{T_{cr}}\right) + \frac{R}{c_p}\left(\frac{\dot{Q}_e}{T_{re}} + \frac{\dot{Q}_c}{T_{cr}}\right)}{\frac{v_e}{\gamma T_{re}} + \frac{V_r}{T_r} + \frac{v_c}{\gamma T_{cr}}} \tag{3.9}$$

where T_{re} and T_{cr} are the temperatures of the gas entering and leaving the hot regenerator end and of the gas entering and leaving the cold regenerator end, respectively. If the change of the gas mass in any chamber is positive then the gas is flowing toward it having the temperature of the corresponding regenerator end,

otherwise it will have the chamber temperature. These temperatures are assigned based on the direction of the gas flow through

$$T_{re} = \begin{cases} T_e, & \dot{m}_e < 0 \\ T_{rh}, & \dot{m}_e \geq 0 \end{cases} \quad 3.10$$

$$T_{cr} = \begin{cases} T_c, & \dot{m}_c < 0 \\ T_{rk}, & \dot{m}_c \geq 0 \end{cases} \quad 3.11$$

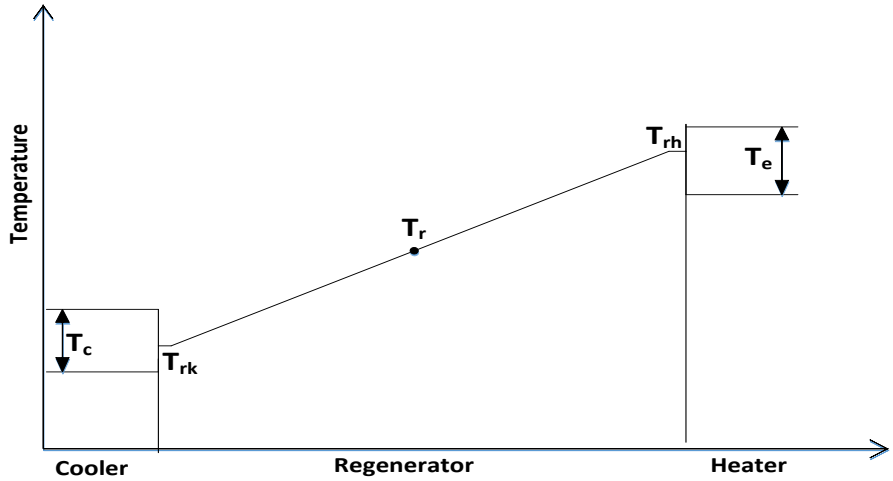

Figure 3-4: Temperature distribution of the three-control volume Stirling engine.

The regenerator temperature is shown in Figure 3-4 and defined as [167]

$$T_r = \frac{T_{rh} - T_{rk}}{\ln \frac{T_{rh}}{T_{rk}}} \quad 3.12$$

where T_{rh} and T_{rk} are the regenerator hot and cold end temperatures, considered as constant temperatures and found from the regenerator energy balance equation

$$\dot{Q}_r + c_p \dot{m}_e T_{re} + c_p \dot{m}_c T_{cr} = \frac{c_v}{R} V_r \dot{p} \qquad 3.13$$

Taking the closed integration of Equation 3.13 over one cycle results in

$$\oint c_p \dot{m}_e T_{re} + \oint c_p \dot{m}_c T_{cr} = 0 \qquad 3.14$$

By assuming ideal regeneration, the energy from the hot regenerator side does not transfer to the cold side and thus for the hot side only the first integral needs to be considered. This integral can be rearranged to

$$\oint [i c_p \dot{m}_e T_e + (1-i) c_p \dot{m}_e T_{rh}] = 0 \qquad 3.15$$

which gives the following equation for T_{rh}

$$T_{rh} = \frac{-\oint i \dot{m}_e T_e}{\oint (1-i) \dot{m}_e} \qquad 3.16$$

Similarly, the temperature of the cold side is given by

$$T_{rk} = \frac{-\oint j \dot{m}_c T_c}{\oint (1-j) \dot{m}_c} \qquad 3.17$$

In Equations 3.15-3.17, the parameters i and j are functions given by

$$i = \begin{cases} 1, & \dot{m}_e < 0 \\ 0, & \dot{m}_e \geq 0 \end{cases} \quad 3.18$$

$$j = \begin{cases} 1, & \dot{m}_c < 0 \\ 0, & \dot{m}_c \geq 0 \end{cases} \quad 3.19$$

The mass flow rate $\dot{m}_e$ is calculated from Equation 3.6 while $\dot{m}_c$ and m_c are calculated from Equations 3.2 and 3.1, respectively.

Once the mass and energy flows are calculated, the output power is evaluated as

$$P_{ins} = \Delta p(\dot{v}_e + \dot{v}_c) \quad 3.20$$

where P_{ins} and Δp are the mechanical instantaneous power and the instantaneous pressure difference across pistons, respectively. The cycle work is calculated as

$$W = \oint \Delta p(\dot{v}_e + \dot{v}_c) \quad 3.21$$

thus, the average power can be written as

$$P = f \times \oint \Delta p(\dot{v}_e + \dot{v}_c) \quad 3.22$$

Engine efficiency is given by

$$\zeta = \frac{P}{\dot{Q}_e} \tag{3.23}$$

The in-cylinder heat transfer of a Stirling engine can be described by Newton's law of cooling, describing convective heat transfer. The added heat into the expansion cylinder is hence given by

$$\dot{Q}_e = hA_e(T_h - T_e) \tag{3.24}$$

and the rejected heat by the compression cylinder is given by

$$\dot{Q}_c = hA_c(T_k - T_c) \tag{3.25}$$

Here h, A_e, A_c, T_h and T_k are the heat transfer coefficient, instantaneous wall area of the expansion cylinder, instantaneous wall area of the compression cylinder, wall temperature of the expansion cylinder and wall temperature of the compression cylinder, respectively. The wall areas of the expansion and compression cylinders are given in Equations 3.26 and 3.27

$$A_e = \frac{4v_e}{D_e} \tag{3.26}$$

$$A_c = \frac{4v_c}{D_c} \tag{3.27}$$

where $D_e \; and \; D_c$ are the expansion and compression piston diameters, respectively.

Equation 3.28 correlates the Nusselt number with the Reynolds number correlation, which was experimentally obtained for the swept volume of an air charged Stirling engine with stroke to bore ratio of 1.75 and for a wide range of Reynolds numbers (1500-40000). In comparison to the heat transfer correlations that can be used with the heat exchangers of the Stirling engine [228]. This correlation from Toda et al. is tailored for heat transfer inside the swept volume of Stirling engines where variable volume, variable pressure, variable speed and undeveloped oscillatory flow with a wide range of Reynolds' numbers can exist. The correlation which holds for Reynolds numbers between 1000-100000 is [225]

$$Nu = \begin{cases} 0.7Re^{0.58}, & expansion\ stroke \\ 0.62Re^{0.53}, & compression\ stroke \end{cases} \quad 3.28$$

where

$$Nu = \frac{hD_x}{k} \quad 3.29$$

Equation 3.30 from Toda directly correlates the heat transfer coefficient with the piston diameter, flow velocity, pressure and temperature [227].

$$\begin{aligned} h_e &= 0.042D^{-0.42}v^{0.58}p^{0.58}T^{-0.19} \\ h_c &= 0.0236D^{-0.47}v^{0.53}p^{0.53}T^{-0.11} \end{aligned} \quad 3.30$$

where $h_e\ and\ h_c$ are the in-cylinder heat transfer during the expansion stroke and compression stroke, respectively. These correlations were developed for air-filled engines working at temperatures up to 400° C.

3.4 Ideal engine performance

The mathematical model from Section 3.3.2 is implemented in Matlab/Simulink and solved using the fourth order Runge-Kutta method with a time step of 10^{-4}s. The results were checked against results with 10^{-5}s time step and gave negligible differences. The model is used to analyse the performance of the proposed Franchot engine at moderate temperatures, i.e. up to 600 K. The parameters of the reference Franchot engine design are shown in Table 1. This configuration is called the reference engine design and is used for most simulations unless otherwise stated.

Instead of changing the stroke length, the diameter of the cylinder is changed to evaluate changes in the stroke to bore ratio. In addition, the phase angle, engine speed, dead volume and charge densities are changed to evaluate their effect on the performance. The hot cylinder wall temperature was kept constant at 600 K due to thermal limitations of the hot piston seal.

Table 3-1: Parameters of the reference cylinder wall heated/cooled engine

Name	***symbol***	***value/unit***
Stroke length	L_e, L_c	25×10^{-2} *m*
Bore diameter	D_e, D_c	2×10^{-2} *m*
Charge gas density	ρ	*1.225 kg/m³*
Charge pressure		*1 atm*
Clearance length	re, rc	1×10^{-3} *m*
Dead volume ratio		*1*
Out-of-Phase angle	θ	*150 deg*
Engine speed	n	*1000 rpm*
Hot, cold temperatures	T_h, T_k	*600 K,300 K*
Working gas	*Air*	
Gas constant	*R*	*287 J/kg.K*

3.4.1 Effect of changing the phase angle

The effect of changing the phase angle on the efficiency and power for the reference engine design is shown in Figure 3-5. It can be seen, that phase angles between 150°-170° have simultaneously high efficiency and high power and are thus the most suitable phase angles for the ideal reference engine. The performance in this phase angle range can be optimised between the highest power and the highest efficiency.

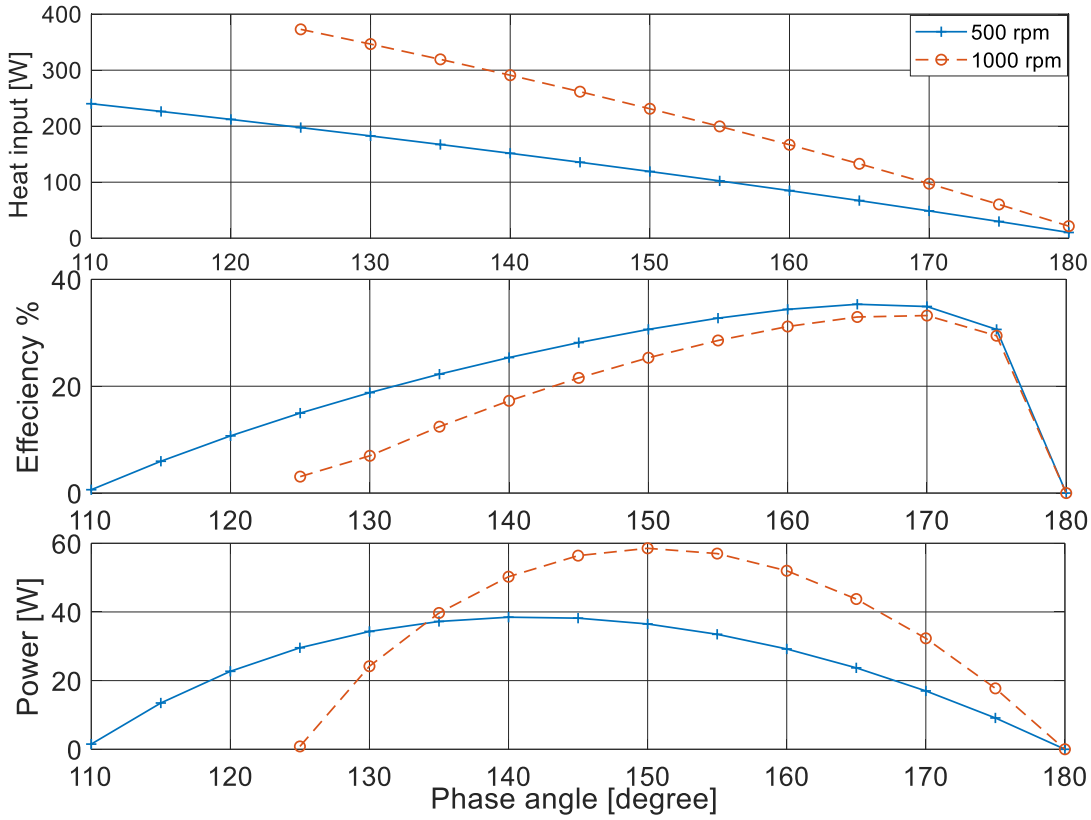

Figure 3-5: Variation of engine input energy, efficiency and power with phase angle for the reference engine at 500 and 1000 rpm.

However, the maximal power phase angle (150°) and maximal efficiency phase angle (170°) are distinct for the reference engine, so that the engine cannot be optimised for both performance criteria simultaneously. While the difference in the phase angle is only 20°, the differences in the efficiency and power at those phase angles are significant: 25.3% efficiency and 58.5 W at 150° and 33% efficiency and 32.3 W at 170°. The efficiency 25.3% at the maximum power shows a good match with the ideal efficiency of 29.3% calculated by Curzon and Ahlborn [79]. At lower speeds, the engine achieves less power but with better efficiencies. This is due to the decrease in the indicated power in comparison to the heat transfer. Hence, at lower speeds the optimum phase angles are shifted towards smaller angles.

Stirling engines are usually designed to operate at speeds that gain maximum power, in order to increase the power densities and hence reduce the capital cost. In the bare cylinder Franchot engine, the power and efficiency could be improved by changing the phase angle without increasing the engine complexity. In Figure 3-6, the P-V

diagram of a half Franchot engine that is a conventional alpha type engine shows that increasing the phase angle decreases the maximum engine pressure and decreases the added and rejected thermal energies. This reduces the internal heating and cooling loads on the corresponding cylinders as well as the gas leakage.

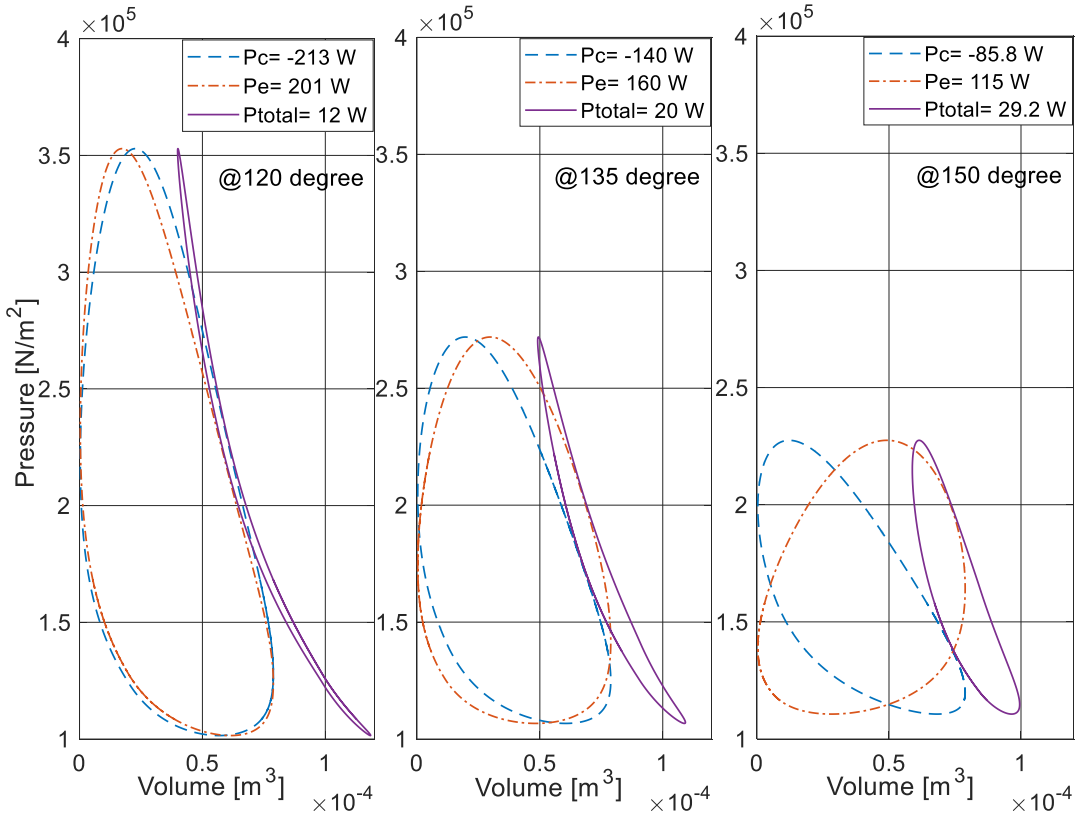

Figure 3-6: P-V diagram of the reference engine at different phase angles.

The instantaneous gas temperatures inside both the expansion and compression volumes can be seen in Figure 3-7. The gas hysteresis losses, which are transient heat transfer losses, occur due to the variation of the gas to wall temperature difference over a cycle. This variation in temperature occurs as the pressure fluctuates with engine volume [229]. However, hysteresis losses don't appear in isothermal and adiabatic spaces [230]. The heat transfer in adiabatic working space does not exist by definition and the temperature variation in an isothermal space is zero and hence no hysteresis loss will occur [172]. At the maximum power point, the engine is endo-reversible which means the heat transfer occurs in one direction. The temperature spike of the hot gas has short duration and occurs during the compression of the hot piston, which results in small heat transfer. In a real engine, the temperature spike is expected to be

smaller than the spike of the engine without dead volume due to reduced pressure variations. This means that the hysteresis losses can be neglected at the maximum power point due to the absence of gas to wall temperature difference. At efficiencies larger than the maximum power efficiency, the Stirling engine cycle becomes closer to isothermal and by definition, hysteresis losses are reduced for isothermal process as it is reversible. At efficiencies smaller than the maximum power efficiency, hysteresis losses become less pronounced because the heat transfer occurs in one direction. Hence, the hysteresis losses will not be considered for the cylinder heated and cooled Stirling engine.

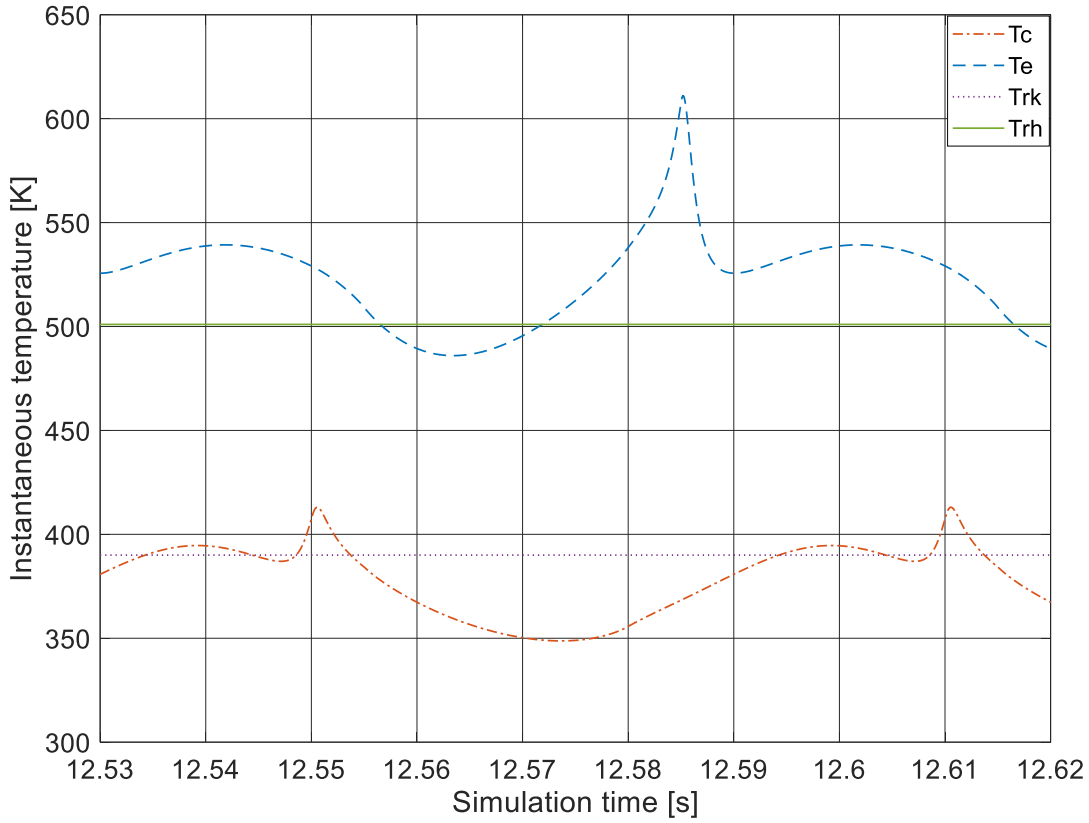

Figure 3-7: The instantaneous gas temperatures in the compression and expansion volume of the basic engine design.

The relationship between the phase angle and engine speed is illustrated in Figure 3-8. It can be seen that the engine output power increases at higher speeds for increasing phase angles and that the efficiency decreases with increasing engine speed. For each engine speed, there is one phase angle, which gives the highest power but not the

highest efficiency. The maximum power efficiency, i.e. the efficiency at the maximum output power, is around 17% for all studied phase angles.

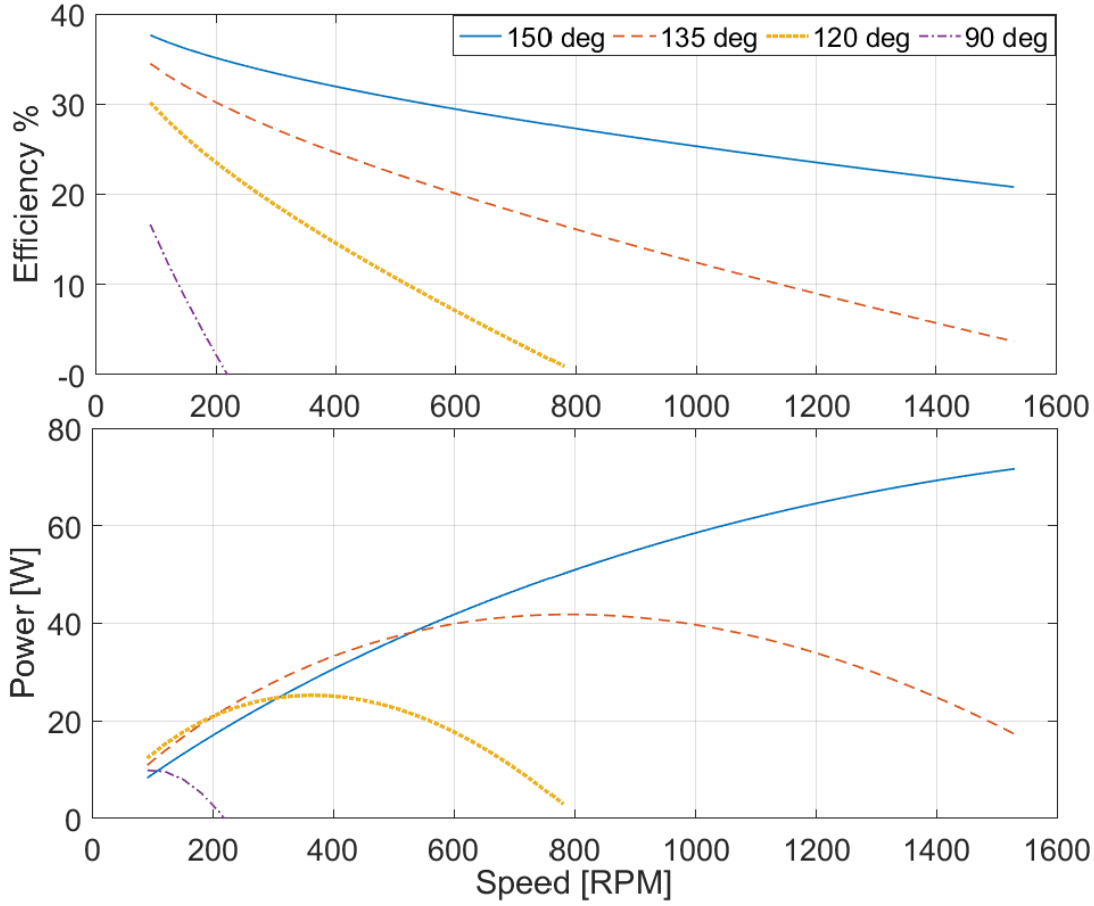

Figure 3-8: Variation of engine efficiency and power against engine speed for various phase angles.

In general, increasing the speed leads to a linear increase in the indicated power given by Equation 3.22 under the assumption that the heat transfer is sufficiently fast. However, the heat transfer rate given by Equation 3.30 increases at a lower rate and thus, the engine power reaches a maximum for a specific engine speed.

3.4.2 Effect of dead volume

The dead volume ratio is the ratio of the clearance volume to the swept volume. The simulations were performed with a dead volume of 25%, 50%, 100% and 200% of the swept volume. The dead volume is at the head of cylinders so an increase in the dead volume increases the cylinder wall area, which acts as heat transfer area. Thus, an

increase in the dead volume increases the energy transferred to the engine. However, the dead volume also decreases the engine power by decreasing pressure variation.

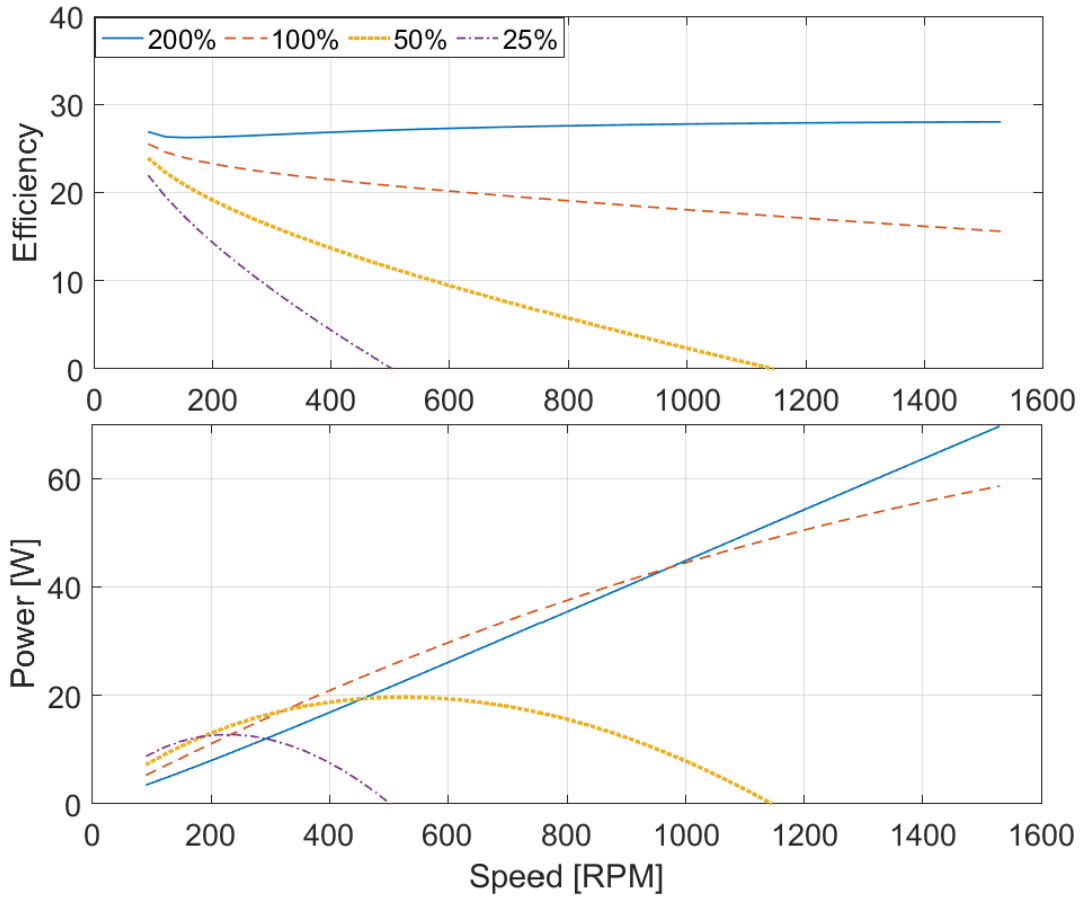

Figure 3-9: Variation of engine efficiency and power against engine speed for various dead volume ratios and 90° phase angle.

Figure 3-9 shows that for a fixed phase angle of 90°, an increase in the dead volume improves the efficiency and increases the maximum power at higher speeds. Thus, an increase in dead volume has a similar effect as an increase in phase angle. However, for every single speed, neither the maximum power nor its efficiency was better than that achieved by varying the phase angle. That is due to the reduced pressure variation and hence temperature to wall difference. Thus, it would be better to increase the number of engines at the optimal phase angle instead of increasing the dead volume to achieve higher engine powers. For example, doubling the engine size by increasing the dead volume does not double the maximum engine power at the same speed. Here, the optimal value of dead volume that maximise the power is a function of the speed.

3.4.3 Effect of cylinder diameter

Figure 3-10 shows the response of the bare cylinder Franchot engine to changing the piston diameter while keeping the stroke length constant. It can be seen that smaller diameters always increase the efficiency but not necessarily the power at a fixed phase angle. The reason for this is that the decrease in swept volume is larger than the decrease in heat transfer. Thus, the heat transfer to swept volume ratio increases with decreasing diameters, which leads to higher efficiencies but lower indicated power.

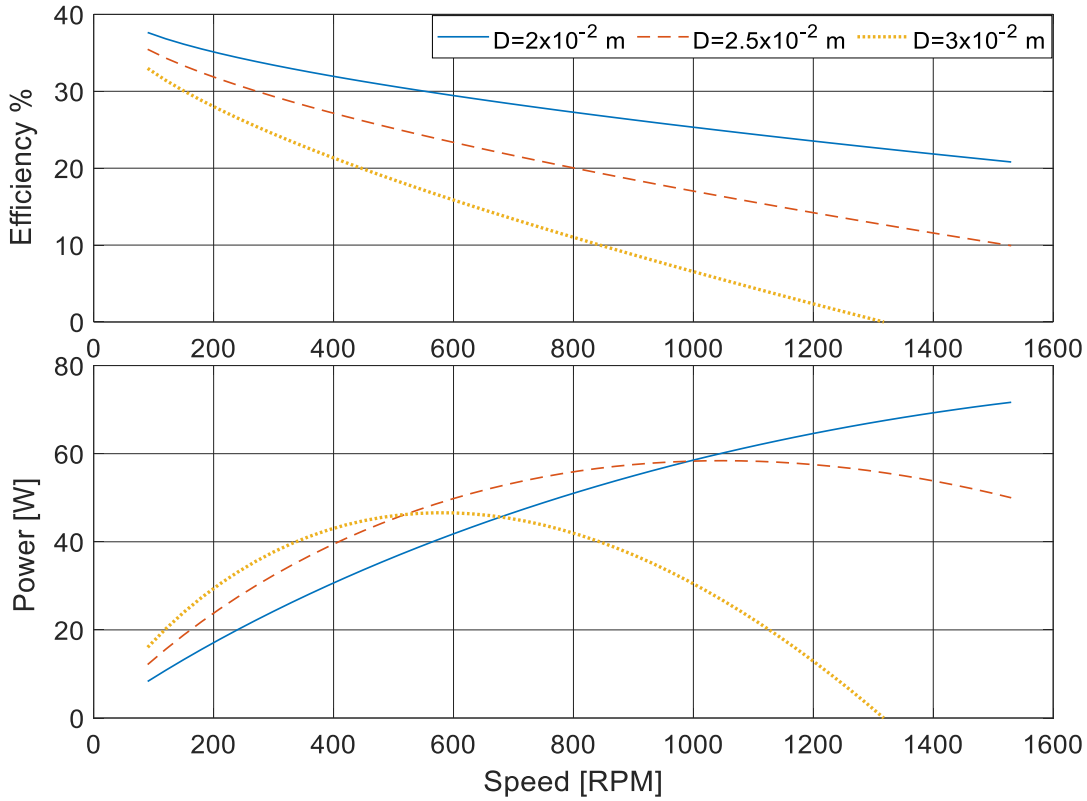

Figure 3-10: Variation of engine output efficiency and power against engine speed for various piston diameters.

At low speeds and a fixed phase angle, larger diameter pistons give higher power because the heat transfer is large enough to deliver the required energy. On the other hand, small piston diameters are not able to compete at low speeds unless the phase angle is reduced to force the engine to work at higher power modes. The maximum power efficiency is around 16.5% for the studied diameters. Increasing the diameter also increases the dead volume which has been ignored in this section due to the assumption of small clearance distance.

3.4.4 Effect of gas charge density

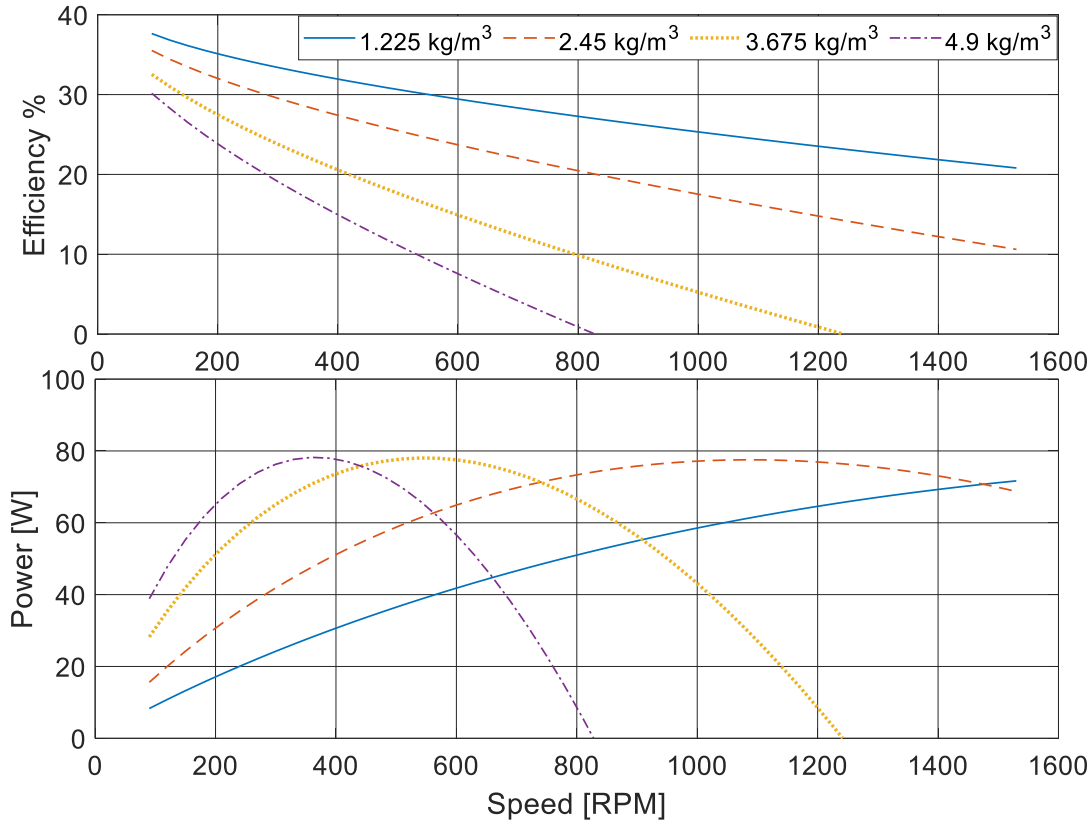

Figure 3-11: Variation of the reference engine output efficiency and power against engine speed for various charge densities.

The effect of the charge density is shown in Figure 3-11. Although the effect on the maximum power is barely noticeable, it decreases the corresponding maximum power speed. In addition, the maximum power efficiency is around 16.5% for all studied densities. This result makes pressurising the working gas unavoidable if a higher power is needed and higher speeds are unfeasible. According to Equations 3.22 and 3.30, both the indicated power and the heat transfer rate are affected in the same way by a change in engine speed or pressure. From the ideal gas law, increasing the gas density linearly increases the pressure if the temperature does not change. At the maximum power point, the efficiency is limited by the Curzon and Ahlborn efficiency and thus, the temperature variation is similar for three charge densities. In combination with the results shown in Figure 3-11, this explains the result of having the same power at a lower speed for an increase in the gas density. However, an increase in charge density increases the requirements on the engine sealing.

Figure 3-12 shows the decrease of both the pressure and pressure difference peaks on the working pistons for increasing phase angles for two charge densities. The lower pressure differences at larger phase angles might result in decreasing gas leakage losses across the power pistons. Figure 3-12 also shows a steep decrease of the pressure and pressure difference peaks for the pressurised engine at 2.45 kg/m3. That is due to the decrease in the fractional volumetric variation with increasing the phase angle. The decrease in the maximum pressure might lower requirements for the engine material and decreases the working gas leakage to the ambient through the piston rod sleeves.

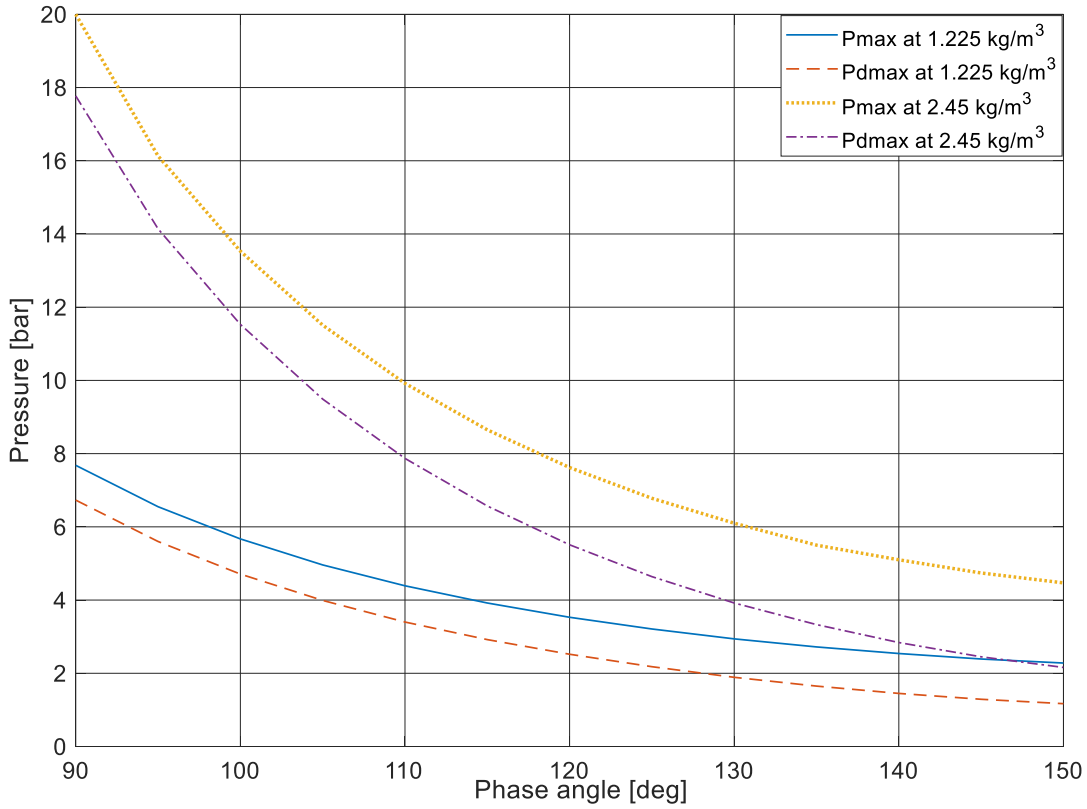

Figure 3-12: Variation of the engine maximum pressure (p_{max}) and maximum pressure difference (p_{dmax}) with phase angle at two gas densities.

3.5 The Franchot-based refrigerator

In this section, the cylinder heated/cooled Franchot refrigerator is investigated and performance curves are obtained. It has the expansion cylinder temperature below the ambient temperature. Hence, it requires mechanical power instead of generating power and works as a refrigerator instead of a prime mover. Stirling-cycle refrigerators have

a performance that ideally approaches Carnot COP. This ideal performance requires the heat transfer to be infinite to make the gas temperature inside the machine equal to the wall temperature. However, due to the limited heat transfer and the non-isothermal processes, the COP approaches Carnot COP if the cold production decreases for which, the temperature of the working gas to approach the cylinder walls temperature. Due to the absence of a natural maximum, the Franchot refrigerator is assumed to have the same size and geometry as the engine listed in Table 3-1. The model derived in section 3.3.2 and the ideal engine assumptions are applied to the refrigerator. The cooling COP is calculated from equations 3.22 and 3.24 as follows

$$COP = \frac{\dot{Q}_e}{P} \qquad 3.31$$

In this section, the expansion and compression cylinder temperatures are fixed at 280K and 300 K respectively which have a Carnot COP of 14. The Franchot refrigerator has some control variables that can be optimised separately: the phase angle, dead volume, piston diameter and gas density.

3.5.1 Effect of changing the phase angle

In the bare cylinder Franchot engine, the cooling capacity and efficiency are theoretically optimised by changing the phase angle. In Figure 3-13, the P-V diagram of a half Franchot cooler that is a conventional alpha type cooler shows that increasing the phase angle decreases the maximum pressure as well as the added and rejected thermal energies. This reduces the internal heating and cooling loads on the corresponding cylinders and hence the mechanical energy input (total energy).

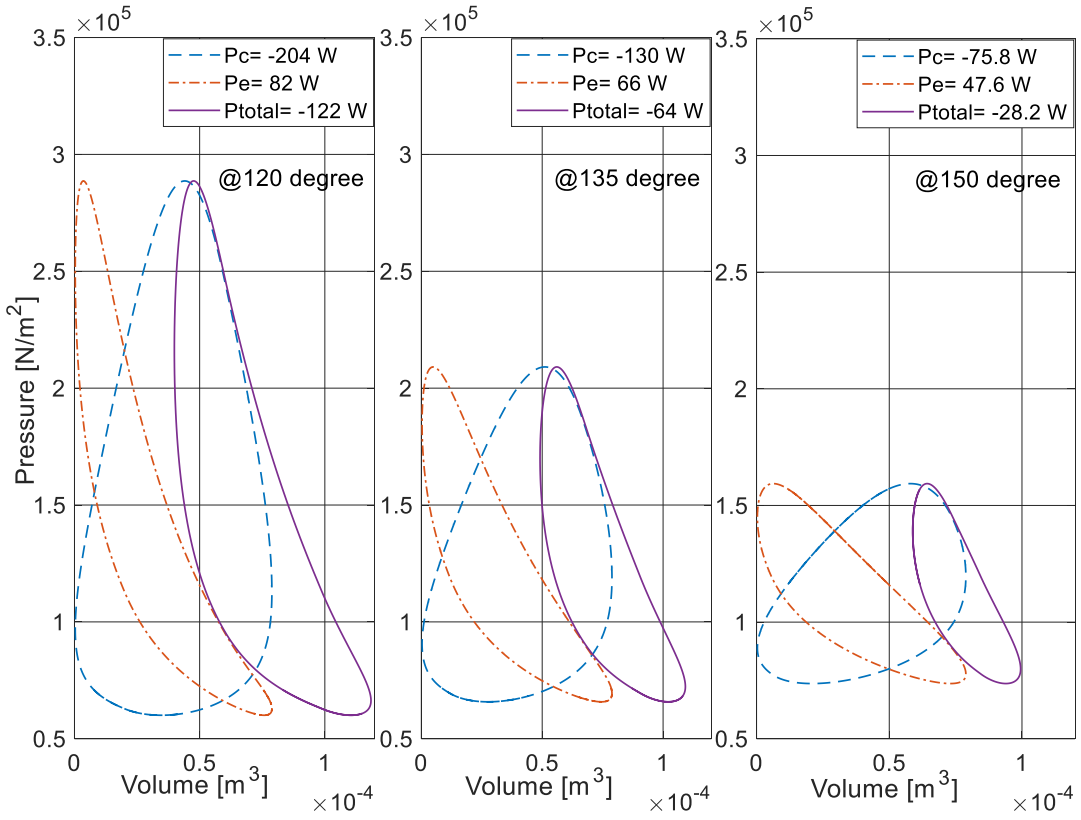

Figure 3-13: P-V diagram of the reference cooling machine at different phase angles.

Figure 3-14 shows the influence of the phase angle on the cooling load and COP of the Franchot-based refrigerator. The cylinder wall heated and cooled Franchot refrigerator has a monotonic response with engine speed and no optimum is found. The COP is enhanced as the phase angle increases and machine speed decreases. Increasing the phase angle decreases the indicated power to heat transfer ratio, which decreases the temperature differences between the gas and cylinder wall hence the cooling load decreases and the COP increases. Increasing the speed enhances the heat transfer at a smaller rate compared to the indicated power. Hence, the cooling rate increases but the COP decreases. Comparing the 170° to 150° phase angle, the 170° achieves a COP = 3.8 and a cooling load of 50 W at 1530 rpm, while the 150° resulted in the same COP = 3.8 but with only 9.5 W of the cooling load at 90 rpm. The increase in the cooling power for the larger angle can be attributed to the increase in the heat transfer due to the speed. At a speed of 1000 rpm, a machine with phase angle of 150° generates cold energy of 92 W but with a COP of 1.65, which is lower than the COP

of the VCC cycle, while the machine performance at 170° is 34 W with a COP of 4.4. Although the speed is fixed, the heat transfer is different, which can be attributed to temperature differences due to gas pressure variations. Increasing phase angle and speed improves the engine characteristics but speed is limited to the prime mover speed and speed related losses. On the other hand, decreasing the speed decreases the cooling power, which requires replicating the cylinders to improve cold production. Therefore, the machine speed would be determined by the prime mover maximum power speed.

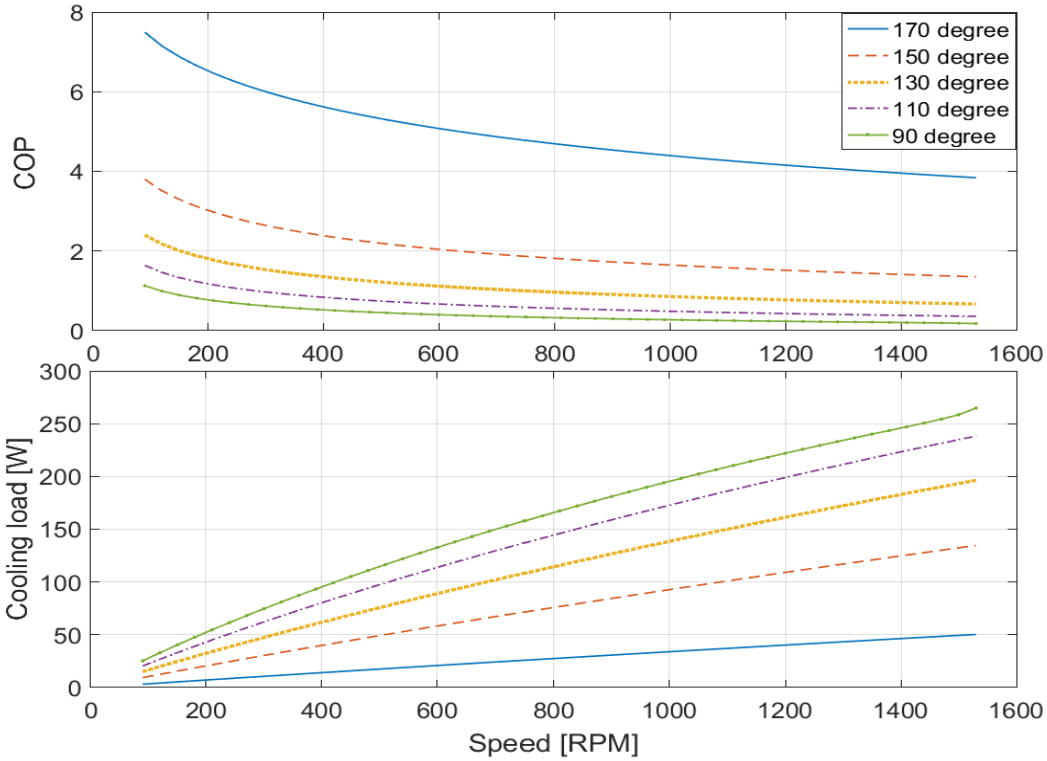

Figure 3-14: Variation of cooling load and COP against machine speed for various phase angles.

3.5.2 Effect of dead volume

Figure 3-15 shows the effect of increasing the expansion and compression dead volume from 25% to 100%. Increasing the dead volume improved the COP but reduced the cooling capacity given that the heat transfer area got larger. The cooling power is reduced due to reducing the pressure variation.

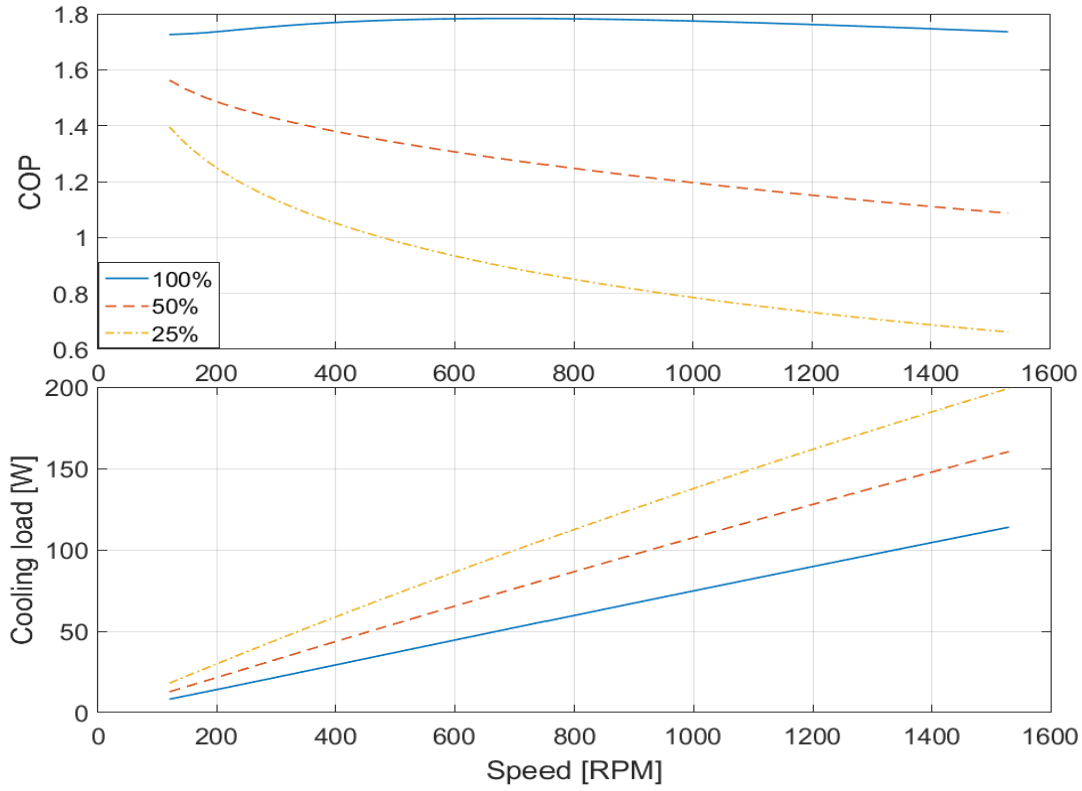

Figure 3-15: Variation of cooling load and COP against machine speed for various dead volume ratios and 90° phase angle.

At 1000 rpm and for equal dead and swept volumes, the machine achieves a COP of 1.77 with a cooling load of 74 W. Interestingly, the same cooling power could be reached with no dead volume by setting the phase angle to 157° which gives a COP of 2.2 (see section 3.5.1). Hence, the phase angle control, which does not increase the heat transfer surface area, is superior to the dead volume control in terms of the thermodynamic performance and geometrical considerations. Therefore, it is better to keep the dead volume as small as possible.

3.5.3 Effect of cylinder diameter

The effect of enlarging the piston diameter of the Franchot-based refrigerator is shown in Figure 3-16. As the diameter increases the cooling power increases but the COP decreases. The increase in cooling power is attributed to the increase in the heat transfer due to increasing Reynold's number. The effect of heat transfer due to the cylinder area is neutralised by the increase in hydraulic diameter (see equations 3.25 and 3.29). The reduction of the COP with the diameter can be explained by the

increased gas to wall temperature difference. The gas temperature variation depends on the swept volume, which linearly depends on the square of the diameter while the heat transfer improves at a slower rate due to Reynold's number (see equation 3.28). At small diameters, the heat transfer is relatively large at a given speed, which increases the COP, but decreases the cooling load. However, small diameters might be difficult to achieve and thus, other methods to increase the COP might be required.

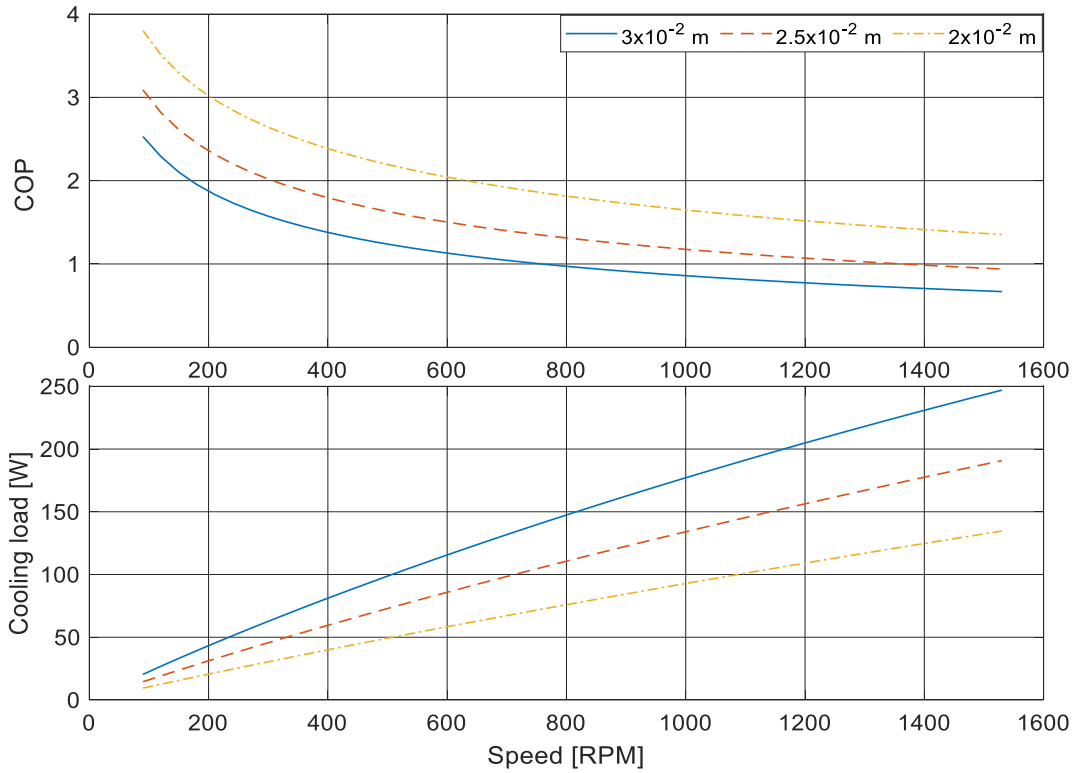

Figure 3-16: Variation of cooling load and COP with machine speed for various diameters.

3.5.4 Effect of gas charge density

Figure 3-17 shows that the gas density increases the load on the prime mover without affecting the heat exchanging area. Increasing gas charge density is equivalent to increasing the speed as both have the same effect on Reynold's number and the power equation. A high COP could be easily obtained with atmospheric charge pressure but at the cost of low cooling capacity. Increasing the charge pressure has the benefit of decreasing the speed due to decreasing mechanical friction losses. However, high pressure needs good sealing, especially across the power pistons to decrease gas leakage losses.

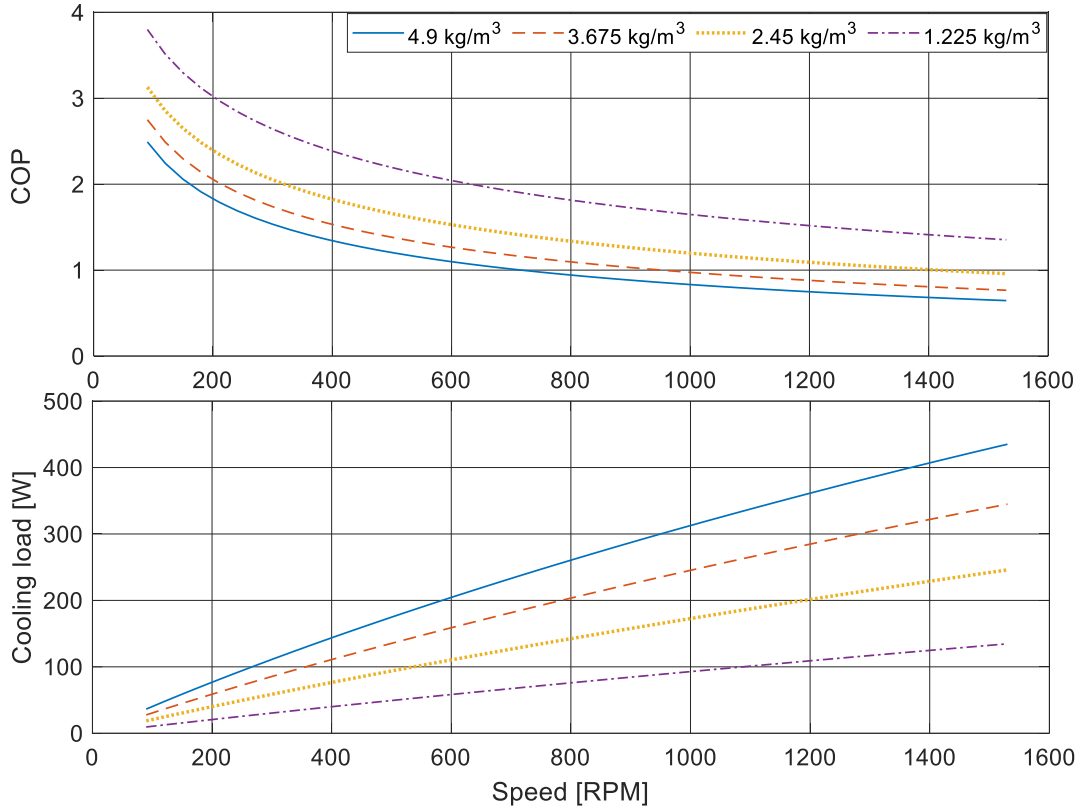

Figure 3-17: Variation of cooling load and COP against machine speed for various charge densities.

3.6 Conclusion

A 2nd order thermodynamic model based on the three-control volume approach with polytropic expansion and compression, limited instantaneous heat transfer and calculated regenerator temperatures has been developed specifically for this study and was implemented in Matlab/Simulink. The model shows good agreement between the maximum power efficiency and the ideal efficiency calculated by Curzon and Ahlborn. The model gives the upper performance expected for the Franchot engine and refrigerator at different machine parameters and working conditions. However, no optimal performance was obtained in this chapter, but many parameters are determined in subsequent chapters such as the phase angle and engine speed and dead volume.

The ideal model shows that working on the maximum power point helps to reduce the engine size hence the cost. Obtaining efficiencies larger than Curzon and Ahlborn's is becoming harder especially when approaching Carnot efficiency. Thus, increasing the

efficiency is mainly affected by increasing the temperature. For the studied temperatures of 600 K and 300 K, the Curzon and Ahlborn efficiency is 29.29% which is 58.6% relative to Carnot efficiency. For the refrigerator, the cooling capability decreases with increasing the COP. Hence, working at high COP and high cooling rates requires increasing the machine size.

Dead volume is found to have inferior characteristics in comparison to the phase angle and is recommended to be as small as possible in both the engine and refrigerator. Pressurising the working gas is equivalent to increasing the speed for the Franchot machine without considering gas losses or forces acting on the pistons. However, the unpressurised machine requires no auxiliary compressor or tight seals, has lower leakage losses, uses simpler materials and is simpler to manufacture. So, using unpressurised air matches one of the goals of this study, which is to simplify the Stirling cycle machine.

The theoretical study revealed that the phase angle is superior to the other control methods for the Stirling-cycle machine. The phase angle can be easily changed, can be used with large diameters, decreases the pressure and pressure differences and improves the performance without adding to the heat transfer area. From the theoretical results of this study, it is possible to increase both engine power and efficiency at lower speeds by varying the phase angle or working gas density. In contrast, the dead volume and piston diameter are difficult to modify after manufacturing.

The engine should always work near the maximum power point to reduce the size hence engine and heat exchanger costs. To obtain a high efficiency beyond Curzon and Ahlborn efficiency, the power density should decrease which will add to the engine drawbacks. The refrigerator has a monotonic response so that its COP increases with decreasing cooling power. As there is no maximum performance, the refrigerator geometry and working conditions are chosen to be the same as those for the engine given that the power ratings for both machines are close.

CHAPTER

4 Isothermalising the Franchot engine

In the previous chapter, the cylinder wall heated/cooled Franchot machine was studied without considering gas friction losses in the machine's cylinders. The machine has limited heat transfer, which is generally improved by increasing the Reynold's number of the gas in the working cylinders. This implies increasing the flow rate of the working gas, which is expected to increase gas pumping losses as the working gas shuttles through the regenerator. Moreover, larger than 90^{o} phase angles and large dead volumes were needed to match the indicated power to the heat transfer as the heat transfer increases slower than the increase in the indicated power. The cylinder wall heating and cooling is simple and benefits from the whole cylinder surface to exchange heat. For these reasons, the power density improvements of the cylinder heated/cooled machine will be discussed in this chapter. The power and efficiency will be enhanced by adding novel simple isothermalisers so that the increase in heat transfer is accompanied with reduced gas flow rates due to reduction in the hydraulic diameter. The isothermalisers have cylindrical geometry that suits the machine introduced in the previous chapter. A parametric study on the effect of the isothermalisers on the cylinder wall heated and cooled Franchot machine has been carried out considering the gas friction losses in the expansion and compression spaces. The optimised response of the Franchot machine with isothermalisers is compared to the bare cylinder, adiabatic and ideal Stirling cycle. Some interesting theoretical results are found that change the perspective of using Stirling cycle machines.

4.1 Introduction

In Section 2.9.3, different methods have been reviewed for isothermalising the Stirling machines. However, none of them is practical for the novel design presented in Chapter 3 for the long heating and cooling path. The interleaving fins must be long

and almost fill the working volume thus, they increase the mass of the reciprocating piston. Two further problems with the interleaving fins are: the exchange of heat with external energy source and conductive heat transfer along the fins. Isothermalising by injecting thermal fluid through slender pipes will not be effective unless many injectors are deployed along the working cylinders, this method does not suit or simplify the novel design especially, when the power needed for injection is larger than the power produced.

4.2 The novel isothermalisers

The piston rod is used to link the engine piston to the connecting rod. It must be designed to withstand the forces acting on it in order to avoid buckling. In the double acting Stirling engine, reducing the piston rod diameter is important as it reduces the swept volume on one side, which must be calculated precisely in order to keep the symmetry on both sides of the piston. The maximum radial force that a piston rod is able to withstand before buckling can be obtained from Euler equation for determining the critical buckling load on struts as [152]

$$F_{max} = \frac{\pi^2 EI}{(kL)^2} \qquad 4.1$$

where, $E, I, k\ and\ L$ are the modulus of elasticity, second moment of area, effective length factor and unsupported length of the piston rod, respectively.

However, an increase in the piston rod diameter will reduce the hydraulic diameter and swept volume, which increases the heat transfer per volume. Thus, acting like a passive isothermaliser, which is not heated or cooled by heat sources. Due to the cylindrical geometry of the piston rod, the hydraulic diameter is fixed along the engine cylinders but the area of the hot and cold external cylinders varies over a cycle based on piston location as shown in Figure 4-1.

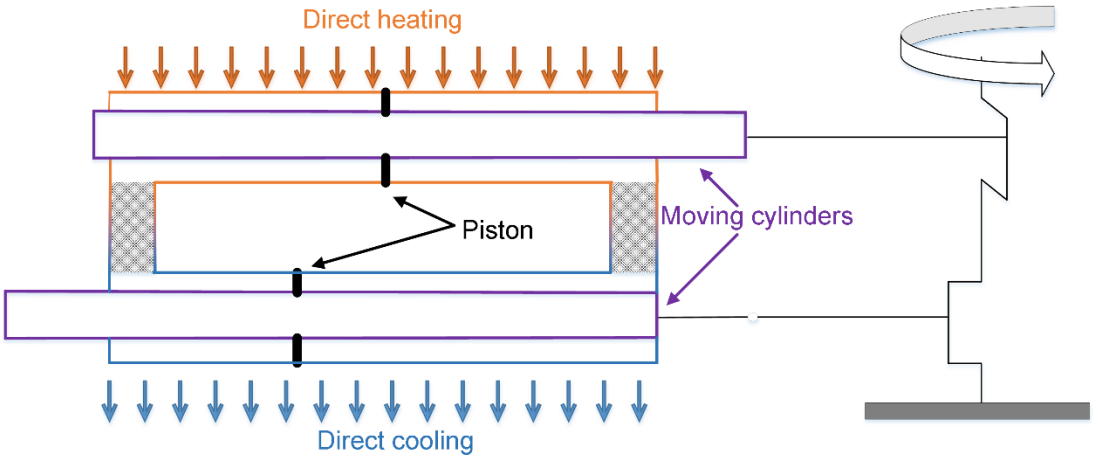

Figure 4-1: The proposed passive isothermalisers (moving cylinders) inside the Franchot engine double-ended cylinders.

Due to the reciprocating nature of the piston rods, heat exchanging between the internal cylinders and external heat sources will be challenging. Supposing no heat transfer from the pistons or piston rod seals occurs, the piston rod only exchanges energy with the working gas by convection. In addition, the cold and hot piston rods are also supposed to be insulated from the ambient air and heat source. Hence, the piston rod, which is externally insulated, has a total heat flow equal to zero

$$\oint \dot{Q}_f = \oint hA_f(T_f - T_g) = 0 \qquad 4.2$$

hence

$$\oint hA_f T_f = \oint hA_f T_g \qquad 4.3$$

where h, A_f, T_f and T_g are the coefficient of heat transfer, internal cylinder area, internal cylinder temperature and gas temperature, respectively.

The fluctuation in the piston rod temperature is ignored because of the higher heat capacity of the stainless steel in comparison to air. Hence, the rod temperature is supposed to be constant during a cycle. So, the average temperature of the piston rod (passive isothermaliser) can be calculated as

$$T_f = \frac{\oint hA_f T_g}{\oint hA_f} \qquad 4.4$$

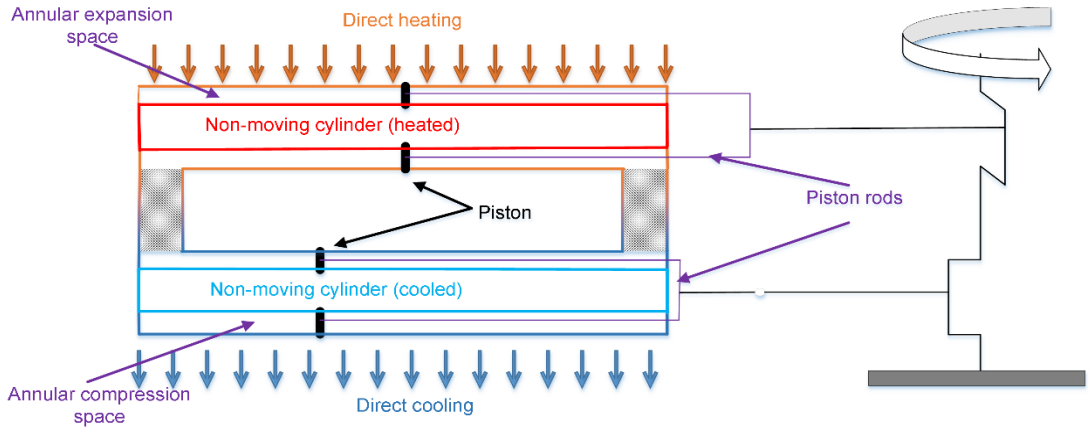

Figure 4-2: The proposed active isothermalisers (heated and cooled), that is heated or cooled with piston rods, in the gap between the external and internal single-ended cylinders.

The double-ended piston rod as a passive isothermaliser is heavy, long, needs sealing from both rod sides and does not benefit from the rod surface area for heat transfer. However, this configuration results in symmetrical swept volumes, unlike the traditional single-ended double-acting engines. Using heated and cooled internal cylinders (active isothermalisers) instead of the passive isothermalisers will increase the heat transfer by increasing the total heat exchange area in addition to the reduction in hydraulic diameter. While it is possible to cool the cold piston rod as it reciprocates through the air, heating the reciprocating rod in the expansion spaces is hard. However, for space cooling, the expansion cylinder can be fully implemented inside the chilled space and thus, an active isothermaliser for the expansion cylinder can be achieved. Figure 4-2 shows another method for heating and cooling the piston rod by replacing it with a fixed internal cylinder. In this single-ended configuration, the piston rods have small diameters and are linked to the piston from one side. These piston rods are assumed not to affect the heat transfer or swept volume. The piston rod guides are only

sealed from one side and the total engine length is shortened. However, sealing the piston rods is expected to be hard due to the available space. In addition, annular pistons must be used; hence, the piston rubbing area and the gas leakage path are large in comparison to the moving isothermaliser design.

Considering the effect of Reynold's number and Nusselt number on heat transfer (see Equations 3.28 and 3.29). The heat transfer enhancement in the working cylinders due to reduction in the hydraulic diameter can be calculated according to equation 3.30.

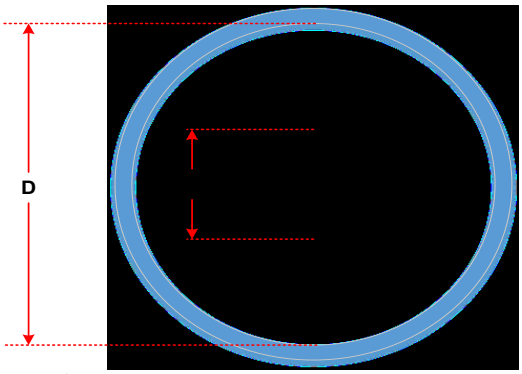

Figure 4-3: A Cross-section of the annular working cylinder.

The hydraulic diameter of the annulus shape (Figure 4-3) is calculated from

$$D_h = \frac{4A}{P} \qquad 4.5$$

where A, P are the cross-sectional free flow area and wetted perimeter respectively. The hydraulic diameter in Equation 4.5 is rewritten as

$$D_h = 4\frac{\frac{\pi}{4}(D^2 - d^2)}{\pi(D + d)} = D - d \qquad 4.6$$

4.3 Gas friction loss

Gas friction inside the heat exchangers is an important factor that affects the Stirling engine design limits. The pumping loss due to gas friction in the heat exchanger may undermine the engine performance. A heat exchanger with the highest possible heat transfer rate is accompanied by large pumping losses. On the other hand, a heat exchanger with poor heat transfer is possible with negligible pumping losses. Thus, compromising between the heat transfers and pumping losses is important to achieve optimal performance.

For the Franchot engine, each cylinder has a constant volume equal to the summation of the dynamic volumes. These cylinders have a constant hydraulic diameter and total length L. The pressure drop in each cylinder is calculated from [231]

$$\Delta p = -\frac{\overline{\tau_w} A_w}{A_{ff}} \tag{4.7}$$

where $\overline{\tau_w}, A_w \; and \; A_{ff}$ are the shear force, flow-wetted area and free flow area, respectively. The flow-wetted area of the annulus cylinder is given by

$$A_w = \pi L(D + d) \tag{4.8}$$

The free flow area of the annulus cylinder is given by

$$A_{ff} = \frac{\pi(D^2 - d^2)}{4} \tag{4.9}$$

Hence, the pressure drop in Equation 4.7 is written as

$$\Delta p = -\frac{4\overline{\tau_w}L}{D-d} = -\frac{4\overline{\tau_w}L}{D_h} \quad 4.10$$

According to Zhao and Cheng [231], the shear force is given by

$$\overline{\tau_w} = 0.5\overline{C_f}\rho U_{max}^2 \quad 4.11$$

The friction factor $\overline{C_f}$ for a turbulent oscillatory flow regime for a range of stroke to bore ratios of 53.4 -113.5 and kinetic Reynolds number of 81-540 [231] is given by

$$\overline{C_f} = \frac{D_h}{X_m}\left(\frac{76.6}{\left(\frac{2D_h Re_{max}}{X_m}\right)^{1.2}} + 0.40624\right) \quad 4.12$$

where X_m are Re_{max} are the maximum fluid displacement at the maximum engine stroke and maximum fluid Reynolds' number which is obtained from

$$Re_{max} = \frac{D_h U_{max}\rho}{\mu} \quad 4.13$$

where U_{max} is the maximum piston speed which can be calculated based on rotational speed n or average linear piston speed from [228]

$$U_{max} = \pi\frac{X_m n}{60} = \frac{\pi}{2}U_{av} \quad 4.14$$

Hence, the pressure loss can be written as

$$\Delta p = -\frac{2\rho U_{max}^2 L}{X_m}\left(\frac{76.6}{\left(\frac{2D_h Re_{max}}{X_m}\right)^{1.2}} + 0.40624\right) \quad 4.15$$

The power loss in each cylinder is calculated from [232][233]

$$P_{lx} = \Delta p_x \times \dot{v}_x \quad 4.16$$

where $\dot{v}$ is the volumetric flow rate of the working gas at a given compartment.

4.4 Model validation

The polytropic model is applied to the alpha type engine with annular heat exchanger made by Karabulut [234]. The annular heat exchanger has the cylinder walls heated and the piston dome is of passive fin type as shown in Figure 4-4.

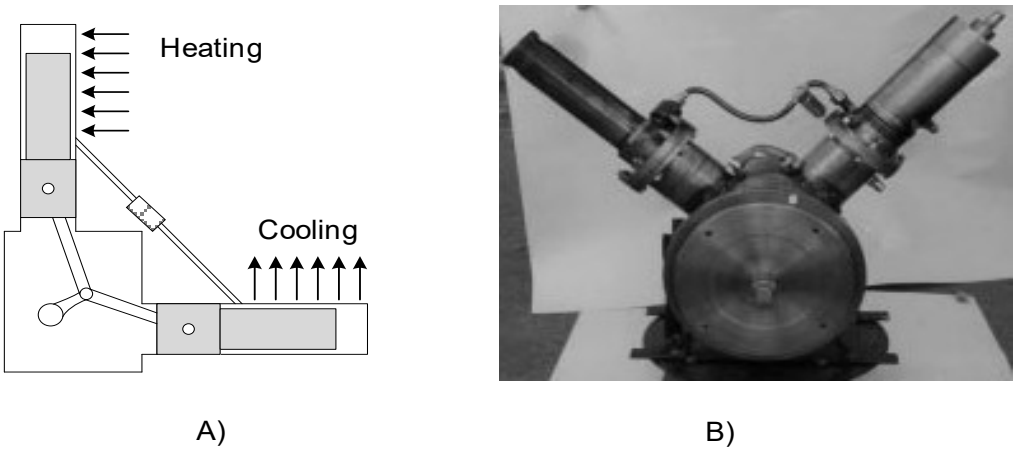

Figure 4-4: Karabulut alpha type engine with annular heat exchangers A) schematic diagram and B) picture of the engine [234].

In the Karabulut engine, the heat exchanging area and volume are constant for the annulus and dynamic for the swept space as the swept volume is sinusoidal. These conditions are replicated in the model for validation purpose. The technical specification of the Karabulut engine is shown in Table 4-1.

Table 4-1: Technical specifications and operating conditions of the Karabulut engine [234].

Name	***value/unit***
Stroke length	$6 \times 10^{-2}\ m$
Bore diameter	$5.24 \times 10^{-2}\ m$
Piston dome diameter	$4.74 \times 10^{-2}\ m$
Hot annulus length	$13.5 \times 10^{-2}\ m$
Cold annulus length	$11 \times 10^{-2}\ m$
Connecting pipe length	$30 \times 10^{-2}\ m$
Connecting pipe diameter	$0.5 \times 10^{-2}\ m$
Regenerator matrix	*Woven wire*
Wire diameter	*100 micron*
Regenerator porosity	*0.7*
Regenerator volume	$12 \times 10^{-6}\ m^3$
Out-of-Phase angle	90^o
Hot, cold temperatures	$1100^o\ C, 20^o\ C$
Working gas	*Air*
Average gas pressure	*1 bar, 2 bar*

To increase the accuracy of the model, the reheat and pressure losses of the regenerator are considered. The effect of having imperfect regeneration is considered by modifying the regenerator gas stream temperatures as [235][194]

$$T_{rho} = T_{rk} + \varepsilon(T_{rh} - T_{rk}) \qquad 4.17$$

$$T_{rko} = T_{rh} - \varepsilon(T_{rh} - T_{rk}) \qquad 4.18$$

where, T_{rho}, T_{rko} and ε are the hot outlet gas temperature, cold outlet gas temperature and regenerator effectiveness, respectively. The enthalpy loss can be quantified by

$$\dot{Q} = c_p \dot{m} \Delta T (1 - \varepsilon) \quad 4.19$$

The effectiveness is calculated according to Tanaka [236] by

$$\varepsilon = \frac{Ntu}{Ntu + 2} \quad 4.20$$

where Ntu is the number of transfer units (indicative of the size of the heat exchanger) and calculated from

$$Ntu = \frac{4\overline{Nu}L_r}{P_r \overline{R_e} d_h} \quad 4.21$$

where $\overline{Nu}, P_r, \overline{R_e}$ and d_h are the average Nusselt number, Prandtl number, average Reynolds number and regenerator hydraulic diameter, respectively. Nusselt number is correlated according to Tanaka as follows

$$\overline{Nu} = 0.33 \overline{R_e}^{0.67} \quad 4.22$$

The pressure loss due to the gas friction with the regenerator material is calculated from

$$\Delta p_{loss} = -\frac{0.5 f_h \rho L_r U^2{}_{max}}{d_h} \quad 4.23$$

where Δp_{loss} is the pressure loss and f_h is the friction factor calculated according to Tanaka from

$$f_h = 1.6 + \frac{175}{Re_{max}} \tag{4.24}$$

The pressure loss due to the connecting pipe is calculated as

$$\Delta p_{loss} = -\frac{2 f_{Re} \mu L_r U_{av}}{d_h} \tag{4.25}$$

where $f_{Re}, \mu, L_r \; and \; d_h$ are the friction factor, dynamic viscosity, connecting pipe length and pipe hydraulic diameter, respectively. f_{Re} is calculated by [232]

$$f_{Re} = \begin{cases} 16 & Re < 2000 \\ 7.343 * 10^{-4} Re^{1.3142} & 2000 < Re < 4000 \\ 0.0791 Re^{0.75} & Re > 4000 \end{cases} \tag{4.26}$$

The mathematical model is applied to Karabulut engine at a range of speeds and two pressures. The comparison between the polytropic model and experimental study is shown in Figure 4-5. The polytropic model has good agreement with the experimental results especially in predicting the trend of engine performance and location of the power peak values. The maximum relative error was calculated as +22% and +30% for the 1 and 2 bar data sets, respectively. Those errors can be attributed to the roughness of the experimental data, the lack of data about gas leakage and mechanical friction. The good agreement shows that the model is able to predict Stirling machine performance.

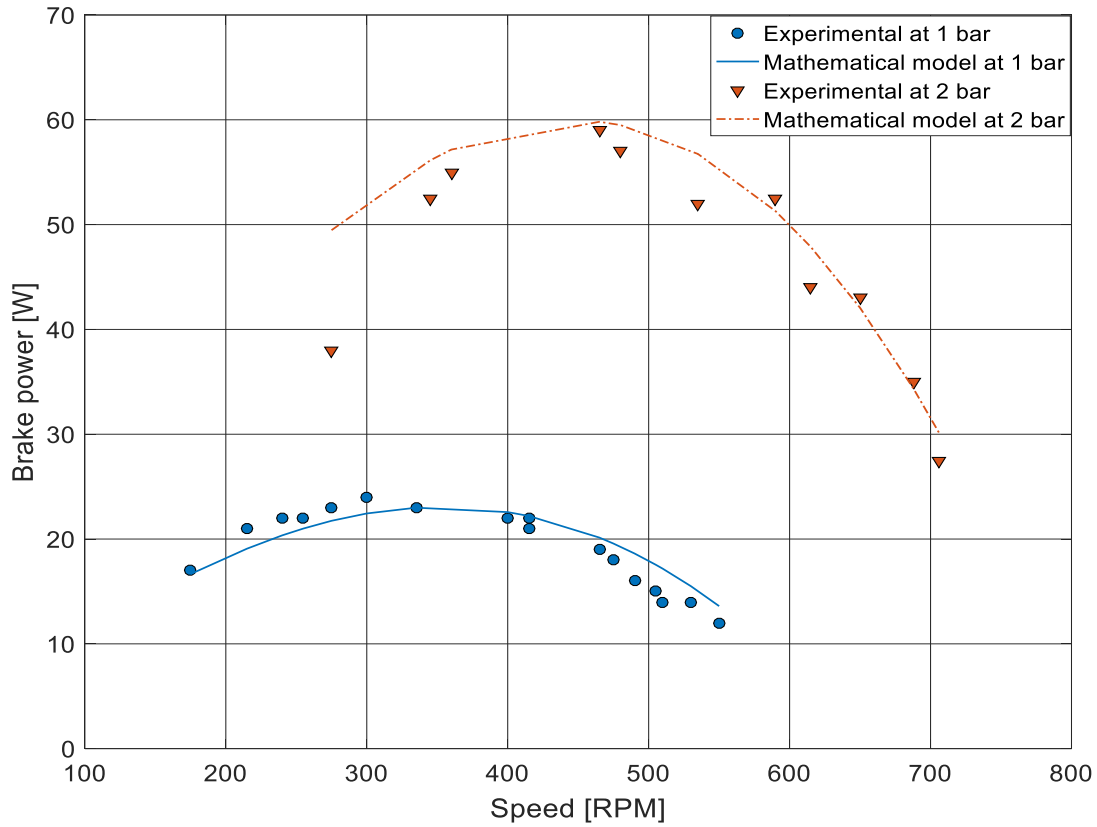

Figure 4-5: Comparison between the 3 control volume polytropic model with regenerator losses and experimental data of Karabulut alpha type engine [234].

4.5 Parametric response

The following study is performed with constant cylinder temperatures. The heat transfer and gas friction loss in the working cylinders are considered. The model is implemented in Matlab/Simulink and solved using the Runge-Kutta method with a time step of 10^{-4}s. All results in this chapter use the reference engine parameters listed in Table 4-2 unless otherwise stated. The Reynolds numbers for Figure 4-8-Figure 4-11 are within the range 1465-15500 and Figure 4-12 has a minimum Reynolds number of 734 for the engine with passive isothermaliser and a maximum of 24530 for the bare cylinder engine in which the gas friction losses are ignored.

Table 4-2: Parameters of the reference engine with isothermalisers

Name	***symbol***	***value/unit***
Stroke length	L_e, L_c	$50 \times 10^{-2}\ m$
Bore diameter	D_e, D_c	$5 \times 10^{-2}\ m$

Charge gas density	ρ	*1.225 kg/m³*
Clearance length	re, rc	0.1×10^{-3} *m*
Gas constant	R	*287 J/kg.K*
Phase angle	θ	90^{o}
Hot, cold temperatures	T_h, T_k	*450 K,300 K*
Working gas	*Air*	

4.5.1 Influence of the passive isothermalisers

Figure 4-6 shows the power increasing with increasing speed until it reaches a maximum. The power drops with speed beyond the maximum because of the inadequate heat transfer at high speeds and the increase in pumping losses due to gas friction, which increase faster than the indicated power. However, gas friction might be ignored up to the maximum power point as it makes less than 5% of the indicated power. The power increased as a function of the piston rod diameter. This can be explained by the increase in heat transfer rate per unit volume, which is due to the decrease in the hydraulic diameter. The increase in heat transfer increases the efficiency at any given speed and moves the maximum power point to larger speeds.

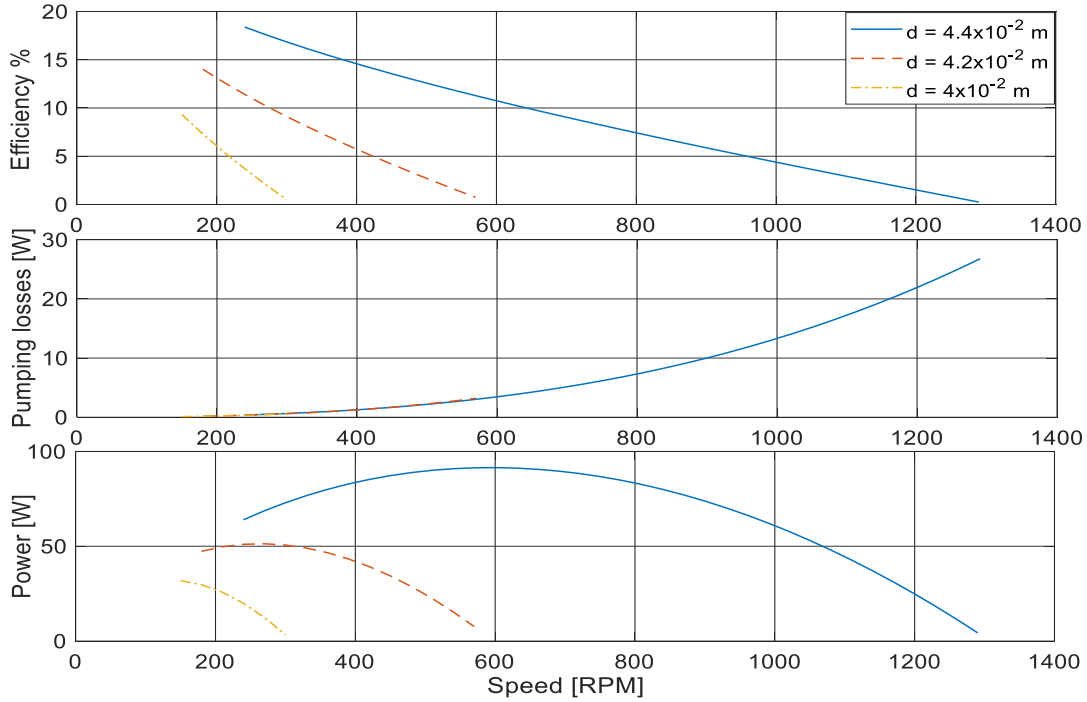

Figure 4-6: Influence of increasing the passive isothermaliser diameter on the Franchot engine performance.

4.5.2 Influence of the active isothermalisers

The influence of changing the internal cylinder diameter on the performance of the Franchot engine with active isothermalisers is shown in Figure 4-7. The power increases with increasing speed until reaching a maximum before dropping to zero. In comparison to the passive isothermaliser design, the power is increased by a factor more than 2 at the maximum. The increase can be attributed to the enhanced heat transfer due to the participation of the internal cylinder area and the increase in the engine speed. Due to the same flow-wetted area, the gas friction losses are the same for both the passive and active isothermalisers at every single speed. However, at the maximum power point the pumping losses are larger in the engine with active isothermaliser due to the higher speed.

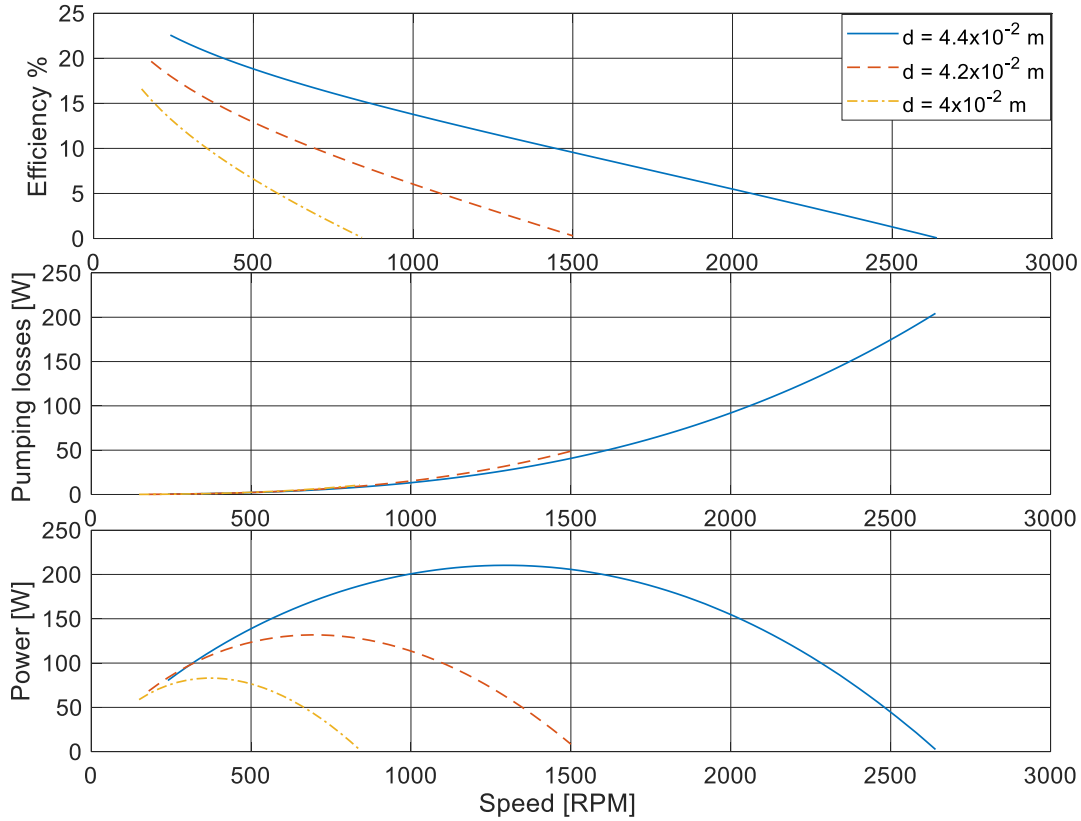

Figure 4-7: Influence of increasing the active isothermaliser diameter on the Franchot engine performance.

Figure 4-8 shows the influence of doubling the working cylinder diameter for different internal cylinders on the performance of the Franchot engine with speed. It shows an

increase in the power without affecting the efficiency or the speed compared to the results in Figure 4-7. The power is enhanced linearly with total heat transfer surfaces for the same speed range and hydraulic diameters. The 10×10^{-2} m diameter engine represents dual 5×10^{-2} m engines at the same hydraulic diameter which gives twice the swept volume. However, the 10×10^{-2} m diameter engine has slightly larger than double the surface area due to the internal cylinder surface. This increases both the power and friction losses by a factor slightly larger than two with doubling the external diameter if the hydraulic diameter is unchanged. A simple increase in the internal cylinder diameter from 9×10^{-2} m to 9.4×10^{-2} m leads to an increase in the maximum power of around 3 folds. Although the internal diameter has been slightly changed, the hydraulic diameter is significantly decreased which increases the heat transfer rate and hence the operating speed. Thus, trebling the power can be attributed to the increase in the speed and heat transfer rate. A further increase in the internal diameter will increase the power, which might require increasing the piston rods diameters or number of rods to avoid buckling.

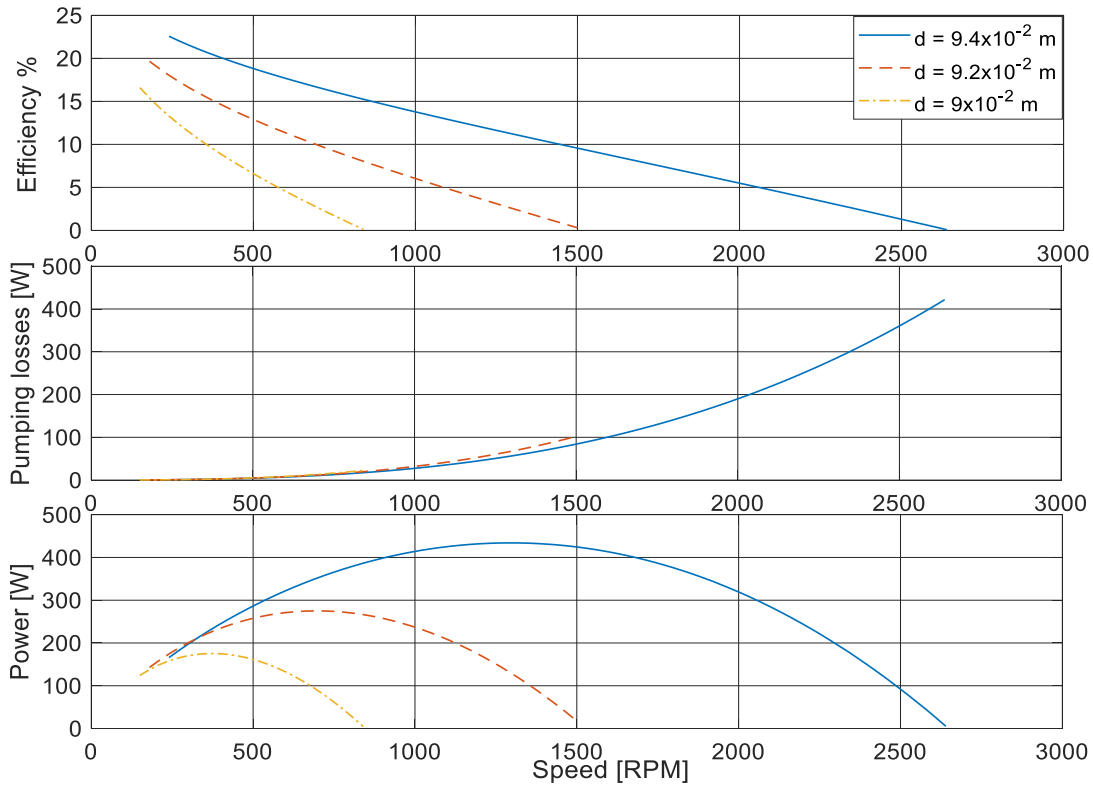

Figure 4-8: Influence of increasing the active isothermaliser diameter on the Franchot engine performance for doubled Franchot engine at cylinder diameter of $0.1\,m$.

The effect of doubling the stroke on the performance of the Franchot engine is shown in Figure 4-9. Although the area is doubled, the generated power of the 1 m stroke is more than twice of the 0.5 m stroke. This is because of the increased heat transfer rates due to doubling the linear velocity. For doubling the stroke, the power improvement at the 4×10^{-2} m internal cylinder is better than that for 4.2×10^{-2} m and 4.4×10^{-2} m in comparison to the 50×10^{-2} m stroke. It is also noticeable that the maximum power point shifted to higher speeds for the 4×10^{-2} m and 4.2×10^{-2} m internal cylinder, while the maximum power speed for the 4.4×10^{-2} m internal cylinder is almost unaffected. This can be attributed to the pumping losses that resist the motion. Interestingly, it is important to consider gas friction in long strokes even at the maximum power point. For d= 4.4×10^{-2} m, the gas friction loss is 152 W which is comparable to the indicated power of 483 W. Therefore, using multiple cylinders or enlarging the diameter instead of elongating the cylinder would be a suitable alternative for increasing the power and reducing the pumping losses.

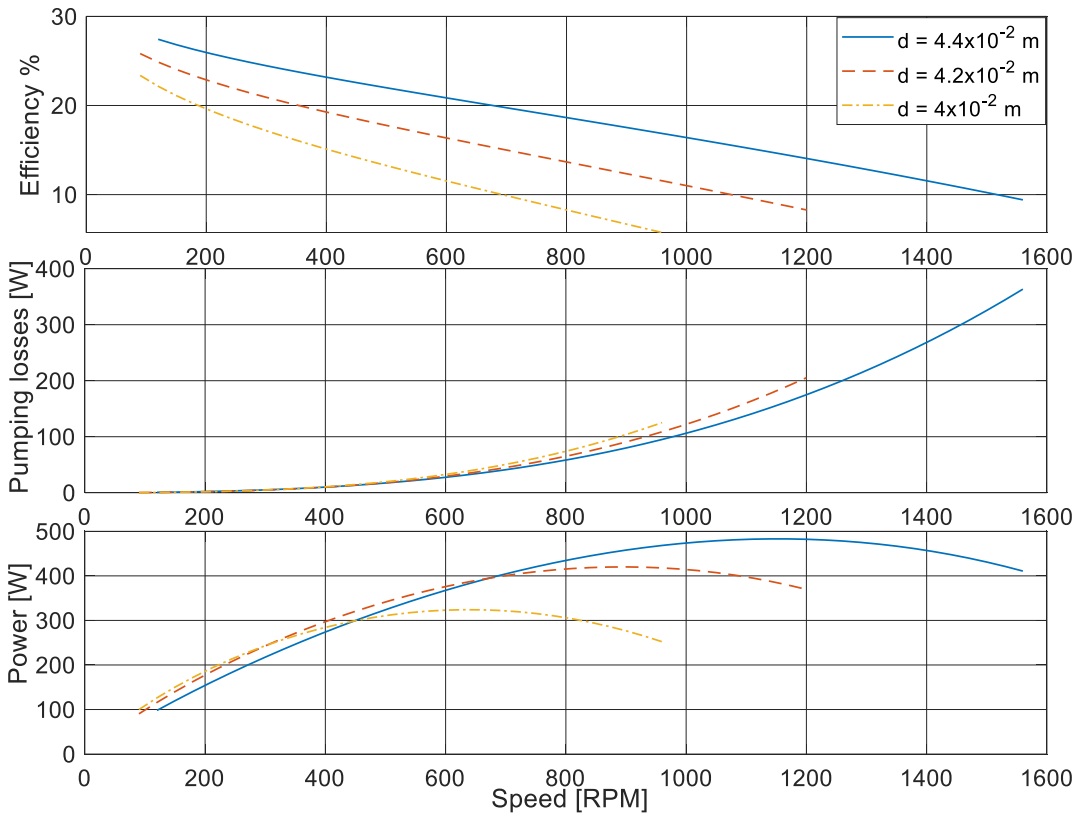

Figure 4-9: Influence of increasing the active isothermaliser diameter on the Franchot engine performance for doubled Franchot engine cylinder length of 0.1 *m.*

4.6 Multi-cylinder engine

Separating the large working cylinder into multiple small cylinders increases the area to volume ratio, which might help in increasing the heat transfer and hence the power generated. The basic engine with active isothermaliser having internal cylinder diameter of 4×10^{-2} m and outer cylinder diameter of 5×10^{-2} m is transformed into multiple cylinders as follows: six cylinders of 1.5×10^{-2} m diameter, seven of 1.28×10^{-2} m, eight of 1.125×10^{-2} m and nine of 1×10^{-2} m diameter. Thus, the total surface area of the multiple cylinders is constant and equals the summation of the external and internal cylinder areas.

Figure 4-10 shows that the multi-cylinder engine performance lies behind that of the active isothermalisrs except for the 9-cylinder engine. They both have the same performance due to the same hydraulic diameter and total swept volume. The performance curves clearly show that the hydraulic diameter is more important than the heat exchanging area itself. That is because the heat transfer rate increases with the hydraulic diameter while swept volume decreases. Manufacturing of multiple cylinders is expected to be more challenging than an engine with isothermalisers due to the number of regenerator connections, pistons, cylinders and piston seals. Also, the theoretical results show that multiple cylinders do not provide better performance than that with using isothermalisers. However, exceptional mechanical and operational characteristics of the engine could be achieved for multi-cylinder engine and are studied in chapters 5, 6 and 7.

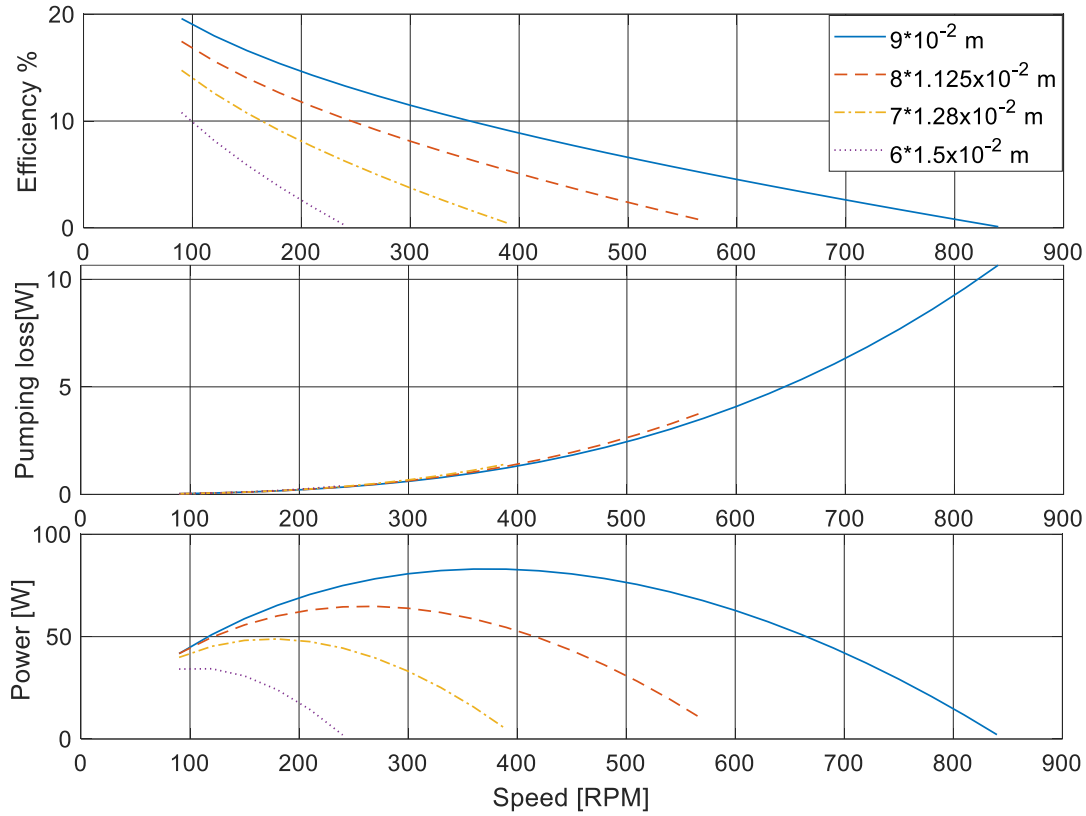

Figure 4-10: the influence of increasing the number of cylinders and keeping the total wall area unchanged.

4.7 The optimised response

In chapter 3, the power improvement by optimising the phase angle was found superior to other methods. The phase angle is easier to change than the piston rod diameter or the number of cylinders for increasing the power. However, using a large phase angle like 150° is far from the recommended phase angles of 90° to 120°. Increasing the phase angle decreases the variation in the engine volume and hence the generated power.

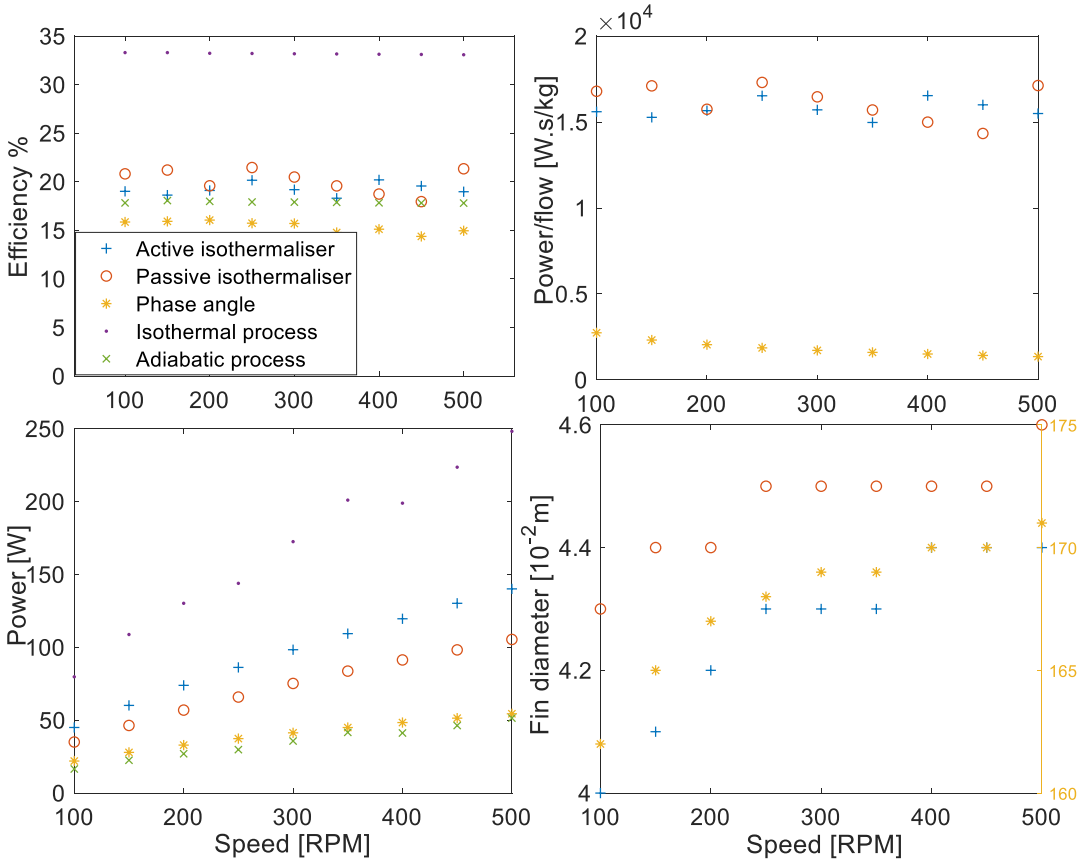

Figure 4-11: Optimised response based on the maximum power for the Franchot engine using passive isothermaliser, active isothermaliser, isothermal processes, adiabatic processes and the bare Franchot engine controlled by the phase angle.

Figure 4-11 shows the optimised response of the system at the maximum power point for different design parameters: phase angle for plain cylinder and internal cylinder diameter of the isothermalised engines. The response of the engine with isothermal and adiabatic expansion and compression processes is shown for comparison. The active-isothermalised, passive-isothermalised and bare-cylinder engines were optimised separately and thus they have different swept volumes. Both the ideal isothermal and adiabatic engines have the same swept volume as the active-isothermalised engine Optimisation of the Franchot engine described in Table 4-2 was performed manually until the maximum power is reached for the speed range 100-500 rpm. Every single speed, phase angle and piston rod diameter was changed with a step size of 50 rpm, 1 degree and 1×10^{-3} m, respectively. The adiabatic-process engine was optimised for the maximum power by increasing its regenerator dead volume with a step size of 10^{-5} m^3. The step sizes are believed to be responsible for the roughness in the figures generated.

It is shown that isothermalising the Franchot engine is superior to the bare engine controlled by the phase angle in terms of power and efficiency. The isothermalised engines work closer to the Curzon and Ahlborn efficiency at the maximum power than the bare engine controlled by changing the phase angle. In addition to that, the power obtained is higher for the isothermalised engine than the bare engine controlled by the phase angle. That is because the isothermalisers increase the heat transfer coefficient and area, while the phase angle matches the available heat transfer to the power.

It is also shown that the optimal internal cylinder diameter increases with speed. The diameter increases to compensate for the increase in required heat at higher speed by decreasing the hydraulic diameter, where the increase in heat transfer due to increasing the speed is insufficient. It is interesting that the hydraulic diameter of the active-isothermalised engine is larger than that with passive-isothermalisers. That's due to the increase in the heat transfer due to the surface area of the internal cylinder of the active isothermalised engine. Large hydraulic diameter eases adding the piston rods to the configuration described in Figure 4-2.

The engine with active isothermalisers has an average power ratio of 43% of the ideal isothermal engine, which is the same ratio of Curzon and Ahlborn to Carnot efficiency. This means that the engine with the active isothermalisers has the maximum possible power density at the maximum power point given that the isothermal engine is impossible to achieve. In the same regard, the ideal adiabatic engine has lower power and efficiency than the isothermalised engines. On average, the active and passive-isothermalised engines produce 2.75 and 2.11 times the power of the ideal adiabatic engine, respectively although the difference between the efficiencies is small. Thus, the isothermalised engine has potential for power density improvement in comparison to the adiabatic engines.

In comparison to the isothermaliser method at 90^{o} phase angle, the phase angle change method resulted in a much lower power to mass flow rate especially for large angles, which increases regenerator losses (i.e reheat and pressure losses) to power generated. However, using isothermalisers fixes the power to mass flow rate to a constant value

by decreasing the swept volume, which allows higher power capabilities at higher speeds. Technically, the bare cylinder design has a larger hydraulic diameter that eases the sealing of the piston rods and pistons. The engines with passive isothermalisers have larger and twice the number of piston rod seals, which increases gas leakage in comparison to the bare-cylinder engine. Moreover, the heavy piston rods are expected to increase the vibrations of the Franchot engine with two cylinders. The active-isothermalised engine in single-ended cylinders has annulus shaped working volume, which requires good sealing to prevent gas leakage across the power pistons. Sealing the piston rods of the active-isothermalised engine might be difficult due to the small hydraulic diameter and the number of piston rods. Also, higher heat transfer compared to the bare cylinder requires good external heat exchanging mechanisms to reduce temperature gradients.

4.8 The isothermalised refrigerator response

The active isothermalisers have potential in direct space cooling. The expansion and compression cylinder can be exposed to the chilled space and the ambient, respectively. Here, the refrigeration cycle is investigated for expansion and compression cylinder temperatures of 280/300 K. Since the Stirling refrigerator COP has a monotonic response with the cooling demand (see section 3.5) the parameters are chosen based on the optimised parameter of the prime mover in the previous section. The prime mover and the refrigerator have the same phase angle, speed, dead volume, stroke and geometry.

Figure 4-12 shows the response of the Franchot refrigerator for different design parameters: phase angle for plain cylinder and internal cylinder diameter for the isothermalised refrigerator. The response of the ideal isothermal machine that has isothermal expansion and compression processes and the adiabatic machine in which the heaters and coolers are isothermal and the expansion and compression processes are adiabatic is shown for comparison. Both the ideal isothermal and adiabatic machines have the same swept volume as the active-isothermalised one. The isothermal cycle presents the maximum possible performance, which result in the

largest cooling power and a COP of 14. Active-isothermalised and passive-isothermalised refrigerator, which have the same heat exchange area as the bare engine, are superior to the phase angle-controlled refrigerator as they achieve higher cooling power at a given efficiency. However, the input power consumption is higher for the active-isothermalised refrigerator than the passive-isothermalised refrigerator due to the higher swept volume of the former one.

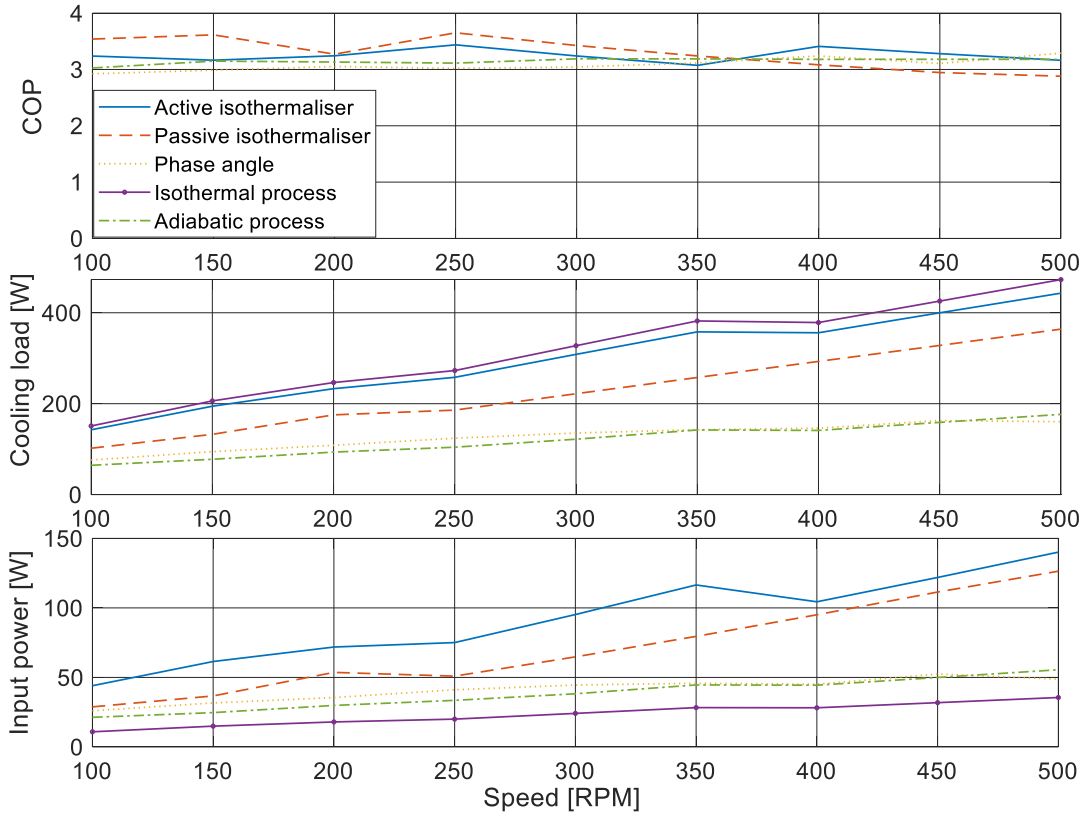

Figure 4-12: Response of the Franchot cycle cooler using passive isothermaliser, active isothermaliser, isothermal expansion, adiabatic expansion and the bare Franchot cooler controlled by the phase angle.

In comparison to the ideal machine with isothermal processes, the machine with active isothermalisers has slightly lower cooling power but has much lower COP. However, the ideal COP is never achievable. In this regard, the ideal adiabatic refrigerator has lower cooling power than the isothermalised refrigerators at nearly the same COP. On average, the active and passive-isothermalised refrigerators have 2.5 and 1.9 times the cooling power of the ideal adiabatic refrigerators at COP of 3.25 and 3.29,

respectively. Also, they have an average cooling power of 94% and 72% of the ideal Stirling-cycle refrigerators, respectively. Interestingly, their consumed power is comparable to the power generated by the prime mover of the same geometry. Hence, the Stirling-cycle heat driven machine would be suggested for near ambient cooling and low temperature activation.

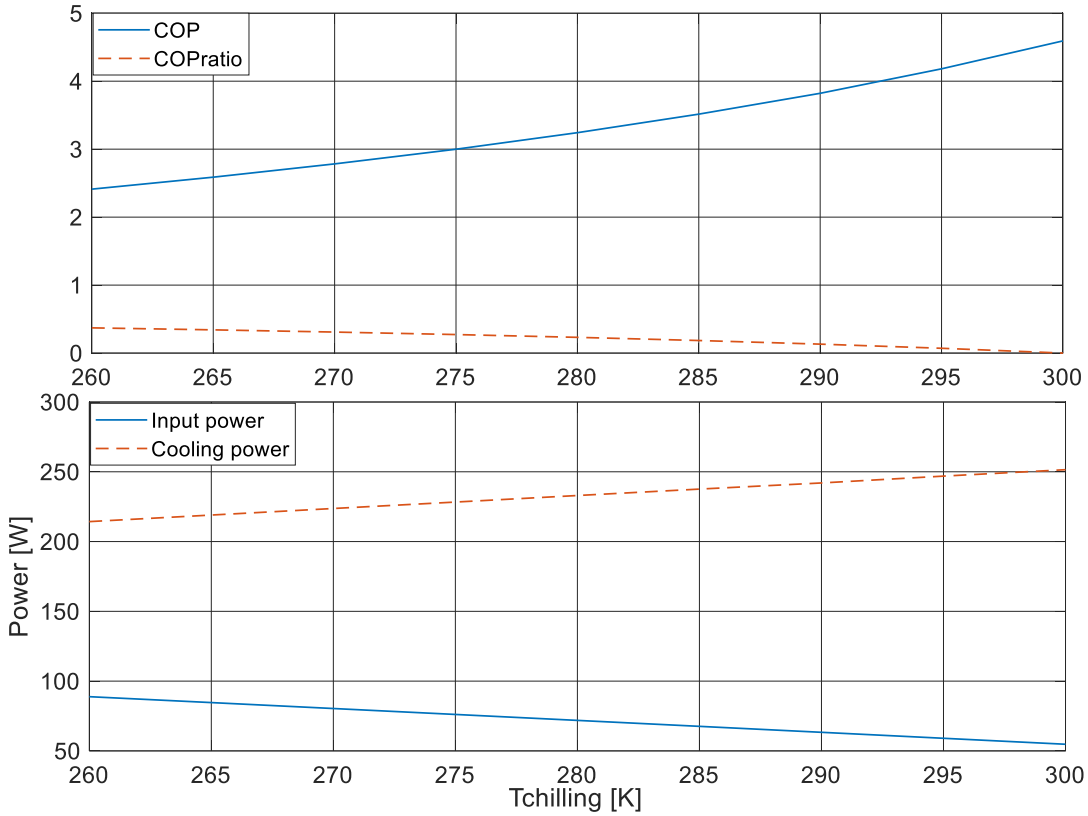

Figure 4-13: Effect of increasing the chilling temperature on the COP, COP ratio, input power and cooling power of the machine with active isothermaliser at $T_k = 300\ K, n = 200$ *rpm and* 0.042 *m internal cylinder diameter.*

For near ambient cooling, the engine with active isothermaliser has a COP range comparable to that of the VCC as shown in Figure 4-13. The polytropic cycle has greater potential compared to the adiabatic cycle for near ambient cold production. The power consumed by increasing the temperature, at which the cold side operates, can cause the prime mover to speed up hence eventually will reach a steady operating point. On the other hand, decreasing the load temperature increases the required power and hence the engine is anticipated to decelerate. The COP ratio, which is the actual

COP to Carnot COP (Equation 2.4), reaches zero at load temperature equal to the ambient temperature although the COP is maximum. The reason for this is that the gas temperature in the polytropic engine needs to be different from the wall temperature for the heat transfer to take place while the temperature difference in the ideal machine is zero.

4.9 Conclusion

Performance investigations using validated mathematical models are done for both the bare and isothermalised Franchot engine by considering the gas friction in the compression and expansion cylinders. The power and efficiency were improved by using active and passive isothermalisers and the Curzon and Ahlborn efficiency is achieved regardless of the friction losses once the power is optimised at every single speed. It is shown that the gas friction losses in the compression and expansion spaces can be ignored for short strokes at the maximum power point. The single cylinder with active isothermalisers is thermodynamically equivalent to the multi-cylinder engine when they have the same heat transfer area and swept volume. However, changing the diameter with speed cannot be done once the engine is manufactured.

Adjusting the phase angle improves the power density and efficiency without the complexity of the isothermalisers but without reaching the Curzon and Ahlborn efficiency in most cases. Large phase angles can be considered with attention given to the regenerator losses due to the mass flow rate. Large phase angles are highly recommended if large hydraulic diameters are needed. Large diameters ease the addition of the piston rods and reduce the number of required machines to achieve a certain power.

The machine with isothermalisers resulted in a higher power to mass flow rate in comparison to the bare cylinder machine for both the engine and refrigerator, which relatively decreases regenerator losses. The simulations show that the isothermalised Franchot engine can achieve the Curzon and Ahlborn efficiency and has the potential to enhance the performance of Stirling engines without using complex heat

exchangers. The active and passive isothermalisers achieve an average of 2.75 and 2.11 higher power density than the adiabatic engine, respectively. The active and passive-isothermalised engines are superior to the adiabatic engine in terms of the power density and hence the regenerator losses. The performance of the Stirling-cycle refrigerator is comparable to the conventional VCC in terms of the COP and has higher power density than the adiabatic cycle refrigerator of an average of 2.5 and 1.9, respectively.

The active-isothermalised machine is expected to have sealing difficulties, especially for small hydraulic diameters and multiple piston rods. Moreover, heating/cooling the internal cylinder adds to the machine complexity. On the other hand, the passive isothermalised machine uses large diameter piston rods, which increase the gas leakage and rod mass. Thus, vibration will be more pronounced due increasing the rod mass.

CHAPTER

5 Multi-cylinder arrangement

In chapter 4, the theoretically studied single-cylinder engine increases the power generated by a factor equal to the number of engines. In this chapter, the multi-cylinder Franchot engine is presented where each pair of hot and cold cylinders has two distinct regenerators. This transforms the engine into multiple independent engines. These engines are distributed around the crankshaft of a slider-crank mechanism to provide unique mechanical characteristics such as self-starting capability and vibration reduction. The slider-crank mechanism is considered in the inline configuration with the Franchot engine cylinders to shorten the regenerator connections, as all cylinders are parallel to each other. The phasor diagram is used here to represent the swept volume and phase angle of the hot and cold spaces, which is referred to in red and blue, respectively. The smallest mechanical angle between any two Franchot engines, which are distributed around the crankshaft, is referred to as the phase shift. The phase angle is the angular mechanical shift between each hot and cold cylinder in a Franchot engine.

5.1 Introduction

There is a lack of research on the start-up of Stirling engines. A kinematic Stirling engine can start up if the total work over a complete cycle is positive [111]. A single-acting Stirling engine with kinematic drive generates negative power sectors of crankshaft rotation due to the compression stroke. To guarantee the power hence motion continuity, a flywheel is commonly used to overcome the negative power sectors of crankshaft rotation and reduce generated harmonics by using some of its stored kinetic energy [237]. For the start-up of kinematic Stirling engines, an external mechanical energy source should be adequate to bring the engine to a certain speed

because otherwise, the engine will not complete a full rotation before being brought to a full stop. The stored energy in a solid cylinder flywheel is given by

$$k_e = 0.5\, J\, \omega^2 \qquad 5.1$$

where J and ω are the flywheel moment of inertia and angular velocity, respectively.

The flywheel kinetic energy decreases quadratically with speed. Therefore, the stored energy might not be sufficient to compensate the negative energy needs by the Stirling engine, which causes the engine to stop even if the total cycle power is positive. If the energy needed is larger than the energy stored in the flywheel, the starting mechanism needs to bring the engine to a higher speed or to use a flywheel with larger moment of inertia.

Here, a strict assumption is made that not only the average power should be positive but also the instantaneous power generated by the engine should always be positive. This implies that the average power is positive and the engine-starts up if there is no negative power portion at low speeds at which the kinetic energy of the flywheel is negligible. The instantaneous power will be used to check the power continuity and power pulses that cause torque pulsations on the crankshaft of a slider-crank mechanism without a flywheel. The instantaneous power represents the instantaneous torque as the speed of rotation is assumed constant over one complete cycle. At start-up or when the engine accelerates the direction of rotation will not change hence, the sign of power portions will be the same as that of the torque. Vibrations due to reciprocating masses and rocking couples are judged based on the phasor diagram and cylinder arrangement.

The total power transferred to the crankshaft of a Franchot engine is the summation of power generated by Stirling engines on both sides of the pistons. Assuming the engine is symmetrical for both sides, the power of the opposite Stirling engine is the power of a Stirling engine shifted by an angle of 180^o. Hence, the instantaneous power of the

Franchot engine will be calculated by considering only one side of the Franchot engine. The ideal instantaneous power given by Equation 3.20 is rewritten as

$$P_{ins} = (p - p`)(\dot{v}_e + \dot{v}_c) = p(\dot{v}_e + \dot{v}_c) + p`(\dot{\grave{v}}_e + \dot{\grave{v}}_c) \qquad 5.2$$

where (`) represents the variables of the opposite piston side. Hence, the total instantaneous power of a Franchot engine is

$$P_{ins} = p(\dot{v}_e + \dot{v}_c) + \ p(\dot{v}_e + \dot{v}_c)\angle 180^o \qquad 5.3$$

where the second part of the equation is the instantaneous power of a Stirling engine shifted by 180°. Similarly, the instantaneous power of any Franchot engine that has one hot and one cold cylinder can be obtained based on the phasor diagram for different phase shifts by

$$P_{ins} = [p(\dot{v}_e + \dot{v}_c) + \ p(\dot{v}_e + \dot{v}_c)\angle 180^o]\angle \theta_s \qquad 5.4$$

where θ_s is the phase shift between a Franchot engine and a reference engine at an arbitrary zero position. By considering only one alpha engine, the number of variables, complexity of the model and simulation time are reduced.

The model is implemented in Matlab/Simulink and solved using the Runge-Kutta method with a time step of $10^{-4}s$. The instantaneous powers were generated in a cycle at steady condition, which is reached after around $9.5s$. All results are obtained mathematically for predicting the Franchot engine performance and use the reference engine parameters listed in Table 5-1 unless otherwise stated.

Table 5-1: Parameters of the reference multi-cylinder engine

Name	***symbol***	***value/unit***
Stroke length	L_e, L_c	*0.5 m*
Bore diameter	D_e, D_c	0.75×10^{-2} *m*
Charge gas density	ρ	1.225 *kg/m*^{3}
Out-of-phase angle	θ	120^o
Hot, cold temperatures	T_h, T_k	*450 K,300 K*
Rotation speed	n	*500 RPM*
Working gas	*Air*	
Gas constant	*R*	*287 J/kg.K*

5.2 Single phase $(1 - ph)$ Franchot engine

This simplest engine configuration has only one pair of hot and cold cylinders connected to each other by two regenerators. The expansion volume v_e is always leading the compression volume v_c by an arbitrary phase angle. The phasor diagram of the $1 - ph$ Franchot engine in Figure 5-1 shows that the masses are not uniformly distributed around the crankshaft, which causes primary vibrations. However, the perfect balance is only achievable at 180 degree phase angle, but at this point the power output approaches zero.

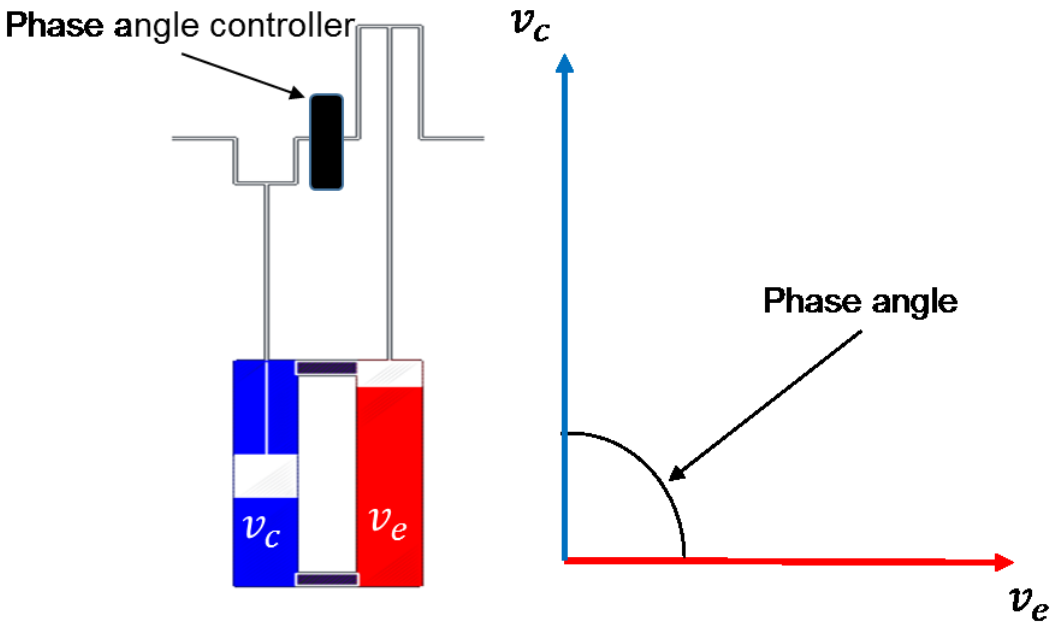

Figure 5-1: 1-ph kinematic Franchot engine and its phasor diagram.

For the start-up capability, the Franchot engine is investigated for the effect of increasing the temperature, phase angle and dead volume. Figure 5-2 shows that negative power is reduced but not eliminated for the studied cases. Increasing the temperature increases the power variation and reduces the negative part of the power by shifting the power curve up due to increasing the pressure in the expansion stroke. Increasing the dead volume to 100% of the swept volume reduces the power variations due to reducing the pressure variations. Increasing the phase angle leads to reduction in the negative part of the power signal due to reduction in the pressure variation and time shift between negative and positive power peaks. The time shift works as filter for the power signal while reducing the pressure variation reduces the power signal amplitude so that it oscillates around zero as the volumes on both sides of the working pistons approaches equality. Thus, an increase in the dead volume increases the impact of the negative power portions.

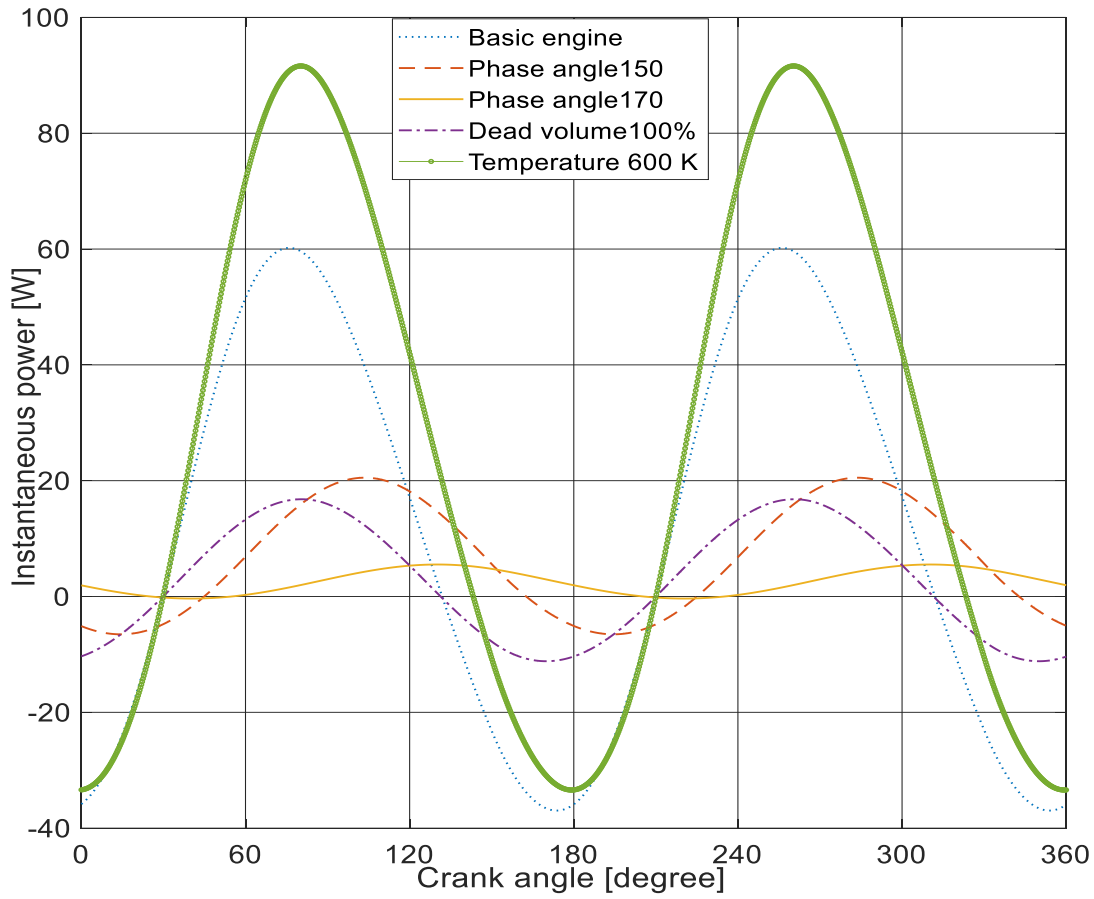

Figure 5-2: Power response for increasing the phase angle, dead volume and temperature of the reference engine.

Figure 5-3 shows that the power calculated from the second part of Equation 5.3 is not equal to the negated power of the first part for which otherwise, the generated power would be zero. In a duplicated alpha engine, the negative powers are added together whilst in the Franchot engine, negative and positive powers are added together which reduces the power variations and hence torque pulsations. The frequency of the combined power signal P_{ins} of the Franchot engine is twice the frequency of an alpha engine because the individual instantaneous powers are not sinusoidal and the shifted power peaks do not match with the original power peaks. Høeg et al. [130] also showed that the torque signal frequency is twice the engine rotation frequency. Therefore, the Franchot engine has two negative power regions in one rotation, which are smaller in magnitude than the negative power of a duplicated alpha engine.

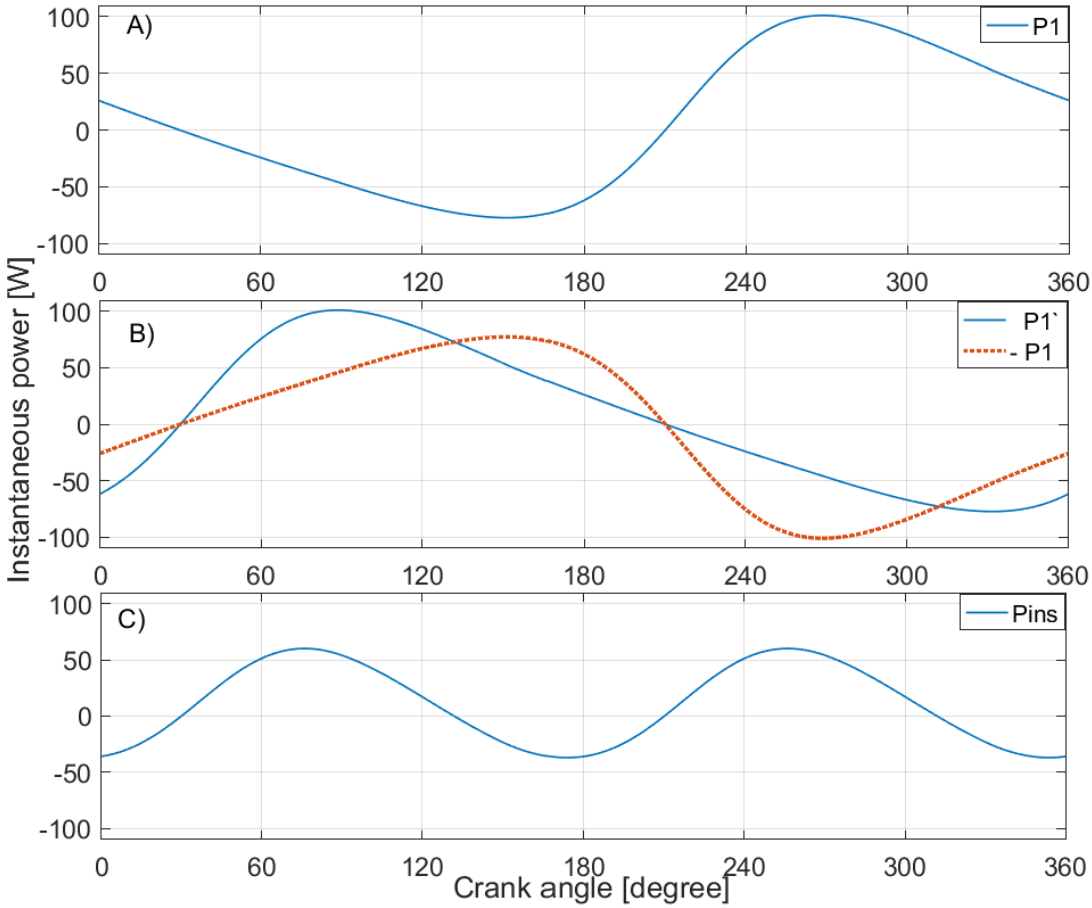

Figure 5-3: Instantaneous power response at the steady state of the reference engine showing A) the power due to one side, B) the difference between the shifted and negated power and C) the total instantaneous power of the reference Franchot engine.

5.3 Dual Phase ($2-ph$) Franchot engine

The Dual Franchot engine can be mechanically coupled to the crankshaft in inline configurations where there is an arbitrary phase shift between any of the two hot or cold cylinders. Figure 5-4 shows a dual Franchot engine where the phase angle is controlled with a single device and which use a common heater and a common cooler.

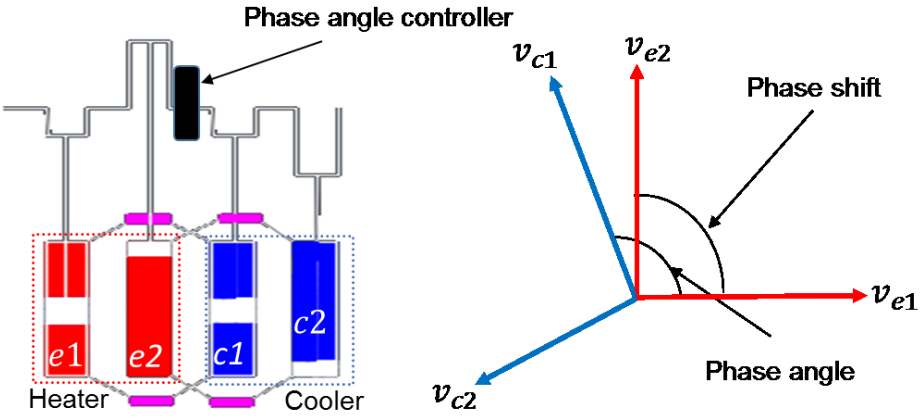

Figure 5-4: Dual kinematic Franchot engine and its phasor diagram.

The phasor diagram shown in Figure 5-4 shows that the dual Franchot engine is liable for primary vibrations due to the uneven distribution of cranks and masses unless the phase shift is set to 180°. However, at a phase shift of 0° and 180°, the thermodynamic performance of the dual Franchot engine is similar to a duplicated $1-ph$ Franchot engine (see Figure 5-5). Other phase shifts are investigated in order to reduce the power variations and check the engine capability to self-start. Figure 5-5 shows that the lowest power variation occurs at the 90° phase shift. The same angle was confirmed experimentally for causing the minimum torque variations by Høeg et al. [130]. Thus, the dependency on a flywheel is reduced and the self-starting properties are better than for the $1-ph$ Franchot engine, although small negative power portions still exist at the studied speed.

The largest reduction in power variation occurs when the instantaneous powers (see Figure 5-3 C) of two Franchot engines are added with a shift of 180°. In this case, each negative power portion is matched with a positive power portion in the opposite engine. The 180° shift in power signal is achieved by a 90° phase shift because the

power wave frequency is twice the engine rotational frequency (see section 5.2). At a 90° phase shift, the power frequency of the $2-ph$ engine is four times the rotational frequency. Similarly, the phase shifts of zero and 180° produce zero and 360° phase shifts in the power wave, respectively and thus no shift in the power signal. Therefore, two or more engines with 0° or 180° phase shift are just a $1-ph$ Franchot engine with multiple cylinders.

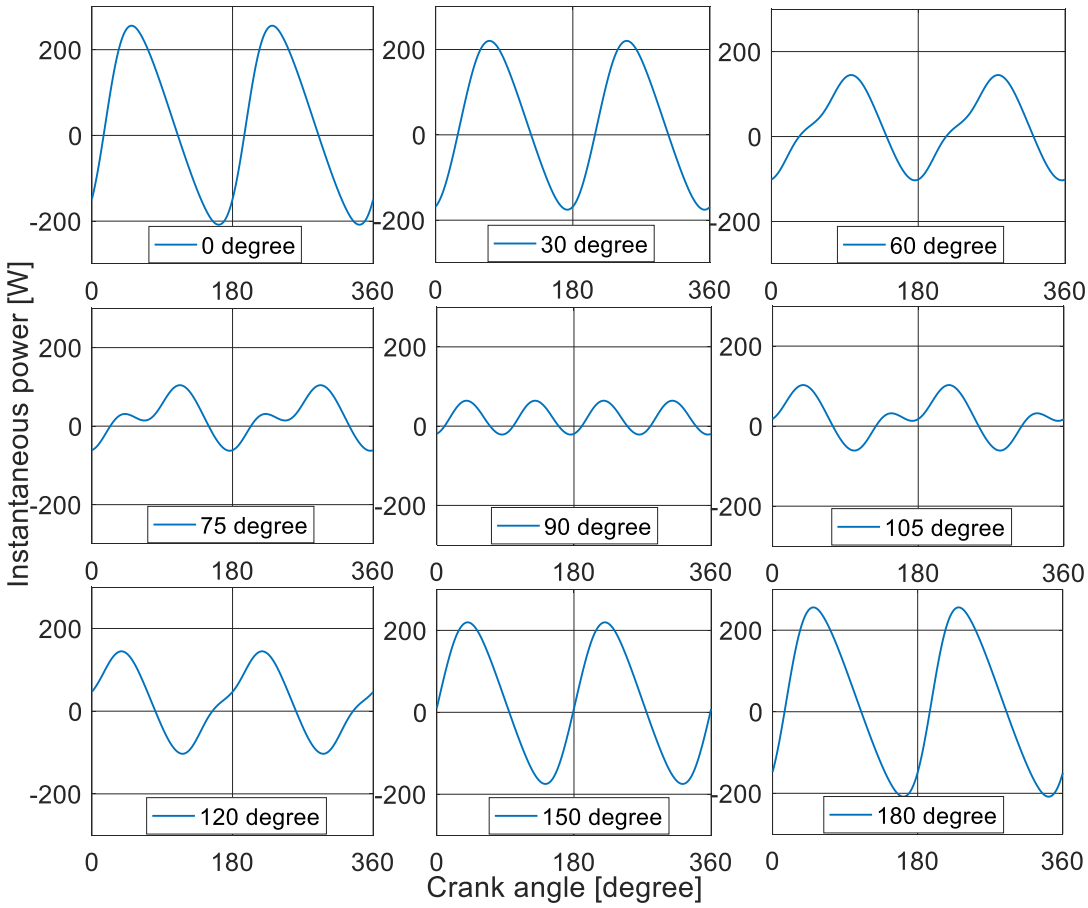

Figure 5-5: Effect of the phase shift on the power variation of a $2-ph$ *Franchot engine at 90° phase angle.*

Figure 5-6 shows the capability of the $2-ph$ Franchot engine with a phase shift of 90° to self-start. This finding is in line with former studies [155][130][156]. The low speed represents the response of the system just after starting at a phase shift of 90°. At low speeds, the compression process is almost isothermal due to the long cycle time, which reduces the negative power needed for compression. Thus, the engine will continue running below 30 rpm with a flywheel as the negative power portion

vanishes at low speeds. Increasing the temperature to 600 K leads to an increase in power variations as well as in the average power. Hence, the positive shift in the average power removed the negative power portions. However, most important is the phase angle, which acts as a filter of the power signal. The instantaneous power for the increased phase angle of 120° leads to a uniform positive power, which has no negative portions. Hence, the $2-ph$ Franchot engine can be self-starting as the negative power portions vanish for increased temperature difference, decreased speed or increased phase angle.

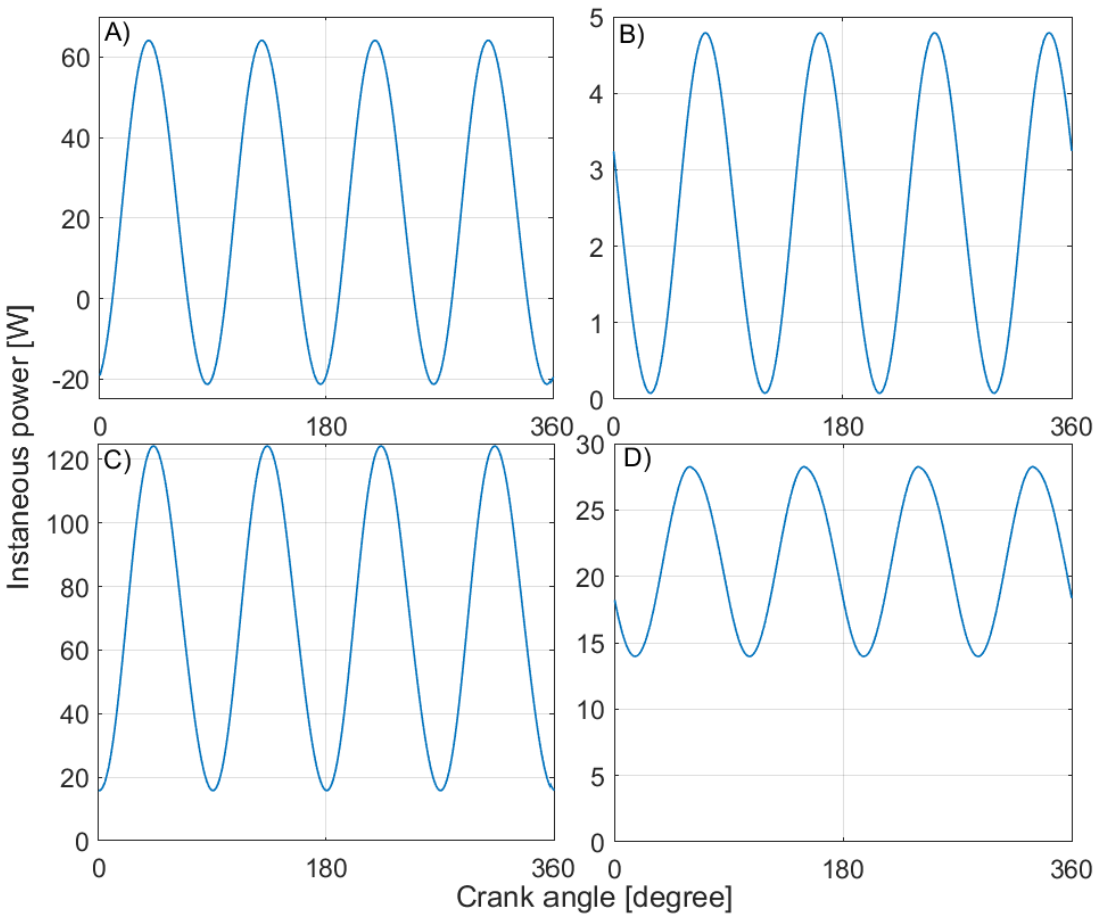

Figure 5-6: Instantaneous power of the reference dual Franchot engine at a phase shift of 90° and A) phase angle of 90°, B) phase angle of 90° and $n = 30\ rpm$ C) phase angle of 90° and T_h = 600 K, and D) reference engine at phase angle of 120°, T_h = 450 K and n = 500 rpm.

5.4 Three phase ($3-ph$) Franchot engine

The $3-ph$ Franchot engine shown in Figure 5-7 is arranged in an inline topology in the slider-crank mechanism so that there are a common heater, a common cooler and one device to control the phase angle. As each Franchot engine has two regenerators, this arrangement has a twin of longer regenerator connections between cylinder $e1$ and $c1$ in comparison to the other connections. The phasor diagram (Figure 5-7) shows a uniform distribution of the masses and forces on the crankshaft which removes the vibrations caused by the unbalanced forces and masses. The phasor diagram shows that the reciprocal vibrations can vanish even if the phase angle is controlled as the vector summation of the forces is zero for arbitrary phase angles. In addition, it is also possible to remove the rocking couples if the phase angle equals the phase shift. At this phase angle, the engine compromises piston twins ($e1-c3, e2-c1$ *and* $e3-c2$) moving with each other. Therefore, to reduce the primary vibrations, both the phase shift and phase angle have to be fixed to 120°. However, the location of cold cylinders $c1$ and $c2$ can be swapped to give equal regenerator lengths but the rocking couples will not be inherently removed.

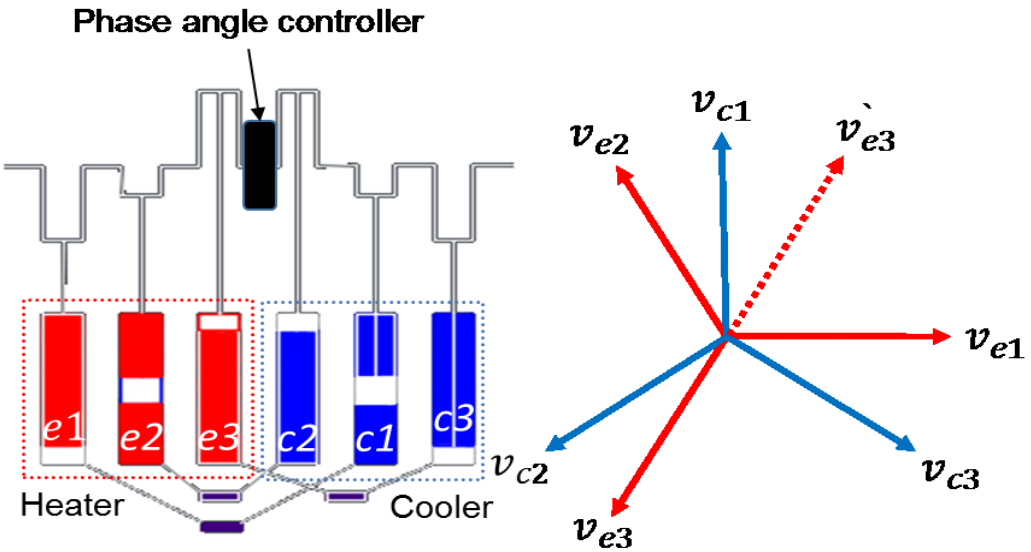

Figure 5-7: 3-ph kinematic Franchot engine showing the regenerator connection on the lower side only and its phasor diagram.

Figure 5-8 shows that there are two phase shifts at which the system has the minimum power variation: at 60° and at 120°. At these angles, the power frequency is three times

the power pulses frequency of a $1-ph$ Franchot engine or six times the rotational frequency. The minimum instantaneous power is shifted to a positive value and the power variation on the crankshaft is reduced.

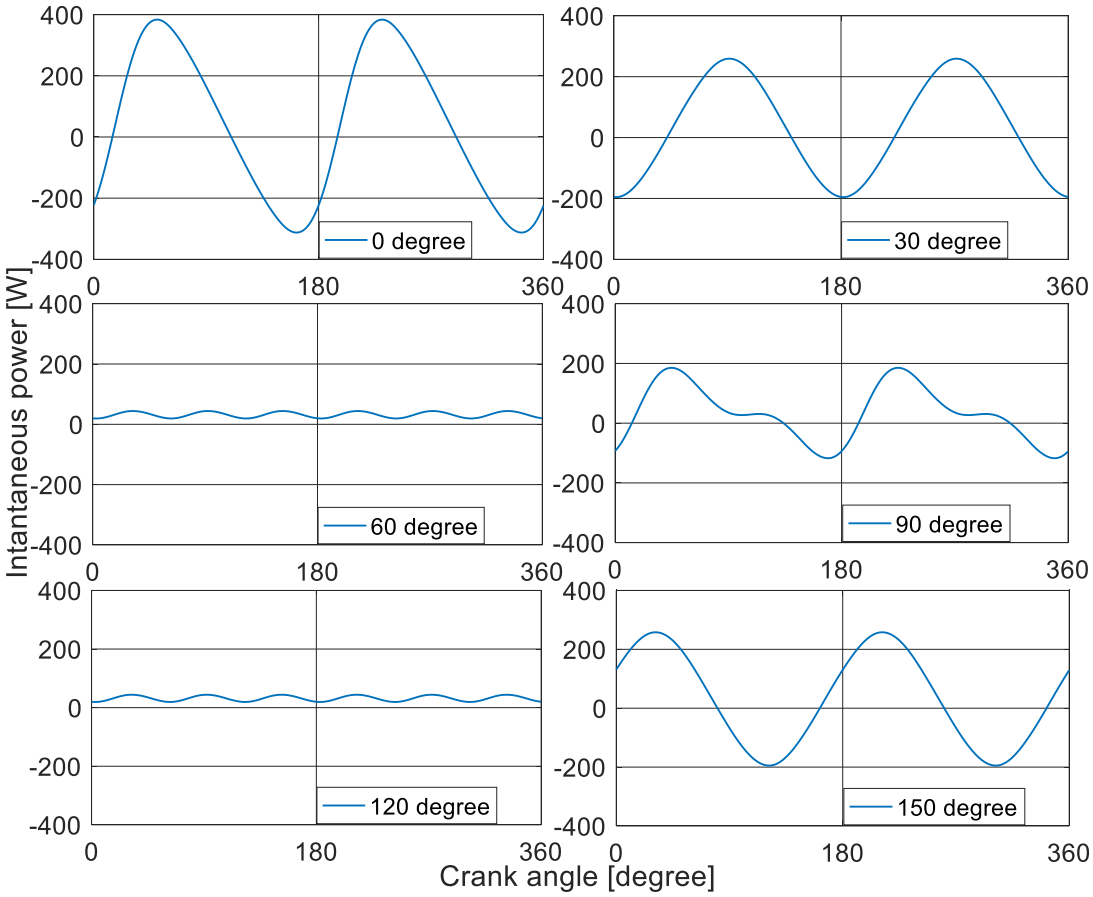

Figure 5-8: Effect of the phase shift on the instantaneous power of the 3-ph Franchot engine at 90° phase angle.

Figure 5-9 shows the power response of the $3-ph$ Franchot engine is similar at phase shifts of 60° and 120° for different phase angles. The reason for this is that the Franchot engine has two Stirling engines mounted mechanically opposite to each other and thus, the phase shift 60° is seen as a shift of 120° by the opposite engine as it is shifted by 180° (see Figure 5-7). In addition, large phase angles lead to smaller power variations hence smoother power signals. These power variations are much smaller than in the $2-ph$ Franchot engine (see Figure 5-5). Therefore, the need for a flywheel is much smaller for the $3-ph$ Franchot engine than for the $2-ph$ engine.

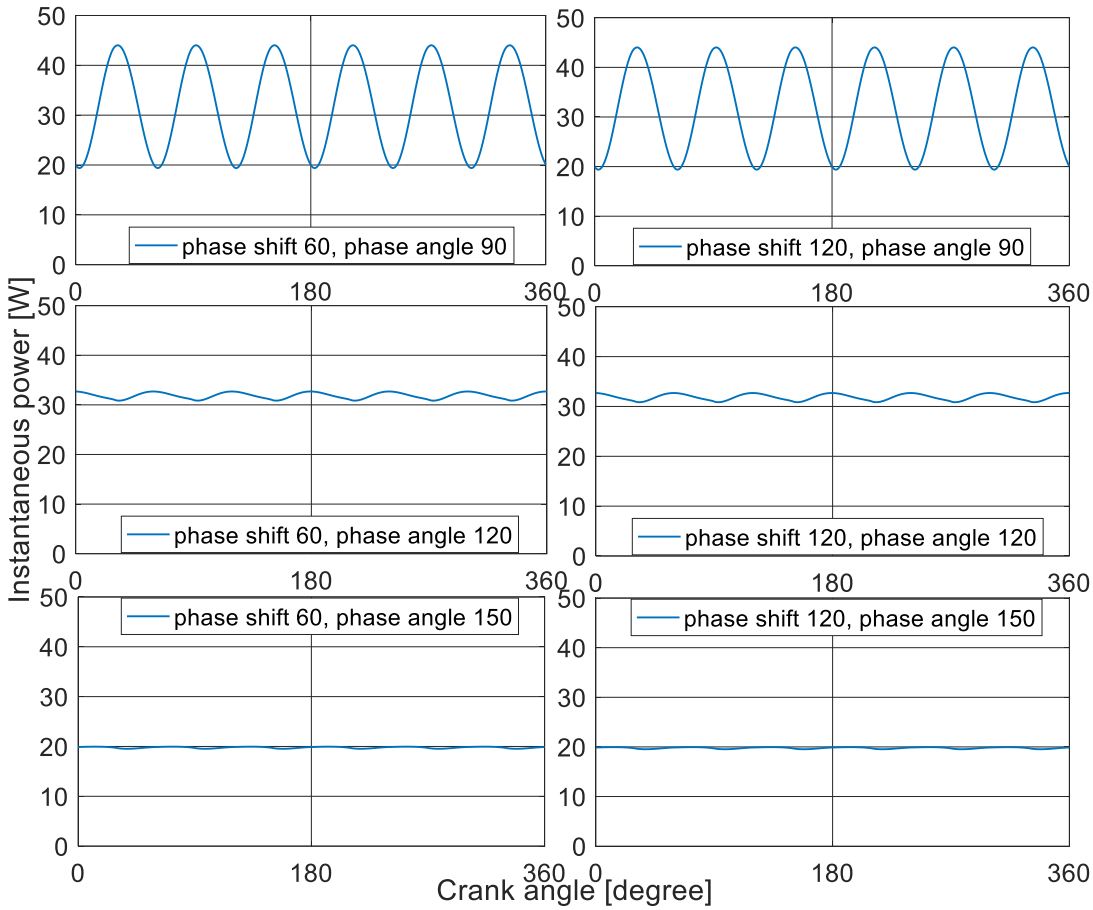

Figure 5-9: Effect of the phase angle on the power variation of a $3-ph$ *Franchot engine at 60° and 120° phase shifts.*

5.5 Multi-phase $(n-ph)$ Franchot engine

The findings from sections 5.2-5.4 are extended to the $n-ph$ engine. The different power signals of a multi-phase engine are added to the crankshaft. As seen in Figure 5-3, each $1-ph$ Franchot engine has a power frequency, which is two times the engine rotational frequency and thus each phase has two maxima and two minima in one cycle. In order to remove the negative power portions, each negative power portion must be balanced by positive power portions. In the multi-phase engine, the phase shifts can be chosen with the aim of cancelling the maxima and minima. Figure 5-10 shows the power amplitude for the $2-ph$ to $7-ph$ Franchot engines over the phase shift. For each $n-ph$ engine, there are $n-1$ different phase shifts, which produce power variation minima.

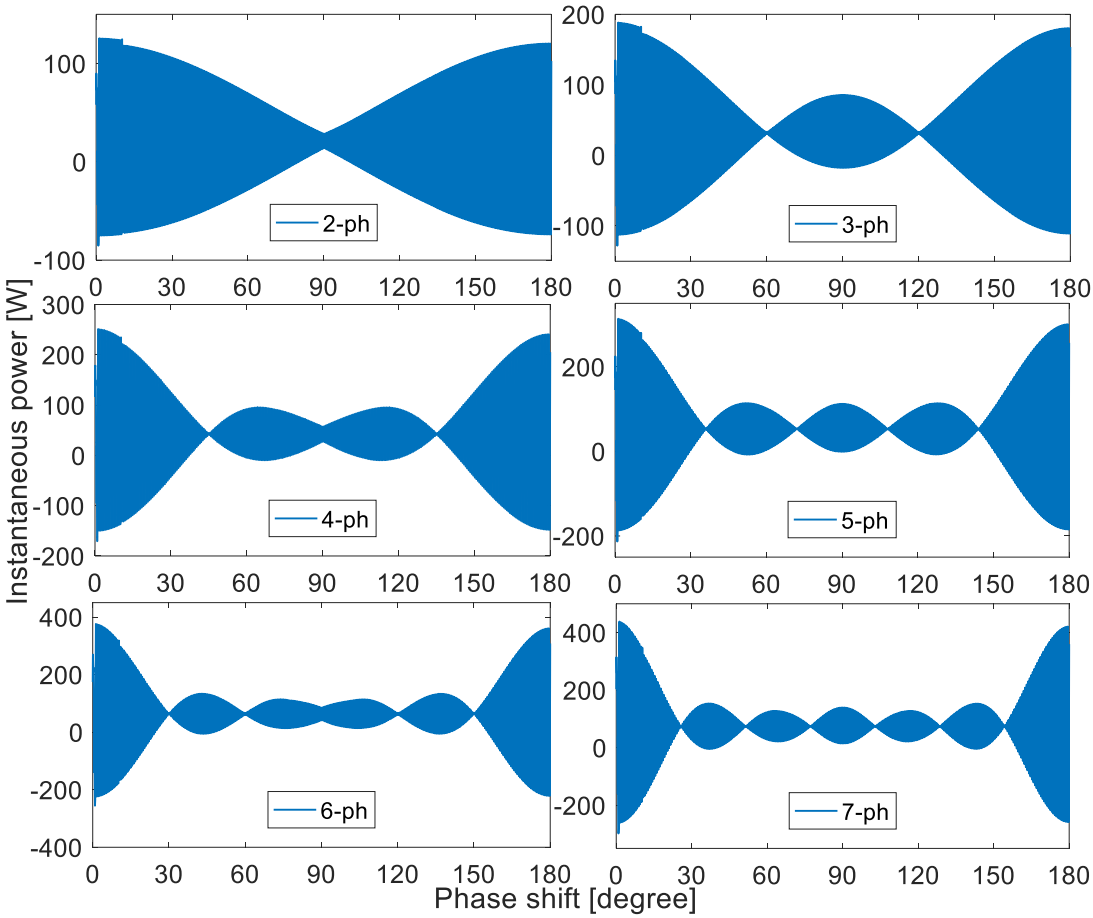

Figure 5-10: Power amplitude response of the multi-phase Franchot engine with the phase shift.

The phase shifts that lead to the lowest power variations are given by

$$\theta_s = \frac{180}{n} y \qquad 5.5$$

where y is an integer between 1 and $n-1$, n is the number of phases (pair of hot and cold cylinders) of the Franchot engine.

For even y values, the Franchot engines will be uniformly distributed around the crankshaft making a symmetric phase shift between the adjacent engines. The phase shift of the $n-ph$ Franchot engine is twice the phase shift of an equivalent Siemens configuration in terms of number of cylinders and is given by

$$\theta_s = \frac{360}{n} \qquad 5.6$$

For odd y values, the Franchot engines will be stacked on one half of the crankshaft making the smallest phase shift equal to

$$\theta_s = \frac{180}{n} \qquad 5.7$$

Those two-phase shifts have the same power signal pattern because the Stirling engines forming a Franchot engine are out of phase. In other words, the power signal frequency of a Franchot engine is twice that of the Stirling engine. Thus, each Franchot engine has a duplicated power cycle each half rotation. As the Franchot engine has two opposite alpha Stirling engines, the instantaneous power at a phase shift of θ is equivalent to the instantaneous power $at\ 180^o - \theta$ and hence, it is mirrored about 90°. At the phase shift of 90°, the angular shift in the power signal is $180n$. Hence, for the even number of phases, this will be turned into a signal duplication for which the signal amplitude is increased rather than being attenuated.

Since the phase shift is valid for $y \leq n - 1$ and y needs to be an even number, the minimum number of phases that results in power minima and symmetric distribution of phases is three. With a symmetric distribution, the power variation is minimum and the first order reciprocal vibrations are reduced due to the uniform distribution of forces and masses on the crankshaft. In order to reduce the vibrations related to the rocking couples, the masses should be uniformly distributed and pairs of expansion and compression pistons should move together in the same direction. Thus, the phase angle must be fixed and match the phase shift. However, for $n > 4$, different straight regenerator connections can be made to obtain different phase angles while removing the rocking couples. For example, for $n = 5$, there are two possible regenerator connections as there are always two compression volumes delayed by 72° and 144°.

Table 5-2 summarises the potential phase angles up to the $8-ph$ Franchot engine where the phases are uniformly distributed around the crankshaft and the rocking couple are removed. These phase angles can be mathematically described by Equation 5.5 where y is an even number. These phase angles are similar to the phase angles of the multi-cylinder single-acting Stirling engine [126]. However, different phase angles can be obtained if cross regenerator connections are considered.

Table 5-2: Possible phase angles of the multi-cylinder Franchot engine.

	3-ph	*4-ph*	*5-ph*	*6-ph*	*7-ph*	*8-ph*
$y=2$	*120°*	*90°*	*72°*	*60°*	*51.4°*	*45°*
$y=4$			*144°*	*120°*	*102.8°*	*90°*
$y=6$					*154.2°*	*135°*

5.6 Conclusion

The phasor diagram and reduced multi-cylinder model are used to obtain the power signal to evaluate the vibrations and self-starting capabilities of multi-cylinder Franchot engines. It is predicted that the multi-cylinder Franchot engines are self-starting if at least two Franchot engines are combined. In addition, the cranks can be evenly distributed for three or more Franchot engines. Finally, the power oscillation could be reduced for the $n-ph$ engine, which agrees with the reported cases. Hence, the slider-crank mechanism is recommended for the $n-ph$ Franchot engine where $n \geq 3$ as it is able to reduce the power pulses, rocking couples and primary vibrations caused by each Franchot engine on the rotating crankshaft. On the other hand, the slider-crank mechanism does not remove the rocking couples in the Siemens configuration. In addition, the $3-ph$ Franchot engine gives a preferable phase angle of 120° in contrast to 60° of an equivalent Siemens configuration. Thus, the multi-cylinder Franchot engine could be self-starting, has significantly reduced vibrations and can use the simple slider-crank mechanism. Multiple Franchot engine are still having the phase angle freely controlled unless rocking vibration reduction is required.

CHAPTER

6 Balanced compounding

In the previous chapter, the mathematically studied kinematic multi-cylinder engine led to favourable characteristics of the Franchot engine such as the vibration reduction and self-starting. On the other hand, it has long cranks and piston rods and uses rotating parts, which increase the mechanical friction, lubrication needs, size and cost. This leads to the investigation of alternative coupling. In this chapter, the multi-cylinder Franchot engine is reconfigured and modelled for the balanced compounding mechanism. The balanced compounding is a free piston technology, which uses the working gas as a gas spring and has each expansion piston rigidly connected to a compression piston (see section 2.8). This chapter will address if the balanced compounding mechanism can maintain synchronisation between pistons without a flywheel and mechanical phase linkage. In addition, the effect of the number of cylinders on the phase shift and of the cylinder arrangements on the piston side forces that cause mechanical friction are mathematically investigated. The engine is designed to drive linear loads under various conditions.

6.1 Introduction

The cylinder wall heated and cooled Franchot engine has long strokes and cranks (see Figure 6-1). Long cranks create problems for the designers such as the size and piston side forces. The free piston concept presented in section 2.8 can reduce the problems generated by the kinematic drives. However, the use of gas or mechanical spring coupling might not be the suitable option for the cylinder wall heated and cooled engine. Long bounce spaces or long mechanical springs increase the engine length. The cylinder wall heated and cooled Franchot engine cannot use the balanced compounding innovated by Finkelstein due to long regenerator connections (see Figure 2-10). Moreover, the configuration of the opposite engine requires distributed

heaters and coolers. Thus, parallel engines offer a solution for the distributed heat exchangers and the crossed and long regenerator connections in the Finkelstein arrangement.

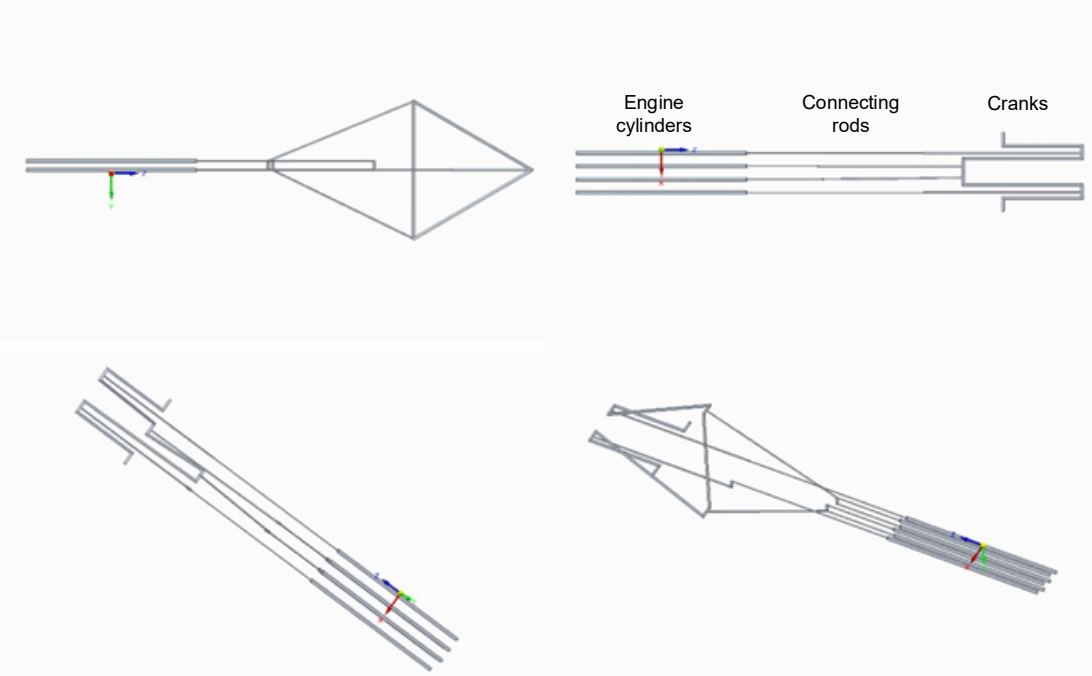

Figure 6-1: Kinematic 3-ph Franchot engine showing real cranks to cylinders size.

Chapter 5 shows that the negative power generated by the multi-cylinder Franchot through some portions of its rotation can be minimised for certain values of the phase shift and number of cylinders. According to the phasor diagrams and Table 5-2, each compression piston moves parallel to an expansion piston at a predefined phase angle. The compression work will be compensated by the expansion work without a crankshaft and flywheel [165]. Hence, the side-by-side balanced compound arrangement, which has the expansion and compression cylinders arranged side by side, is conceptually suggested. It requires a minimum of three phases to have a fixed phase angle with straight and short regenerator connections. In addition, the expansion and compression pistons must move together. The engine will run at one of the predefined phase angles for which the positive power can always be generated. Other phase angles create either negative power portions or large power variations, which hinder the motion of the piston. Hence, all the working volumes of the balanced compounded Franchot engine will have the same phase angle.

The top and side view of the balanced compound cylinder wall heated and cooled $n-ph$ engine are shown in Figure 6-2. Each compression piston is rigidly coupled with a conjugate expansion piston via an external linkage. Thus, the power needed for compression is instantly drawn from the expansion power. Each hot and cold cylinder that composes a distinct engine is coupled through two distinct regenerators. Each linkage connects two Franchot engines and each Franchot engine is connected to two linkages according to the ordering shown. Only one long but straight regenerator connection is needed in the engine En. However, the zero side forces obtained by the Finkelstein arrangement are not achievable by this configuration. The side forces in this arrangement are expected to be smaller than the forces of the slider-crank engine due to the short length of the external linkage between the hot and cold cylinders. Besides their role to guide the pistons, the guiding cylinders can be used as an additional machine to serve as a prime mover or as a load such as a heat pump or fluid pump. This will be evaluated for refrigeration in section 6.4.3.

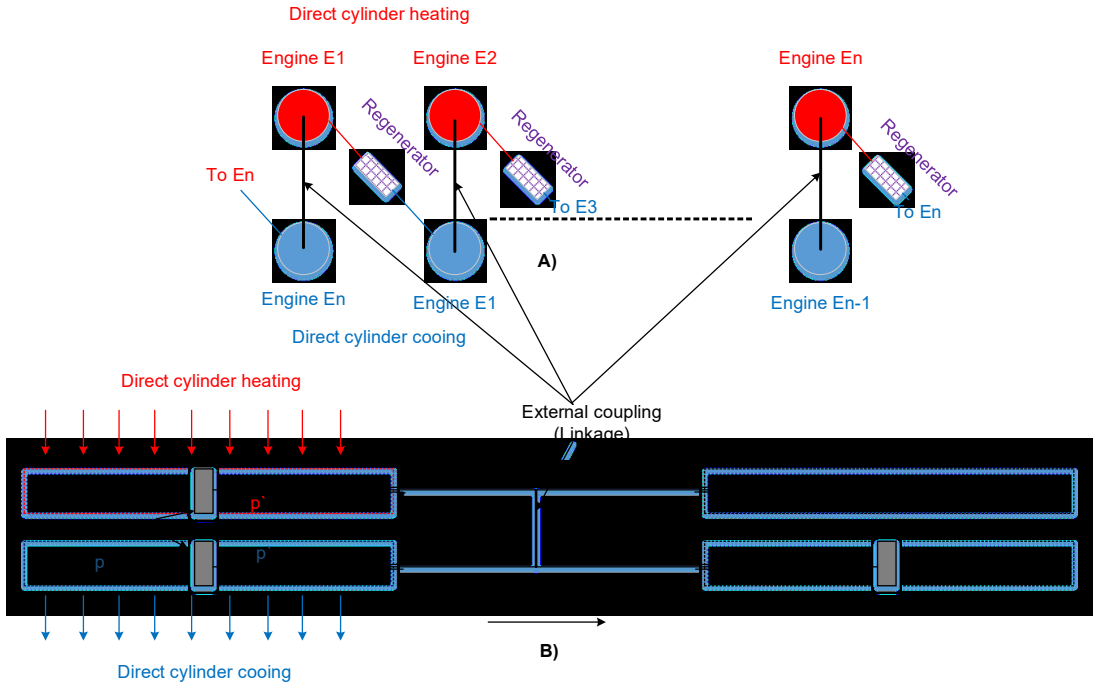

Figure 6-2: Balanced compounding of the multi-cylinder Franchot engine. A) cross-sectional view showing the $n-ph$ engine and B) side view showing two cylinders of the multi-cylinder configuration.

6.2 Mathematical representation

In section 5.1, the power shifting method was used to predict the power variations and led to very important results about how to connect different Franchot engines with each other. However, it cannot be applied to the free piston arrangement as the phase angle, speed and stroke are not initially defined as by the slider-crank mechanism. Herewith a model based on dynamic engine analysis of the balanced compound Franchot engine is developed for determining the piston speed, stroke and phase angle.

Figure 6-3 shows the relationship between the forces, reciprocators and displacement of each component of the balanced $n-ph$ Franchot engine. The $n-ph$ Franchot engine is composed from $2*n$ alpha type Stirling engines. In which, each alpha type Stirling engine is modelled separately.

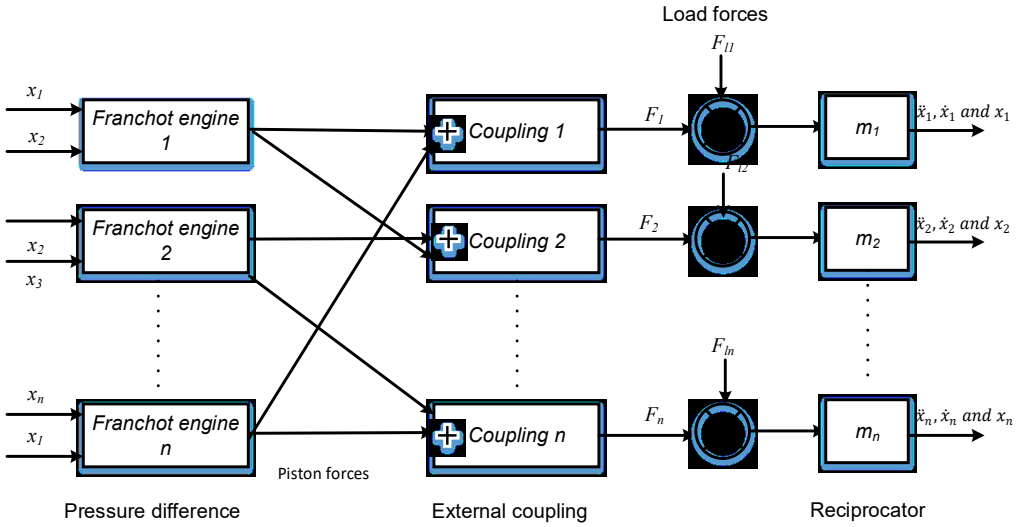

Figure 6-3: Schematic diagram of the $n-ph$ balanced compound Franchot engine, which shows the forces and nomenclature.

Applying Newton's second law of motion, the force balance equation applies

$$\begin{bmatrix} F_1 \\ F_2 \\ \vdots \\ F_n \end{bmatrix} = \begin{bmatrix} m_1 \\ m_2 \\ \vdots \\ m_n \end{bmatrix} [\ddot{x}_1 \quad \ddot{x}_2 \quad \dots \quad \ddot{x}_n] + \begin{bmatrix} F_{l1} \\ F_{l2} \\ \vdots \\ F_{ln} \end{bmatrix} \qquad 6.1$$

where F_i is the thermal driving force, m_i is the total mass of the reciprocating elements(linkage, piston rods and pistons), F_l is the load force, x_i is the reciprocator displacement. The parameter i goes from 1 to the number of reciprocators. The power is calculated for the $n-ph$ Franchot engine as follows

$$P = F_1\dot{x}_1 + F_2\dot{x}_2 + \cdots + F_n\dot{x}_n \qquad 6.2$$

The thermal forces applied to each piston rod are calculated from

$$\begin{bmatrix} F_1 \\ F_2 \\ \vdots \\ F_n \end{bmatrix} = \begin{bmatrix} \Delta p_{E1} & \Delta p_{En} \\ \Delta p_{E2} & \Delta p_{E1} \\ \vdots & \vdots \\ \Delta p_{En} & \Delta p_{En-1} \end{bmatrix} \begin{bmatrix} A_{h1} & A_{h2} & \cdots & A_{hn} \\ A_{kn} & A_{k1} & \cdots & A_{kn-1} \end{bmatrix} \qquad 6.3$$

where $A_{hi}\ and\ A_{ki}$ are the cross-sectional area of the hot and cold pistons respectively, $\Delta p_{Ei}$is the pressure difference across the pistons of the Franchot engine and the subscript E denotes the Franchot engine.

If all reciprocators have the same cross-sectional area and mass then the acceleration of the pistons can be calculated by combining Equations 6.1 and 6.3 to get

$$\begin{bmatrix} \ddot{x}_1 \\ \ddot{x}_2 \\ \vdots \\ \ddot{x}_n \end{bmatrix} = \frac{1}{m}\left(A \begin{bmatrix} \Delta p_{E1} + \Delta p_{En} \\ \Delta p_{E2} + \Delta p_{E1} \\ \vdots \\ \Delta p_{En} + \Delta p_{En-1} \end{bmatrix} - \begin{bmatrix} F_{l1} \\ F_{l2} \\ \vdots \\ F_{ln} \end{bmatrix} \right) \qquad 6.4$$

The speed and displacement of the pistons are calculated by calculating the integral and double integral of the acceleration matrix, respectively. The displacement relative to the opposite piston space is taken by

$$\begin{bmatrix} \grave{x}_1 \\ \grave{x}_2 \\ \vdots \\ \grave{x}_n \end{bmatrix} = L - \begin{bmatrix} x_1 \\ x_2 \\ \vdots \\ x_n \end{bmatrix} \qquad 6.5$$

The free piston Stirling engine is considered a mass damper system where the generic load acting on its moving pistons can be approximated by a damping load in which the load force is written as [152][164][166][167][238][239][240][241]

$$\begin{bmatrix} F_{l1} \\ F_{l2} \\ \vdots \\ F_{ln} \end{bmatrix} = \begin{bmatrix} c_1 \\ c_2 \\ \vdots \\ c_n \end{bmatrix} [\dot{x}_1 \quad \dot{x}_2 \quad \dots \quad \dot{x}_n] \qquad 6.6$$

where c is the damping coefficient.

The friction is another type of load that reduces the Stirling engine performance and needs to be minimised. For sliding pistons, the coefficient of friction is around 0.2 [135]. There are two mechanical friction sources in this configuration: friction due to the weight of the reciprocating masses and friction due to the side forces created by the cylinder offset. The side forces can be obtained by analysing the free body diagram of the engine as shown in Figure 6-4. The analysis considers the worst case when the side forces caused by the axial forces are loaded on the rod seals.

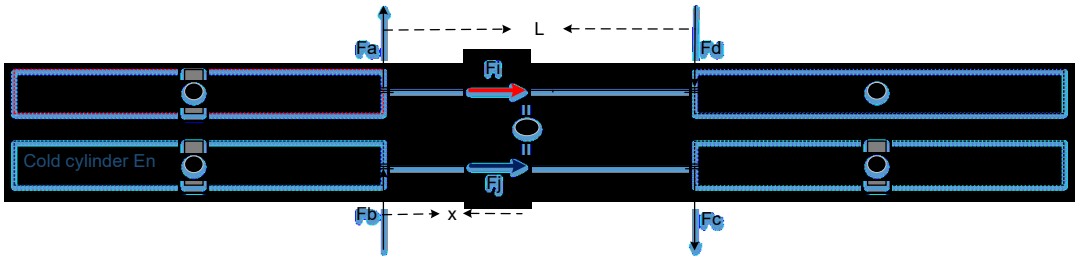

Figure 6-4: Free body diagram of the balanced compound Franchot engine.

Taking the moment of force around the non-rotating point *e* applies

$$\sum M_e = 0 \qquad 6.7$$

hence,

$$\frac{y}{2}(F_j - F_i) - x(F_a + F_b) - (L - x)(F_c + F_d) = 0 \qquad 6.8$$

As the piston rod is only free to move along the cylinder axis (x) then the summation of forces in the y direction is

$$\sum F_y = 0 \qquad 6.9$$

This implies that

$$F_a + F_b = F_c + F_d \qquad 6.10$$

hence, the reciprocator total side force is calculated from Equations 6.8 and 6.10 as

$$F_a + F_b + F_c + F_d = \frac{y * (F_j - F_i)}{L} = \frac{y}{L}\Delta F \qquad 6.11$$

where y is the crank length and L is the distance between engine and guide cylinders, respectively. The force difference ΔF for n number of phases is modelled as

$$\Delta F = \begin{bmatrix} \Delta F_1 \\ \Delta F_2 \\ \vdots \\ \Delta F_n \end{bmatrix} = A \begin{bmatrix} \Delta p_{En} - \Delta p_{E1} \\ \Delta p_{E1} - \Delta p_{E2} \\ \vdots \\ \Delta p_{En-1} - \Delta p_{En} \end{bmatrix} \tag{6.12}$$

The load force due to mechanical frictions caused by the weight of the reciprocators and dynamic forces on each phase is written as

$$\begin{bmatrix} F_{l1} \\ F_{l2} \\ \vdots \\ F_{ln} \end{bmatrix} = \begin{bmatrix} \begin{cases} 0.2(m_1 g + \frac{y}{L}|\Delta F_1|) & \dot{x}_1 < 0 \\ -0.2(m_1 g + \frac{y}{L}|\Delta F_1|) & \dot{x}_1 > 0 \end{cases} \\ \begin{cases} 0.2(m_2 g + \frac{y}{L}|\Delta F_2|) & \dot{x}_2 < 0 \\ -0.2(m_2 g + \frac{y}{L}|\Delta F_2|) & \dot{x}_2 > 0 \end{cases} \\ \vdots \\ \begin{cases} 0.2(m_n g + \frac{y}{L}|\Delta F_n|) & \dot{x}_n < 0 \\ -0.2(m_n g + \frac{y}{L}|\Delta F_n|) & \dot{x}_n > 0 \end{cases} \end{bmatrix} \tag{6.13}$$

where g and 0.2 are the gravitational acceleration and dry coefficient of friction given by Hirata [135].

The resonant frequency of the free piston Stirling engine is a function of the reciprocating mass and spring stiffness as [242][153]

$$\omega_o = \sqrt{\frac{k}{m}} \tag{6.14}$$

The spring stiffness of the balanced compound Franchot engine can be calculated from the stiffness of the working gas. As the gas stiffness is non-linear, the instantaneous piston forces are calculated from Equation 6.3. To calculate the engine frequency over one rotation and at steady state condition, the gas stiffness is averaged over one rotation. The working gas stiffness has a maximum value if the expansion and compression processes are adiabatic which is given by [146]

$$k = \frac{\gamma p A^2}{V} \qquad 6.15$$

The stiffness has a minimum value if the expansion and compression processes are isothermal which is given by [146]

$$k = \frac{p A^2}{V} \qquad 6.16$$

Since the expansion and compression processes are polytropic then the working gas stiffness can be written as

$$k = \frac{n p A^2}{V} \qquad 6.17$$

where n is the polytropic index which can be calculated from [215] as

$$n = -\frac{V}{p}\frac{dp}{dv} \qquad 6.18$$

To study the effect of gas leakage across the power pistons on the performance of the balanced compound mechanism, the total mass of the working gas was considered variable. Hence, Equation 3.2 is written as

$$\dot{m}_l = \dot{m}_e + \dot{m}_c + \dot{m}_r \qquad 6.19$$

where $\dot{m}_l$ is the mass leakage in this engine, it is equal to the summation of the leakage on the hot and cold pistons and is written as

$$\dot{m}_l = \dot{m}_{le} + \dot{m}_{lc} \qquad 6.20$$

The energy balance equation of the expansion volume is written by considering the enthalpy due to the gas leakage at the expansion piston as follows

$$\dot{Q}_e + \dot{H}_e + c_p \dot{m}_e T_{re} = p\dot{v}_e + c_v(\dot{m_e} T_e) \qquad 6.21$$

By rearranging equation 6.21, the mass flow rate in the expansion chamber results in

$$\dot{m}_e = \frac{\frac{p\dot{v}_e}{R} + \frac{v_e\dot{p}}{\gamma R} - \frac{\dot{Q}_e + \dot{H}_e}{c_p}}{T_{re}} \qquad 6.22$$

Similarly, the mass flow rate in the compression chamber is written as

$$\dot{m}_c = \frac{\frac{p\dot{v}_c}{R} + \frac{v_c\dot{p}}{\gamma R} - \frac{\dot{Q}_c + \dot{H}_c}{c_p}}{T_{cr}} \qquad 6.23$$

By combining Equations 3.8, 6.21, 6.22 and 6.23 the pressure equation becomes

$$\dot{p} = \frac{-p\left(\frac{\dot{v}_e}{T_{re}} + \frac{\dot{v}_c}{T_{cr}}\right) + \frac{R}{c_p}\left(\frac{\dot{Q}_e + \dot{H}_e}{T_{re}} + \frac{\dot{Q}_c + \dot{H}_c}{T_{cr}}\right) + R\dot{m}}{\frac{v_e}{\gamma T_{re}} + \frac{V_r}{T_r} + \frac{v_c}{\gamma T_{cr}}} \qquad 6.24$$

The Franchot engine enjoys small enthalpy loss as the leaks shuttle between similar temperature chambers. The enthalpy loss due to the gas leakage across the power pistons is calculated as [230]

$$\dot{H} = c_p \dot{m}_{lx} T \qquad 6.25$$

where T depends on the mass leakage direction between opposite expansion or compression spaces. It is the source temperature for positive mass flow rate and working space temperature for negative mass flow rate. The mass leakage through a clearance seal where the flow is laminar is calculated from [52][230]

$$\dot{m}_l = \pi D \frac{p + \dot{p}}{4RT_g}\left(\dot{x}\delta - \frac{\delta^3}{6\mu}\frac{p - \dot{p}}{L_g}\right) \qquad 6.26$$

where $\dot{p}, T_g, \dot{x}, \delta, \mu \; and \; L_g$ are pressure at opposite chamber, gas temperature, linear piston velocity, piston to cylinder wall gap, gas viscosity and gap length, respectively.

6.3 Model validation

The multi-cylinder model has been applied to Der Minassians [152] double acting $3-ph$ FPSE prototype shown in Figure 6-5 (A). The system has three cylinders, which each have two diaphragm pistons. One diaphragm motion is reversed using a novel mechanical reverser. In addition to the working gas spring, each engine uses springs due to the diaphragm pistons, flexure and magnetic coupling.

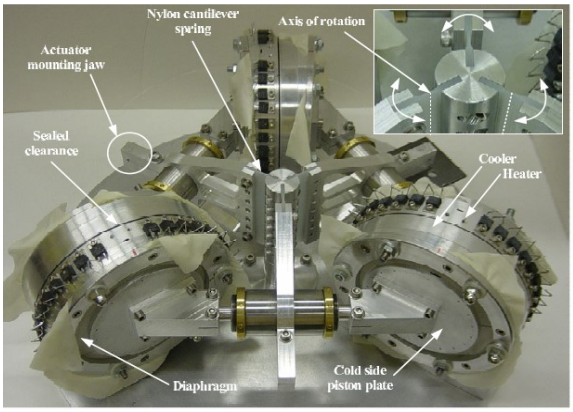

(A)

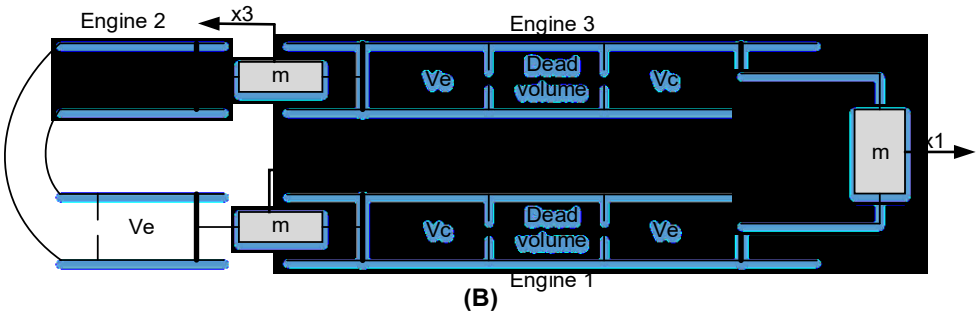

(B)

Figure 6-5: Der Minassians engine A) Picture from[146] B) schematic diagram with reverser.

According to Figure 6-5, Equation 6.4 is rewritten to consider the reversal of one piston and the use of external springs as

$$\begin{bmatrix}\ddot{x}_1\\ \ddot{x}_2\\ \vdots\\ \ddot{x}_n\end{bmatrix}=\frac{1}{m}\left(A\begin{bmatrix}p_{E1}+p_{En}-2p_o\\ p_{E2}-p_{E1}\\ \vdots\\ p_{En}-p_{En-1}\end{bmatrix}-\begin{bmatrix}F_{l1}\\ F_{l2}\\ \vdots\\ F_{ln}\end{bmatrix}-k_p\begin{bmatrix}x_1\\ x_2\\ \vdots\\ x_n\end{bmatrix}\right) \qquad 6.27$$

where $x_n, p_o \; and \; k_p$ are the hot side piston motion, ambient pressure and piston system stiffness, respectively. The engine expansion volume is calculated from

$$\begin{bmatrix} V_1 \\ V_2 \\ \vdots \\ V_n \end{bmatrix} = \begin{bmatrix} V + Ax_1 \\ V + Ax_2 \\ \vdots \\ V + Ax_n \end{bmatrix} \qquad 6.28$$

The compression swept volume, which is reversed for the last piston, is calculated from

$$\begin{bmatrix} \acute{V}_1 \\ \acute{V}_2 \\ \vdots \\ \acute{V}_n \end{bmatrix} = \begin{bmatrix} V - Ax_2 \\ V - Ax_3 \\ \vdots \\ V + Ax_1 \end{bmatrix} \qquad 6.29$$

To apply the three-control volume model, the regenerator end temperatures were set to source temperature and the heat transfer to the swept volume is ignored. The Der Minassians engine parameters and experimental and simulation outputs are tabulated in Table 6-1.

Table 6-1: The parameters of 3-ph Der Minassians engine

Name	***symbol***	***value/unit***
Swept volume	V	$93.2 \times 10^{-6}\ m^3$
Piston area	A	$45.6 \times 10^{-4}\ m^2$
Reciprocating mass	m	$0.64\ kg$
Total dead volume	V_r	$163.2 \times 10^{-6}\ m^3$
Hot, cold temperatures	T_h, T_k	$420\ K, 300\ K$
Working gas pressure	p	$100\ kPa$
Ambient air constant	MR	$0.119\ J/K$
Reciprocator mass	m	$0.1\ kg$
Number of phases	n	3
Piston system stiffness	k_p	$3.58\ kN/m$
Damping factor	c	$11.2\ N.s/m$

Table 6-2 shows a comparison between the experimental data, Der Minassians calculation and this work. The phase shift and phase angles match exactly. The frequency is slightly higher than that calculated by Der Minassians because this work assumes adiabatic swept volumes which increase the gas stiffness and hence the frequency. The frequency discrepancy with experimental data is attributed to the effective piston area that reduces the working gas stiffness. The swept volume does not increase linearly with the stroke as the flat shape of the diaphragm piston deforms with the stroke. The model in this work anticipates that the system starts-up at a temperature of $400\ K$ with the damping load considered. It is higher than the calculated temperature by Der Minassians as the isothermal model assumes that the real gas temperature differences are larger than in the adiabatic model. In contrast to the experimental engine, the discrepancy in estimating the stroke and frequency is due to the finite heat transfer and effective piston diameter in the test engine, respectively. Thus, the start-up temperature is overestimated because the damping losses are increased due to the higher anticipated frequency. However, both the phase shift and phase angle for the multiphase engine were accurately obtained. The model, which considered the exact speed, piston diameter and heat transfer, is validated in section 4.4. Thus, the model can be extended for the balanced compound engine.

Table 6-2: Comparison between this work, Der Minassians model and experimental data

Variable	***Experimental***	***Der Minassians isothermal model***	***This work***
Phase shift	60^o	60^o	60^o
Phase angle	120^o	120^o	120^o
Frequency	$16\ H_z$	$19\ H_z$	$20\ H_z$
Start-up temperature at cold side temperature of 313K	$373\ K$	$367\ K$	$400\ K$
Stroke	$1.4 \times 10^{-2}\ m$		$1.7 \times 10^{-2}\ m$

6.4 Results

All simulation results are taken for the engine design parameters in Table 6-3 unless otherwise stated. The reference engine is considered ideal according to assumptions mentioned in section 3.3.1 but the mechanical friction and regenerator pumping losses

are considered as friction and damping load, respectively. Also, the initial and boundary conditions assumed in this study are listed in Table 6-4.

Table 6-3: Parameters of the reference balanced compound Franchot engine.

Name	***Symbol***	***Value/unit***
Cylinder length	L_e, L_c	$0.5\ m$
Bore diameter	D_e, D_c	$2.5 \times 10^{-2}\ m$
Charge gas density	ρ	$1.225\ kg/m^3$
Link length	y	$4\times 10^{-2}\ m$
Hot, cold temperatures	T_h, T_k	$450\ K, 300\ K$
Working gas	Air	
Gas constant	R	$287\ J/kg.K$
Reciprocator mass	m	$0.1\ kg$
Number of phases	n	3

Table 6-4: Initial and boundary conditions of the balanced compound 2-ph Franchot engine.

Name	***Symbol***	***Value/unit***
Initial piston position	x_0	$0.5\ L_e$
Maximum stroke	x_{max}	L_e
Initial piston speed	$\dot{x}$	$0\ m/s$
Initial pressure difference	Δp	$0\ bar$
Working gas temperature	T_e, T_c	T_h, T_k

6.4.1 Effect of Friction

The start-up of the balanced compound engine is highly dependent on the static friction. Figure 6-6 shows the dynamic response of the $3-ph$ balanced compound Franchot engine in which, a minimum pressure difference of $3.67\ kN/m^2$ is needed to allow start-up. The force generated by this difference overcame the static friction, which is caused mainly by the side forces. In a real application, pistons must be shifted from the mid-stroke point so that a pressure difference can develop. Otherwise, an external starter might be required. However, it is very unlikely that all pistons stop exactly at the mid-stroke due to the mechanical friction, especially when the engine temperature difference is reduced. The mid-stroke equilibrium point may be affected by the difference in the regenerator volumes or the reduction of the swept volume due to the piston rod. Unlike the balanced compound engine, the kinematic engine has the stroke, phase angle, phase shift and the instantaneous position of pistons exactly

defined. Hence, pressure variations occur once the engine is heated which cause the kinematic engine to start-up regardless of the crank angle.

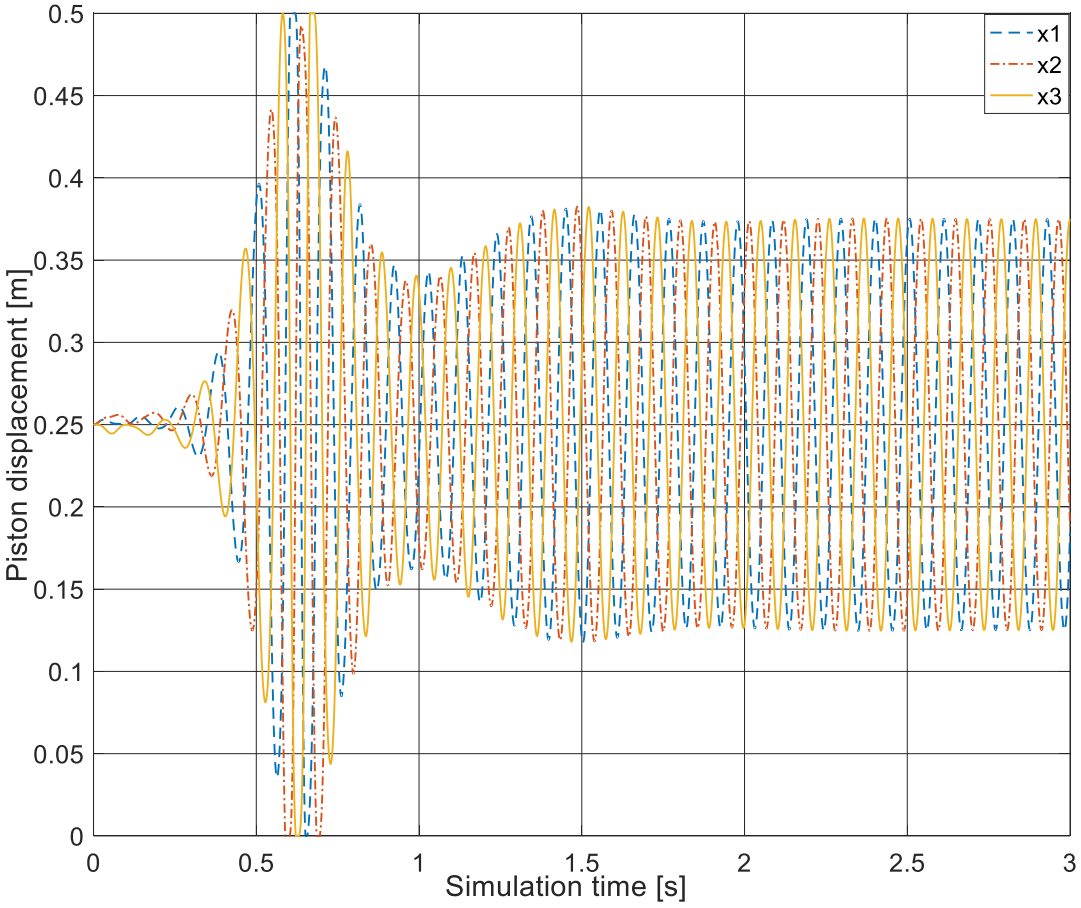

Figure 6-6: No-load dynamic start-up response of the reference 3-ph Franchot engine considering the mechanical friction.

The dynamic response shows that the volume and phase angles are exactly 120°. Different angles are less likely to happen due to the anticipated negative power, which hinders the piston motion (see chapter 5). At the steady state, piston displacements are symmetric and can be represented by sinusoidal functions [179]. The system experiences overshoots before reaching the steady state, that is due to the continuous heat addition while starting which increases the stroke to above steady response.

The driving force and the side force acting on the $3-ph$ balanced compound Franchot engine are shown in Figure 6-7. The maximum driving force occurs at the full stroke while the side forces are minimum. The worst case occurs around mid-stroke where the largest side forces and smallest driving force exist. However, at mid-

stroke, the kinetic energy is maximum and acts similar to the flywheel to overcome negative loads such as friction or speed dependent loads.

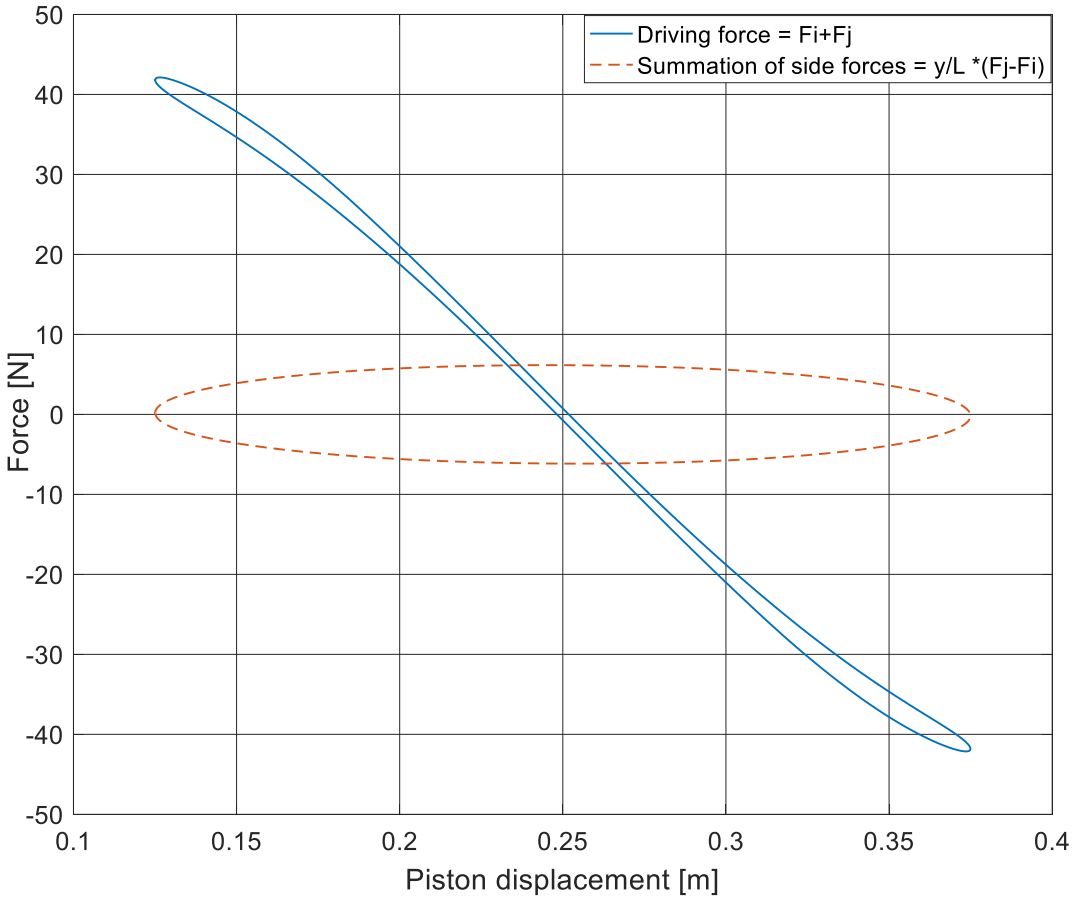

Figure 6-7: Loading forces of the 3-ph balanced compound Franchot engine.

6.4.2 Effect of gas leakage

In Stirling engines, gas leakage must be prevented in order to achieve the design performance. Different methods are used to overcome gas leakage such as using pressurised crankcase, tight seals, diaphragm pistons, liquid pistons and gas compensation. In this study, tight clearance seals are being suggested. The effect of gas leakage due to a typical radial clearance of 25 μm [122] between the piston and cylinder wall is considered in Figure 6-8 for changing piston length. The gas leakage has almost no effect on the engine operation for piston lengths above $3\times 10^{-2}\ m$. However, for smaller piston lengths, the engine stroke decreases as a response to increasing gas leakage while the engine frequency is only slightly affected. Hence, no

special gas compensation techniques is required. For large gas leakage, even the kinematic engine will stall and contact seals are recommended for engines with high gas leakage.

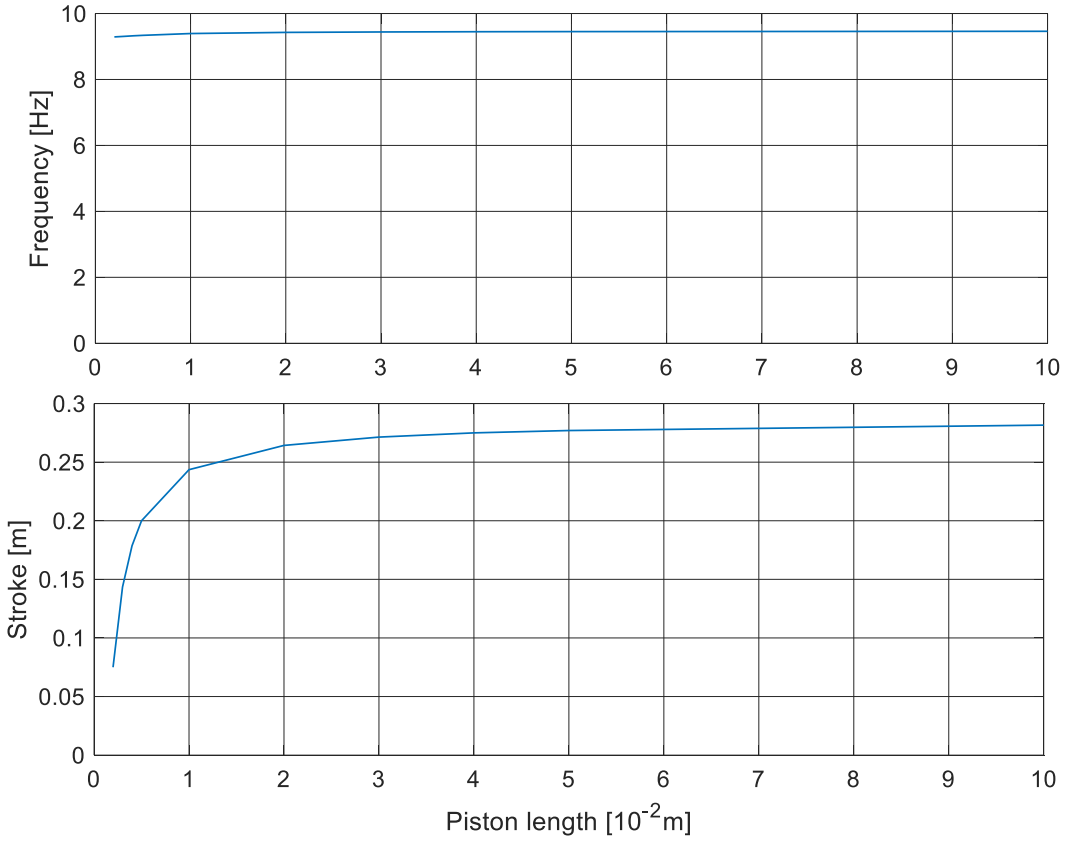

Figure 6-8: Steady state response of the reference engine with changing piston length L_g at no-load condition.

6.4.3 Loading the balanced compound engine

In the kinematic engine, the engine stroke and piston instantaneous location are predetermined. The engine varies its speed as a response to the load. At no-load, the kinematic engine will accelerate until engine losses match the power generated and thus, the brake power is zero and engine speed is maximum. Loading the kinematic engine decreases its speed as well as the speed-accompanied losses. In contrast, the balanced compound engine has its speed determined by the stiffness of the gas spring and the reciprocator mass (see Equation 6.14) and its stroke is undetermined.

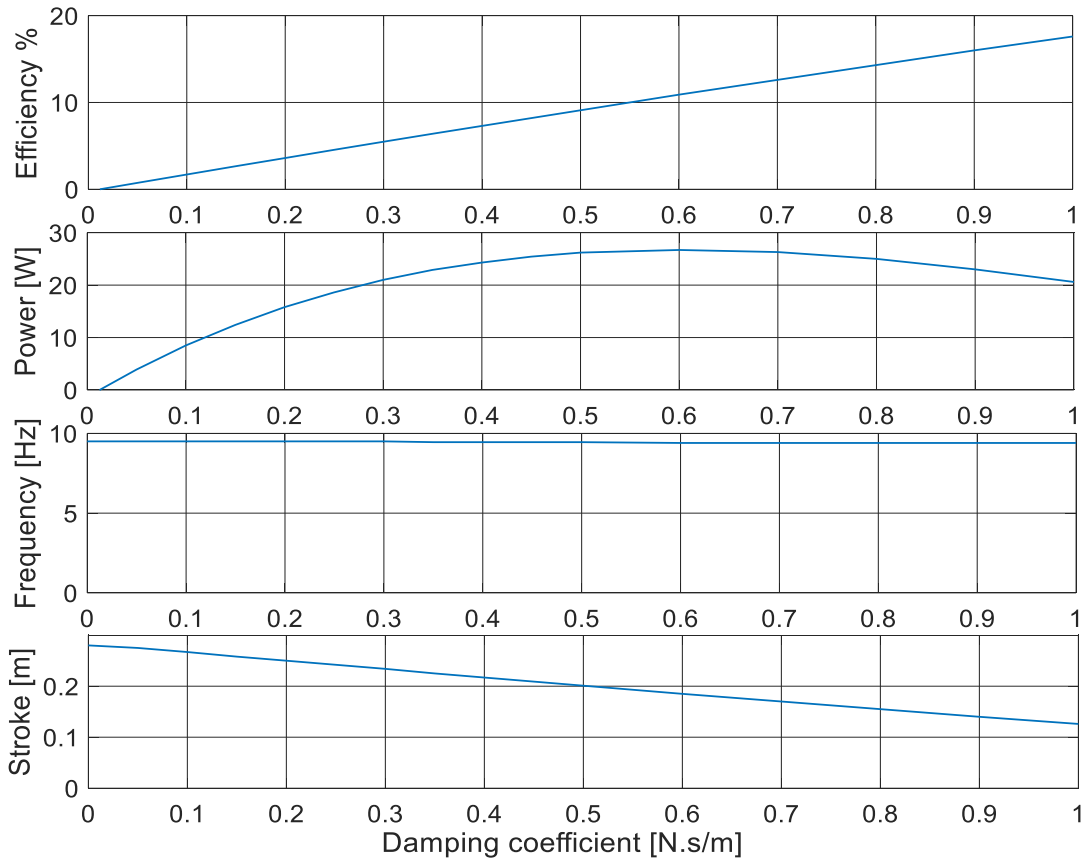

Figure 6-9: Steady state response of the reference engine for changing the damping load.

Figure 6-9 shows the effect of loading the $3-ph$ balanced compound engine by increasing the damping coefficient. The balanced compound Franchot engine has a slight frequency drop but a considerable stroke decrease as a response to increasing the load, which makes it suitable for fixed frequency applications like electricity generation. At no-load, the pistons reciprocate at the maximum stroke allowing heat to be transferred from the hot space to the cold space at highest rate without generating any useful power. At high engine loads, a stall point might be reached where no motion exists. Consequently, no heat will be exchanged and no power will be generated. Hence, a power maximum can be found at a point between the no-load and stall point while the efficiency is maximised as the load increases towards the stall point. The power could be enhanced up to a point where the stroke is slightly smaller than cylinder length but the pistons will hit the cylinder head at no-load. Hence, the no-load condition should be carefully considered even if the engine is always loaded. The phase angle is unaffected by the dynamic load and the engine starts-up for various load values.

Figure 6-10 shows the PV diagram of the $3-ph$ balanced compound engine at the no-load, medium power and maximum power conditions. At the no-load condition, a butterfly-shaped PV diagram shows two negative power regions where the compression overlaps with the expansion process and hence behaves like a gas spring [243]. This spring is important to the balanced compound engine to prevent the pistons from hitting the cylinder head by making gas cushions, but it decreases the indicated work to zero at no-load. At medium and maximum powers, no negative work is found and both the pressure variation and swept volume are smaller than in the no-load case.

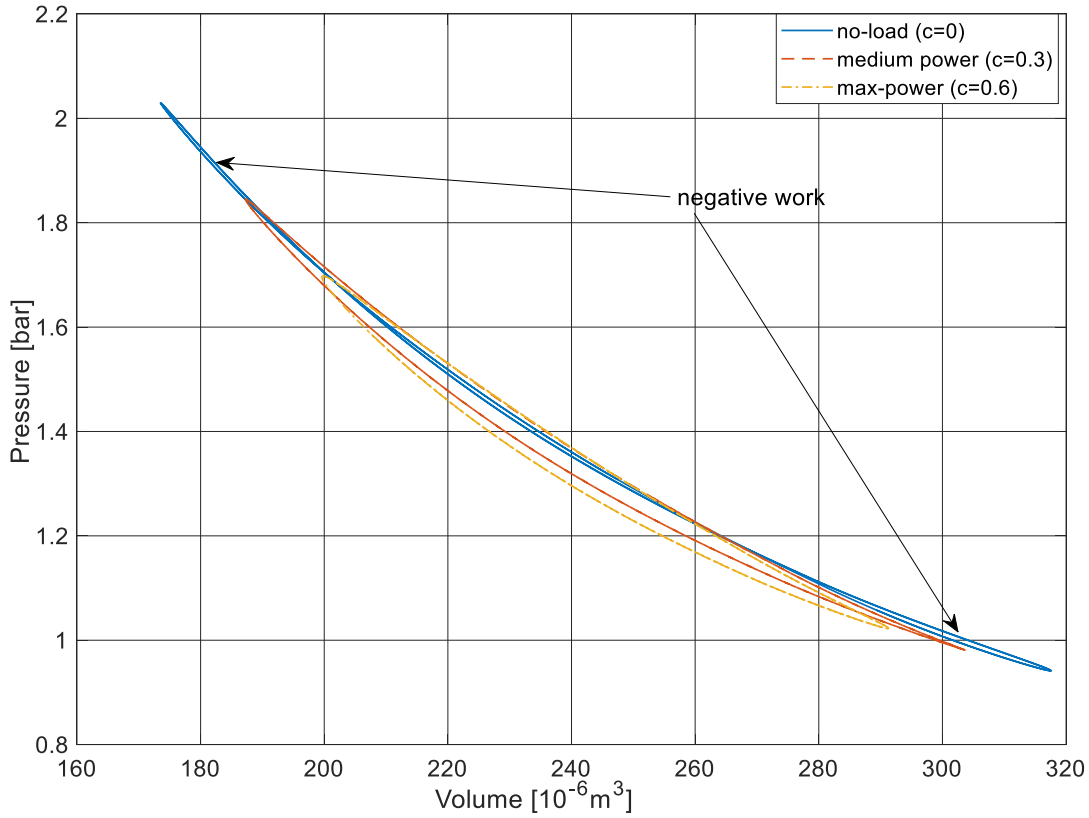

Figure 6-10: PV diagram of the balanced compound engine at no-load and maximum power conditions.

Piston guides (shown in Figure 6-2) play an important role in keeping the pistons and piston rods on track. However, they can be used as a Stirling-cycle refrigerator without requiring additional reciprocating masses, cylinders or cranking mechanism. Only regenerators are connected correctly so that advancing pistons are attached to chilling cylinders and lagging pistons are located in the compression cylinders, which always reject heat. The effect of adding refrigeration load on this duplex machine is shown in

Figure 6-11. The frequency of the duplex machine is higher than the frequency of the engine because of the addition of the refrigerator gas spring. However, the frequency of the duplex machine is nearly constant for increasing temperature difference. The cooling load, stroke and machine COP decreases for increasing temperature difference although the motor efficiency increases. However, the COP_r, which is the ratio of the COP to Carnot COP, increases as the lift temperature increases.

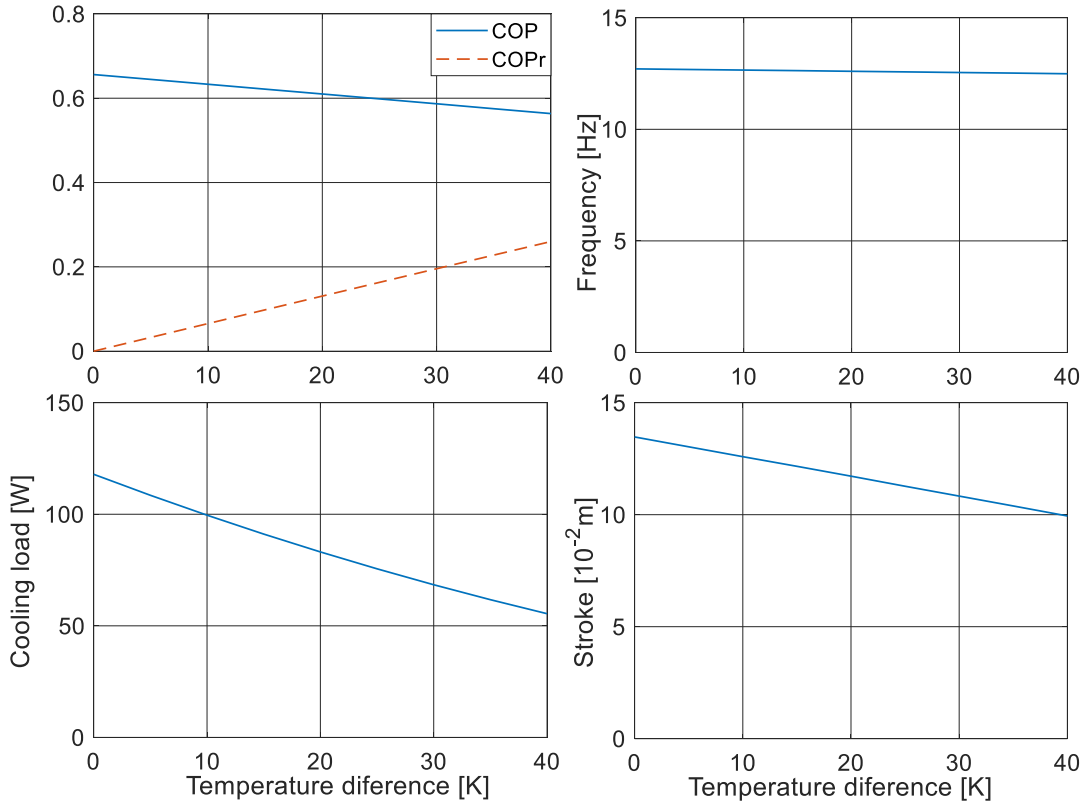

Figure 6-11: Effect of increasing the temperature difference ($T_k - T_{chilling}$) on cooling power, COP, frequency and stroke of the duplex engine having a consistent geometry.

Each machine reciprocator is composed of four pistons (see Figure 6-4) and hence, four force signals are contributing in the total reciprocator driving force as shown in Figure 6-12. These forces are different in amplitude and phase shift but share the same frequency. Due to these differences, the reciprocator generates unwanted moment forces, which increase the friction between the pistons and cylinders. The side forces can be reduced by reducing the length of the crank length y, increasing the length of the piston rod and decreasing the coefficient of friction according to Equations 6.11 and 6.13.

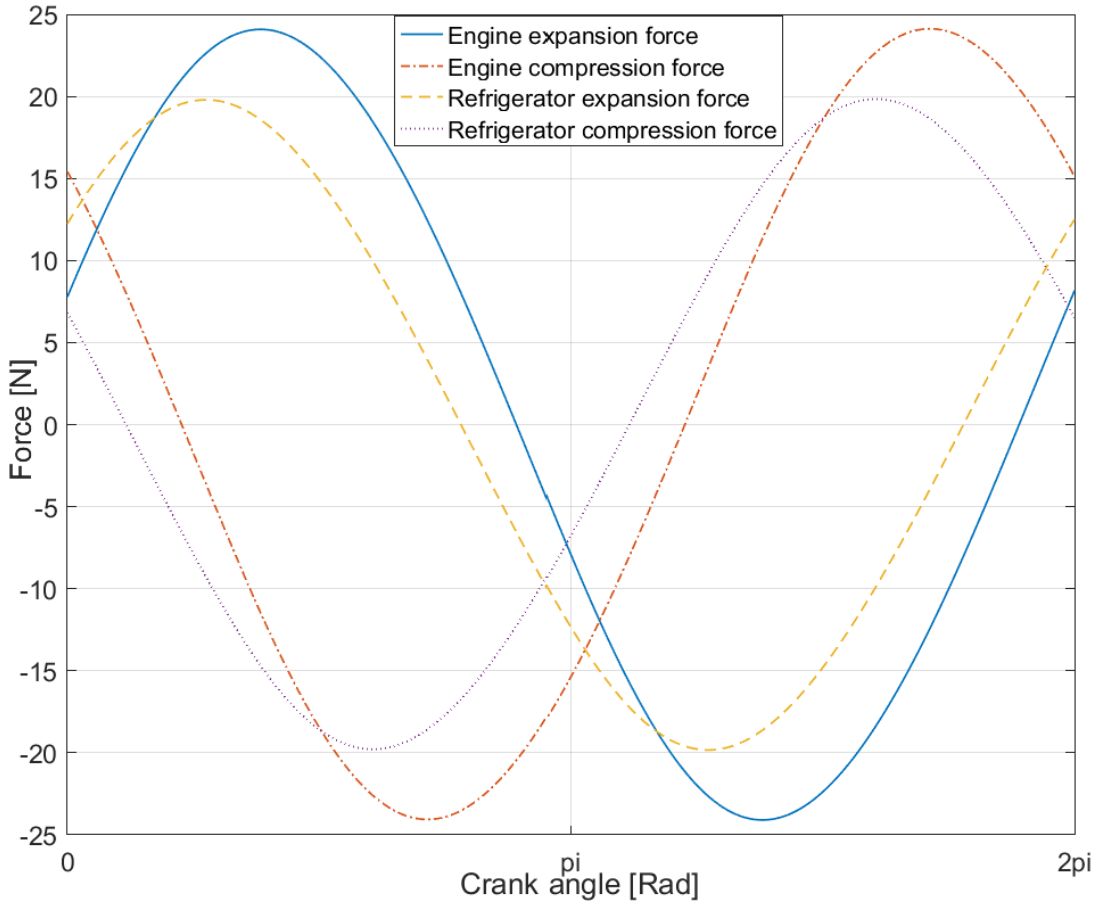

Figure 6-12: The four-piston forces acting on one reciprocator over one crank rotation at $T_l = 300\ K$.

In addition, the expansion and compression cylinders of the refrigerator can be easily interchanged by changing the regenerator connections. If the refrigerator has the same regenerator connecting order as the engine, the expansion cylinders of the refrigerator will be inline with the expansion cylinders in the engine and similarly for the compression cylinders. This is the forward regenerator connection. If instead, the expansion cylinders are inline with the compression cylinders of the refrigerator (reversed regenerator connection), a more balanced force combination leads to reduced side forces. However, no other change can be made to the arrangement of the refrigerator cylinders. Figure 6-13 shows the effect of interchanging the refrigerator cylinders on the side forces. The side force in the case of reversed regenerator connection is reduced to around 20% of the side force for the forward regenerator connection. Thus, according to Equation 6.13,the mechanical friction associated with the side forces will be also reduced to around 20% of the mechanical friction for the

forward regenerator connection. However, the side forces are not completely cancelled out by interchanging the refrigerator cylinders because of the phase shift between the piston forces shown in Figure 6-12. The moment force would only be removed if the refrigerator works as an engine with the same temperature levels as the engine. In his case, the two engines generate identical force signals.

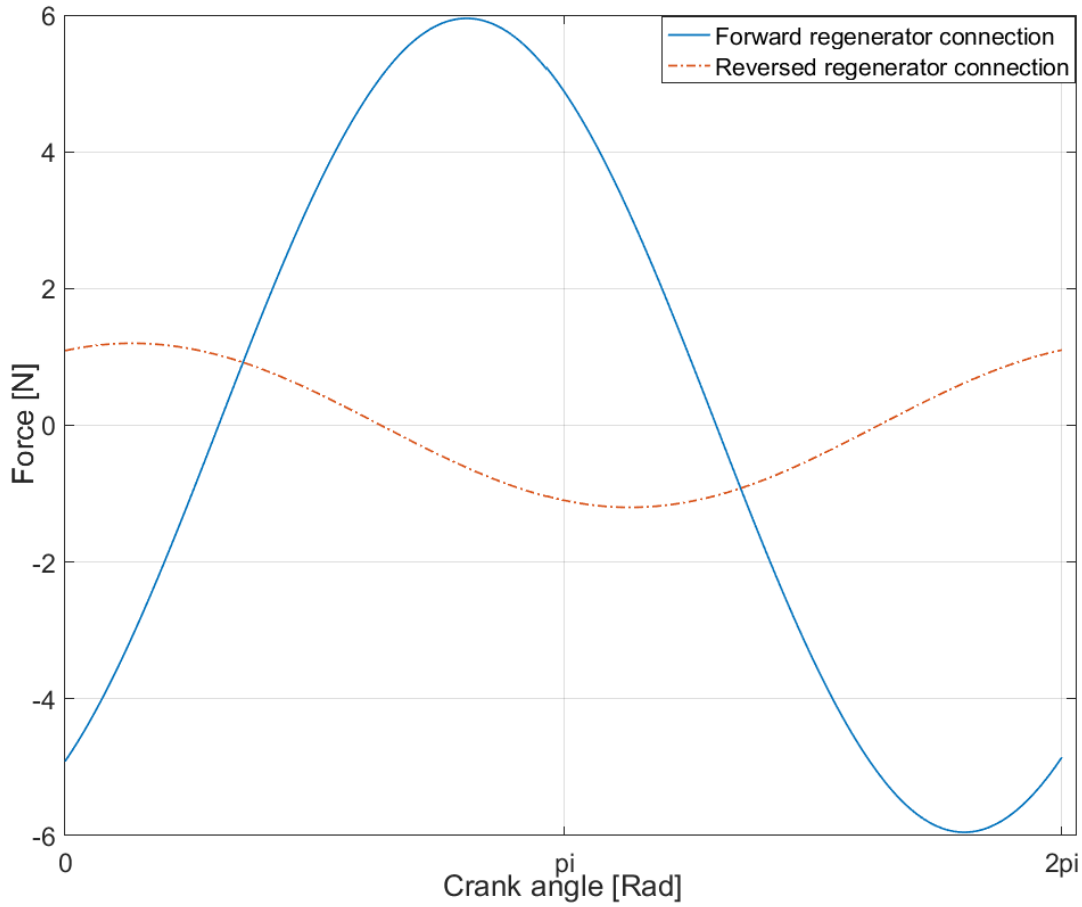

Figure 6-13: Total side forces of the duplex engine for the forward regenerator connection (expansion cylinders of the engine are in line with the refrigerator expansion cylinders) and reversed regenerator connection at $T_l = 300\ K$.

6.4.4 Effect of geometry

Frequency, swept volume, heat transfer and piston forces are all functions of engine dimension. All contribute to the performance of the balanced compound engine with heated and cooled cylinders.

Figure 6-14 shows the effect of increasing the engine cylinder diameters and lengths on the stroke and frequency of the unloaded engine. The increase in the diameter results in a linear increase of the resonant frequency which is in accordance with Equations 6.14 and 6.17. Thus, the engine stroke is reduced so that no total negative power is generated due to the increased swept volume and frequency. For long cylinders, the resonant frequency decreases because of reducing the working gas stiffness according to equation 6.17. In addition, longer cylinders also increase the heat transfer, which in turn leads to longer strokes. It is found that the phase angle is kept unchanged by changing the cylinder geometry and the engine self-starts at no-load.

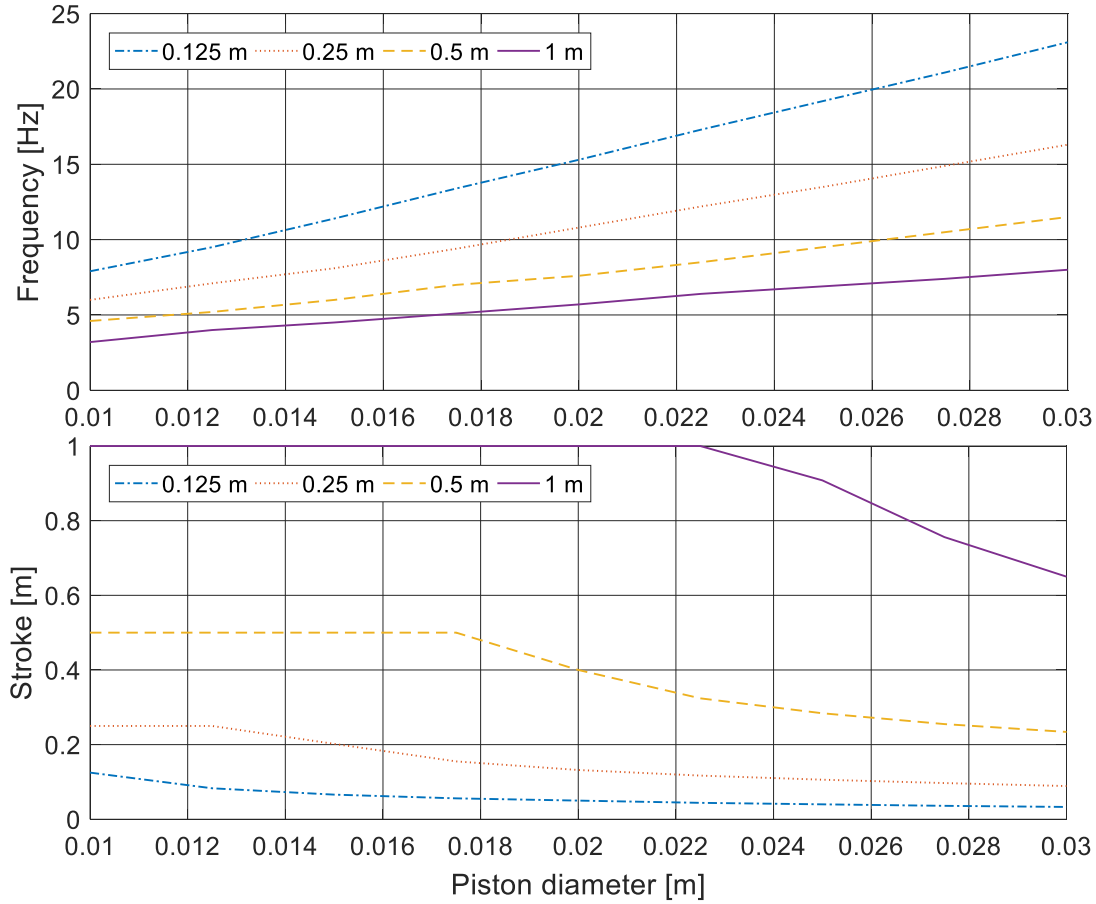

Figure 6-14: Steady state response of the reference engine for changing piston diameter at no-load and for various cylinder lengths (0.125, 0.25, 0.5 and 1 m).

Figure 6-15 shows the influence of changing the diameter on the engine performance at the maximum power condition. It is found that increasing the diameter increases the maximum power and efficiency. The heat transfer increases due to increasing the

Reynolds' number inside the engine cylinders, which increases due to the diameter and the frequency of oscillation. The engine regulates itself by decreasing the stroke until reaching the maximum power as a response to increasing the diameter. Thus, the dead volume increases and hence the efficiency is enhanced.

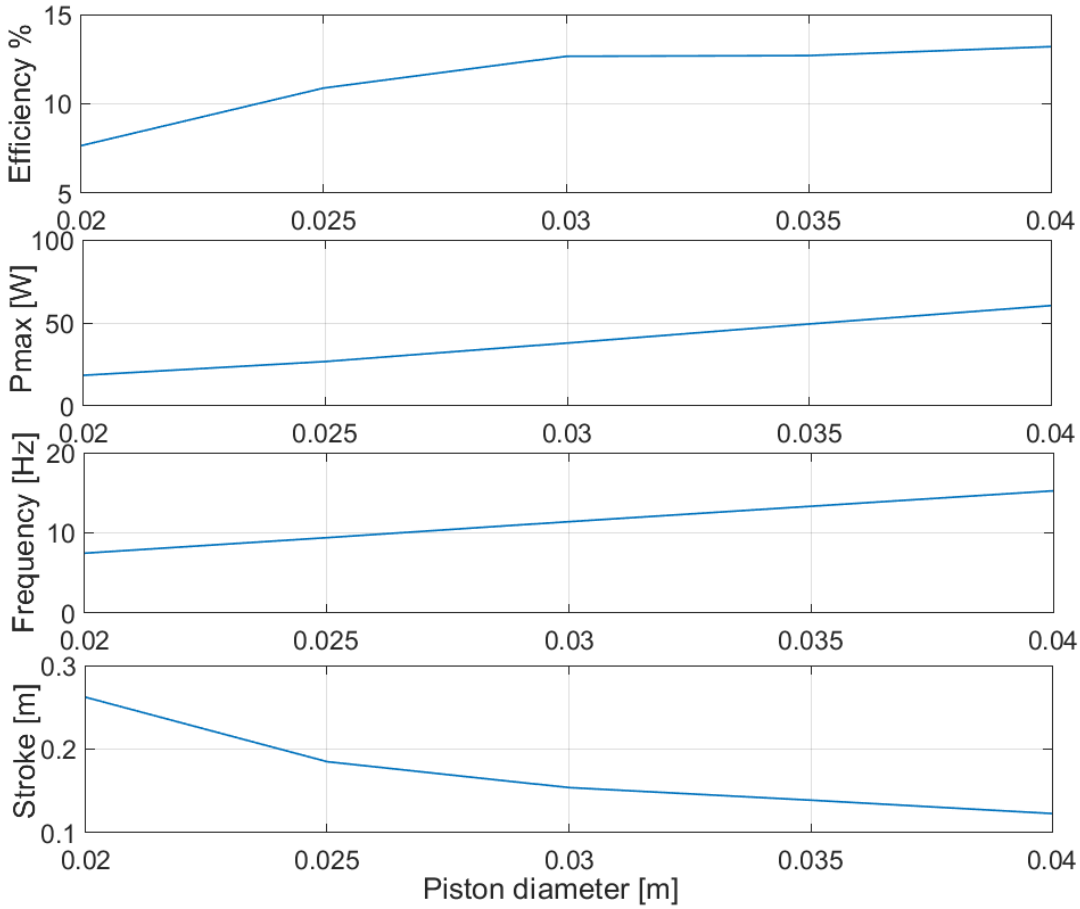

Figure 6-15: Performance of the balanced compound Franchot engine at the maximum power optimised by the damping factor with changing piston diameter.

For the same swept volume, large diameters and short strokes generate large forces which help to overcome potential static mechanical frictions and loads hence ease the start-up of the balanced compound Franchot engine. Moreover, they prevent the pistons from hitting the cylinder head especially at no-load condition.

6.4.5 Effect of temperature

The heat source temperature is the easiest parameter to control in the balanced compound engine and it has a major effect on engine power and efficiency. High-

temperature differences induce high-pressure variations and generate more cycle work than low temperature differences. Thus, both the frequency and stroke increase with increasing temperature differences as shown in Figure 6-16.

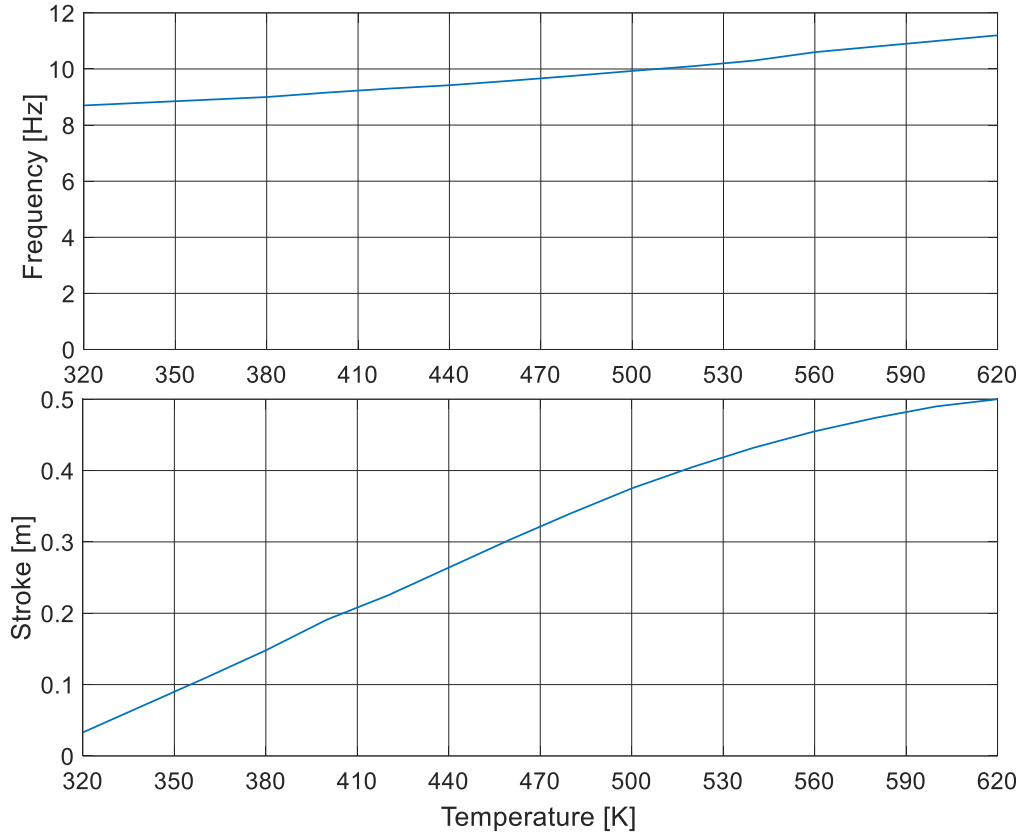

Figure 6-16: Steady state response of the reference engine for changing hot cylinder temperatures and at no-load condition.

The increase in the frequency can be attributed to the increase in the stiffness, which is in turn increased as a response to the increased pressure variation. The phase angle stays constant over the temperature range and the engine is self-starting for dynamic load. However, similar to Figure 6-14, high temperature might cause the piston to hit the cylinder head. Hence, large temperatures require large diameters to decrease the stroke but this will also increase the frequency. Alternatively, the engine load can be increased which will reduce the stroke without affecting the frequency and thus prevents the piston from hitting the cylinder head (see Figure 6-9). Accordingly, increasing the temperature can be used during the start-up to overcome the static friction.

6.4.6 Effect of regenerator dead volume

Increasing the dead volume decreases the pressure variation, which reduces the gas stiffness and hence, engine frequency. Moreover, an increased dead volume increases the engine thermal efficiency as it decreases the indicated power to heat transfer ratio. Thus, an increase in the stroke and decrease in the frequency are predicted for increasing the dead volume, which can be seen in Figure 6-17 .

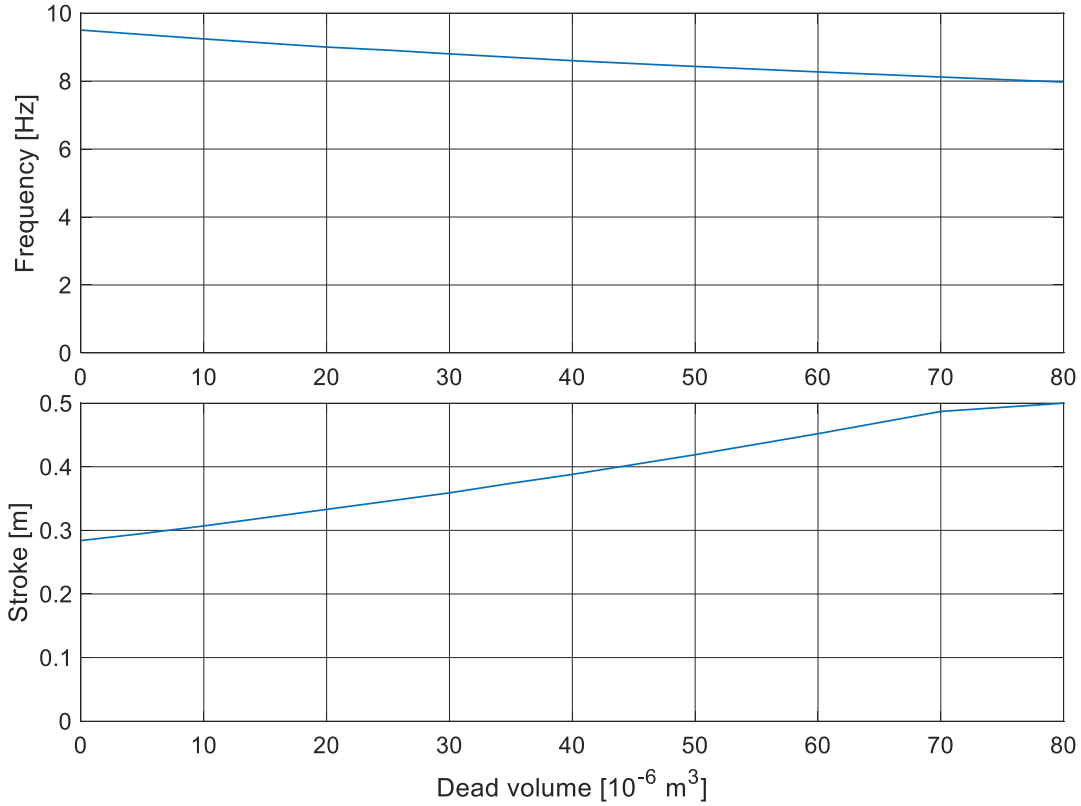

Figure 6-17: Steady state response of the reference engine for changing regenerator dead volumes and at no-load condition.

At start-up, a large regenerator dead volume could prevent the pistons from moving due to the small pressure variation, especially near the equilibrium point. Moreover, a large regenerator has high heat capacity and it takes a long time to create a temperature gradient which is due to the working gas oscillation. Hence, an external kick-start or appropriate piston positioning method might be required to start the motion. In addition, the dead volume can lead to the piston hitting the cylinder head hence causing an unstable operation but it could be optimised to maximise the power or enhance the

efficiency (see section 3.4.2). However, the self-starting capability and fixed phase angle are obtained for the $3-ph$ engine at no-load and dynamic load conditions for different regenerator volumes.

6.4.7 Effect of reciprocator mass

Piston length should be as small as possible in ordered to have the lowest effect on the engine swept volumes, heat transfer area and friction due to reciprocator weight. Reciprocating mass includes the pistons, piston rods and the link between the piston rods. The effect of the mass on engine dynamics is shown in Figure 6-18. Increasing the reciprocator mass causes the stroke to increase and frequency to decrease. Light reciprocators increase the resonant frequency similarly to increasing piston area. The self-starting capability and fixed phase angle are obtained for the $3-ph$ engine at the no-load condition for the reciprocator mass range shown in Figure 6-18.

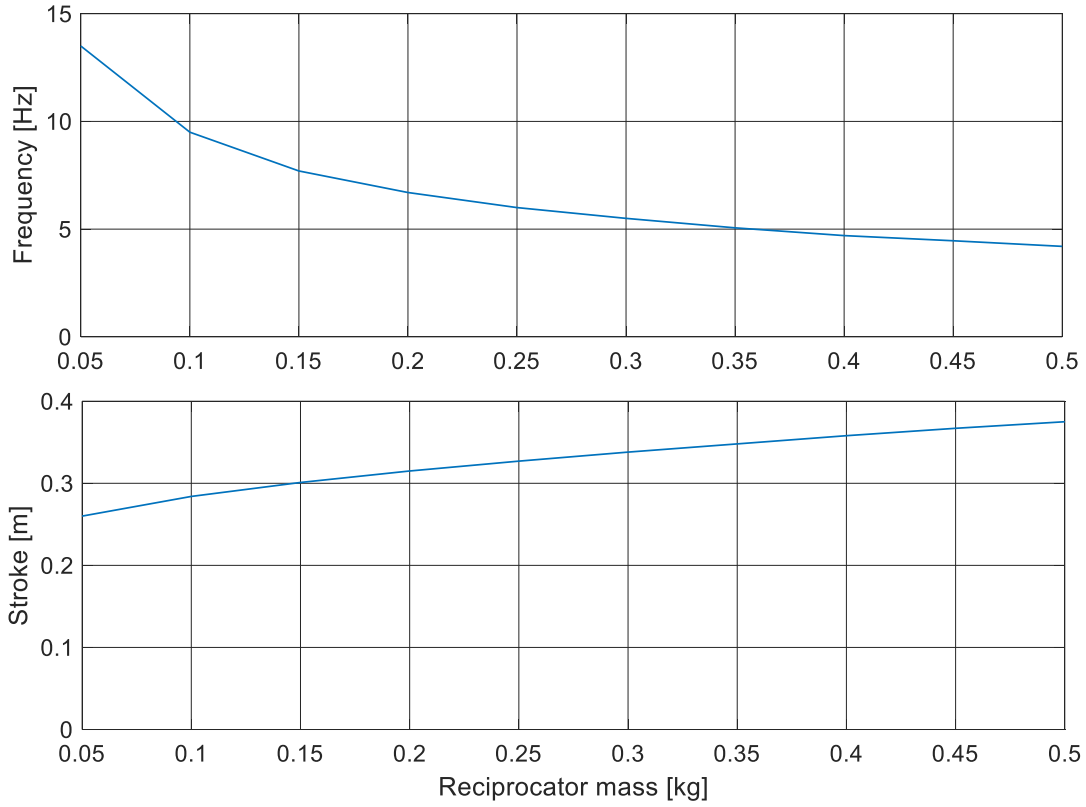

Figure 6-18: Steady state response of the reference engine for changing reciprocator mass and at no-load condition.

6.4.8 Effect of number of cylinders

The Franchot engine has the advantage of a flexible phase angle. For the balanced compound configuration, the phase angle is determined from the order of piston motion and regenerator connection. The number of cylinders is directly linked to the phase angle according to Table 5-2. The phase angle can be predicted for the $3-ph$ and $4-ph$ Franchot engine since they have only the single-phase angles 120^{o} and 90^{o}, respectively. In the $n-ph$ Franchot engines where n is larger than four, the phase angle can take several values in the kinematic engine. Berchowitz and Kwon [154] anticipated the phase angle will decrease for increasing the number of cylinders of the stepped piston design.

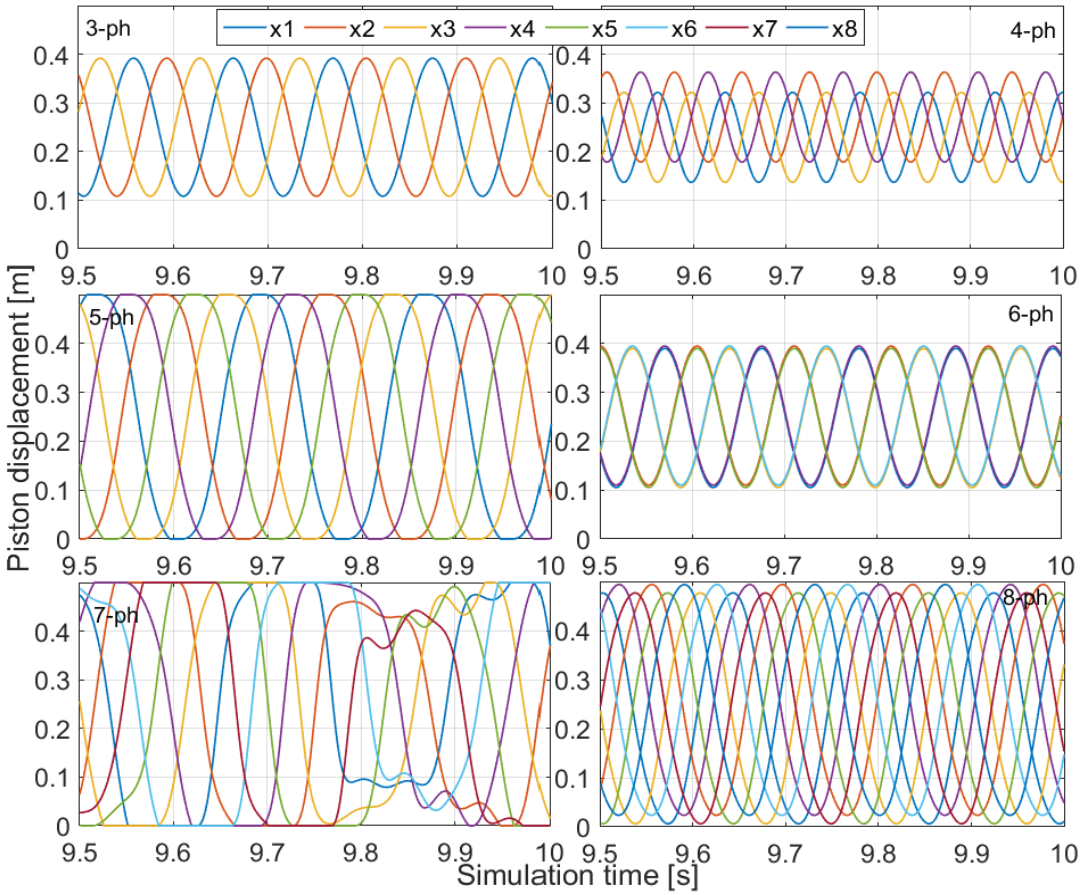

Figure 6-19: No-load steady response for three to eight phase Franchot engine. The reciprocators' motion is given according to the displacement notation.

Figure 6-19 shows that the $n-ph$ balanced compound Franchot engine always works on a single-phase angle unlike the kinematic engine which can be forced to work on

different phase angles (see Table 5-2). Although small phase angles where anticipated for engines with large number of cylinders [154] the balanced compound Franchot engine always operates at the largest possible phase angle. At this phase angle, the pistons encounter the smallest possible piston forces due to the lower pressure difference compared to smaller phase angles. This means the balanced compound Franchot engine prefers the least resisting phase angle among the ones listed in Table 5-2. Thus, the phase angle of the balanced compound $n-ph$ Franchot engine is given as the largest even value of y in Equation 5.5. So y_m can be written as

$$y_m = \begin{cases} n-1 & for\ odd\ n \\ n-2 & for\ even\ n \end{cases} \qquad 6.30$$

Hence, the phase angles of the balanced compound Franchot engine where all regenerator connections are straight can be obtained by substituting Equation 6.30 in Equation 5.5

$$\theta = \begin{cases} 180 - \dfrac{180}{n} & for\ odd\ n \\ 180 - \dfrac{360}{n} & for\ even\ n \end{cases} \qquad 6.31$$

The phase angle in Figure 6-19 is determined from the lagging of a cold working volume of cylinder x_{i+1} to the neighbouring hot cylinder x_i because the regenerator connections are fixed. Hence, the motion sequence of the pistons in corresponding cylinders is used. Due to the even distribution of curves, the phase shift in a cycle is determined by dividing 360 by the number of distinguished phases. Following from this, the phase angle is calculated based on the number of phase shift peaks between the advancing and lagging curves $x_i\ and\ x_{i+1}$, respectively. For example, the $5-ph$ engine has a phase shift of 72° due to five phases and each cold space x_{i+1} lags the corresponding hot space x_i by two peaks, which equals 144°. The $6-ph$ engine has

only three distinguished phases, which result in a phase shift of 60^{o}, and hence a phase angle of 120^{o} due to only two peaks.

The $4-ph$ Franchot engine has the smallest possible phase angle of 90^{o}. This engine has the shortest stroke and largest frequency because a small phase angle increases the pressure variation, which in turn increases the stiffness. Accordingly, the smallest frequency and the longest stroke are found at the largest phase angle at which hitting the cylinder might occur. The $3-ph$ and $6-ph$ Franchot engines have a different number of cylinders but have nearly the same dynamic response due to having the same phase angle. Large phase angles such as in the $7-ph$ engine have an unsteady response, due to the large durations of hitting the cylinder head, while other pistons reciprocate creating pressure variations. Hitting the cylinder head must be avoided for the engine longevity, durability, quietness and efficiency.

The odd-phase balanced compound Franchot engines have similar phase angles and number of cylinders to the multi-cylinder Siemens configuration but different phase shifts as two pistons are moving together at the same time. The phase angle of the even-phase Franchot engines lags behind odd phase engines as the number of cylinders increases. The smallest possible number of cylinders is 3, 4 and 6 in the Siemens configuration, Finkelstein arrangement and balanced compound Franchot engine, respectively.

The balanced compound Franchot engine still has linear vibration problems due to rocking couples. However, two engines can inherently remove the rocking couples if the cylinders are in the correct location and most importantly if the motion of the piston is synchronised. The $6-ph$ engine, as an example, has the pistons already synchronised achieving the same phase angle of the $3-ph$ engine. Hence, the inline cylinders arrangement will be capable to remove the rocking couples. It is expected according to Equation 6.31 that $2n-ph$ engines can remove the vibrations where n is an odd number. The phase angle for this $2n-ph$ engine is the same as the $n-ph$ according to Equation 6.31.

6.5 Conclusion

The balanced compounding of the cylinder wall heated and cooled Franchot engine is mathematically modelled with appropriate validation. The engine response with respect to changes in friction, load, geometry, temperature, dead volume and reciprocating mass has been discussed. The novel $3-ph$ Franchot engine has a favourable phase angle of 120^{o} and short regenerator connections.

The dynamic model of the balanced compound Franchot engine confirms the potential phase angles that were found using the instantaneous power method for the 3-ph and 4-ph Franchot engines, which equals the phase shift. In addition, it is shown that the $n-ph$ balanced compound Franchot engine always prefers the largest possible phase angle so that it operates with the least resisting loads.

In the balanced compounding, the Franchot engine can have only a single-phase angle, which limits its advantages. However, a design choice of the phase angle can be made by changing the number of cylinders. The simplest form of the $n-ph$ free piston engine is the 3-ph engine. It has the shortest regenerator connections, smallest number of cylinders, a favourable phase angle and potential for electricity generation. In contrast to the Finkelstein configuration, the side-by-side balanced compound 3-ph engine has a 120^{o} phase angle, shorter regenerator connections and long engine strokes but it could not eliminate the side forces on the piston rods. The balanced compound engine is suggested for pumping and power generation applications as its response has nearly constant frequency with the load.

Due to the absence of the crankshaft, the balanced compound Franchot engine could have incomplete strokes but with a fixed phase angle and nearly constant frequency as a response to increasing load. The performance of the free piston engine depends on the engine dimension, temperatures, dead volume, reciprocator mass, number of cylinders and load. Small loads, high temperatures, large dead volumes and low diameters increase the stroke, which might lead to the pistons hitting the cylinder heads.

The mechanical friction created by side forces can be decreased by increasing the length of the piston rods, decreasing the offset between the cylinders and by choosing suitable cylinder arrangement for the duplex machine. The friction losses can be reduced to 20% of the maximum friction by selecting the reversed regenerator connection. The engine could be self-starting because the friction prevents the engine from stopping exactly at mid-stroke. Thus, the conceptually suggested balanced compound engine will have great potential as a prime mover for liquid or heat pumps.

CHAPTER

7 Solar powered refrigeration

This chapter discusses a novel idea for placing the Stirling engine cylinders inside the evacuated tubes of a solar collector. The novel idea offers direct thermal coupling to the solar collector without requiring active heat transfer mechanisms. In this chapter, mathematical models with realistic assumptions that take various engine losses into consideration are being used for optimisation of the solar powered machine. The capabilities of the machine have been discussed. To the best of my knowledge, no Stirling machine has been designed to directly work inside the evacuated tubes or is directly exposed to the solar irradiance reflected by line reflectors.

7.1 Evacuated tube collectors (ETC)

The evacuated tube technology has two concentric tubes usually made of borosilicate glass in which air between them is evacuated to reduce heat transfer by convection [244]. Copper tubes placed inside the inner tube are used to allow pressurised HTF to directly flow through the inner pipe (see Figure 7-1A). A metallic tube absorber and only one glass tube (e.g. Schott PTR70 [245]) can be used which allows direct and high-pressure fluid flow for power applications (i.e. Rankine engine).Solar irradiance is absorbed by the surface of the inner tube with a close-fitting aluminium or copper plate attached to the inner glass and copper tubes. Similarly, solar irradiance can be directly absorbed by an inner metallic tube or a fin attached to an inner copper tube where only one glass tube is used. The heat can alternatively be conveyed to nearby thermal loads by heat pipes. Heat pipes are highly conductive thermal devices that use a two-phase fluid inside the copper tube to transfer the heat to its cold bulb end (see Figure 7-1B). The fluid is heated in the evaporation section and turned into vapour. The vapour's heat is then rejected at the cold end where it condenses and becomes liquid again. In comparison to the direct flow method, which uses pumps to circulate

the HTF in the copper pipes, heat pipes use a self-driving mechanism caused by natural convection. However, transferring the heat from the bulb to remote loads still needs a HTF pump. For domestic water heating purpose where pressures are low, the water-in-glass method, which has the water in touch with the internal surface of the evacuated tube, can be used for which it resembles a heat pipe (see Figure 7-1C).

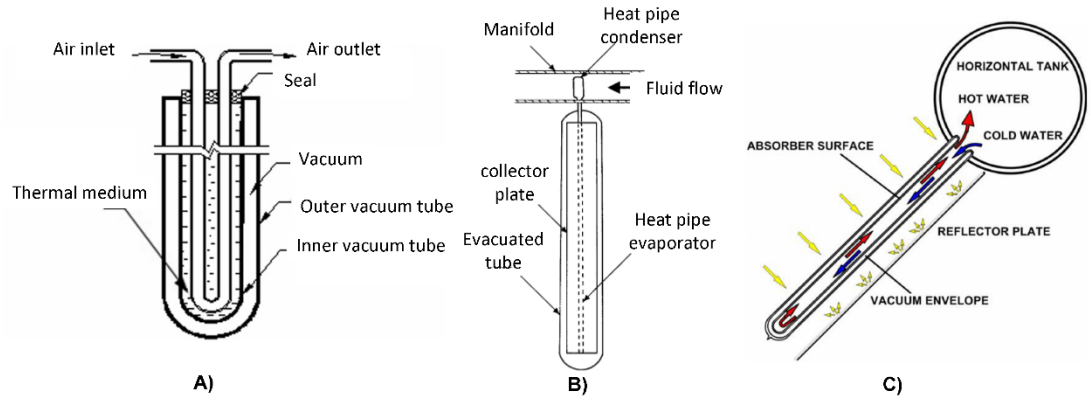

Figure 7-1: Heat transfer methods from the ETC to load, A) direct flow [246], B) heat pipe [6] and C) water-in-glass method [247].

7.2 Solar thermal concentrators

A reflector can be added to the solar collector to increase the collection area and hence the energy and temperature [248]. The reflector surface is usually made of aluminium or silver [249]. The receiver has a small absorbing surface which reduces both the module cost and heat losses which leads to higher temperatures [34]. For example, the parabolic dish which is an imaging point concentrator can achieve temperatures >450° C concentrated in a very small area [33]. However, imperfect tracking can cause complete energy loss. This technology is economically feasible for large-scale applications due to the 2-axis tracking system and high-temperature technologies [249]. A line concentrator can use a reflector to focus the solar radiation in a focal line where an absorbing tube is placed. The line-focus concentrator has lower temperatures than the dish collector due to the larger absorber area. The parabolic reflector which is an imaging reflector perfectly concentrates the parallel solar radiation in a single line achieving temperatures as high as 400° C with non-evacuated tubes [6]. Higher temperatures can be reached with evacuated tubes. However, at least, a good single

axis tracking system is required. This technology has been commercially deployed for industrial applications and uses both evacuated and non-evacuated tubes [250][251][252].

The compound parabolic concentrator (CPC) is a non-imaging reflector, which uses two parabolic reflectors to concentrate the received solar irradiance within an acceptance angle into a focal tube. The CPC concentration ratio is usually up to 5 based on the acceptance angle [6]. The CPC enhances the performance by reflecting the direct and diffused irradiance that passes between the ETC gaps. Hence, the CPC collectors can be stationary (see Figure 7-2), are cheaper and easier to fabricate and operate than other solar concentrators [253]. With a non-evacuated tube, the CPC collector can provide about 35% more energy at a temperature of 95° C than the flat plate collector [254][246]. A stationary CPC collector can also generate a moderate temperature of 200° C at 50% efficiency with ETC and presents a good compromise between simplicity and thermal performance [255]. The collector must be oriented to the south or north if it is in the northern or southern part of the earth, respectively. Thus, creates an angle measured from horizontal called tilt angle. The performance of stationary collectors is improved by selecting an optimal tilt angle close to the latitude angle with a variation in the tilt angle of 10°-15° based on the application. A single axis tracker collects about 15% more than the stationary CPC collector but requires tracking power [256].

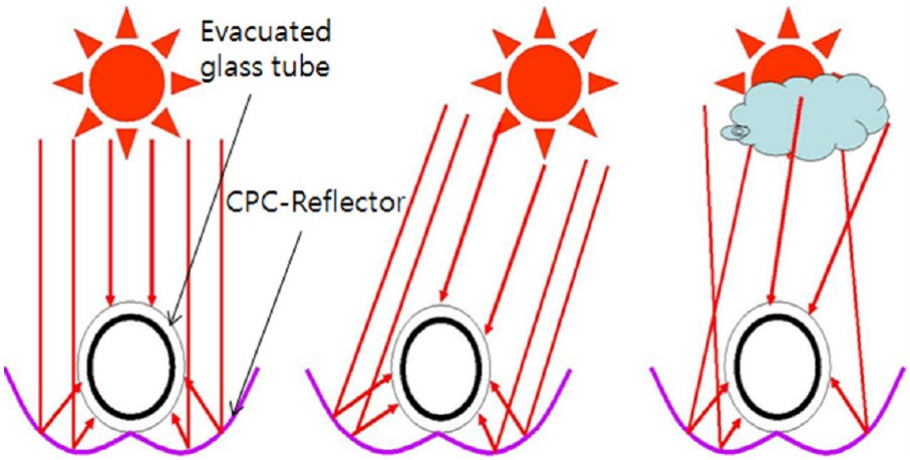

Figure 7-2: CPC reflector with evacuated tube collector and various incident angles [257].

7.3 Direct thermal coupling of the Franchot engine with CPC

The solar CPC collector has a number of evacuated tube and parabolic reflectors. The line absorbers are particularly suitable to heat the multi-cylinder Franchot engine directly due to the similarity in geometry. A novel direct thermal coupling is achieved by deploying the cylinders of the multiphase Franchot engine inside the evacuated tubes. The heat is transferred to the hot cylinder by closely attaching it to the inner surface of the absorber pipe as depicted in Figure 7-3A. A thermally conductive fitting or wire mesh can be added to the annulus between the glass tube and hot cylinders to reduce the effect of the cylinder thermal expansion and vibration on the glass tube. In the future, it might be possible to directly use the absorber glass tube as engine cylinder if a strong and vibration resistant glass is manufactured especially for engines with low maximum pressure. The direct thermal coupling removes the need for extra components such as heat transfer fluid, heat exchangers, piping, auxiliary power supply and fluid pump. Thus, the direct thermal coupling simplifies the design and can potentially lead to systems with higher efficiencies and lower costs. To eliminate the gas static pressure caused by the piston weight, the machine cylinders are placed horizontal for all tilt angles of the CPC collector (see Figure 7-3A).

The large surface area of the cold cylinders of the engine enables the heat exchange with the ambient air by either natural or forced convection. Additional fins can be attached to the cold pipes, which increase the heat transfer area and thus improve the heat flow. It is also important to acknowledge the potential of using the CPC reflector as an external fin (unless it is hot) by attaching it to the cold cylinders to benefit from its large surface area. An annular heat exchanger filled with heat transfer fluid such as water or water-glycol mixture might also be used if even higher heat transfer rates are required. The glycol is used to prevent water from freezing hence it protects the pipes from bursting and guarantees continuous heat transfer. For heat pumping, it must be considered that the glycol degrades by overheating which requires replacing it almost once a year which is expensive [258]. In domestic air conditioning, water can also be used where the minimum temperature is around 7^{o}C.

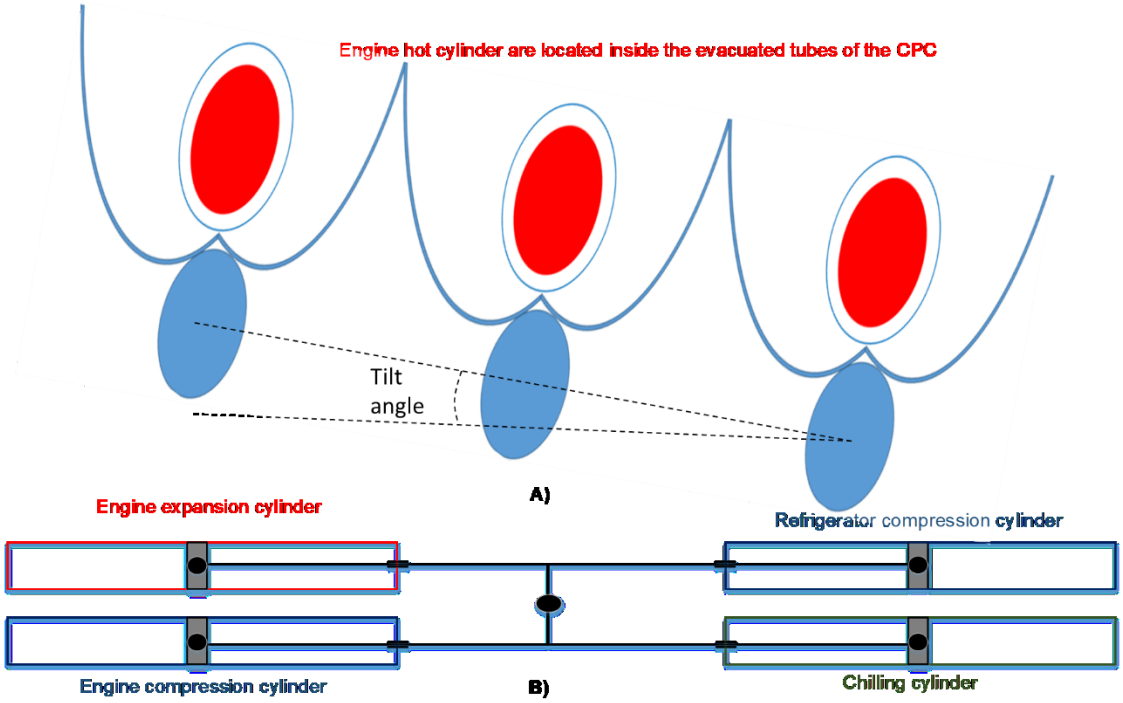

Figure 7-3: Schematic of the proposed solar powered refrigerator A) multi-cylinder Franchot engine inside the evacuated tube of a CPC collector, B) side view of the machine cylinders where the expansion cylinder of the engine is in line with the compression cylinder of the refrigerator.

For solar refrigeration, the Stirling refrigerator is mechanically coupled to the engine using the balanced compounding mechanism discussed in chapter 6. The compression cylinder in the machine rejects heat to the ambient similarly to the compression cylinder of the engine. For transferring cold energy from the expansion cylinder of the refrigerator to the chilled space, the expansion cylinders can be directly deployed in the chilled space. Additionally, fins or an annual heat exchanger can be added to improve the heat transfer.

7.4 Base design of the coupled solar cooler

The CPC collector XL15/26P [259] made by Ritter-XL is chosen as a reference in this case study. The collector is commercially available for the domestic sector and has high performance. It can achieve temperatures of 185° C above ambient at a solar to thermal efficiency of 50%. In addition, it can achieve high stagnation temperature of 338° C above ambient at a solar irradiance of 1000 W/m^2. However, the useful energy

at the stagnation temperature is zero. The high temperatures of this collector positively affect the engine performance at high loads and enable the engine to self-start (see section 6.4.5). The full specifications of the XL15/26P collector are presented in Appendix 1. The machine dimensions are governed by the dimensions of the XL15/26P collector and the $3-ph$ engine. Each ETC has a collector sheet of 11.6×10^{-2} m times 1.5 m. However, shorter lengths of 0.5 and 1.0 m are investigated as well. The chiller and engine are chosen to have the same geometry. The engine diameter is fixed to 2.5×10^{-2} m so that it fits inside the evacuated tube. The machine is assumed horizontal and the effect of gravity on the piston dynamics is eliminated. The crank length is fixed at 4×10^{-2} m due to the ETC diameter. A piston length of 5×10^{-2} m is chosen to reduced gas leakage as shown in section 6.4.2. The reciprocating mass including the link, piston rods and pistons mass was calculated to be 0.31 kg, 0.6 kg and 0.9 kg for the cylinder lengths of 0.5 m, 1 m and 1.5 m, respectively. The regenerator length is kept constant at 0.1 m to fit between the collector cylinders. The regenerator wire mesh diameter is fixed at 90 microns. For simplicity and friction reduction, the $3-ph$ balanced compound Franchot machine is used with the reversed regenerator connection (see section 6.4.3). As the refrigeration cycle has monotonic performance and is directly driven by a Stirling cycle engine, the cooler is assumed to have the same dimensions and operating conditions as the driving engine.

The solar energy intercepted by the collector is calculated from

$$\dot{Q}_{collector} = AG \qquad 7.1$$

where $A\ and\ G$ are the solar collector area and solar radiation intensity per unit of collector area in W/m^2, respectively. The energy absorbed by the collector is calculated using

$$\dot{Q}_i = \zeta \, \dot{Q}_{collector} \qquad 7.2$$

where ζ is the solar collector efficiency calculated by

$$\zeta = \zeta_o - \frac{a_1 \Delta T}{G} - \frac{a_2 \Delta T^2}{G} \qquad 7.3$$

where the constants $\zeta_o, a_1 and \; a_2$ are given by the CPC manufacturer (see Appendix 1). ΔT is the temperature difference between the hot engine cylinder and ambient temperature. Hence, the hot temperature is calculated from

$$T_h = T_k + \Delta T \qquad 7.4$$

The solar collector model is validated against the performance curves provided in Appendix 1. The balanced compounding model (see section 6.2) considers the regenerator losses.

Cooling machines are usually manufactured based on maximum loads [21][260] and optimised for constant irradiance [261]. For example, the irradiance is often fixed at a midday peak of 1 kW/m^2 which coincides with the maximum cooling need. For design purpose, the compression cylinders of the engine and refrigerator are assumed to have a constant and consistent temperature of 27^o C and the chilling cylinders are assumed to have a constant temperature of 7^o C. The effect of different load temperatures is studied in section 7.6.

The regenerator diameter and porosity were optimised for the maximum cold production using the 'Particle Swarm Optimisation (PSO)' function in Matlab while the other parameters are not changed. For example, the phase angle is defined by the

number of cylinders, the piston diameter is limited to the ETC diameter and speed is governed by the moving masses and engine geometry. In addition to the PSO, the regenerator diameter and porosity are manually rounded to the nearest centimetre and and integer number, respectively.

7.5 Optimised solar cooler

The performance of the optimised solar powered machine for different cylinder lengths is summarised in Table 7-1. It is assumed that there is no gas leakage through tight piston rod seals. The regenerator diameter and porosity were optimised for maximum cold production. For example, the optimised regenerator diameter of 0.1 m and porosity of 89% are obtained for a cylinder length of 0.5 m and charging pressure of one atm. The maximum cooling power in this case is 55.7 W. This gives a solar COP (COPs) of 0.334 for a collector temperature of about 135^o C at an efficiency of 58.6%.

Table 7-1: The optimised engine parameters and characteristics at a nominal load of 7^o C, irradiance of 1 kW/m^2 and charging pressure of one atm.

Parameters	***Le=0.5 m***	***Le=1 m***	***Le=1.5 m***
Reciprocator mass	*0.31 kg*	*0.6 kg*	*0.9 kg*
Regenerator diameter	*0.1 m*	*0.11 m*	*0.11 m*
Regenerator porosity	*89%*	*90%*	*89%*
Average stroke	*0.44 m*	*0.94 m*	*1.41 m*
Frequency	*3.22 Hz*	*1.95 Hz*	*1.48 Hz*
Collector temperature	*135^o C*	*134.5^o C*	*142^o C*
Collector efficiency	*58.6%*	*58.6%*	*57.3%*
Engine solar efficiency	*7.1%*	*7.1%*	*8.95%*
Cooling power	*55.7 W*	*114.6 W*	*168.4 W*
Maximum solar COP	*0.334*	*0.344*	*0.337*
Peak cooling power per m^2	*334.2 W/m^2*	*343.8 W/m^2*	*336.8 W/m^2*

The prime mover works at an efficiency smaller than Curzon and Ahlborn efficiency and at low collector temperature. Based on Curzon and Ahlborn efficiency and the efficiency of the XL15/26P collector for T_k =27^o C, the maximum solar engine efficiency is 10.1%. This means that the performance of this machine can be further enhanced if more parameters are optimised for the maximum cold generation. For example, when the engine and refrigerator regenerators were optimised separately, a

maximum cooling power of 61 W was generated for a cylinder length of 0.5 m. The engine regenerator diameter of 0.1 m with a porosity of 90% and the refrigerator regenerator diameter of 7.35×10^{-2} m with a porosity of 89% were obtained. The cold production improved to around 10% which is very close to the Curzon and Ahlborn efficiency.

By considering leakage through the piston rod seals, the average working pressure of the machine is assumed to be 1 atm. Interestingly, the optimised regenerator diameter of 8.7×10^{-2} m at a porosity of 88% for the engine and refrigerator is smaller than for the machine without leaking. It also gives a cooling power of 61 W which gives a specific solar cooling power of 367.5 W/m^2. However, the engine efficiency is 9% and can only be enhanced to 10% by separately optimising the regenerator of the prime mover and refrigerator.

The solar powered machine might also be optimised based on the phase angle in order to decrease the size of the regenerator (see sections 3.4.1 and 3.5.1) by increasing the number of cylinders, which in addition, increases the total cold production. The machine performance can be enhanced by choosing different dimensions for the engine and refrigerator. Moreover, the refrigerator can be isothermalised to improve cold production (see chapter 4) while the engine power maximum is limited by the solar irradiance and maximum power point efficiency. Hence, isothermalising the engine does not increase the total power generated. The high in-cylinder heat transfer results in decreasing the collector temperature. Hence, the efficiency increases for the solar collector and decreases for the engine. In terms of the solar coefficient of performance (COPs), this technology is comparable to the basic PV powered VCC and adsorption coolers. For example, the PV powered VCC has a solar COP of 0.35 for air conditioning. The single stage absorption chiller has a cycle COP of 0.7 and the solar collector efficiency is 0.5 which result in a solar COP of 0.35. However, the Stirling cycle technology conceptually developed in this thesis has the advantages of using stationary thermal collectors, fewer components and devices, no toxic materials, the same technology for the engine and refrigerator and benign refrigerants. In addition, it

enjoys quiet operation, low maintenance requirements and a wide range of temperatures for refrigeration and heat pumping without changing the refrigerant (air).

7.6 Influence of irradiance

Cooling requirements vary based on solar irradiance and ambient temperature. Hence, the machine is investigated for different load conditions and different irradiances as shown in Figure 7-4. It shows that the cold production improves for higher solar irradiance, which adds more energy to the engine and for higher load temperature, which reduces the load on the engine. The solar COP and machine stroke are increased although the solar collector temperature decreased. However, the solar collector efficiency increases for decreasing hot cylinders temperature, consequently more energy is absorbed by the engine.

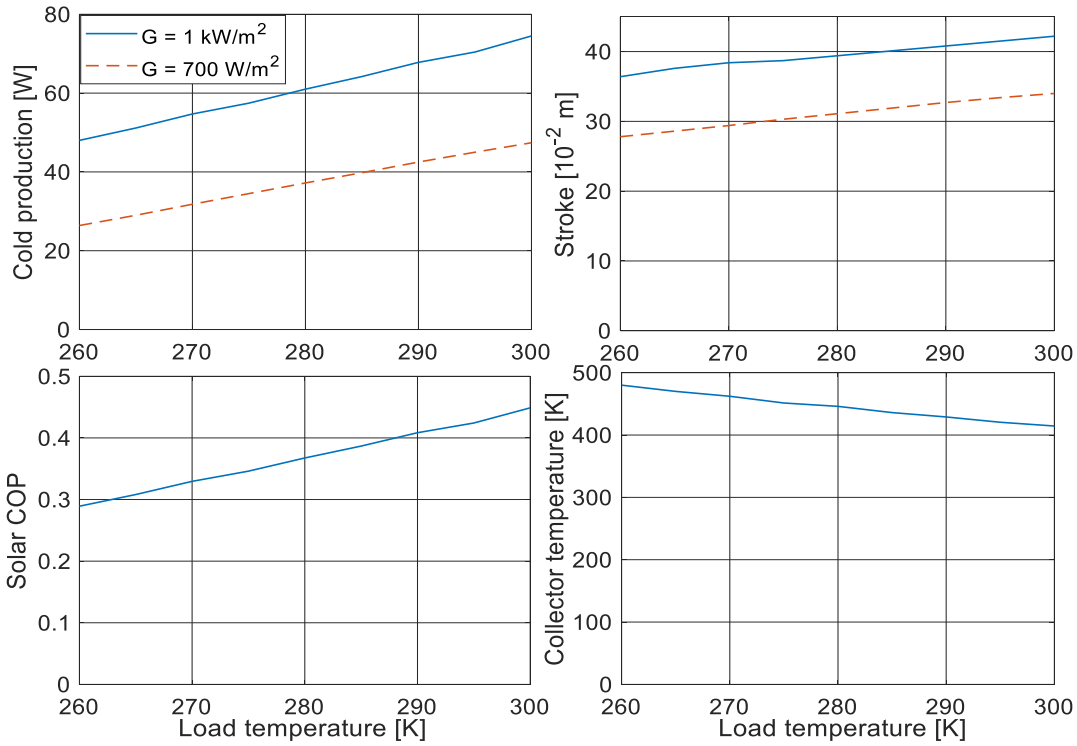

Figure 7-4: Effect of increasing the load temperature on cooling power, solar COP, stroke and CPC temperature at mean machine pressure of 1 atm and solar irradiances of 1 kW/m² and 700 W/m².

For the range of load conditions investigated, no change was observed for the machine frequency, which is almost constant at 3.4 Hz. At load temperature above 300 K and solar irradiance of 1 kW/m^2, the pistons might hit the cylinder heads. Therefore, the engine must be kept loaded at high solar irradiances unless hitting the cylinder heads is prevented by an additional mechanism such as using spring cushioning. However, using mechanical springs is impractical due to the number of springs in the multi-cylinder design and due to the high cylinder temperature (in case of in-cylinder spring placing). Gas cushioning can easily be implemented by decreasing the regenerator dead volume, but it decreases the cold production.

7.7 Conclusion

A novel solar powered refrigerator based on direct thermal coupling of a Stirling engine with a solar collector has been introduced and evaluated with a validated mathematical model. The hot cylinders of the 3-ph duplex Franchot engine are deployed directly inside evacuated tube collectors. This eliminates the need for heat transfer components, such as heat transfer fluid, pumps, complex heat exchangers and an external power supply. Moreover, the cold and chilling cylinders can directly exchange heat with the cooling or chilled spaces due to their large surface area. Fins, fans or cylindrical exchangers could be used to improve the heat transfer if higher heat transfer rates are required. This novel design can produce more efficient and cheaper solar coolers because of the simplified design and removal of intermediate heat transfer steps.

A validated mathematical model of the novel machine has been implemented in Matlab/Simulink. The model has been used to evaluate the performance for different machine configurations and to optimise the regenerator configuration. The results show a promising machine concept for near ambient cooling. The cooling rate per square meter of solar collector can be up to 367 W/m^2 for the basic cycle by only optimising the regenerator dead volume. Moreover, the machine might achieve the optimised response without hitting cylinder heads and hence no additional stroke control mechanism could be needed. The simulation showed good results for air

conditioning and sub-zero cooling using only air at atmospheric pressure as the working fluid. Thus, the Stirling technology is conceptually suggested for near ambient solar cooling.

The solar powered engine performance is determined by the solar collector and Curzon and Ahlborn efficiency. On the other hand, for near ambient cooling, the refrigerator is still open for further improvements due to the monotonic response of cooling power to COP and high Carnot COP. This technology could be further optimised for higher power densities by improving the cooling machine performance such as by using distinct regenerators or isothermalising the refrigerator. For the studied machine, the COP is about four, while the Carnot COP is 14 for 300/280^{o} C. For high temperature solar collectors, the engine might be capable to increase power density without hitting the cylinder head by decreasing the dead volume and phase angle or increasing the pistons diameter. However, the smallest phase angle is 90^{o} for the four cylinder configuration and the piston diameter is determined by the solar collector.

CHAPTER

8 Conclusion and recommendation

The main aim of this thesis is to design a solar powered refrigeration system based on the Stirling cycle. Simplicity in design that maintains the power density is important as it might lead to reduced costs. Thus, a literature review in chapter 2 is performed to determine the parts, which are responsible for increasing the complexity of the design and to show some other alternatives. The complexity in power dense Stirling machines was attributed to the use of light gases, complex materials, heat exchangers, drive mechanisms and solar coupling. To reduce design complexity, air was adopted in this study, as it is readily available, free and easily replenished. Moderate temperatures between 450 K and 600 K are studied as they allow the use of simple materials like graphite seals and simple solar collectors. However, the efficiency and power density of the moderate temperature engines are smaller than for engines with high temperature, which for example, are using point focus collectors. For further reduction in the complexity, the Franchot machine was used due to its reduced losses and potential for cylinder wall heating and cooling. However, these solutions create challenges of improving the power density, efficiency, drive mechanism and solar collector coupling. Thesis challenges are addressed in this thesis.

Finding alternative heating and cooling methods for Stirling machines is one of the goals of this study. It is addressed in chapter 3 by a novel engine design that benefits from the Franchot engine cylinders to work as large stroke to bore ratio heat exchangers. This method is able to reduce the dead volume, complexity and heat losses. A mathematical model was derived for this engine which takes the reduced number of control volumes and the polytropic process of the expansion and compression into account. The regenerator end temperatures are also defined based on the working gas temperatures due to the polytropic processes. The engine and refrigerator are investigated separately and without considering the gas flow losses to understand their performance behaviour and characteristics due to cylinder wall

heating and cooling. It is anticipated that changing the phase angle is superior to changing the dead volume for maximising the generated power. However, the power density using cylinder wall heating and cooling is low but could be slightly improve by increasing the machine speed or working gas pressure. The engine could achieve Curzon and Ahlborn efficiency with negligible effect of hysteresis losses. The refrigerator has monotonic response and can theoretically approach Carnot efficiency at small cooling loads.

To increase the Stirling machine power density with reduced gas flow rate, a novel isothermaliser is introduced in chapter 4. The mathematical model is extended to consider the effect of the isothermalisers and is validated against an experimental study. Performance comparisons between the bare cylinders with optimal phase angle, the isothermal and adiabatic cycle and the novel isothermalisers are made for the engine and refrigerator separately. In comparison to the adiabatic engine, it is found that the active isothermalisers increase the power per swept volume to 275% while the passive isothermalisers increase it to 211% at the maximum power point. However, the active and passive isothermalisers produce only 57% and 44% of the ideal isothermal engine power, respectively. For the active and passive-isothermalised refrigerator, the cooling power density improvements are 250% and 190% at a COP of 3.25 in comparison to the adiabatic cycle, respectively. The bare cylinder engine with phase angle method is found to be inferior to the isothermaliser method due to lower heat transfer and higher gas flow rate. The latter results in larger pumping and enthalpy losses as the gas passes through the regenerator. The isothermaliser increases the heat transfer by decreasing the hydraulic diameter, which also decreases the swept volume and hence the gas flow rate. It is also found that the isothermaliser method is equivalent to using multiple cylinders having the same total cylinder area, hydraulic diameter and phase angle in terms of power generation and efficiency but only uses two cylinders, which results in less moving parts and eases the maintenance, sealing and drive mechanism.

The effect of using multiple cylinders with the kinematic drive is studied for some mechanical and dynamic attributes in chapter 5. The study is performed based on an

extended model of that derived in chapter 3. The performance was assessed based on the mechanical configuration, negative power generations and vibration reduction. In addition to power enhancement, the multi-cylinder Franchot engine might have the ability to work without a flywheel, to self-start and to reduce the primary vibrations. That is because the power needed for compression is instantly compensated by the expansion power generated by another Franchot engine. It is anticipated that to remove the vibration due to rocking couples, at least three Franchot engines each with a pair of hot and cold cylinders should be used while in comparison, the Siemens engine cannot remove the rocking couples. For the $3-ph$ and $4-ph$ Franchot engine, there is only one feasible phase angle each to reduce the power pulses, remove the rocking couples and reciprocal vibrations while there are multiple angles for the engine with more than four phases.

Given that the negative power could be eliminated for the kinematic engine especially at specific phase shifts, the pistons have potential to reciprocate without the need for a rotating drive. The key step is to directly couple an expansion and compression piston via the piston rods so that the compression piston power is directly drawn from the expansion piston power. This method is known as the balanced compounding mechanism. Thus, no rotary motion is generated which limits the potential applications of the engine. In chapter 6, the balanced compounding is studied by modifying the piston coupling. The mathematical model is extended to include the effect of gas leakage and potential mechanical loads. The model is validated against an experimental Siemens engine, which uses mechanical springs instead of gas springs in the balanced compound engine. The model anticipated that the engine has nearly constant operating frequency depending on the gas spring stiffness and reciprocating rod mass. Hence, for increased input energy or reduced load, the engine responds by increasing its strokes. Moreover, increasing the piston diameter, decreasing the dead volume or number of phases increases the frequency and decreases the stroke. The balanced compound Franchot engine has only one operating phase angle determined by the number of cylinders, which is the largest possible phase angle. For heat pumping, it is expected that the piston side forces are minimised if the expansion piston of the engine is in line with the compression piston of the refrigerator.

To address the main goal of the study, the solar powered machine is studied for the CPC collector in chapter 7. Due to the similiarities in geometry, the balanced compound Franchot engine is installed inside the evacuated tubes of the CPC collector. Thermal coupling between hot engine cylinders and the collector tubes is also discussed. A model that takes into account the collector temperature and potential losses due to gas flow and mechanical friction is implemented. The regenerator dead volume and porosity were optimised for maximum cold production because the phase angle is unchangeable. The cold production per square meter of solar collector is 367.5 W/m^2 for the basic machine design and air conditioning application. For the long evacuated tube, the performance of the solar powered refrigerator does not change. The solar to mechanical efficiency is comparable to a PV module with 10% efficiency. The mechanical energy is directly obtained without an electric motor, which adds to the cost and complexity and reduces the efficiency of the system. The COP of the refrigerator at temperatures of 280/300° C is four, which is comparable to that of the VCC.

The developed cooling system in this study is characterised by material simplicity, quietness, use of unpressurised air as a working fluid, safety, self-starting, simplified heat exchanger, direct thermal coupling with solar collector, similar technology for engine and refrigerator, working on sub-zero temperatures without changing the working gas and lack of electronics, rotational elements and external power supply. As a result, the current technology could be suitable for solar near ambient refrigeration.

8.1 Recommendation and future work

For the $3-ph$ solar cooler working directly with the CPC collector, the regenerator dead volume is around 93% of the total engine swept volume. Hence, decreasing the dead volume requires increasing the phase angle to keep high performance. So, changing the number of cylinders would be the only option to increase the phase angle and to decrease the dead volume.

The $4-ph$ engine has a phase angle of 90°, which is the smallest possible phase angle for the balanced compound Franchot engine. Small phase angles decrease the stroke making the Franchot engine more suitable to work with high temperature solar collectors and hence high-power generation such as with the parabolic trough collectors. However, the $3-ph$ and $6-ph$ engines have a phase angle of 120° and can work on temperatures higher than those obtained by the CPC collector by decreasing the dead volume to avoid hitting the cylinder heads. The $6-ph$ balanced compound Franchot machine is particularly interesting due to its ability to remove rocking couples with the smallest number of cylinders. Moreover, the $3-ph$ and $6-ph$ engines have potential for $3-ph$ electricity generation due to the phase shift between pistons.

Instead of using a water-cooling jacket for cold cylinders or using isothermalising cylinders, it might be better to benefit from the solar reflector surface for exchanging heat. However, the effect of wind, natural and forced cooling of these cylinders needs further studies. It is also suggested for the hot pistons to be directly installed inside the glass tube to reduce material cost given that the pressures are near atmospheric. However, the vibration of the engine and the brittle nature of the glass need to be addressed.

The friction and gas leakage have negative effect on the balanced compound machine performance and hence using honed cylinders is recommended. For the temperature range obtained by the CPC collector, various dry sealing options can be used such as PTFE and graphite seal. The latter has low thermal expansion comparable to stainless steel and good thermal conductivity.

To eliminate the effect of gravity (e.g in case of solar tracking or inclined piston mounting) and hence the corresponding gas leakage through the pistons, the cylinders of the balanced compounding machine need to be horizontally installed. Although it is expected to be small the effect of gravity, in the case of inclined mounting and using clearance seals, might be balanced by adding mechanical springs which need to be

long or by using an air pump to replenish the gas leakage from the lower to the upper side of a Franchot engine. However, gas leakage can be reduced by using contact seals.

The maximum generated mechanical power is governed by the CPC power and temperature and the Stirling engine efficiency. The refrigerator might still increase its COP to high values, as the Carnot COP at temperatures of 280/300 K is 14. Hence, cold production improvements could be achieved if the refrigerator has isothermalisers. Moreover, it might be interesting to use PV panels with the isothermalised Stirling cycle refrigerator given that the electrical energy generated by the cheap PV collectors and the solar powered Franchot engine are of the same order. Thus, the refrigerator can be dislocated from the engine for more installation flexibilities.

The solar powered refrigerator might be modified to work as a heat pump or electricity generator. Thus, the machine may benefit from the loss of cooling need without considering energy storage. However, excessive cold generation needs to be stored to cater for the cooling demand during the temporary loss of solar irradiance (e.g. at night). Storing near ambient cold is better than storing the hot input energy. That is due to the safe temperature level, two-phase storage material availability (water) and lower storage energy in comparison to the hot energy.

Appendix 1

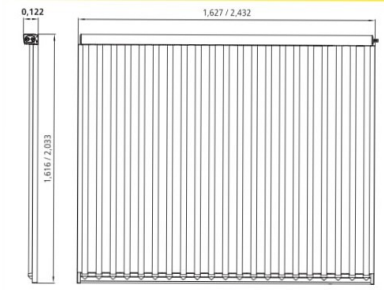

Vakuumröhrenkollektoren Baureihe XL P

- Hochleistungsvakuumröhren nach dem Thermoskannenprinzip (Dewar-Röhren)
- Antireflexbeschichtung
- Witterungsbeständiger CPC-Spiegel (Compound Parabolic Concentrator)
- U-Rohr-Register aus Spezialstahl
- Optimiert für sehr große Felder und industrielle Anwendungen

Technische Angaben

Baureihe		XL 15 / 26 P	XL 15 / 39 P	XL 19 / 33 P	XL 19 / 49 P
Anzahl der Vakuumröhren		14	21	14	21
η_0 (Apertur), DIN 4757-4 bzw. EN 12975	%	68,7	68,7	68,7	68,8
a_1 mit Wind, bez. auf Apertur	W/(m²K)	0,613	0,613	0,613	0,583
a_2 mit Wind, bez. auf Apertur	W/(m²K²)	0,003	0,003	0,003	0,003
$K_{\theta,IAM}$ (50°)		0,94	0,94	0,94	0,94
$K_{\theta,d}$ (50°)		0,90	0,90	0,90	0,90
Rastermaße (Länge x Breite x Tiefe)	m	1,616 x 1,627 x 0,122	1,616 x 2,432 x 0,122	2,033 x 1,627 x 0,122	2,033 x 2,432 x 0,122
Bruttofläche	m²	2,63	3,93	3,31	4,94
Aperturfläche	m²	2,33	3,49	3,00	4,50
Kollektorinhalt	Liter	2,13	3,19	2,53	3,79
Gewicht	kg	39,9	58,7	49,1	72,4
Betriebsüberdruck, max. zulässig	bar	10	10	10	10
Stillstandstemperatur, max.	°C	338	338	338	338
Anschluss-Weite, Klemmverschraubung	mm	15	15	15	15
Material Kollektor		Aluminium / Stahl / Kupfer / Glas / Silicon[1] / PBT / EPDM / TPE			
Material Glasröhre		Borosilicat 3.3			
Absorberschicht		hochselektiv			
Glasröhre (Außend./Innend./Wandst.)	mm	47 / 36,2 / 1,6			
Farbe (Alu-Rahmenprofile, Eloxal)		Aluminiumgrau (bzw. Natureloxal / A6CO)			
Farbe (Kunststoffteile)		Schwarz (bzw. Schwarz / RAL 9004)			
Prüfbericht EN 12975-2	ITW-Prüfberichtnr.	11COL1008/2OEM02	11COL1008/2OEM02	11COL1008/2OEM02	11COL1007/1OEM02
DIN CERTCO-Registernummer	Solar KEYMARK	011-7S2434R	011-7S2434R	011-7S2434R	011-7S2425R
Wärmeträger		Wasser			

[1] Siliconfreie Variante auf Anfrage

Kollektorkennlinien bei unterschiedlicher Einstrahlung

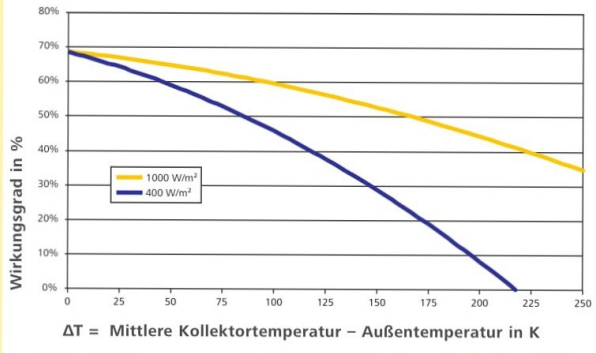

Ritter XL Solar – Eine Marke der Ritter Energie- und Umwelttechnik GmbH & Co. KG

Kuchenäcker 2
72135 Dettenhausen
Deutschland

Tel. +49 7157 5359 - 254
Fax +49 7157 5359 - 125
info@ritter-xl-solar.com
www.ritter-xl-solar.com

TH-2410 V1.5 07/2017

Bibliography

[1] J. M. Daoud and D. Friedrich, "Performance investigation of a novel Franchot engine design," *Int. J. Energy Res.*, Aug. 2017.

[2] J. M. Daoud and D. Friedrich, "Parametric Study of an Air Charged Franchot Engine with Novel Hot and Cold Isothermalizers," *Inventions*, vol. 2, no. 4, p. 35, Dec. 2017.

[3] J. M. Daoud and D. Friedrich, "Design of the multi-cylinder Stirling engine arrangement with self-start capability and reduced vibrations," *Appl. Therm. Eng.*, vol. 151, no. January, pp. 134–145, 2019.

[4] J. M. Daoud and D. Friedrich, "A novel Franchot engine design based on the balanced compounding method," *Energy Convers. Manag.*, vol. 169, pp. 315–325, Aug. 2018.

[5] J. Khan and M. H. Arsalan, "Solar power technologies for sustainable electricity generation - A review," *Renew. Sustain. Energy Rev.*, vol. 55, pp. 414–425, 2016.

[6] S. A. Kalogirou, "Solar thermal collectors and applications," *Prog. Energy Combust. Sci.*, vol. 30, no. 3, pp. 231–295, Jan. 2004.

[7] K. F. Fong, T. T. Chow, C. K. Lee, Z. Lin, and L. S. Chan, "Comparative study of different solar cooling systems for buildings in subtropical city," *Sol. Energy*, vol. 84, no. 2, pp. 227–244, 2010.

[8] M. Gräber and C. Kirches, "Nonlinear model predictive control of a vapor compression cycle based on first principle models," *Proc. 7th Vienna Int. Conf. Math. Model.*, p. 6, 2012.

[9] G. liang Ding, "Recent developments in simulation techniques for vapour-compression refrigeration systems," *Int. J. Refrig.*, vol. 30, no. 7, pp. 1119–1133, 2007.

[10] N. Hariharan and B. P. Rasmussen, "Parameter estimation for dynamic HVAC models with limited sensor information," in *Proceedings of the 2010 American Control Conference*, 2010, pp. 5886–5891.

[11] N. Rona, *Solar Air-Conditioning Systems: Focus on components and their working principles*. 2004.

[12] M. Alobaid, B. Hughes, J. K. Calautit, D. O'Connor, and A. Heyes, "A review of solar driven absorption cooling with photovoltaic thermal systems," *Renew. Sustain. Energy Rev.*, vol. 76, no. March, pp. 728–742, 2017.

[13] N. Aste, C. Del Pero, and F. Leonforte, "Active refrigeration technologies for food preservation in humanitarian context - A review," *Sustain. Energy Technol. Assessments*, 2016.

[14] B. P. Rasmussen and A. G. Alleyne, "Dynamic modeling and advanced control of air conditioning and refrigeration systems," ACRC TR-244, 2006.

[15] U. Eicker, D. Pietruschka, A. Schmitt, and M. Haag, "Comparison of photovoltaic and solar thermal cooling systems for office buildings in different climates," *Sol. Energy*, vol. 118, pp. 243–255, 2015.

[16] B. Abdullahi, "Development and Optimization of heat pipe based Compound Parabolic Collector," University Of Birmingham, 2015.

[17] M. Jradi and S. Riffat, "Medium temperature concentrators for solar thermal applications," *Int. J. Low-Carbon Technol.*, vol. 9, no. 3, pp. 214–224, Sep. 2014.

[18] J. A. Duffie, W. A. Beckman, and W. M. Worek, "Solar Engineering of Thermal Processes, 2nd ed.," *J. Sol. Energy Eng.*, vol. 116, no. 1, p. 67, 1994.

[19] L. A. Chidambaram, A. S. Ramana, G. Kamaraj, and R. Velraj, "Review of solar cooling methods and thermal storage options," *Renew. Sustain. Energy Rev.*, vol. 15, no. 6, pp. 3220–3228, Aug. 2011.

[20] A. Munir, O. Hensel, and W. Scheffler, "Design principle and calculations of a Scheffler fixed focus concentrator for medium temperature applications," *Sol. Energy*, vol. 84, no. 8, pp. 1490–1502, Aug. 2010.

[21] M. Yaqub and S. M. Zubair, "Capacity Control for Refrigeration and Air-Conditioning Systems: A Comparative Study," *J. Energy Resour. Technol.*, vol. 123, no. 1, p. 92, 2001.

[22] S. Huang, P. M. Rich, R. L. Crabtree, C. S. Potter, and P. Fu, "Modeling Monthly Near-Surface Air Temperature from Solar Radiation and Lapse Rate: Application over Complex Terrain in Yellowstone National Park," *Phys. Geogr.*, vol. 29, no. 2, pp. 158–178, 2008.

[23] J. I. Prieto, J. C. Martínez-García, and D. García, "Correlation between global solar irradiation and air temperature in Asturias, Spain," *Sol. Energy*, vol. 83, no. 7, pp. 1076–1085, Jul. 2009.

[24] Jen-hu Chang and B. Root, "On the relationship between mean monthly global radiation and air temperature," *Arch. für Meteorol. Geophys. und Bioklimatologie Ser. B*, vol. 23, no. 1–2, pp. 13–30, Mar. 1975.

[25] S. Dumais and G. Doré, "An albedo based model for the calculation of pavement surface temperatures in permafrost regions," *Cold Reg. Sci. Technol.*, vol. 123, pp. 44–52, Mar. 2016.

[26] R. Yacef, A. Mellit, S. Belaid, and Z. Şen, "New combined models for estimating daily global solar radiation from measured air temperature in semi-arid climates: Application in Ghardaïa, Algeria," *Energy Convers. Manag.*, vol. 79, pp. 606–615, Mar. 2014.

[27] K. L. Bristow and G. S. Campbell, "On the relationship between incoming solar radiation and daily maximum and minimum temperature," *Agric. For. Meteorol.*, vol. 31, no. 2, pp. 159–166, May 1984.

[28] J. P. Praene, O. Marc, F. Lucas, and F. Miranville, "Simulation and experimental investigation of solar absorption cooling system in Reunion Island," *Appl. Energy*, vol. 88, no. 3, pp. 831–839, Mar. 2011.

[29] S. A. Klein and D. T. Reindl, "Solar Refrigeration," *ASHRAE J.*, vol. 47, no. 9, 2005.

[30] "Solar photovoltaics (PV)." [Online]. Available: https://www.navitron.org.uk/products/solar-photovoltaics. [Accessed: 16-Feb-2018].

[31] Y. Chu, "Review and Comparison of Different Solar Energy Technologies," *Glob. Energy Netw. Inst.*, no. August, 2011.

[32] D. S. Kim and C. A. Infante Ferreira, "Solar refrigeration options – a state-of-the-art review," *Int. J. Refrig.*, vol. 31, no. 1, pp. 3–15, Jan. 2008.

[33] S.-Y. Wu, L. Xiao, Y. Cao, and Y.-R. Li, "A parabolic dish/AMTEC solar thermal power system and its performance evaluation," *Appl. Energy*, vol. 87, no. 2, pp. 452–462, Feb. 2010.

[34] D. Kaliakatsos, M. Cucumo, V. Ferraro, M. Mele, S. Cucumo, and A. Miele, "Performance of Dish-Stirling CSP system with dislocated engine," *Int. J. Energy Environ. Eng.*, vol. 8, no. 1, pp. 65–80, 2017.

[35] M. Zeyghami, D. Y. Goswami, and E. Stefanakos, "A review of solar thermo-mechanical refrigeration and cooling methods," *Renew. Sustain. Energy Rev.*, vol. 51, pp. 1428–1445, Nov. 2015.

[36] S. A. Montzka *et al.*, "An unexpected and persistent increase in global emissions of ozone-depleting CFC-11," *Nature*, vol. 557, no. 7705, pp. 413–417, May 2018.

[37] A. Allouhi, T. Kousksou, A. Jamil, P. Bruel, Y. Mourad, and Y. Zeraouli, "Solar driven cooling systems: An updated review," *Renew. Sustain. Energy Rev.*, vol. 44, pp. 159–181, 2015.

[38] S. Jain and C. W. Bullard, "Capacity and Efficiency in Variable Speed , Vapor Injection and Multi-Compressor Systems," ACRC TR-227, 2004.

[39] C. Infante Ferreira and D. S. Kim, "Techno-economic review of solar cooling technologies based on location-specific data," *Int. J. Refrig.*, vol. 39, pp. 23–37, 2014.

[40] "Harnessing the power of the sun to save human lives n.d." [Online]. Available: https://www.solarchill.org/english/the-solution/. [Accessed: 20-Jan-2018].

[41] G. Walker, G. Reader, R. Fauvel, and E. R. Bingham, "Stirling, Near-Ambient Temperature Refrigerators: Innovative Compact Designs," in *27th Intersociety Energy Conversion Engineering Conference*, 1992, pp. 5.93-5.96.

[42] A. C. Ferreira, R. F. Oliveira, M. L. Nunes, L. B. Martins, and S. F. Teixeira, "Modelling and Cost Estimation of Stirling Engine for CHP Applications," in *Proceedings of the 2014 International Conference on Power Systems, Energy, Environment*, 2014, vol. Energy, En, pp. 21–29.

[43] L. Bauwens, "Adiabatic Losses in Stirling Refrigerators," *J. Energy Resour. Technol.*, vol. 118, no. June 1996, pp. 120–127, 1996.

[44] H. Hachem, R. Gheith, F. Aloui, and S. Ben Nasrallah, "Optimization of an air-filled beta type stirling refrigerator," *Int. J. Refrig.*, vol. 76, pp. 296–312, 2017.

[45] D. Haywood, "Investigation of Stirling-type Heat-pump and Refrigerator Systems Using Air as the Refrigerant," 2004.

[46] K. Mahkamov, G. Hashem, B. Belgasim, K. Hossin, and I. Mahkamova, "Parametric Analysis of a Dynamic Solar Cooling System Based on a Liquid Piston Converter," *17th Int. Stirling Engine Conf.*, no. December, pp. 59–74, 2016.

[47] D. M. Berchowitz and R. Unger, "Experimental Performance of a Free-Piston Stirling Cycle Cooler for Non-CFC Domestic Refrigeration Applications," in *18th International congress of refrigeration*, 1991.

[48] D. M. Berchowitz, "Stirling Coolers for Solar Refrigerators," in *International appliance technical conference*, 1996.

[49] D. M. Berchowitz, J. Mcentee, and S. Welty, "Design and testing of a 40 W free-piston Stirling cycle cooling unit," in *20th International Congress of Refrigeration*, 1999, no. 1998.

[50] E. Oguz and F. Ozkadi, "Experimental Investigation Of A Stirling Cycle Cooled Domestic Refrigerator," in *International Refrigeration and Air Conditioning Conference*, 2002.

[51] H. Wang *et al.*, "Performance of a combined organic Rankine cycle and vapor compression cycle for heat activated cooling," *Energy*, vol. 36, no. 1, pp. 447–458, 2011.

[52] M. H. Ahmadi, M.-A. Ahmadi, and F. Pourfayaz, "Thermal models for analysis of performance of Stirling engine: A review," *Renew. Sustain. Energy Rev.*, vol. 68, no. October 2016, pp. 168–184, 2017.

[53] K. Wang, S. R. Sanders, S. Dubey, F. H. Choo, and F. Duan, "Stirling cycle engines for recovering low and moderate temperature heat: A review," *Renew. Sustain. Energy Rev.*, vol. 62, pp. 89–108, Sep. 2016.

[54] H. Hachem, R. Gheith, F. Aloui, and S. Ben Nasrallah, "Technological challenges and optimization efforts of the Stirling machine: A review," *Energy Convers. Manag.*, vol. 171, no. March, pp. 1365–1387, 2018.

[55] R. U. and N. W. L. S. James G. Wood, "A Stirling-Rankine Fuel-Fired Heat Pump," in *International Compressor Engineering Conference*, 2000, pp. 761–768.

[56] G. electric Company, "Development and demonstration of a Stirling/Rankine heat activated heat pump:Final Report:PhaseIIIB-Engine Technology Development testing," Pennsylvania, ORNL/Sub/82-17485/1, 1984.

[57] W. D. C. Richards and W. L. Auxer, "Performance of a Stirling engine powered heat

activated heat pump," *Proc. 13th Intersoc. Enegy Convers. Eng. Conf.*, 1978.

[58] P. D. Fairchild and C. D. West, "Heat-activated heat-pump development and potential application of Stirling-engine technology.," in *20th Automotive Technology Development Contractor Coordination Meeting October*, 1982.

[59] J. English and J. Corey, "Design of Refrigerant Compressor with Hydraulically Coupled,Hermetically Sealed Linear Drive," in *International Compressor Engineering Conference*, 1982.

[60] Ackermann R.A., "Free-Piston Stirling Engine Diaphragm-Coupled Heat-Actuated Heat Pump Component Technology Program," ORNL/Sub/83-47985/1, 1988.

[61] D. O. Jones, R. J. Vincent, and G. Pfleiderer, "Performance Predictions and Test Results of a Free Piston Stirling Engine Driven Heat Pump," in *International Compressor Engineering Conference*, 1986.

[62] and R. A. A. Moynihan, T. M., "Test Results for a Stirling-Engine-Driven Heat-Actuated Heat Pump Breadboard System," in *Proc., Intersoc. Energy Convers. Eng. Conf.;(United States)*, 1984.

[63] J. A. Shonder, G. Chen, and J. McEntee, "Proof of Concept of a Magnetically Coupled Stirling Engine-Driven Heat Pump," in *27th Intersociety Energy Conversion Engineering Conference*, 1992.

[64] R. J. Vincent and W. D. Waldron, "A Magnetically Coupled Stirling Engine Driven Heat Pump: Design Optimization And Operating Cost Analysis," in *Proceedings of the 25th Intersociety Energy Conversion Engineering Conference*, vol. 2, pp. 204–210.

[65] G. Chen and J. McEntee, "Hardware Development And Initial Subassembly Tests Of A Gas-fired Stirling Engine/refrigerant Compressor Assembly," in *Proceedings of the 25th Intersociety Energy Conversion Engineering Conference*, vol. 5, pp. 258–263.

[66] G. Chen, "Dynamic characteristics concerned in the design of a free-piston Stirling engine/magnetic coupling/compressor system," in *Proceedings of the 24th Intersociety Energy Conversion Engineering Conference*, 1989, pp. 2219–2223.

[67] R. J. Vincent, "Dynamic Behavior of a Free-Piston Stirling Engine Driven Heat Pump With Magnetic Coupling," in *International Compressor Engineering Conference*, 1988.

[68] P. Schwartz, "The Natural Gas Heat Pump and Air Conditioner 2014." [Online]. Available: https://energy.gov/sites/prod/files/2014/11/f19/BTO 2014 Peer Review Presentation - ThermoLift 4.4.14.pdf. [Accessed: 14-Feb-2018].

[69] S. Convey and P. Schwart, "Modernizing the Vuilleumier Cycle: Recent developments for a novel natural gas air-conditioner and heat pump Seann," in *IEA Heat Pump Centre Pump (HPC) Newsletter*, 2015, vol. 33, no. 4, pp. 19–23.

[70] D. G. Thombare and S. K. Verma, "Technological development in the Stirling cycle engines," *Renew. Sustain. Energy Rev.*, vol. 12, no. 1, pp. 1–38, Jan. 2008.

[71] D. M. Berchowitz, "Stirling-Engines-in-Developing-Countries," in *The conference on small engines and their fuels in developing countries, University of reading*, 1984, pp. 140–149.

[72] "Stirling Engine." [Online]. Available: https://www.nms.ac.uk/stirlingengine. [Accessed: 08-Jun-2018].

[73] A. R. Tavakolpour, A. Zomorodian, and A. Akbar Golneshan, "Simulation, construction and testing of a two-cylinder solar Stirling engine powered by a flat-plate solar collector without regenerator," *Renew. Energy*, vol. 33, no. 1, pp. 77–87, Jan. 2008.

[74] S. Alfarawi, R. AL-Dadah, and S. Mahmoud, "Influence of phase angle and dead volume on gamma-type Stirling engine power using CFD simulation," *Energy Convers. Manag.*, vol. 124, pp. 130–140, 2016.

[75] K. J. Laidler, *Energy and the Unexpected*. Oxford university press, 2002.

[76] T. Finkelstein and A. J. Organ, *Air Engines*. 2001.
[77] N. C. J. Chen and F. P. Griffin, "A Review of Stirling Engine Mathematical Models," ORNL/CON-135, 1983.
[78] H. G. Ladas and O. M. Ibrahim, "Finite-time view of the Stirling engine," *Energy*, vol. 19, no. 8, pp. 837–843, 1994.
[79] F. L. Curzon and B. Ahlborn, "Efficiency of a Carnot engine at maximum power output," *Am. J. Phys.*, vol. 43, no. 1, pp. 22–24, Jan. 1975.
[80] A. Vaudrey, F. Lanzetta, and M. Feidt, "H. B. Reitlinger and the origins of the efficiency at maximum power formula for heat engines," *J. Non-Equilibrium Thermodyn.*, vol. 39, no. 4, pp. 199–203, 2014.
[81] C. Wu, "Power Optimization of a Finite-Time," vol. 13, no. 9, pp. 681–687, 1988.
[82] S. . Kaushik and S. Kumar, "Finite time thermodynamic analysis of endoreversible Stirling heat engine with regenerative losses," *Energy*, vol. 25, no. 10, pp. 989–1003, Oct. 2000.
[83] D. A. Blank, G. W. Davis, and C. Wu, "Power optimization of an endoreversible stirling cycle with regeneration," *Energy*, vol. 19, no. 1, pp. 125–133, Jan. 1994.
[84] J. Chen, "The maximum power output and maximum efficiency of an irreversible Carnot heat engine," *J. Phys. D. Appl. Phys.*, vol. 27, no. 6, pp. 1144–1149, Jun. 1994.
[85] H. Yavuz, "Optimization of the Irreversible Stirling Heat Engine," *Energy*, vol. 873, no. September 1998, pp. 863–873, 1999.
[86] M. Feidt, "Optimal thermodynamics-new upperbounds," *Entropy*, vol. 11, no. 4, pp. 529–547, 2009.
[87] D. Ladino-luna, P. Portillo-díaz, and R. T. Páez-hernández, "On the Efficiency for Non-Endoreversible Stirling and Ericsson Cycles," *J. Mod. Phys.*, vol. 4, no. December, pp. 1–7, 2013.
[88] P. C. T. de Boer, "Maximum Attainable Performance of Stirling Engines and Refrigerators," *J. Heat Transfer*, vol. 125, no. 5, pp. 911–915, 2003.
[89] L. Chen, F. Sun, and C. Wu, "Effect of heat transfer law on the performance of a generalized irreversible Carnot engine," *J. Phys. D. Appl. Phys.*, vol. 32, no. 2, pp. 99–105, Jan. 1999.
[90] D. Ladino-Luna, R. T. Páez-Hernández, and P. Portillo-Díaz, "Linear Approximation of Efficiency for Similar Non- Endoreversible Cycles to the Carnot Cycle," in *Recent Advances in Thermo and Fluid Dynamics*, InTech, 2015.
[91] G. Walker, G. Reader, O. R. Fauvel, and E.R.Bingham, *The Stirling Alternative*. Gordon and Breach Publishers Inc., 1994.
[92] H. S. Leff and W. D. Teeters, "EER, COP, and the second law efficiency for air conditioners," *Am. J. Phys.*, vol. 46, no. 1, pp. 19–22, Jan. 1978.
[93] C. H. Blanchard, "Coefficient of performance for finite speed heat pump," *J. Appl. Phys.*, vol. 51, no. 5, p. 2471, 1980.
[94] C. WU, "Maximum Obtainable Specific Cooling Load of a Refrigerator," *Energy Convers.Mgmt*, vol. 36, no. 1, pp. 7–10, 1995.
[95] J. Chen, "Minimum power inputof irreversible Stirling refrigerators for given cooling rate," *Energy Convers. Manag.*, vol. 39, no. 12, pp. 1255–1263, 1998.
[96] C.-Y. Cheng and C.-K. Chen, "Performance optimization of an irreversible heat pump," *J. Phys. D. Appl. Phys.*, vol. 28, no. 12, pp. 2451–2454, Dec. 1995.
[97] C. Wu, L. Chen, and F. Sun, "Optimization of steady flow heat pumps," *Energy Convers. Manag.*, vol. 39, no. 5–6, pp. 445–453, Mar. 1998.
[98] L. Chen, F. Sun, N. Ni, and C. Wu, "Optimal configuration of a class of two-heat-reservoir refrigeration cycles," *Energy Convers. Manag.*, vol. 39, no. 8, pp. 767–773, 1998.

[99] S. C. Kaushik, S. K. Tyagi, S. K. Bose, and M. K. Singhal, "Performance evaluation of irreversible Stirling and Ericsson heat pump cycles," *Int. J. Therm. Sci.*, vol. 41, no. 2, pp. 193–200, 2002.

[100] B. Souvik and D. A. Blank, "Design considerations for a power optimized regenerative endoreversible Stirling cycle," *Int. J. Energy Res.*, vol. 24, no. February 1999, pp. 539–547, 2000.

[101] J. R. Senft, "Theoretical limits on the performance of Stirling engines," *Int. J. Energy Res.*, vol. 22, no. May, pp. 991–1000, 1998.

[102] B. Penswick and I. Urieli, "Duplex stirling machines," in *Proc., Intersoc. Energy Convers. Eng. Conf.;(United States), vol. 3, no. CONF-840804-. Sunpower, Inc., Athens, Ohio*, 1984.

[103] J. Y. Hu, E. C. Luo, W. Dai, and L. M. Zhang, "Parameter sensitivity analysis of duplex Stirling coolers," *Appl. Energy*, vol. 190, pp. 1039–1046, 2017.

[104] L. B. Erbay, M. M. Ozturk, and B. Doğan, "Overall performance of the duplex Stirling refrigerator," *Energy Convers. Manag.*, vol. 133, pp. 196–203, 2017.

[105] R. W. Dyson and G. A. Bruder, "Progress Towards the Development of a Long-Lived Venus Lander Duplex System," E-17389-1, 2011.

[106] R. Vuilleumier, "Method and apparatus for inducing heat changes," U.S. Patent 1,275,507, 1918.

[107] G. Walker and J. R. Senft, *Free Piston Stirling Engines*, First edit., vol. 12. Berlin, Heidelberg: Springer Berlin Heidelberg, 1985.

[108] C. Pan, T. Zhang, Y. Zhou, and J. Wang, "Experimental study of one-stage VM cryocooler operating below 8K," *Cryogenics (Guildf).*, vol. 72, pp. 122–126, 2015.

[109] H. Carlsen, "Development of a gas fired Vuilleumier heat pump for residential heating," in *Proceedings of the 24th Intersociety Energy Conversion Engineering Conference*, 1989, pp. 2257–2263.

[110] W. R. M. Martini, "Stirling engine design manual," DOE/NASA/3194-I, 1983.

[111] J. Mou and G. Hong, "Startup mechanism and power distribution of free piston Stirling engine," *Energy*, vol. 123, pp. 655–663, Mar. 2017.

[112] F. Normani, *Stirling Engine Manual*. 2013.

[113] A. Asnaghi, S. M. Ladjevardi, P. Saleh Izadkhast, and A. H. Kashani, "Thermodynamics Performance Analysis of Solar Stirling Engines," *ISRN Renew. Energy*, vol. 2012, pp. 1–14, 2012.

[114] B. Kongtragool and S. Wongwises, "Performance of low-temperature differential Stirling engines," *Renew. Energy*, vol. 32, no. 4, pp. 547–566, 2007.

[115] C. Çinar and H. Karabulut, "Manufacturing and testing of a gamma type Stirling engine," *Renew. Energy*, vol. 30, no. 1, pp. 57–66, Jan. 2005.

[116] H. Karabulut, F. Aksoy, and E. Öztürk, "Thermodynamic analysis of a β type Stirling engine with a displacer driving mechanism by means of a lever," *Renew. Energy*, vol. 34, no. 1, pp. 202–208, 2009.

[117] J. D. Van de Ven, "Mobile hydraulic power supply: Liquid piston Stirling engine pump," *Renew. Energy*, vol. 34, no. 11, pp. 2317–2322, 2009.

[118] A. Sripakagorn and C. Srikam, "Design and performance of a moderate temperature difference Stirling engine," *Renew. Energy*, vol. 36, no. 6, pp. 1728–1733, Jun. 2011.

[119] T. Mancini *et al.*, "Dish-Stirling Systems: An Overview of Development and Status," *J. Sol. Energy Eng.*, vol. 125, no. 2, p. 135, 2003.

[120] H. P. Trolove and J. K. Raine, "The design and heat pipe tests for a line focus solar Stirling domestic generation system," *Proc. Inst. Mech. Eng. Part A J. Power Energy*, vol. 209, no. 1, pp. 27–36, Feb. 1995.

[121] H. P. Trolove, "Line Focus Solar Stirling Domestic Power Generation," University of

Canterbury, 1994.
[122] B. Hoegel, "Thermodynamics-based design of stirling engines for low-temperature heat sources.," University of Canterbury, 2014.
[123] G. Walker, *Cryocoolers*, Part 2: Ap. Boston, MA: Springer US, 1983.
[124] G. Walker, *Cryocoolers*, Part 1: Fu. Boston, MA: Springer US, 1983.
[125] M. A. White, J. E. Augenblick, and A. A. Peterson, "Double acting thermodynamically resonant free-piston multicylinder Stirling system and method," U.S. Patent 7,134,279 B2, 2006.
[126] S. Chatterton and P. Pennacchi, "Design of a Novel Multicylinder Stirling Engine," *J. Mech. Des.*, vol. 137, no. 4, p. 042303, 2015.
[127] G. Walker, "Coal-fired Stirling engines for railway locomotive and stationary power applications," *Proc Instn Mech Engrs*, vol. 197A, no. October, pp. 233–246, 1983.
[128] B. Hoegel, D. Pons, M. Gschwendtner, and A. Tucker, "Theoretical investigation of the performance of an Alpha Stirling engine for low temperature applications," *ISEC Int. Stirling Engine Comm.*, no. January, 2012.
[129] T. RABALLAND, "Etude de faisabilité d ' un concept d ' étanchéité pour machines volumétriques à pistons oscillants," University of Bordeaux, 2007.
[130] A. Høeg, T.-M. Tveit, T. Aase, and T.-A. Asphjell, "Mechanical Design of the 4-500 KWth stirling cycle heat pump SPP 4-106," in *The 17th International Stirling Engine Conference*, 2016, pp. 21–33.
[131] C. M. Bartolini, V. Naso, and F. Suraci, "Stirling engine," U.S. Patent 4,760,698, 1988.
[132] C. m. Bartolini, "Franchot-Bartolini Stirling engine," in *international Stirling engine conference, ISEC3, Rome, Italy*, 86AD, pp. 515–525.
[133] C. M. Bartolini and F. Rispoli, "The Simulation of Franchot-Bartolini Stirling engine for Design purposes," in *23rd Intersociety Energy Conversion Engineering Conference*, 1988, pp. 45–48.
[134] C. M. Bartolini and F. Rispoli, "Franchot-Bartolini Stirling engine with Ross linkage," in *Intersociety Energy Conversion Engineering Conference*, 1988, pp. 151–156.
[135] K. Hirata, "A10 Development of 2-cylinder Double-Acting Stirling Engine," in *The Proceedings of the Symposium on Stirlling Cycle*, 2006, vol. 10, pp. 93–96.
[136] E. Effron and H. E. Hoelscher, "Graphite oxidation at low temperature," *AIChE J.*, vol. 10, no. 3, pp. 388–392, May 1964.
[137] L. Xiaowei, R. Jean-Charles, and Y. Suyuan, "Effect of temperature on graphite oxidation behavior," *Nucl. Eng. Des.*, vol. 227, no. 3, pp. 273–280, 2004.
[138] T. Tveit, D. Manager, S. P. As, and N. Vakås, "Performance Analysis and Verification of a Novel High Temperature Difference Heat Pump," in *11th IEA Heat Pump Conference*, 2014, pp. 1–10.
[139] C. Bergmann and J. A. D. R. Prise, "Numerical prediction of the instantaneous regenerator and in-cylinder heat transfer of a stirling engine," *Int. J. Energy Res.*, vol. 15, no. 8, pp. 623–635, Oct. 1991.
[140] H. El Hassani, N. Boutammachte, and M. Hannaoui, "Study of Some Power Influencing Parameters of a Solar Low Temperature Stirling Engine," *Eur. J. Sustain. Dev.*, vol. 3, no. 2, pp. 109–118, Jun. 2014.
[141] A. J. Organ, *Stirling cycle engines: inner workings and design*. JohnWiley & Sons, Ltd, 2014.
[142] B. Hoegel, D. Pons, M. Gschwendtner, A. Tucker, and M. Sellier, "Thermodynamic peculiarities of alpha-type Stirling engines for low-temperature difference power generation: Optimisation of operating parameters and heat exchangers using a third-order model," *Proc. Inst. Mech. Eng. Part C J. Mech. Eng. Sci.*, vol. 228, no. 11, pp. 1936–1947, Aug. 2014.

[143] W. Arias, H. . Velásquez, D. Florez, and S. Oliveira Junior, "Thermodynamic analysis, performance numerical simulation and losses analysis of a low cost Stirling engine V-Type, and its impact on soc Efficiency, Cost, Optimization, Simulation and Environmental Impact of Energy Systems, ECOS 2011ial development in rem," *Proc. 24th Int. Conf.*, pp. 3767–3778, 2011.

[144] J. R. Senft, "Optimum Stirling engine geometry," *Int. J. Energy Res.*, vol. 26, no. 12, pp. 1087–1101, 2002.

[145] N. Martaj and P. Rochelle, "1D modelling of an alpha type Stirling engine," *Int. J. Simul. Multidiscip. Des. Optim.*, vol. 5, p. A07, Feb. 2014.

[146] A. Der Minassians, "Stirling Engines for Low-Temperature Solar-Thermal- Electric Power Generation," University of California at Berkeley, 2007.

[147] H. Carlsen, M. B. Commisso, and B. Lorentzen, "Maximum Obtainable Efficiency For Engines And Refrigerators Based On The Stirling Cycle," in *Proceedings of the 25th Intersociety Energy Conversion Engineering Conference*, 1990, vol. 5, pp. 366–371.

[148] V. K. Gopal, "Active Stirling Engine," University of Canterbury, 2012.

[149] R. Li and L. Grosu, "Parameter effect analysis for a Stirling cryocooler," *Int. J. Refrig.*, vol. 80, pp. 92–105, Aug. 2017.

[150] Y. Tekin and O. E. Ataer, "Performance of V-type Stirling-cycle refrigerator for different working fluids," *Int. J. Refrig.*, vol. 33, no. 1, pp. 12–18, 2010.

[151] G. Fenies, F. Formosa, J. Ramousse, and A. Badel, "Double acting Stirling engine: Modeling, experiments and optimization," *Appl. Energy*, vol. 159, pp. 350–361, 2015.

[152] A. Der Minassians and S. R. Sanders, "Multiphase Stirling Engines," *J. Sol. Energy Eng.*, vol. 131, no. 2, p. 021013, 2009.

[153] D. M. Berchowitz and Y.-R. Kwon, "Multiple Cylinder Free-Piston Stirling Machinery," *J. Power Energy Syst.*, vol. 2, no. 5, pp. 1209–1220, 2008.

[154] D. M. Berchowitz and Y.-R. KWon, "Multiple-cylinder, free-piston, alpha configured Stirling engines and heat pumps with stepped pistons," U.S. Patent 7,171,811 B1, 2007.

[155] J. Arthur A. Varela, "Hybrid electric propulsion system," U.S. Patent 5,172,784 A, 1992.

[156] P. Fette, "A Stirling Engine Able to Work with Compound Fluids Using Heat Energy of Low to Medium Temperatures," in *Sixth International Stirling Engine Conference*, 1993, pp. 13–18.

[157] N. W. Lane and W. T. Beale, "Free-piston Stirling design features," *Eighth International Stirling Engine Conference*. 1997.

[158] T. Finkelstein, "Optimization of phase angle and volume ratio for Stirling engines," Jan. 1960.

[159] K. Lee, N. Clark, A. George, V. Petrucci, and J. E. Smith, "Thermodynamic implications of the Stiller-Smith Mechanism," in *Scientific Reports*, 1987, vol. 7, no. 1, p. 4503.

[160] C. Çınar, F. Aksoy, H. Solmaz, E. Yılmaz, and A. Uyumaz, "Manufacturing and testing of an A-type Stirling engine," *Appl. Therm. Eng.*, vol. 130, pp. 1373–1379, 2018.

[161] T. K. Garrett, K. Newton, and W. Steeds, "Engine balance," in *Motor Vehicle*, Elsevier, 2000, pp. 25–46.

[162] W. T. Beale, "Free Piston Stirling Engines - Some Model Tests and Simulations," 1969, pp. 1–10.

[163] W. T. BEALE, "Stirling cycle type thermal device," U.S. Patent 3,552,120, 1971.

[164] E. D. Rogdakis, N. A. Bormpilas, and I. K. Koniakos, "A thermodynamic study for the optimization of stable operation of free piston Stirling engines," *Energy Convers. Manag.*, vol. 45, no. 4, pp. 575–593, 2004.

[165] T. Finkelstein, "balanced compounding of Stirling machines," in *Intersociety Energy Conversion Engineering Conference,13th*, 1978, pp. 1791–1797.

[166] H. Karabulut, "Dynamic analysis of a free piston Stirling engine working with closed and open thermodynamic cycles," *Renew. Energy*, vol. 36, no. 6, pp. 1704–1709, 2011.
[167] R. W. Redlich and D. M. Berchowitz, "Linear Dynamics of Free-Piston Stirling Engines," *Proc. Inst. Mech. Eng. Part A Power Process Eng.*, vol. 199, no. 3, pp. 203–213, Aug. 1985.
[168] W. T. Beale, "Pressure modulation system for load matching and stroke limitation of Stirling cycle apparatus," U.S. Patent 4,458,495, 1984.
[169] F. Formosa, A. Badel, and J. Lottin, "Equivalent electrical network model approach applied to a double acting low temperature differential Stirling engine," *Energy Convers. Manag.*, vol. 78, pp. 753–764, 2014.
[170] A. der Minassians, "Stirling three-phase engine." [Online]. Available: https://www.youtube.com/watch?v=EO_bJ0A_CTg. [Accessed: 13-Dec-2018].
[171] P. Fette, "A Twice Double Acting a - Type Stirling Engine Able to Work with Compound Fluids Using Heat Energy of Low to Medium Temperatures." [Online]. Available: http://www.stirling-fette.de/english.htm. [Accessed: 02-Nov-2017].
[172] C. D. West, "Liquid-piston Stirling machines," in *2nd International Conference on Stirling engines*, 1984, pp. 15–36.
[173] J. W. Mason and J. W. Stevens, "Characterization of a solar-powered fluidyne test bed," *Sustain. Energy Technol. Assessments*, vol. 8, pp. 1–8, 2014.
[174] W. T. Beale, "A Free Cylinder Stirling Engine Solar Powered Water Pump," *Sunpower Incorporated*. 1979.
[175] K. Mahkamov, G. Hashem, B. Belgasim, and I. Mahkamova, "A Novel Solar Cooling system based on a Fluid Piston Convertor," *16th Int. Stirling Engine Conf. ISEC2014*, 2014.
[176] S. Langdon-Arms, M. Gschwendtner, and Martin Neumaier, "Development of a heat-actuated unconstrained 4 cylinder double-acting alpha-type liquid piston Stirling cooler," in *The 17th International Stirling Engine Conference*, 2016, pp. 34–52.
[177] T. Finkelstein, "Method and device for balanced compounding of Stirling cycle machines," U.S. Patent 4,199,945, 1980.
[178] T. Finkelstein, "Analysis of Heat-Activated Stirling Heat Pump," in *Intersociety Energy Conversion Engineering Conference*, 1980, pp. 1788–1796.
[179] T. Finkelstein, "Isothermal Sinusoidal Analysis of Balanced Compound Vuilleumier Heat Pumps," in *27th Intersociety Energy Conversion Engineering Conference*, 1992.
[180] Robert F. McConaghy, "Multi-cylinder free piston Stirling engine," U.S. Patent 0,193,266 A1, 2007.
[181] M. W. Dadd, "Linear multi-cylinder Stirling cycle machine," U.S. Patent 8,820,068 B2, 2014.
[182] C. D. West, "Stirling machines: adiabatic to isothermal," in *international Stirling engine conference, ISEC3, Rome, Italy*, 1986.
[183] S. Le'an, Z. Yuanyang, L. Liansheng, and S. Pengcheng, "Performance of a prototype Stirling domestic refrigerator," *Appl. Therm. Eng.*, vol. 29, no. 2–3, pp. 210–215, 2009.
[184] B. Kongtragool and S. Wongwises, "A four power-piston low-temperature differential Stirling engine using simulated solar energy as a heat source," *Sol. Energy*, vol. 82, no. 6, pp. 493–500, 2008.
[185] B. Kongtragool and S. Wongwises, "Performance of a twin power piston low temperature differential Stirling engine powered by a solar simulator," *Sol. Energy*, vol. 81, no. 7, pp. 884–895, Jul. 2007.
[186] J. H. Shazly, A. Z. Hafez, E. T. El Shenawy, and M. B. Eteiba, "Simulation, design and thermal analysis of a solar Stirling engine using MATLAB," *Energy Convers. Manag.*,

vol. 79, pp. 626–639, Mar. 2014.
[187] B. Kongtragool and S. Wongwises, "A review of solar-powered Stirling engines and low temperature differential Stirling engines," *Renew. Sustain. Energy Rev.*, vol. 7, no. 2, pp. 131–154, 2003.
[188] Eugene W. White, "Solar heated engines," 4,414,814, 1983.
[189] B. Kongtragool and S. Wongwises, "Optimum absorber temperature of a once-reflecting full conical concentrator of a low temperature differential Stirling engine," *Renew. Energy*, vol. 30, no. 11, pp. 1671–1687, 2005.
[190] P. Kerdchang, M. MaungWin, S. Teekasap, J. Hirunlabh, J. Khedari, and B. Zeghmati, "Development of a new solar thermal engine system for circulating water for aeration," *Sol. Energy*, vol. 78, no. 4 SPEC. ISS., pp. 518–527, 2005.
[191] N. Boutammachte and J. Knorr, "Field-test of a solar low delta-T Stirling engine," *Sol. Energy*, vol. 86, no. 6, pp. 1849–1856, 2012.
[192] J. Wu, "A new approach to determining the intermediate temperatures of endoreversible combined cycle power plant corresponding to maximum power," *Int. J. Heat Mass Transf.*, vol. 91, pp. 150–161, 2015.
[193] A. A. El-Ehwany, G. M. Hennes, E. I. Eid, and E. A. El-Kenany, "Development of the performance of an alpha-type heat engine by using elbow-bend transposed-fluids heat exchanger as a heater and a cooler," *Energy Convers. Manag.*, vol. 52, no. 2, pp. 1010–1019, Feb. 2011.
[194] B. Kongtragool and S. Wongwises, "Thermodynamic analysis of a Stirling engine including dead volumes of hot space, cold space and regenerator," *Renew. Energy*, vol. 31, no. 3, pp. 345–359, Mar. 2006.
[195] Y. Timoumi, I. Tlili, and S. Ben Nasrallah, "Design and performance optimization of GPU-3 Stirling engines," *Energy*, vol. 33, no. 7, pp. 1100–1114, Jul. 2008.
[196] H. Hosseinzade, H. Sayyaadi, and M. Babaelahi, "A new closed-form analytical thermal model for simulating Stirling engines based on polytropic-finite speed thermodynamics," *Energy Convers. Manag.*, vol. 90, pp. 395–408, 2015.
[197] J. D. Van de Ven and P. Y. Li, "Liquid piston gas compression," *Appl. Energy*, vol. 86, no. 10, pp. 2183–2191, 2009.
[198] A. H. Orlowska, "An investigation of some heat transfer and gas flow problems relevant to miniature refrigerators," Oxford university, 1985.
[199] S. G. Hauser, W. R. Martini, and W. A. Scheffler, "Experimental measurements of enhanced heat transfer in a Stirling engine model with interleaving fins," in *Intersociety Energy Conversion Engineering Conference, 16th, Atlanta, GA, Proceedings. Volume 2. (A82-11701 02-44) New York, American Society of Mechanical Engineers, 1981, p. 1925-1928.*, 1981.
[200] G. M. Benson, "Isothermalizer system," U.S. Patent 4,446,698, 1984.
[201] T. A. Alexandravichus, "Double-Acting Stirling Engine with the Inner Heat Exchangers," in *27th Intersociety Energy Conversion Engineering Conference*, 1992.
[202] W. L. Chen, K. L. Wong, and L. W. Po, "A numerical analysis on the performance of a pressurized twin power piston gamma-type Stirling engine," *Energy Convers. Manag.*, vol. 62, pp. 84–92, 2012.
[203] A. Siegel, Kai, and Schiefelbein, "Stirling engine with injection of heat transfer medium," U.S. Patent 5,638,684, 1997.
[204] L. S. Smith, S. P. Weaver, B. P. Nuel, and W. H. Vermeer, "Direct contact thermal exchange heat engine or heat pump," US 2009/0038307 Al, 2009.
[205] S.-J. Jang, Y.-P. Lee, and K. Sim, "Experimental Feasibility Study on Low-Temperature Differential Stirling Engines with Water Spray Heat Transfer," *Trans. Korean Soc. Mech.*

Eng. B, vol. 38, no. 6, pp. 475–482, Jun. 2014.

[206] K. Sim, M.-S. Jeong, Y.-P. Lee, and S.-J. Jang, "Mechanical Load Performance Measurements of a Low Temperature Differential Stirling Engine with Water-Sprayed Heat Transfer according to Supply Water Flow Rates and Temperatures," *KSFM J. Fluid Mach.*, vol. 18, no. 1, pp. 29–36, 2015.

[207] J. D. Van de Ven, P. B. Gaffuri, B. J. Mies, and G. Cole, "Developments Towards a Liquid Piston Stirling Engine," in *International Energy Conversion Engineering Conference*, 2008.

[208] M. Schober, M. Deichsel, and E. Schlucker, "Power and efficiency analysis of liquid piston Stirling engines," in *The 17th International Stirling Engine Conference*, 2016, pp. 481–500.

[209] J. W. Stevens, R. O. Kerns, and J. W. Mason, "Operational Characteristics of Liquid-Piston Heat Engines," in *Energies-Whither Energy Conversion? Present Trends, Current Problems and Realistic Future Solutions"*, 2014, pp. 1–12.

[210] J. W. Stevens, "Low capital cost renewable energy conversion with liquid piston Stirling engines," in *Proceedings of ASME 2010 4th International Conference on Energy Sustainability ES2010*, 2010.

[211] F. Kyei-Manu and A. Obodoako, "Design and Development of a Liquid Piston Stirling Engine," 2006.

[212] M. M. H. Al-Hazmy, "A Computational Model for Resonantly Coupled Alpha Free-Piston Stirling Coolers," Oregon State University, 1998.

[213] D. M. Clucas, "Development of a Stirling engine charger based on a low cost Wobble mechanism," University of Canterbury, 1993.

[214] K. Kraitong, "Numerical modelling and design optimisation Of Stirling engines for power production," University of Northumbria at Newcastle, 2012.

[215] M. Babaelahi and H. Sayyaadi, "Modified PSVL: A second order model for thermal simulation of Stirling engines based on convective-polytropic heat transfer of working spaces," *Appl. Therm. Eng.*, vol. 85, pp. 340–355, 2015.

[216] M. Babaelahi and H. Sayyaadi, "A new thermal model based on polytropic numerical simulation of Stirling engines," *Appl. Energy*, vol. 141, pp. 143–159, 2015.

[217] R. Li, L. Grosu, and W. Li, "New polytropic model to predict the performance of beta and gamma type Stirling engine," *Energy*, vol. 128, pp. 62–76, 2017.

[218] M. Babaelahi and H. Sayyaadi, "Analytical closed-form model for predicting the power and efficiency of Stirling engines based on a comprehensive numerical model and the genetic programming," *Energy*, vol. 98, pp. 324–339, Mar. 2016.

[219] N. Martaj, L. Grosu, and P. Rochelle, "Thermodynamic study of a low temperature differences Stirling engine at steady state operation," *Int. J. Appl. Thermodyn.*, vol. 10, no. 4, pp. 165–176, 2007.

[220] M. Tarawneh, F. Al-Ghathian, M. A. Nawafleh, and N. Al-Kloub, "Numerical Simulation and Performance Evaluation of Stirling Engine Cycle," *Jordan J. Mech. Ind. Eng.*, vol. 4, no. 5, 2010.

[221] M. C. Campos, J. V. C. Vargas, and J. C. Ordonez, "Thermodynamic optimization of a Stirling engine," *Energy*, vol. 44, no. 1, pp. 902–910, 2012.

[222] A. A. Kornhauser, B. C. Kafka, D. L. Finkbeiner, and F. C. Cantelmi, "Heat Transfer Measurements for Stirling Machine Cylinders," 1994.

[223] R. P. Adair, E. B. Qvale, and J. T. Pearson, "Instantaneous heat transfer to cylinder wall in reciprocating compressors," *Int. Compress. Eng. Conf.*, pp. 521–526, 1972.

[224] C. A. Finol and K. Robinson, "Thermal modelling of modern engines: a review of empirical correlations to estimate the in-cylinder heat transfer coefficient," *Proc. Inst.*

Mech. Eng. Part D J. Automob. Eng., vol. 220, no. 12, pp. 1765–1781, Jan. 2006.

[225] F. Toda, S. Iwamoto, M. Matsuo, and Y. Umezane, "Heat Transfer on a Small Stirling Engine -Heat Transfer in Expansion Chamber Wall -," *Bull. M.E.S.J*, vol. 19, no. 1, pp. 49–59, 1991.

[226] G. Xiao, C. Chen, B. Shi, K. Cen, and M. Ni, "Experimental study on heat transfer of oscillating flow of a tubular Stirling engine heater," *Int. J. Heat Mass Transf.*, vol. 71, pp. 1–7, 2014.

[227] F. Toda, S. Iwamoto, M. Matsuo, and Y. Umezane, "Heat Transfer on a Small Stirling Engine," *J. Mar. Eng. Soc. JAPAN*, vol. 25, no. 6, pp. 358–365, 1990.

[228] M. Kuosa, K. Saari, A. Kankkunen, and T.-M. Tveit, "Oscillating flow in a stirling engine heat exchanger," *Appl. Therm. Eng.*, vol. 45–46, pp. 15–23, 2012.

[229] J. R. Senft, *Mechanical Efficiency of Heat Engines*. Cambridge: Cambridge University Press, 2007.

[230] R. Li, L. Grosu, and D. Queiros-condé, "Losses effect on the performance of a Gamma type Stirling engine," *Energy Convers. Manag.*, vol. 114, pp. 28–37, 2016.

[231] T. S. Zhao and P. Cheng, "Experimental studies on the onset of turbulence and frictional losses in an oscillatory turbulent pipe flow," *International Journal of Heat and Fluid Flow*, vol. 17, no. 4. pp. 356–362, 1996.

[232] M. Babaelahi and H. Sayyaadi, "Simple-II: A new numerical thermal model for predicting thermal performance of Stirling engines," *Energy*, vol. 69, pp. 873–890, May 2014.

[233] M. Abbas, N. Said, and B. Boumeddane, "Thermal analysis of Stirling engine solar driven," *Rev. des Energies Renouvelables*, vol. 11, no. 4, pp. 503–514, 2008.

[234] H. Karabulut, H. S. Yucesu, and A. Koca, "Manufacturing and testing of a V-type Stirling engine," *Turkish J. Eng. Environ. Sci.*, vol. 24, no. 2, pp. 71–80, 2000.

[235] C. H. Cheng and Y. J. Yu, "Numerical model for predicting thermodynamic cycle and thermal efficiency of a beta-type Stirling engine with rhombic-drive mechanism," *Renew. Energy*, vol. 35, no. 11, pp. 2590–2601, 2010.

[236] M. Tanaka, I. Yamashita, and F. Chisaka, "Flow and Heat Transfer Characteristics of the Stirling Engine Regenerator in an Oscillating Flow," *JSME Int. J.*, vol. 33, no. 2, pp. 283–289, 1990.

[237] M. Pfabe and C. Woernle, "Reducing torsional vibrations by means of a kinematically driven flywheel - Theory and experiment," *Mech. Mach. Theory*, vol. 102, pp. 217–228, 2016.

[238] S. Kwankaomeng, B. Silpsakoolsook, and P. Savangvong, "Investigation on stability and performance of a free-piston Stirling engine," *Energy Procedia*, vol. 52, pp. 598–609, 2014.

[239] L. B. Gordon, "Loss Terms in Free-Piston Stirling Engine Models," 1992.

[240] G. Benvenuto and F. de Monte, "Analysis of free-piston Stirling engine/linear alternator systems. Part I - Theory.," *J. Propuls. Power*, vol. 11, no. 5, pp. 1036–1046, 1995.

[241] J. Mou, W. Li, J. Li, and G. Hong, "Gas action effect of free piston Stirling engine," *Energy Convers. Manag.*, vol. 110, pp. 278–286, 2016.

[242] S.-Y. Kim and D. Berchowitz, "Specific Power Estimations for Free-Piston Stirling Engines," in *4th International Energy Conversion Engineering Conference and Exhibit (IECEC)*, 2006, no. June.

[243] C. Fernández-Aballí-Altamirano, M. Calcoen, E. Vandermeersch, and J. J. González-Bayón, "Experimental Tailer like Thermal Lag Engine to obtain pressure and volume diagrams," *Ing. Mecánica*, vol. 16, no. 1, pp. 35–40, 2013.

[244] A. Abdollahpour, M. H. Ahmadi, and A. H. Mohammadi, "Thermodynamic model to study a solar collector for its application to Stirling engines," *Energy Convers. Manag.*, vol. 79, pp. 666–673, Mar. 2014.

[245] "SCHOTT PTR®70 Receivers." [Online]. Available: http://www.schott.com/d/csp/2ad9cb93-5b86-4a51-aead-a49b4e869ef8/1.0/schott_ptr70_4th_generation_datasheet.pdf. [Accessed: 09-May-2018].

[246] P.-Y. Wang, H.-Y. Guan, Z.-H. Liu, G.-S. Wang, F. Zhao, and H.-S. Xiao, "High temperature collecting performance of a new all-glass evacuated tubular solar air heater with U-shaped tube heat exchanger," *Energy Convers. Manag.*, vol. 77, pp. 315–323, Jan. 2014.

[247] Mahmut Sami Büker, "Building integrated solar thermal collectors for heating & cooling applications," University of Nottingham, 2015.

[248] H. Tabaei and M. Ameri, "Improving the effectiveness of a photovoltaic water pumping system by using booster reflectors and cooling array surface by a film of water," *IJST, Trans. Mech. Eng.*, vol. 39, no. M1, pp. 51–60, 2015.

[249] A. Poullikkas, G. Kourtis, and I. Hadjipaschalis, "Parametric analysis for the installation of solar dish technologies in Mediterranean regions," *Renew. Sustain. Energy Rev.*, vol. 14, no. 9, pp. 2772–2783, Dec. 2010.

[250] H. Al-ansary and O. Zeitoun, "Heat loss experiment on a non-evacuated parabolic trough receiver employing a thermally insulating layer in the annular gap," in *Proceedings of the ASME 2013 7th International Conference on Energy Sustainability ES2013*, 2013, pp. 1–6.

[251] M. Larcher, M. Rommel, A. Bohren, E. Frank, and S. Minder, "Characterization of a parabolic trough collector for process heat applications," *Energy Procedia*, vol. 57, pp. 2804–2811, 2014.

[252] N. Basbous, M. Taqi, and N. Belouaggdia, "Effect of Humidity on Thermal Performances of a Non-evacuated Parabolic Trough Solar Collector," vol. 5, no. 3, 2015.

[253] A. S. Gudekar, A. S. Jadhav, S. V. Panse, J. B. Joshi, and A. B. Pandit, "Cost effective design of compound parabolic collector for steam generation," *Sol. Energy*, vol. 90, pp. 43–50, 2013.

[254] M. Collares-Pereira, "Description and Testing of a Non- Evacuated 1.5XCPC Collector Thermal Performance Comparison With Other Collector Types," *J. Sol. Energy Eng.*, vol. 107, no. November 1985, pp. 277–280, 1985.

[255] L. Jiang, B. Widyolar, and R. Winston, "Characterization of Novel Mid-temperature CPC Solar Thermal Collectors," *Energy Procedia*, vol. 70, pp. 65–70, 2015.

[256] Y. Kim, G. Han, and T. Seo, "An evaluation on thermal performance of CPC solar collector," *Int. Commun. Heat Mass Transf.*, vol. 35, no. 4, pp. 446–457, Apr. 2008.

[257] G. H. Lee, "A Study for the Use of Solar Energy for Agricultural Industry - Solar Drying System Using Evacuated Tubular Solar Collector and Auxiliary Heater -," *J. Biosyst. Eng.*, vol. 38, no. 1, pp. 41–47, Mar. 2013.

[258] P.-L. Paradis, D. R. Rousse, S. Hallé, L. Lamarche, and G. Quesada, "Thermal modeling of evacuated tube solar air collectors," *Sol. Energy*, vol. 115, pp. 708–721, May 2015.

[259] "Vakuumröhrenkollektoren Baureihe XL P." [Online]. Available: https://www.ritter-xl-solar.de/wp-content/uploads/2018/01/Datenblatt-XL-P-DE-V1-4_02.pdf. [Accessed: 01-Apr-2019].

[260] N. Jain and A. G. Alleyne, "Thermodynamics-Based Optimization and Control of Vapor-Compression Cycle Operation: Control Synthesis," *ASME 2011 Dyn. Syst. Control Conf. Bath/ASME Symp. Fluid Power Motion Control. Vol. 1*, no. 1, pp. 827–834,

2011.

[261] M. H. Ahmadi, H. Sayyaadi, S. Dehghani, and H. Hosseinzade, "Designing a solar powered Stirling heat engine based on multiple criteria: Maximized thermal efficiency and power," *Energy Convers. Manag.*, vol. 75, pp. 282–291, Nov. 2013.